INFLUENCE OF ACTIVE EFFLUX TRANSPORT ON THE DISTRIBUTION OF TARGETED AGENTS TO BRAIN TUMORS

A DISSERTATION
SUBMITTED TO THE FACULTY OF THE GRADUATE SCHOOL
OF THE UNIVERSITY OF MINNESOTA
BY

RAJNEET KAUR OBEROI

IN PARTIAL FULFILLMENT OF THE REQUIREMENTS
FOR THE DEGREE OF
DOCTOR OF PHILOSOPHY

William F. Elmquist

July 2014

ACKNOWLEDGEMENTS

I would like to take this opportunity to thank and acknowledge the following persons who have influenced me throughout the graduate school and contributed to this thesis;

First and foremost, my advisor *Dr. William Elmquist* for giving me an opportunity to work in his group and under his guidance. I sincerely thank him for believing in me, his endless patience in mentoring me and encouraging me throughout my research work. I am grateful to him for inspiring me to be a good scientist and explore my research interests. I am thankful to him for giving me wonderful projects to work on since my first day in his lab; from calibrating pipettes to an awesome research project that culminated in this thesis. I would also like to thank him for allowing me to gain industrial experience as an intern at the Clinical Pharmacology division at Covidien, during my graduate program.

I am especially grateful to *Dr. Richard Brundage* for serving on my thesis committee and helping and encouraging me in pursuing my research interests in pharmacometrics. His enthusiasm in teaching and allowing me to lead research topics in the readings class helped me greatly improve my research and teaching skills. Thank you for the wonderful lectures on population pharmacokinetic modeling in the Fall 2011 that helped me shape my interest in this area of research.

I am thankful to my second committee member, *Dr. Jann N. Sarkaria,* for showing interest in my research work and guiding me with his immense knowledge and resources. Thank you for your support and stimulating discussions in greatly improving this work.

I would also like to thank my third committee member and the chair of my committee, *Dr. Jayanth Panyam* for helping and guiding me in understanding the principles of tumor biology. I am grateful to him for his patience and allowing me to sit in his lectures on angiogenesis.

Most importantly I would like to thank all my committee members for their careful review and suggestions on my manuscripts and my research work.

I would like to especially thank *Dr. Cheryl Zimmerman* for sharing her vast knowledge in pharmacokinetics in the readings class. It was a wonderful experience working with her as her teaching assistant in basic pharmacokinetics course. I learned a lot from her.

I am also grateful to *Dr. Terri Morton*, who mentored me during my summer internship at Covidien. Thanks are due to Dr. Krishna Devarakonda for his valuable inputs on my internship project.

I am especially grateful to *Chani Becker*, graduate student in department of neuroscience, and *Jenny Pokorny* (Senior Research Technologist I, Mayo Clinic) for their immense help and support for the research work in this thesis. Without their valuable suggestions, I do not think this work would have been completed. I would also like to thank *Joey McFarren* and *Daniel Muldoon,* undergraduate students who immensely helped us with all the imaging work.

I would like to thank Dr. Ronald Sawchuk Fellowship in Pharmacokinetics for funding my research work. I also thank Jim Fisher at CPAS lab for his help and support over the last four years.

I would like to thank fellow members of the Elmquist lab, both seniors and current members - *Tianli, Ramola, Raj, Sagar, Li Li, Shruthi, Karen, Brynna* and *Shuangling* for their friendship, guidance and support during my graduate program at the UMN.

Special thanks to *Candice McDermott, Erica Flynn* and *Jeanene Noll* for all department related issues.

Many thanks to fellow graduate students *Mehak, Nidhi, Ameya, Pinal, Khushboo and Kinjal* for their valuable discussions, for patiently listening to my stories of failed experiments and not getting the results I had expected. Your warm friendship helped me cope up with not only the grueling coursework and numerous exams but the severe wind chills of Minnesota.

Thanks are due to my friends, *Sudeepto, Mamta & Himanshu, Rashmi, Varun and Mukul* for making my days of graduate life the most memorable ones. I would like to take this opportunity to express special thanks to *Mukul* for being a wonderful friend. I cannot

express how much I have learned from you. I would also like to thank my besties – *Shaili, Chaitali, Sameer and Sameer* for being there for me. You guys are awesome.

And now I would like to acknowledge the most important person. I would like to express my gratitude to my *Dad*. Without his support I would not have been able to take the step of joining the program at Minnesota as a transfer student. His belief in me, his continuous encouragement and the lessons he taught me about leading a good educated life made me stronger and helped me move forward. He taught me to be assertive and liberal at the same time, to be an independent thinker and as he always says, '*no matter how hard the problem is, there is always a solution. It is you who has the key to the door'*. There are no words to express how deeply I am indebted to him for whom I am today.

I express my sincere thanks to my *Mom* for her unconditional love and support. She has always been my source of strength and given me the final push I needed to pursue my interests. No words or act can express the gratitude to her. She is just adorable.

My sincere thanks to my brother, *Gurmeet*, for being there with me to cry, laugh, dance, fight and play. Even though you are younger to me, you have always been like an elder brother to me- protective and caring. Thank you.

Finally, I thank my grandfather, *Darji*, for his unending love and support.

This thesis is dedicated to my parents, Harjinder and Rashpal Oberoi

Rajneet Kaur Oberoi

415 words

Abstract:

Glioblastoma multiforme (GBM) is a lethal disease of the whole brain. Despite complete surgical resection of the tumor, recurrence is inevitable and leads to patient death. Several molecularly-targeted agents have shown promising results preclinically, although clinical results have been disappointing. One plausible explanation for clinical failure of drugs is their inability to effectively target the invasive glioma cells that reside in areas away from the tumor core. These regions of the brain have an intact blood brain barrier (BBB), which through a combination of endothelial tight junctions and active efflux transporters restricts brain penetration of several drugs. The objective of this thesis was to investigate the influence of active efflux transporters, P-glycoprotein (P-gp) and breast cancer resistance protein (Bcrp) on the brain distribution of molecularly targeted agents. To enhance our understanding of brain distribution with statistical certainty, we proposed a population-based analysis method to estimate variability around the brain partition coefficient (Kp).

We showed that the brain distribution of sunitinib (a tyrosine-kinase inhibitor) is limited by active efflux mediated by P-gp and Bcrp at the BBB. We further demonstrated that brain distribution could be enhanced by administration of a dual P-gp/Bcrp inhibitor. To statistically ascertain the variability associated with Kp in a serial sacrifice design, we

developed a pharmacokinetic model to simultaneously describe plasma and brain concentration time profile data. We further evaluated the influence of study design features such as between subject variability (BSV) and sample size at each time point on bias and precision of estimation of Kp. Our results show that bias is unaffected by the assumptions regarding the magnitude of BSV and sample size, however, precision improves with sample size.

We further examined the influence of BBB on delivery and efficacy of dual PI3K/mTOR inhibitors, GNE-317 (higher BBB permeability) and GDC-0980 (restricted BBB penetration) using three glioma mouse models, GL261-luc-GFP model, GBM10 and U87. Disruption of the BBB in the tumor core resulted in higher drug concentrations for GDC-0980. However, intact BBB in the areas adjacent to the core restricted the brain concentrations of GDC-0980. Contrary to this, the brain concentrations of GNE-317 were similar in all the three regions of the brain. Furthermore, results from survival studies indicated that although both GNE-317 and GDC-0980 significantly improved survival compared to placebo, the treatment groups were not significantly different from each other. Therefore, it is important to consider that effective treatment of GBM relies not only on effective delivery across the BBB to invasive glioma cells but also on an effective drug.

……. …….. ……...

Name of the advisor **Sign of the advisor** **Date**

TABLE OF CONTENTS

LIST OF TABLES

CHAPTER II

CHAPTER III

CHAPTER IV

LIST OF FIGURES

CHAPTER I

CHAPTER II

CHAPTER III

LIST OF ABBREVIATIONS

GBM, Glioblastoma multiforme;

VEGFR, Vascular Endothelial Growth Factor Receptor;

PDGFR, Platelet Derived Growth Factor Receptor;

EGFR, Epidermal Growth Factor Receptor;

bFGF, basic Fibroblast Growth Factor Receptor;

BBB, blood brain barrier;

ABC, ATP-Binding Cassette;

P-gp, P-glycoprotein;

Bcrp, Breast cancer resistance protein;

Sunitinib, (N-(2-diethylaminoethyl)-5-[(Z)-(5-fluoro-2-oxo-1H-indol-3 ylidene)methyl]-2,4-dimethyl-1H-pyrrole-3-carboxamide);

TKI, tyrosine kinase inhibitor;

MRP2, multi-drug resistance protein-2;

AUC, area under the curve;

GF120918, elacridar, **N**-(4-[2-(6,7-dimethoxy-3,4-dihydro-1**H**-isoquinolin-2-yl)ethyl]-5-methoxy-9-oxo-10**H**-acridine-4-carboxamide;

Ko143, (3S,6S,12aS)-1,2,3,4,6,7,12,12aoctahydro-9-methoxy-6-(2-methylpropyl)-1,4-dioxopyrazino(1',2':1,6) pyrido(3,4-b)indole-3-propanoic acid 1,1-dimethylethyl ester;

LY335979 (zosuquidar), (R)-4-((1aR,6R,10bS)-1,2-difluoro-1,1a,6,10btetrahydrodibenzo-(a,e)cyclopropa(c)cycloheptan-6-yl)-α-((5-quinoloyloxy)

methyl)-1-piperazine ethanol, trihydrochloride;

FVB, Friend leukemia virus strain B;

Kp, tissue partition coefficient;

LC-MS/MS, liquid chromatography-tandem mass spectrometry;

DTI, drug targeting index;

LLOQ, lowest limit of quantification;

Cmax, maximum observed concentration;

CL/F, apparent clearance;

Css, steady-state concentration;

MRI, magnetic resonance imaging

NONMEM, non-linear mixed effect modeling

PsN, Perl speaks NONMEM

BSV, between subject variability

η, eta (standard deviation associated with BSV)

σ^2 = variance associated with eta

RUV, residual unexplained variability

ω^2, omega squared, variance associated with RUV

θ, theta, symbolized parameter such as clearance

SSE, stochastic simulations and estimations

MPE, mean prediction error

λ_z, terminal rate constant

VPC, visual predictive check

CHAPTER I

OVERVIEW

1.1 INTRODUCTION

Brain tumors are solid neoplasms that occur inside the cranium and the brain stem. They can be malignant or benign in nature. A brain tumor can either originate in the brain (primary brain tumor) or metastasize from peripheral sites to the brain (metastatic brain tumor). Metastatic brain tumors are more common than primary brain tumors. Almost 20-40% of peripheral tumors spread to the brain, most commonly from lung, breast, melanoma and colon cancer (Soffietti et al., 2002). The Central Brain Tumor Registry of United States (CBTRUS) estimated approximately 70,000 cases of primary brain tumors to be diagnosed in 2013 based on age-sex-race groups (www.cbtrus.org) (Walker et al.). On an average, the prevalence of a brain tumor is 221.8 per 100,000 persons. In 2010 alone, approximately 700,000 persons were living with a diagnosis of a primary brain tumor (Porter et al., 2010).

Meningiomas are the most common primary brain tumor, representing 34% of all primary brain tumor cases reported. Glioma, a broad class of primary brain tumors that originate in the glial tissue of the brain represents 30% of all brain tumors, of which 80% are malignant (Porter et al., 2010) (www.cbtrus.org). Glial tumors can be astrocytic, oligodendroglial or oligoastocyitc in nature. The World Health Organization (WHO) has categorized astrocytic glial tumors into four grades, based on morphology, molecular genetics and biomarkers, prognosis and malignancy (Louis et al., 2007). Grade I, pilocytic astrocytomas, are rare, slow-growing benign tumors that are usually associated with prolonged survival. Grade II, astrocytomas, are relatively slow growing tumors. They tend

to infiltrate to other parts of the brain and can recur as a high-grade glioma. Median survival is approximately 10 years. Grade III, anaplastic astrocytoma, are malignant tumors with a greater tendency to spread in other parts of the brain and often recur as a higher-grade tumor. Median survival in these patients is usually 2 years. Grade IV, glioblastoma multiforme (GBM) is the most malignant and most common primary brain tumor in adults. The median survival is approximately 14.6 months after radiation and chemotherapy (Stupp et al., 2005). The tumor cells in GBM have a characteristic morphology. The existing vasculature is highly permeable, with thickened basement membrane and hyperplasic endothelial cells. This makes GBM one of the most angiogenic solid tumors (Brem et al., 1972; Rong et al., 2006; Onishi et al., 2011). Certain reports in literature have indicated that growth of a glial tumor from low-grade to high-grade is dependent on the formation of new blood vessels (Brem, 1976). Histological hallmarks of GBM include a necrotic center with extensive proliferation on the growing edge. This makes tumor cells appear as if arranged in a glomerular capillary loop in a garland-like fashion. Thus, highly hypoxic pseudo-palisading cells surrounding the necrotic tumor core define a unique framework to GBM tumor cells (Onishi et al., 2011). GBMs are particularly notorious for their heterogeneity and invasion into the other healthy parts of the brain (Levin et al., 1975; Berens and Giese, 1999).

1.2 CURRENT TREATMENT OPTIONS:

With high mortality rates, heterogeneous nature of the tumor and aggressive relapse, treatment of GBM remains difficult. Most patients undergo multi-modal treatments that

include surgery, radiation and chemotherapy. With the advancement in research and discovery of tumor growth pathways along with understanding of multiple mechanisms and barriers in drug delivery, molecularly targeted agents appear to be more promising. Several of these drugs are in clinical trials alone or in combination with chemotherapeutic agents or radiation (Bai et al., 2011).

The first line of treatment for GBM is the surgical resection of the tumor without injuring the brain tissue and neurological functions such as motor skills. Most benign tumors are treated by surgery alone, however malignant tumors require radiation and/or chemotherapy in addition to surgery. Various surgical techniques can be utilized for efficient removal of the tumor such as stereotactic surgery (Romanelli et al., 2009), laser surgery (Lee Titsworth et al., 2014) and ultrasonic aspiration (Beckner et al., 2007). Surgery is usually guided by use of contrast agents (gadolinium) or fluorescent agents (5-aminolevulinic acid (5-ALA)), which concentrate in the tumor core, making it easier for the surgeons to detect and remove tumor mass. Although surgery is the primary care for GBM patients, tumor recurrences have been observed due to tumor cells that infiltrate to zones beyond the tumor core. Cells in this region are highly migrating and infiltrative and often go undetected in MRI (Albert et al., 1994). Therefore, surgery is often followed by radiation therapy or chemotherapy to help the brain get rid of as many tumor cells as possible.

Radiation therapy (RT) forms an integral part of treatment option for high-grade gliomas. RT is a specific treatment that only targets the tumor tissue. In some cases, RT is used alone but otherwise it is often used in combination with surgery and/or chemotherapy. Here, high energy X-rays are directed at the tumor core. There are three primary ways by which a radiation therapy can be employed for treating brain tumor cells. External beam radiation therapy (EBRT) utilizes a machine that targets the cancer cells from outside while internal beam radiation therapy (IBRT) also known as brachytherapy, places a radioactive substance, usually sealed in needles or implants are placed near the tumor. Stereotactic radiation therapy (SRT), also called a gamma knife therapy, is a site-specific radiation therapy when the tumor is localized (Oh et al., 2012). In severe cases, patients receive whole brain radiation therapy (WBRT) when the tumor cells can be seen scattered in a MRI. The addition of RT to surgery has shown an increase in survival (Walker et al., 1978; Stupp et al., 2005), but response of GBM patients to RT varies. Use of radio sensitizers, such as chemotherapeutics and anti-angiogenic drugs may show improvement in response to RT (Rodrigus, 2003; Duda et al., 2007).

The goal of chemotherapy is to kill as many tumor cells as possible, which have been left behind after surgery and/or radiation therapy (Berens and Giese, 1999). Several reports in literature have suggested significant survival benefits in GBM patients on chemotherapy (Brandes et al., 1999; Stupp et al., 2005). Chemotherapeutics most commonly employed for GBM treatment are cytotoxic such as alkylating agents (temozolomide (TMZ)) and nitrosoureas (carmustine (BCNU) and lomustine (CCNU)) and cytostatic agents such as

thalidomide and tamoxifen) (Parney and Chang, 2003; van den Bent et al., 2006). With promising results in clinical trials of GBM, FDA approved TMZ as a single agent standard care of treatment in 2005 (Darefsky et al., 2012). Concomitant administration of TMZ and radiation was found to significantly increase the progression-free survival compared to radiation alone (14.6 months vs. 12.1 months) (Stupp et al., 2005). Since its approval, several other chemotherapeutics have been tried in combination with TMZ but none of the combinations showed encouraging results due to myelosuppression as a dose-limiting toxicity. Carmustine (BCNU) was the first systemic chemotherapeutic approved for the treatment of brain tumors in United States. It was formulated as interstitial wafers (Gliadel® wafers) and increased the 6-month survival rate by 20% compared to placebo, though serious intracranial infections were reported after (Brem et al., 1995; Bota et al., 2007)

1.3 MOLECULARLY-TARGETED THERAPY

In recent years, understanding of the molecular mechanisms involved in tumor growth and identification of several aberrant pathways has led to the development of molecularly targeted agents. Several studies have evaluated the role of signal transduction pathways that are up regulated in GBM (Rasheed et al., 1999; Liang et al., 2002; Inda et al., 2010; Suvasini et al., 2011; Yi et al., 2011). These agents act by inhibiting the intracellular phosphorylation of protein-kinase domains (such as tyrosine, serine or threonine) of tumor growth pathway receptors or by interfering with the binding of the specific ligand to its receptor located on the tumor cell or on the blood vessel endothelium. The tumor growth

factor receptor pathways most commonly altered in GBM are vascular endothelial growth factor receptor (VEGFR) (Reardon et al., 2008), platelet derived growth factor receptor (PDGFR) (Kim et al., 2012), epidermal growth factor receptor (EGFR) (Inda et al., 2010), scatter factor/hepatocyte growth factor (MET) (Abounader and Laterra, 2005), neuronal and glioma-derived stem cell factor receptor (Sun et al., 2006) and fibroblast growth factor receptor (FGFR) (Stefanik et al., 1991).

Bevacizumab, anti-VEGF monoclonal antibody, is an anti-angiogenic drug. It was approved in May 2009 by the US-FDA for treatment of recurrent glioblastoma. In combination with irinotecan, bevacizumab improved 6-month progression-free survival to 46% compared to 21% with TMZ (Vredenburgh et al., 2007). Recently, dysregulation in downstream signaling pathways such as phosphatidylinositol-3-kinase (PI3K/mTOR) and Ras/MAPK pathway has been reported in GBM (Maity et al., 2000; Hu et al., 2005). Significant crosstalk among these pathways makes it difficult to treat a tumor, as inhibition of one pathway may lead to compensatory up-regulation of another target. More recently, the use of multi-targeted molecularly targeted agents has become an attractive treatment option, in conjunction with surgery, radiation and chemotherapy.

1.3.1 VASCULAR ENDOTHELIAL GROWTH FACTOR RECEPTOR (VEGFR) AND PI3K/AKT/MTOR PATHWAY

Glioma is a highly vascular tumor with significant infiltration into the surrounding healthy tissue of the brain. Immunohistochemistry analysis and ELISA of several brain tumors has

suggested that there is an increased expression of many tumor growth factors and their receptor pathways, in particular VEGF in GBM (Takano et al., 2010). VEGF is a pro-angiogenic factor and one of the main mediators of glioma-angiogenesis (Wong et al., 2009). VEGF is a ligand, which is released by tumor cells in response to several oncogenes as well as hypoxic or acidic conditions in the tumor core. Once released, VEGF binds to its receptors, located on the tumor cell surface and the blood vessel endothelium. There are six glycoprotein isoforms of VEGF; VEGFA-E and placental growth factor. VEGF is recognized by its receptors, VEGFR1, -2 or -3. VEGFR-1 is involved in activation of haematopoiesis, recruitment of monocytes and bone marrow derived cells for enhancing tumor growth and activation of matrix metalloproteinases (Gerber et al., 2002). VEGFR-3 mediates lymph-angiogenesis. VEGF-A, also known simply as VEGF, plays a prominent role in brain tumor growth. It was discovered as a permeability factor and is considered to increase BBB disruption. VEGF-A binds to two receptors, VEGFR1 and VEGFR2, which have been implicated as being most important in glioma-angiogenesis, with VEGFR-2 playing a dominant role in mediating the mitogenic, angiogenic and permeability enhancing effects of VEGFA (Xu et al., 2013a; Yao et al., 2013). Once VEGF is bound to its receptors, it causes dimerization of the intracellular tyrosine-kinase domains and phosphorylates tyrosine residues. This process promotes activation via phosphorylation of downstream secondary messengers of the PI3K/Akt/mTOR (phosphoinositide 3-kinase, the serine/threonine protein kinase AKT and the mammalian target of rapamycin (mTOR)) pathway. This pathway is considered central to VEGF signaling because it inhibits endothelial cell apoptosis by interfering with apoptotic

signaling (Cheng et al., 2009). It has also been reported that this pathway exhibits a feedback communication loop with the angiogenic factors via hypoxia inducible factor (HIF) which influences release of VEGF by the tumor cells (Mazure et al., 1997). In addition, VEGF-A also called as vascular permeability factor, is considered to be conducive for the disruption of BBB at the tumor "core". Enhanced vessel leakiness in the tumor region increases the overall interstitial fluid pressure (IFP) of the tumor, thus compromising distribution of chemotherapeutics to the tumor core (Jain et al., 2007) **(Figure 1.1).**

There are several small molecule drugs that inhibit VEGFR by inhibiting the intracellular tyrosine-kinase domains and interfering with the signaling cascade. These drugs include cediranib, vandetanib, pazopanib and sunitinib and have been tried in several preclinical models as an anti-VEGF agent (Wedge et al., 2005; Christensen, 2007; Siemann et al., 2009). Sunitinib and sorafenib are two multi-targeted agents that inhibit VEGFR and PDGFR and possess both anti-tumor and anti-angiogenic activities. These drugs have been found to show anti-glioma and anti-VEGF activity in preclinical glioma xenograft models (Siegelin et al., 2010; D'Amico et al., 2012; Czabanka et al., 2013). Bevacizumab is an anti-angiogenic drug that binds to VEGF circulating in the blood stream and interferes with its binding to the VEGFR2. Aflibercept (a fusion protein), also called as a VEGF-trap, is another drug that binds to circulating VEGFA, VEGFB and placental growth factor by acting as a soluble decoy receptor (Stewart, 2011). It is approved by the US-FDA for

wet macular degeneration (Ohr and Kaiser, 2012) and metastatic colorectal cancer (Andre and Chibaudel, 2013).

1.3.2 PLATELET-DERIVED GROWTH FACTOR RECEPTOR (PDGFR)

PDGFR is another commonly over-expressed tumor growth receptor in glioma and contributes significantly to the aggressive nature of the tumor (Nazarenko et al., 2012). This receptor plays a central role embryonic development and response to tissue damage in normal physiological conditions. In a tumor state, it is considered as being an essential pro-angiogenic factor involved in glioma-angiogenesis (Pierce et al., 1991). PDGFR-alpha and ß are the two major receptor isoforms of PDGFR that play an important role in the development and differentiation of the vessel wall (Zhang et al., 2009). Like VEGFR, downstream effects of PDGFR are mediated by receptor dimerization, phosphorylation of intracellular residues followed by activation and phosphorylation of intracellular signaling pathways, PI3K/Akt, MAPK/ERK and STAT3. Amplification of PDGF and PDGFR is observed in 11% of GBM patients (Hermanson et al., 1996; Lokker et al., 2002; Nazarenko et al., 2012)

Figure 1.1: Schematic representation of receptor tyrosine kinase pathways and PI3K/mTOR pathways and therapies for glioblastoma

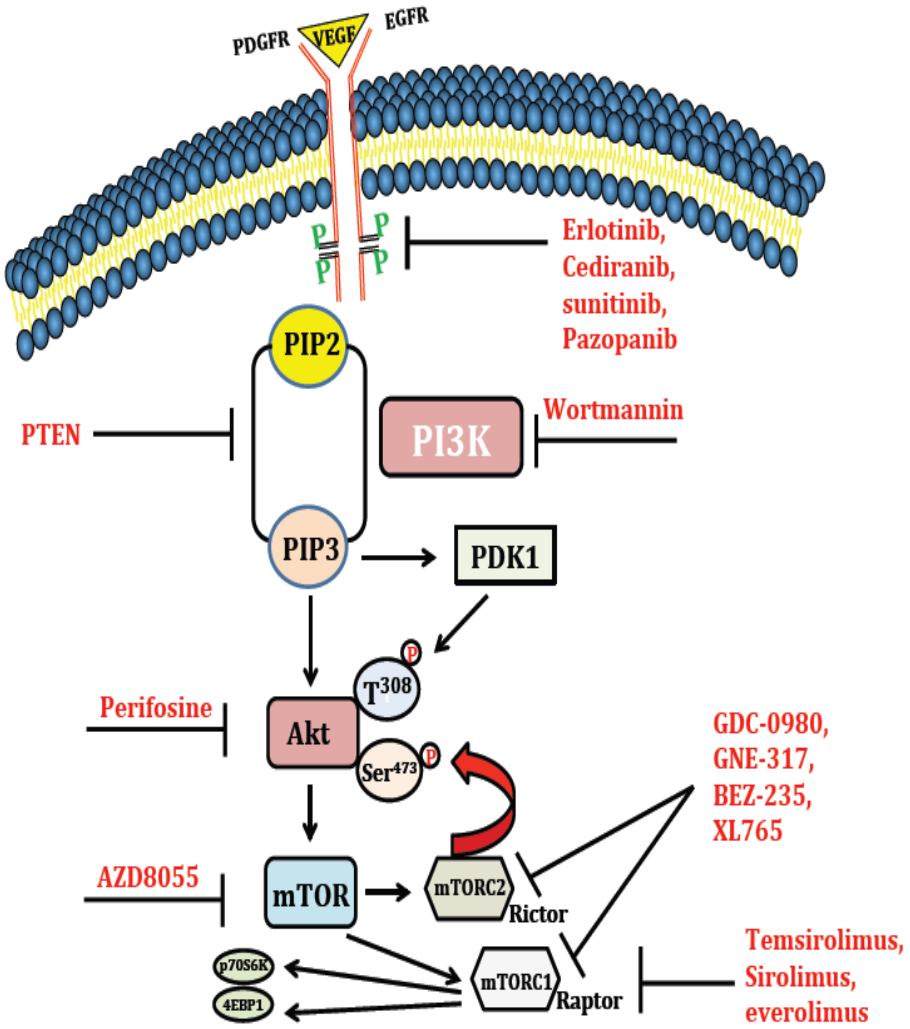

1.3.3 EPIDERMAL GROWTH FACTOR RECEPTOR (EGFR)

EGFR is yet another tumor growth factor receptor involved in cellular proliferation via activation of downstream effector targets, PI3K/Akt/mTOR and ERK/MAPK pathway. EGFR-gene is one of the most frequently amplified and mutated forms in GBM pathophysiology, indicating high-grade glioma. The most common variant form of EGFR-gene is *EGFRvIII, which* results in a constitutively activated receptor, lacking a ligand-binding domain (Gupta and Salunke, 2012). Gefitinib and erlotinib are two tyrosine kinase inhibitors that showed potent anti-EGFR activity but failed to show significant survival benefit in GBM patients (Franceschi et al., 2007; Reardon et al., 2010)

1.3.4 PI3K/AKT/MTOR PATHWAY

Current understanding in molecular mechanisms of GBM pathogenesis and limited efficacy of aggressive treatment modalities have led to development of molecularly-targeted agents that inhibit intracellular pathways. Although treatment with bevacizumab improved survival compared to conventional chemotherapeutics, but effect on long-term efficacy was impeded by the heterogeneous nature of the tumor (Wen et al., 2012) and existence of tumor cells beneath an intact BBB forming a sanctuary. Hence, combination therapies have been proposed wherein the drugs in combination inhibit more than one target (Reardon and Wen, 2006; Lassen et al., 2013).

PI3K/Akt/mTOR belongs to a family of intracellular lipid kinases, comprising of three effectors; phosphoinositide 3-kinase (PI3K), the serine/threonine protein kinase AKT, and the mammalian target of rapamycin (mTOR). Present downstream of several tumor growth receptors, this pathway has been implicated in several physiological and pathological functions such as cellular proliferation, cell differentiation, cell migration, metabolism and genetic mechanisms such as translation and transcription of tumor growth genes and cell cycle functions such as apoptosis. This makes it a very attractive target. (Guertin and Sabatini, 2007; Busaidy et al.; Wen et al., 2012). Alterations in the phosphatase and tensin homolog (PTEN) tumor suppressor gene have often been related to the activation of this pathway (Gruber Filbin et al., 2013) (Figure 1.1).

Binding of ligands such as insulin growth factor (IGF) to insulin growth factor receptor (IGFR) or VEGF to VEGFR, activates intracellularly located PI3K, which is then transported to the plasma membrane catalyzing the formation of phosphatidylinositol 3,4,5-triphosphate (PIP_3) through phosphorylation of phosphatidylinositol-4,5-diphosphate (PIP_2). PIP_3 is a critical activator of Akt (also known as protein kinase B). Activation is mediated via recruitment of Akt to the membrane and phosphorylation of PDK1 and mTORC2. Akt subsequently activates mTOR complex. The mTOR complex comprises of two multi-protein isoforms, mTORC1 and mTORC2. In mTORC1, mTOR is associated with a regulator subunit, Raptor, which regulates mRNA translation and is sensitive to rapamycin and its analogs (Huang and Manning, 2009). Rapamycin and its analogs act by dissociating the raptor from mTORC1, leading to uncoupling of its substrate proteins.

mTORC2, on the other hand, is associated with a rapamycin insensitive protein called Rictor (Sarbassov et al., 2005; Guertin and Sabatini, 2007). Certain studies in literature suggest the existence of feedback loop for activation of Akt and mTORC1 via mTORC2 in an Akt-independent manner (Matheny and Adamo, 2009).

mTORC1 inhibitors (rapamycin, everolimus and temsirolimus) have undergone extensive preclinical and clinical evaluation, both as single agents and in combination for several cancers such as GBM (Goudar et al., 2005; Kreisl et al., 2009), breast cancer (Gadgeel et al., 2013; Ma et al., 2013), (Xu et al., 2013b) and prostate cancer (Zhang et al., 2012; Armstrong et al., 2013; Ellis et al., 2013). As a single agent, mTORC1 inhibitors have shown disappointing results in clinical trials (Cloughesy et al., 2008).

Recent studies have indicated that inhibition of both mTORC1 and mTORC2, in addition to inhibition of PI3K and Akt, are needed to effectively suppress the activities of this pathway (Prasad et al., 2011; Fan and Weiss, 2012; Sami and Karsy, 2013). This led to the development of dual PI3K/Akt/mTOR inhibitors as an effective therapeutic approach. Some of the drugs in this category include GDC-0980, GNE-317, BEZ235, XL765, GDC-0084 and PF-4691502.

The current thesis is focused on

- Sunitinib malate, an anti-angiogenic and anti-tumor agent with activity against VEGFR1-3, PDGFR-beta and other tumor growth regulators. It was approved as an anti-angiogenic agent for the treatment of advanced renal cell carcinoma (RCC) in May 2006

and subsequently for imatinib-resistant gastro-intestinal stromal tumors (GIST) (Rock et al., 2007). Recently, sunitinib was approved for advanced pancreatic neuroendocrine tumor (PNET) (Delbaldo et al., 2012).

- GNE-317 and GDC-0980, dual PI3K/Akt/mTOR inhibitors. GDC-0980 is currently in clinical trials for GBM and GNE-317 is currently under investigation.

1.4 BARRIERS TO DRUG DELIVERY

Despite major developments to improve brain delivery of drugs, treatment of primary and metastatic brain tumors remains one of the most challenging issues. Though brain is a highly perfused organ, it is well protected from the peripheral circulation by the presence of barriers that regulate the passage of several endogenous and exogenous (xenobiotics such as drugs and toxins) substances to the central nervous system (CNS) (Mangas-Sanjuan et al., 2010). Several studies have suggested and indicated the correlation between physiochemical properties of drug molecules and BBB permeability such as lipophilicity, favorable size and charge state, appropriate polar surface area and its hydrogen-bonding potential. In spite of these favorable characteristics, several drug molecules still have limited distribution into the brain, which is affected by other factors that include plasma and/or brain protein binding and interaction with efflux transport systems (Summerfield et al., 2007; Hammarlund-Udenaes et al., 2008; Friden et al., 2009; Hammarlund-Udenaes et al., 2009). These barriers include the blood-brain barrier (BBB), blood-cerebrospinal fluid

barrier (BCSFB) and the ependyma (a layer of epithelial cells). Of these, the BBB is one of the most determinant barriers to drug delivery to the CNS (Abbott, 2000).

1.4.1 BLOOD-BRAIN BARRIER (BBB)

The BBB is not only a physical barrier but also a biochemical barrier that affects the rate and extent of drug distribution into the brain. The BBB is comprised of endothelial cells lining the cerebral microvessels. These cells confer a unique structure to the BBB compared to the microvessels elsewhere in the body, by the presence of tight-junctions and absence of fenestrae and pinocytic vesicles.

1.4.1.1 Physical Barrier

Presences of tight junction (TJ) protein complexes within the brain microvasculature restrict entry of solutes from the systemic circulation into the brain. *zonulae occludentes* are the extremely tight TJ and one of the key features of the BBB. They significantly affect paracellular diffusion across BBB (Begley and Brightman, 2003; Abbott et al., 2010). Other junction complexes include adherens junctions wherein cadherin proteins provide a structural support to the tissue (Wolburg and Lippoldt, 2002). Further, TJ complexes comprising of occludins, claudins (-3, -5, -12), cingulins and junctional adhesion molecules (JAM-A, -B, -C) impede paracellular movement. In addition to TJ between endothelial cells, presence of astrocytic glial endfeet and pericytes at the abluminal side, maintain the barrier properties of the BBB, restricting transport of

hydrophilic and low-molecular weight compounds (Abbott et al., 2006). It has been observed that absence of TJ complex protein, claudin-3, is related to the loss of BBB integrity in GBM (Wolburg et al., 2003). Therefore, translocation of essential polar nutrients such as amino acids and glucose occurs by presence of specific solute carriers present on the luminal or abluminal side of the BBB (Betz et al., 1980; Abbott, 2002; Zhang et al., 2002).

1.4.1.2 Biochemical Barrier

Despite appropriate physiochemical properties, presence of solute carriers, other influx transport systems and carrier-mediated pathways at the BBB, small molecules that are able to diffuse across the endothelial cells are still subjected to active efflux back into the blood stream by efflux transport systems present at the BBB (Pardridge, 2007). Even though lipophilicity has been considered a favorable component for drug delivery, increasing the lipid solubility of a drug beyond a certain level can become counter-productive by increasing its likelihood of becoming a substrate for the ATP-Binding Cassette (ABC) family of efflux transporters (Begley, 2004; Eilers et al., 2008). These are ATP-dependent efflux proteins expressed on the luminal and/or abluminal side of the BBB (Kusuhara and Sugiyama, 2001). The three important members of the ABC family are P-glycoprotein (P-gp, ABCB1), breast cancer resistance protein (BCRP, ABCG2) and multidrug-resistance associated proteins (MRPs, ABCC1-7).

P-glycoprotein (P-gp) is one of the most important and extensively studied ABC efflux protein. It is expressed and located on the luminal side of the brain capillary endothelial cells (Cordon-Cardo et al., 1989; Decleves et al., 2002). Several in-vivo studies have been conducted assessing the role of P-gp in restricting delivery of drugs to the brain. In mice, two genes *mdr1a* and *mdr1b*, encode for P-gp; however *mdr1a* is localized on the BBB (Demeule et al., 2002). Development of P-gp double knockout mice (*Mdr1a/b(-/-)*) has aided researchers in these studies extensively (Schinkel et al., 1994).

Breast cancer resistance protein (BCRP) is another important member of ABC family that plays a significant role, often in tandem with P-gp, in limiting brain distribution of drugs. It was first identified when Doyle and colleagues observed resistance of anthracycline accumulation in breast cancer cell line, MCF-7 (Doyle et al., 1998). In a separate study around the same time, this transporter was observed to cause resistance to mitoxantrone accumulation in cancer cells in a P-gp independent fashion. BCRP is expressed in a variety of tissues which include placenta, intestine, kidney and BBB (Sharom, 2008). At the BBB, BCRP is located on the luminal side of the capillary endothelial cells. Several studies have shown overlapping substrate specificities of BCRP and P-gp (Schinkel and Jonker, 2003).

Further, development of transgenic mouse model knocked out for both the genes (*Mdr1a/b(-/-)Bcrp1(-/-)*) significantly contributed to our understanding of the potential role of these two transporters in limiting the brain distribution of several drugs including

molecularly targeted agents such as tyrosine-kinase inhibitors (de Vries et al., 2007; Chen et al., 2009; Polli et al., 2009) and PI3K/Akt/mTOR inhibitors (Salphati et al., 2012). It has been shown that both P-gp and Bcrp show co-operation at the BBB and inhibition of both these transporters enhances brain delivery (Agarwal et al., 2011a). Moreover, recent studies have shown that lack of P-gp and BCRP results in greater than additive effect compared to absence of single transporter, P-gp or BCRP alone for several dual substrates such as lapatinib (Polli et al., 2009), dasatinib (Chen et al., 2009), gefitinib (Agarwal et al., 2010) and imatinib (Breedveld et al., 2005). Until recently, compensation of the activity of one transporter by the other was considered as a plausible explanation for this effect. However, in a recent study by Agarwal et al., the authors showed via quantitative proteomics approach that genetic deletion of either P-gp or Bcrp does not influence the expression of other transport systems at the BBB and therefore, P-gp and Bcrp do not show compensation effect (Agarwal et al., 2012).

The blood brain barrier is a major impediment in drug delivery into the brain parenchyma. The problem is further complicated by the fact that both P-gp and Bcrp work in tandem to limit brain distribution of drugs. Therefore, there is a need to develop and investigate strategies to effectively target tumors in the brain.

1.5 CHARACTERIZATION OF BRAIN DISTRIBUTION IN A SERIAL SACRIFICE DESIGN USING POPULATION-BASED APPROACH

Preclinical pharmacokinetic investigations to estimate influence of drug efflux transporters are often determined in small animals such as mice and rats. The size of these animals limits the number of samples that can be obtained from each animal. Therefore, for a time-course study over 24 hours, cohorts of animals are sacrificed at each time point to obtain plasma and corresponding tissue concentrations. This kind of sample design is called as 'serial sacrifice design' or destructive sampling design (Ette et al., 1995). Usually, data analysis in this case is determined using naïve-pooled average approach through non-compartmental analysis (NCA) to estimate the exposures (area under the curve (AUC)) in the plasma and the corresponding tissue. The ratio of exposures is used to determine tissue distribution coefficient or K_p (*brain distribution coefficient in this case*). This approach of data analysis has disadvantages. First, we lose information on within animal correlations by averaging concentrations at each time point. Second, we cannot statistically compare between treatment/groups as we only obtain a point estimate of K_p, with no information on associated variance.

To statistically compare transporter functions, we propose a population based modeling approach to estimate K_p of sunitinib in FVB-wild type, *Mdr1a/b(-/-)*, *Bcrp1(-/-)*, and *Mdr1a/b(-/-)Bcrp1(-/-)* mice. In addition, we investigated the influence of design elements (sample size at each time point and varying between-animal variability) on bias and precision of estimation of Kp using stochastic simulations and estimations.

STATEMENT OF PROBLEM

Despite major advancements in discovery of novel targets and development of molecularly targeted drugs, treatment of GBM remains a challenge, particularly because of failure of drugs in improving efficacy and survival of patients in clinical trials. One of the explanations indicated for drug failure in clinical studies relates to the correct identification of the target or mutation in the gene. Development of resistance to previously responding drugs has also been attributed to various mechanisms such as upregulation of alternative signaling pathways, selection of more aggressive tumor cells, invasion and spread of glioma stem cells via different angiogenic mechanisms such as vessel cooption (Grepin and Pages, 2010). However, little attention is given to the issue of delivery of drugs across the BBB in treatment regimens. With prior knowledge and extensive research in preclinical xenograft glioma models we are aware of the mechanisms that can limit the delivery of several drugs into the brain and the tumor cell.

The BBB not only poses a physical barrier by the presence of tight endothelial junctions but is also a functional barrier comprising of active efflux transporters, P-glycoprotein (P-gp) and breast cancer resistance protein (BCRP). These two transporters work in concert to restrict drug delivery to the brain. Furthermore, presence of active efflux on the tumor cell also restricts delivery of drugs into the tumor cell (Agarwal et al., 2011b). These dual barriers, BBB and brain tumor cell barrier, in conjunction with biochemical and physical barriers, can significantly impair drug distribution to the tumor cell resulting in little to no

efficacy (Agarwal et al., 2013). Several molecularly targeted agents have been found to be substrates for P-gp and Bcrp.

In addition, infiltration of highly invasive GBM cells into the surrounding brain tissue poses another challenge for effective treatment and drug delivery to the tumors. Harboring beneath an intact BBB, these tumor cells are not enhanced by contrast agents and are not removed by surgery. These cells further escape the effects of chemotherapy leading to recurrence of the tumor.

Therefore, effective treatment of glioblastoma multiforme requires identification of the correct target and an effective multi-targeted drug or combination of drugs that evade active efflux at the BBB.

RESEARCH OBJECTIVE

Thus, the overall research objective of this thesis is to investigate the role of active efflux mechanisms, mediated by P-glycoprotein and breast cancer resistance protein, in the blood brain barrier in influencing the brain distribution of molecularly targeted agents. To achieve our research objective we used the following research approach:

1. To pharmacokinetically assess the role of P-gp and Bcrp in limiting the brain distribution of sunitinib and examine influence of co-administration of pharmacological inhibitors in improving the brain delivery of sunitinib.
2. To statistically evaluate variability associated with the brain partition coefficient (K_p) using non-linear mixed effect modeling approach and assess the influence of study design elements such sample size at each time point and between-subject variability on the estimation of K_p.
3. To demonstrate that the blood brain barrier is heterogeneously disrupted in the tumor core and is intact in the areas away from the tumor core in glioma mouse models.
4. To study the influence of P-gp and Bcrp on efficacy of dual PI3K/mTOR inhibitors with different brain permeability characteristics in three glioma bearing mouse models- GL261 syngeneic mouse model, patient-derived GBM10 xenograft model and cell-line derived U87 mouse model.

RESEARCH PLAN

Chapter 2 reviews the different strategies to enhance brain drug delivery for the treatment of glioblastoma multiforme. This chapter reviews issues inherent to treatment of GBMs such as heterogeneity in the tumor and the microenvironment that influences drug delivery. Further, this chapter discusses strategies that can overcome tight junctions chemically or physically (such as transient BBB disruption by osmotic or ultrasound methods), evade or overcome active efflux mechanisms (by the use of pharmacological inhibitors or chemical modification of drugs), local delivery strategies (such as convection enhanced delivery, intracerebral, intracranial and intratumoral injections and intranasal delivery of drugs to the brain), use of drug carriers (such as nanoparticles and lipid based delivery methods) and drug modification by conjugating moieties like amino acids that can assist in drug delivery by using influx transport systems.

Sunitinib malate (Sutent®) is an orally available anti-angiogenic drug approved for the treatment of imatinib resistant metastatic renal cell carcinoma (mRCC), gastro intestinal tumors (GIST) and pancreatic neuro-endocrine tumors (pNET). Since GBM is a highly angiogenesis driven tumor we investigated the role of efflux transporters, P-gp and BCRP, in limiting brain distribution of sunitinib in mice. Chapters 3, 4 and 5 discuss pharmacokinetic and statistical analysis of brain distribution of sunitinib.

Chapter 3 discusses the development and validation of a robust analytical method for determination of plasma and brain concentrations of sunitinib by liquid-chromatography

tandem mass spectrometry (LC-MS/MS). Sunitinib is a light sensitive drug that undergoes light-induced E-to-Z isomerism. All experiments and sample preparation was done in light-protected conditions and this is discussed in this chapter.

Chapter 4 quantitatively assesses the role of transport mechanisms that restrict brain delivery of sunitinib and the use of combination strategies such as pharmacological inhibition of active efflux to improve its brain delivery. In addition, this chapter pharmacokinetically assesses the extent of brain distribution of sunitinib as calculated by AUC brain-to-plasma ratio, steady state brain-to-plasma concentration ratio and transient steady state brain-to-plasma ratio for a drug exhibiting non-saturable, linear distributional kinetics.

Chapter 5 statistically examines the brain distribution coefficient in a serial sacrifice design using population based non-linear mixed effect modeling approach. Further, this chapter evaluates the influence of design elements such as sample size at each time point and between-animal variability, on the estimation of Kp for sunitinib.

The PI3K-pathway is considered central to the several surface receptor pathways such as vascular endothelia growth factor (VEGFR). Several dual PI3K/mTOR inhibitors are currently being investigated in clinical trials for GBM, including GNE-317 and GDC-0980. Chapter 6 discusses the influence of BBB (tight junctions and active efflux) on the brain distribution of GNE-317 (brain penetrant) and GDC-0980 (brain impenetrant) in

GL261 tumor bearing mice and FVB non-tumor bearing mice. In addition, we studied brain permeability and heterogeneity in the tumor using Texas Red dextran, a permeability marker. We also evaluated the regional brain distribution of GNE-317 and GDC-0980 in tumor-bearing mouse models.

To summarize, this dissertation shows that there are regions of partially intact BBB in the tumor core suggesting heterogeneity in the tumor that may impact drug distribution. The studies suggest that both P-gp and BCRP restrict delivery of molecularly targeted agents, sunitinib and GDC-0980, while sparing GNE-317. Further, we could statistically determine brain distribution using a novel population based approach to serial-sacrifice data. Simulations show that sample size and magnitude of between-animal variability does not influence the bias in estimate of Kp. However, an increase in sample size at each time point results in higher precision in estimating Kp.

CHAPTER II

STRATEGIES FOR IMPROVING DELIVERY OF ANTI-CANCER DRUGS TO INVASIVE GLIOMA

2.1 INTRODUCTION

Glioblastoma multiforme (GBM) is the most common and aggressive primary brain tumor that remains essentially incurable despite decades of intensive research on conventional and novel therapeutic strategies. Due to the diffusely invasive nature of GBM, even aggressive surgical resection is insufficient to control tumors, and following maximal surgical resection, the addition of partial brain irradiation combined with temozolomide chemotherapy significantly extends time to recurrence and improves survival (Furnari et al., 2007). Unfortunately, despite this aggressive treatment regimen, the median survival for GBM patients remains approximately 12-15 months and only 2% of patients survive longer than 5 years (Stupp et al., 2005). GBM is highly vascular and invasive , and exhibit a complex pattern of molecular heterogeneity and variation (Agnihotri et al., 2013). With the increasing understanding of molecular mechanisms that mediate gliomagenesis and progression, integration of molecularly-targeted agents into the conventional chemo-radiation regimen may provide a significant therapeutic benefit for patients with GBM. However, several factors may limit the efficacy of promising therapeutic strategies: including intra-tumoral molecular heterogeneity, diffuse invasion of single cells well beyond the bulk tumor core that is delineated upon imaging or surgery, and the unique anatomic structure of the brain microvasculature that provides a protective blood-brain barrier (BBB) that prevents accumulation of xenobiotics within the central nervous system. These first 2 issues have been reviewed previously in this journal (Vartanian et al., 2014), and here we provide an overview of the influence of the BBB in

GBM on delivery, and hence, treatment efficacy and potential strategies to overcome this limitation.

2.2 DRUG DELIVERY INTO THE CNS

2.2.1 INFLUENCE OF THE BBB ON DRUG DELIVERY

Despite progress in discovery and development of anticancer drugs for treatment of primary brain tumors, drug delivery into the CNS remains a major challenge, and the BBB is a predominant factor that limits the distribution of many drugs into the brain. The BBB is an anatomical and biochemical barrier that protects the brain from xenobiotics in the systemic circulation. Unlike the microvasculature for much of the rest of the body, brain capillary endothelial cells are interconnected by tight junctions, with limited fenestrations or pinocytic vesicles that form a physical barrier to prevent unimpeded diffusion into the brain. This physical barrier can significantly limit accumulation of small hydrophilic drugs, as well as large molecules that cannot diffuse readily across lipid bilayers such as antibodies and antibody-drug conjugates. For those molecules that are able to traverse the luminal endothelial cell membrane, many molecules are efficiently removed by the activity of efflux transporters that reside in the luminal capillary membrane. Many small molecule compounds employed in medicine are substrates for various efflux pumps located at the BBB. Therefore both physical and biochemical barriers within the BBB significantly limit the concentrations achievable within the brain, which consequently leads to limited efficacy **(Figure 2.1)**.

Drug delivery of hydrophilic molecules by paracellular diffusion and penetration of macromolecules is severely restricted by the physical presence of 'tight junctions' called as *zonulae occludentes.* The junctional complex holding the endothelial cells together is comprised of a multiplex of proteins such as claudins (3, 5 and 12), occludins (1, 2 and 3) and junctional-adhesion molecules (JAM-A, -B and -C). In addition, CNS microvessels are surrounded by, and in communication with, a plethora of cells such as astrocytic glia cells, pericytes and neurons. These together not only provide structural support but also a vasodynamic environment, now known as the neurovascular unit (Hawkins and Davis, 2005), that significantly increases resistance of the BBB towards drug transport (Mangas-Sanjuan et al., 2010).

In addition to the tight junctions, polarized expression of efflux transporters on the luminal and abluminal side of the BBB significantly limit delivery of numerous therapeutics that can otherwise diffuse across the BBB due to their favorable physicochemical characteristics. P-glycoprotein (P-gp) and breast cancer resistance protein (BCRP) are the two major efflux transporters on the BBB that have been extensively studied and reported to influence brain distribution of several cytotoxic and molecularly-targeted agents (Agarwal et al., 2011b).

Although presence of active efflux restricts drug distribution, there are pathways that facilitate brain penetration of several small and large molecules. These pathways can be broadly classified into carrier-mediated influx transporters and receptor-mediated

endocytosis. Different transport pathways present at the BBB are shown in **Figure 2.1.** These nutrient based influx transporters, such as LAT1, OATPs, and GLUT1 translocate polar nutrients such as glucose, amino acids, vitamins and hormones (Tamai and Tsuji, 2000). Receptor mediated endocytosis is involved in transporting large molecules such as insulin, transferrin and some vitamins, e.g., folic acid (Smith, 2003).

In this review, we discuss current and novel strategies for circumventing or modulating the BBB with the goal of improving drug delivery to invasive glioma. The overall goal of the review is to identify and discuss key factors that will help inform the discovery and choice of drug delivery strategies that can overcome these limitations. The structure and function of the BBB provide a dynamic barrier, responsive to size, location and stage of gliomas that controls drug delivery into sites of invasive glioma. Some of these processes may exclude drug molecules while others may enhance drug penetration into the brain.

Figure 2.1: Schematic representation of the neurovascular unit (i.e., BBB) and the different pathways for drug transport

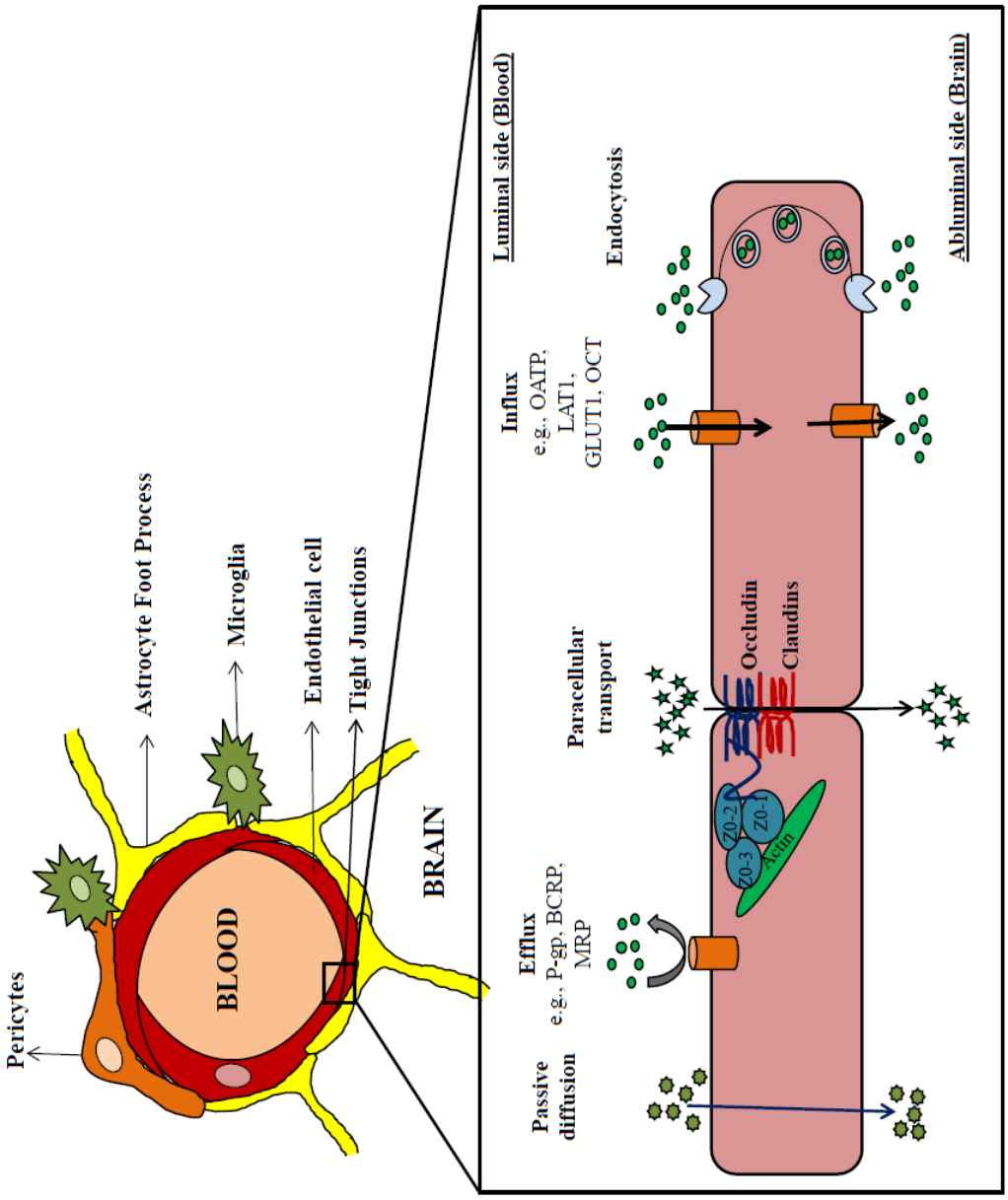

2.2.2 DRUG RELATED ISSUES

Penetration of drugs across brain capillary endothelial cells not only relies on the physical structure of the BBB but is also highly dependent on the physicochemical properties of the drug candidate. The rate and extent of drug distribution into a tissue such as the CNS depends on the overall absorption, elimination, distribution and metabolism (ADME) processes that influence the drug concentrations in the plasma, the degree of specific protein-binding to the plasma proteins and non-specific binding to the lipophilic brain tissue, the intrinsic permeability of the molecule in lipid-membranes, and the presence of moieties that can be utilized to enhance drug penetration (Groothuis, 2000; Alavijeh et al., 2005). Systemic drug ADME depends upon several factors, including lipophilicity and solubility of the drug (Bergstrom, 2005). For many drugs, transcellular passage across the BBB occurs by simple passive diffusion across the endothelial cell membranes. In addition to increasing permeability, lipophilicity also increases the likelihood for metabolism and protein binding (Alavijeh et al., 2005). High binding of drugs to blood proteins affects distribution as only the unbound drug crosses the lipid bilayer and demonstrates pharmacological activity. High lipophilicity can further contribute to non-specific binding to brain tissue, which may influence active unbound concentrations.

To summarize, there are major limitations in effective drug delivery to the brain tumors due to the restrictive nature of the BBB and the physiochemical properties of the drug

molecule. However, several strategies have been, and are being, investigated in preclinical and clinical studies to increase drug distribution to invasive glioma cells.

2.2.3 BLOOD-BRAIN BARRIER WITHIN TUMORS

Essentially all newly diagnosed GBM exhibit disruption of the BBB. Clinically, this is manifest as the accumulation of gadolinium-based contrast agent within regions of the tumor on magnetic resonance imaging. The various clinical formulations of gadolinium are hydrophilic and do not readily cross cellular membranes. As such, contrast does not accumulate in normal brain tissue where the tight-junctions between endothelial cells provide an intact physical BBB. As discussed below, cytokines secreted by GBM tumor cells can lead to disruption of the physical BBB, and in these regions, accumulation of contrast provides a visual demonstration that essentially all GBM patients have significant disruption of the BBB. In the past, this fact has been used by many to argue that the BBB is not a major factor that influences the efficacy of therapies in GBM (Vick et al., 1977).

However, without a doubt, all GBM patients have regions of tumor with an intact BBB, as determined by MRI. Even when surgeons achieve a gross total resection of all contrast-enhancing regions of tumor, 100% of these patients will recur the GBM within several months of treatment (Hou et al., 2006). Several biopsy studies also have demonstrated that significant tumor burden exists in the T2/FLAIR regions outside of the contrast enhancing regions seen on MRI. Moreover, using an (18)F-DOPA radiotracer

that readily crosses the BBB, an anatomical comparison of (18)F-DOPA (3,4-dihydroxy-6-[18F]fluoro-L-phenylalanine (18F-DOPA)) uptake versus contrast enhancement demonstrates significant regions of gross tumor in which there is no significant accumulation of contrast media (**Figure 2.2**) (Pafundi et al., 2013). In a comparison of 10 patients with 23 biopsies, 13 of 16 high-grade biopsy specimens had regions of FDOPA positivity, and image-guided biopsies of these regions demonstrated significant tumor burden. Beyond grossly positive regions of tumor, the highly invasive nature of GBM is well known and in autopsy series, infiltrating single cells have been found throughout the brain (Onda et al., 1989). Again based on surgical biopsy studies demonstrating infiltration of single cells extending beyond the T2/FLAIR tumor volume, radiation target volumes for GBM typically extend 1-2 cm beyond any visible radiographic abnormality (Pafundi et al., 2013). Thus, based on well-established and accepted natural history, surgical and radiographic information on GBM, all GBM patients have regions of a disrupted BBB AND all GBM patients have significant regions of a relatively intact BBB sufficient to prevent the distribution of a small molecule to those invasive sites. These data all support our central contention that delivery of therapeutic agents across the BBB to all regions of a GBM is essential to make significant progress in GBM (Agarwal et al., 2011b)).

Figure 2.2 (Pafundi et al., 2013): Representative image of (A) (18)F-DOPA PET-CT, (B) T1 CE-MRI, (C) T2-FLAIR MRI contours drawn by a neuroradiologist.

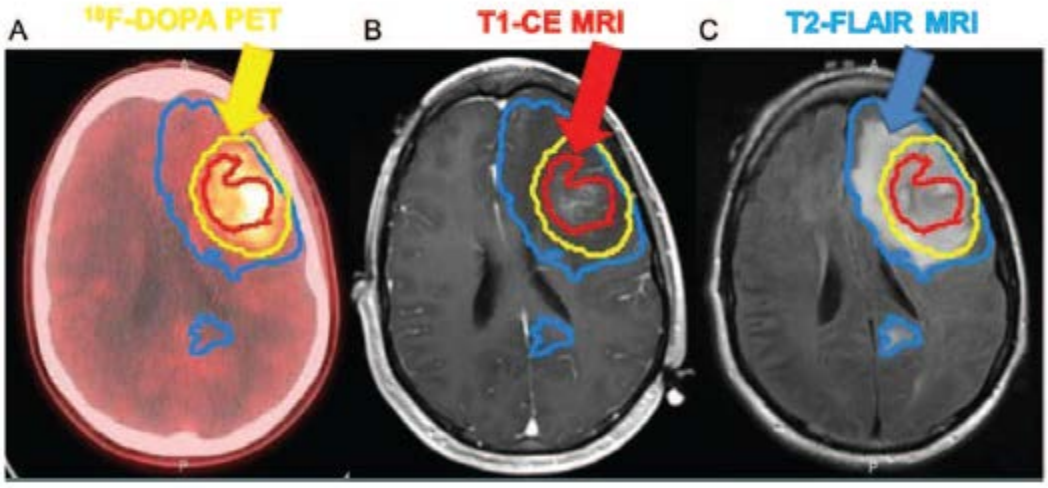

During gliomagenesis, the BBB becomes more permeable due to release of chemical and chemotactic mediators such as adenosine triphosphate (ATP), nitric oxide (NO), macrophage inflammatory protein-2 (MIP-2), interleukin-β (ILβ) and tumor necrosis factor-α (TNF-α) which are produced by the astrocytes. (Ballabh et al., 2004). In particular, the angiogenic pathways are closely related to the invasiveness and proliferative potential of brain tumors mediated by release of vascular endothelial growth factor (VEGF), discovered as the vascular permeability factor (Lee et al., 2006; Jain et al., 2007). Leibner et al. reported loss in expression of claudin-1 and significant down regulation of claudin-5 and occludin in brain microvessels in human GBM (Liebner et al., 2000). Release of pro-angiogenic factors such as VEGF and scatter factor/hepatocyte

growth factor (cMET) and inflammatory mediators such as cytokines have been linked to alterations in tight junction proteins (de Vries et al., 1996; Lamszus et al., 1999). Interacting with the brain tumor microenvironment, the inflammatory pathways and cascades are also involved which may promote protumorigenic activities, glioma growth and metastases with assistance from microglia and other supporting cell types via tumoral-stromal, pericytic-endothelial, and astrocytic-related communications (Charles et al., 2012). Although disruption of BBB in the tumor core (Lee et al., 2006) provides a window of opportunity for the use of novel therapeutics as the BBB becomes more "leaky" due to tumor infiltration, providing exposure to the underlying microenvironment which contains potentially viable molecular therapeutic targets involving the TGFβ(beta), VEGF, and hypoxia-driven pathways (Barcellos-Hoff et al., 2009), the real issue lies in effective drug delivery to invasive glioma cells that remain behind an intact BBB, escaping chemotherapy (**Figure 2.3)**.

As a result, determination of drug transport issues across an intact BBB becomes essential for maximizing the potential ability for novel neurotherapeutics to reach the microenvironment of the tumor, and to engage the target. Brain delivery enhancing methods such as pro-drugs, brain drug-targeting and chimeric peptide technologies have been proposed as strategies for enhancing brain delivery by discovery (Scherrmann, 2002) of BBB-penetrant drugs with desired anti-glioma activities clinically (Pardridge, 2002; Mangas-Sanjuan et al., 2010; Salphati et al., 2012a).

Figure 2.3: Schematic representation of the issues for effective delivery of drugs to the tumor cells and the invasive glioma cells. The presence of intact blood brain barrier and expression of efflux transporters limit distribution of chemotherapeutics to the invasive glioma cells.

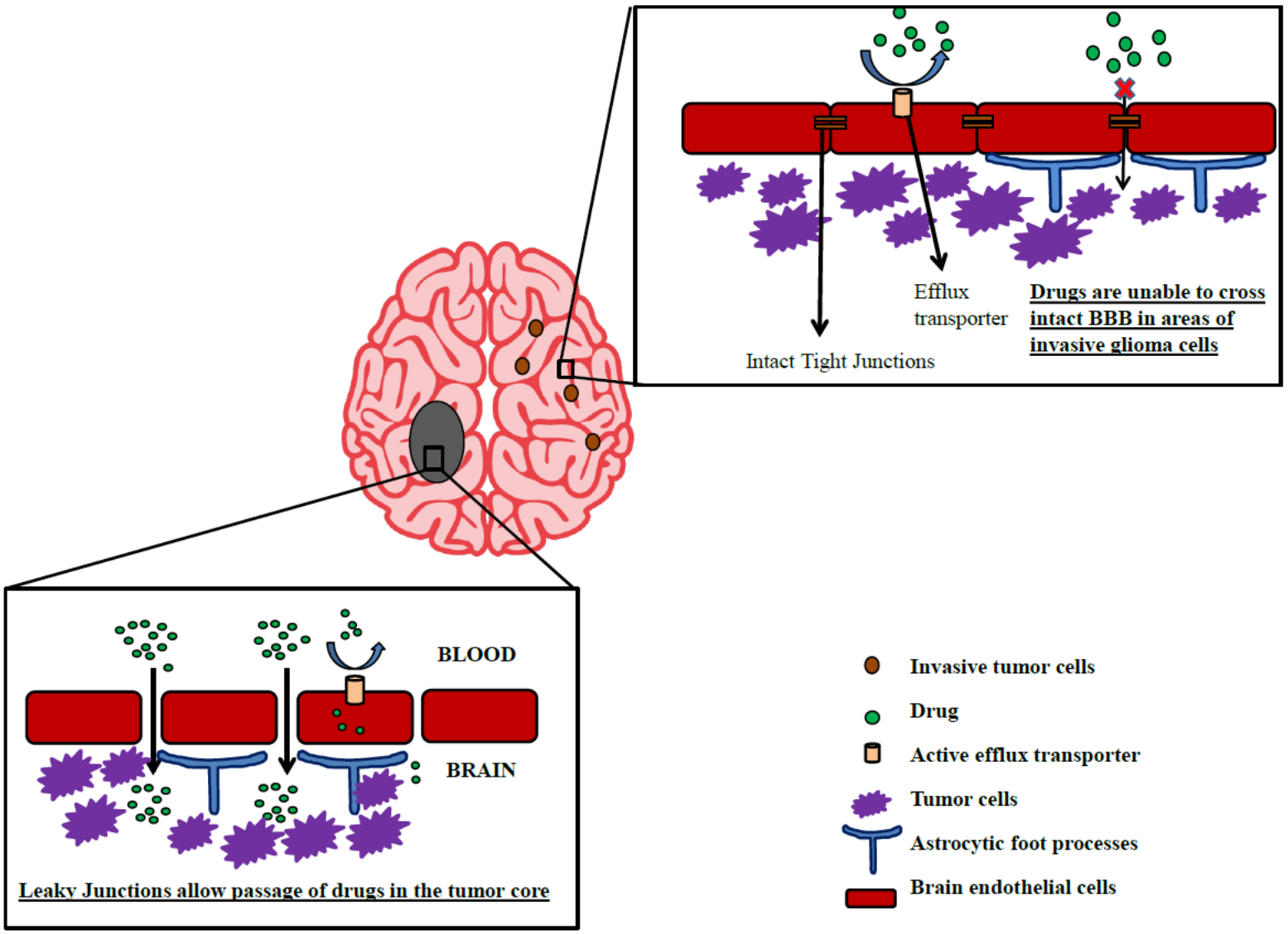
Efflux
transporter
Drugs are unable to cross
intact BBB in areas of
invasive glioma cells
Intact Tight Junctions
BLOOD
BRAIN
Leaky Junctions allow passage of drugs in the tumor core
Invasive tumor cells
Drug
Active efflux transporter
Tumor cells
Astrocytic foot processes
Brain endothelial cells

2.2.4 HETEROGENEITY OF BBB INTEGRITY AND DRUG CONCENTRATIONS

Given the highly infiltrating nature of GBM cells, it is well established that the tumor cells are capable of extending into the surrounding tissue away from the tumor core (Berens and Giese, 1999; On et al., 2013). Although the BBB presents a physical and functional barrier to drug delivery, mounting evidence suggests that recurrence of GBM can be related to the residual group of cells that reside in regions adjoining the resected tumor core (Burger et al., 1983; On et al., 2013).

This has significantly impacted the clinical outcome for patients; emphasizing the clinical risk presented by the migratory, infiltrative and invasive glioma cells. This characteristic of glioma invasion and migration questions the role of BBB in hindering drug delivery of chemotherapeutics to the invasive tumor cells. Ample preclinical evidence suggests breakdown of BBB in the core via increased accumulation of gadolinium-based contrast enhancement (Larsson, 1960), and high drug concentrations (e.g., PD991 (Michaud et al., 2010)). However, drug concentrations measured in this area does not truly represent the drug concentrations in the tumor cells that are left behind and not removed by surgery (away from core). This intratumoral heterogeneity in BBB breakdown has also been observed in glioma patients as well, wherein the microvasculature in the core is highly tortuous, disorganized and permeable while areas adjacent to the core have nearly intact structural integrity (Brightman and Broadwell, 1976). In a seminal study by de Groot and colleagues, the authors observed that tumor progression in GBM followed a unique

pattern of non-contrast enhancing tumor after treatment with an anti-VEGF agent (de Groot et al., 2010). These tumor cells are invisible to the surgeon and lie beneath an intact BBB and escape chemotherapy.

This makes estimation of BBB permeability critical as different methods could influence our interpretation of an effective drug. The most commonly used *in-vivo* measurement is brain-to-blood (or plasma) equilibrium partition coefficient, commonly referred to as Kp brain (Mangas-Sanjuan et al., 2010). This parameter relates the extent of drug exposure in the brain to the extent of drug exposure in the blood or plasma, and is usually obtained by extensive preclinical studies. Nonetheless, attempts to increase BBB permeability and predicting efficacy solely based on Kp brain ratios is risky and often does not lead to desired brain concentrations at the target. Heterogeneity in BBB disruption and presence of invasive tumor cells some distance away from the tumor core can lead to different Kp brain ratios in different regions of the brain, depending upon the integrity of the BBB at the site of measurement. Therefore, it is critical to fully understand the pharmacokinetics and pharmacodynamics of the drug in a tumor-bearing brain, in order to achieve efficacious concentrations throughout. Agarwal et al. studied the regional brain distribution of erlotinib in U87 rat xenograft glioma model. The authors observed that erlotinib concentrations in the tumor core were significantly greater compared to the brain around the tumor core (brain-around-tumor (BAT) also called the tumor 'rim') and the contralateral hemisphere. The corresponding Kp brain ratios in the core, rim and contralateral hemisphere suggest the presence of an intact BBB directly around the tumor

core and in areas away from the tumor, whereas the core had leaky vasculature, which then explained high drug concentrations measured within the core (Agarwal et al., 2013).

2.3 STRATEGIES TO IMPROVE DRUG DELIVERY TO GBM

GBM is a disease of the whole brain (Agarwal et al., 2011b) and its treatment remains one of the major challenges in clinical oncology. Since GBM is one of the most aggressive and infiltrative brain tumors, there are regions where the glioma cells reside behind an intact BBB, which results in poor penetration of drugs into this region of brain parenchyma. Therefore, in the context of invasive gliomas, there is an urgent need to develop effective strategies to enhance delivery of chemotherapeutics across the BBB. Penetration of drugs through BBB, like other membranes in the body, occurs by three major mechanisms: passive diffusion, endocytosis and carrier-mediated active transport. These mechanisms have been explored in various ways to enhance penetration of drugs into the brain. In the sections below, we have reviewed various methods that have been explored to increase delivery of chemotherapeutics into the brain.

2.3.1 DISRUPTION OF TIGHT JUNCTIONS IN THE BBB

Although the BBB integrity may be compromised in the regions of the core tumor mass, the infiltrating tumor cells beyond the tumor core are protected by an intact BBB. The BBB is one of the major physiological impediments for drug delivery to the brain. It acts as an endothelial physical barrier composed of tight junction proteins between the

endothelial cells that limit passage of chemotherapeutics from the systemic circulation into the brain parenchyma. However, if the tight junctions are pharmacologically or pathologically disrupted, one could increase penetration of drugs across the BBB throughout the region of infiltrating tumor cells. This could also enhance delivery of large molecules such as antibodies and proteins, across the BBB.

2.3.1.1 BBB DISRUPTION VIA OSMOTIC MECHANISMS OR ULTRASOUND

Osmotic BBB disruption is a mechanism-based technique that has been investigated for transiently disrupting the BBB to increase permeability to drug molecules. This method relies on administration of hypertonic solutions that lead to shrinkage of the endothelial cells, and disruption of the tight junction complexes creating gaps that allow for paracellular diffusion of molecules (Rapoport, 1970). In 1972, Rapoport and colleagues reported that osmotic opening of the BBB by hypertonic arabinose led to staining of the brain tissue by Evans blue in mouse models (Rapoport et al., 1972) Similar hyperosmolar solutions that have been used preclinically include mannitol, contrast agents and lactamide (Kroll and Neuwelt, 1998; Kemper et al., 2004). Neuwelt and his group pioneered the clinical application of this concept of using hypertonic solutions to osmotically open the BBB to enhance drug delivery of chemotherapeutics (Kroll and Neuwelt, 1998). The group reported promising results with carboplatin (intra-arterially) and etoposide (intravenously) administered in conjunction with mannitol (infusion into the internal carotid artery) to osmotically disrupt the tight junctions in the treatment of malignant astrocytomas, neuroectodermal tumors and CNS lymphoma (Williams et al.,

1995). In another study consisting of 41 malignant glioma patients (21 GBM patients and 20 anaplastic astrocytoma patients), the authors compared the effect of blood-brain barrier disruption (BBBD) with mannitol in patients treated with intra-arterial chemotherapy alone vs. chemotherapy administered in conjunction with BBBD. The authors reported enhanced median survival with BBBD therapy (~90 weeks) compared to chemotherapy alone group (~40 weeks) (Kraemer et al., 2002). Since BBBD is performed using arterial infusion, this process leads to rapid equilibration of the drug even into the contralateral hemisphere, thus providing a uniform drug delivery throughout the brain.

The ultrasound-based BBB disruption method is a focal, selective and non-invasive targeted approach to enhance delivery of drugs into the brain through thermal or mechanical mechanisms. Focused ultrasound (FUS) relies on transcranial delivery of low-frequency ultrasound waves that result in opening of the tight junctions between the endothelial cells (Hynynen et al., 2006). Typically, the ultrasonic exposures last for 20-30 seconds and are given at a frequency of 1 Hz (Hynynen, 2008). This technique was first successfully applied to enhance delivery of BBB impermeable liposome-encapsulated doxorubicin in rats with glioma (Etame et al., 2012). Recently, the microbubble (MB) enhanced focused ultrasound (FUS) approach has shown to temporarily and reversibly disrupt the tight junctions in the brain endothelial cells to increase permeability of drugs across the BBB. The microbubbles act as drug carrier vehicles that can enhance penetration of BBB impermeable drugs and also protect them from degradation.. In

combination with ultrasound, MB can collapse the tight junctions and vessel stability at high acoustic pressures (Sheikov et al., 2004; Aryal et al., 2014). Using this approach, Ting and colleagues reported enhanced brain penetration of carmustine (BCNU) into the brain by using multifunctional microbubbles whose transport into the local brain environment was increased due to the presence of focused ultrasound (Ting et al., 2012). In a similar study, Liu *et al.* reported increased brain delivery of BCNU into both tumor and surrounding normal brain using a 400-kHz focused external ultrasound generator (Liu et al., 2010).

2.3.1.2 PHARMACOLOGICAL APPROACHES TO MODULATE TIGHT JUNCTION PERMEABILITY

The BBB is a protective physical and biochemical barrier that not only maintains neural homeostasis but also limits passage of molecules across the endothelium into the brain parenchyma by interfering with paracellular diffusion of solutes through a network of tight junctional complexes and supportive glia cells. Recently, Alvarez et al. reported that glia cells, such as astrocytes, secrete Sonic hedgehog (Shh, a glycoprotein), which binds to and inactivates the Patched-1 receptor. This hypothesized mechanism would allow activation of the Smoothened (SMO) pathway and subsequent induction of Gli transcription factors thus providing stability to BBB integrity by affecting expression of gene targets that control tight junction formation (Alvarez et al., 2011). It is further posited that SMO inhibitors act by destabilizing vessel integrity thus opening tight

junctions between the endothelial cells. This postulate would suggest that co-administration of a SMO inhibitor could increase brain delivery of concomitantly administered drugs. Currently, 3 SMO inhibitors are in clinical trials for use in medullablastoma, a pediatric brain tumor that in some cases is uniquely driven by hyperactivation of SMO (Romer et al., 2004). Although SMO inhibitors have shown promising results in preclinical models of medullablastoma, their application as adjuvant therapy for chemotherapeutics to improve drug delivery to the brain requires further investigation.

Bradykinin-like compounds (histamine, leukotrienes and bradykinin) act by disrupting the tight junctions by stimulating B_2 receptors preferentially expressed on tumor cells and in the process induce second messenger systems that transiently increases cytosolic Ca^{2+}, resulting in opening of the tight junctions (Kemper et al., 2004). There are reports that have indicated the role of nitric oxide in selectively increasing the brain tumor permeability after administration of bradykinin (Nakano et al., 1996). A low dose of bradykinin selectively increased blood tumor barrier permeability in intracerebral tumor when administered as an infusion through the ipsilateral internal carotid artery (Inamura and Black, 1994). These finding led to the development of Cereport (RMP-7), a 100-fold more potent bradykinin analog and a selective agonist for B_2 receptors. RMP-7 is resistant to degradation by bradykinin-metabolizing enzymes (Doctrow et al., 1994)and has enhanced delivery of a hydrophilic compound, carboplatin, to tumor cells in a RG2 rat-glioma model by 30-80% (Elliott et al., 1996; Borlongan and Emerich, 2003).

However, the combination showed disappointing results when tested in a randomized, double-blind, placebo controlled, phase 2 trial in recurrent malignant glioma patients (Prados et al., 2003). The end point, determined as the median time to tumor progression, was not significantly different between the group treated with RMP-7 and chemotherapy alone group. Kroll and colleagues conducted a direct comparison of BBBD by osmotic methods to bradykinin treatment in nude rats with 6-day intracerebral human small cell lung carcinoma tumors. The group reported that use of hypertonic mannitol resulted in global delivery of variety of agents whereas bradykinin treatment was not effective in increasing delivery of drugs in this human brain tumor xenograft model. These data indicate that the goal of using an adjuvant therapy to open tight junctions remains elusive.

2.3.2 OVERCOMING ACTIVE EFFLUX at the BBB

While the BBB is primarily formed of capillary endothelial cells that are interconnected by tight intercellular junctions, , the BBB is also an efficient functional barrier to several solutes by the presence of active efflux transporters such as P-gp and Bcrp (Agarwal et al., 2011a). In order to effectively deliver drugs across the BBB and evade active efflux, several approaches have been investigated. These include modification of the drug structure to diminish affinity to efflux transporters or co-administration of transport inhibitors to enhance delivery of anti-cancer drugs. **Table 2.1** lists molecularly-targeted agents that have demonstrated substrate liability for P-gp and Bcrp. Given the number of targeted agents, exemplified by table 2.1, approved or in development that are substrates for active efflux at the BBB, the treatment options to effectively administer these

compounds for GBM will require methods to engineer the transporter liability out of the molecule, or use other means to overcome active efflux.

Table 2.1: List of molecularly targeted agents that have been examined for treatment of glioblastoma and their P-gp/Bcrp substrate status

a- Steady state conc ratios

b- AUC ratios

c- With dual inhibitor (GF120918)

d- Pbrain

e- B/P ratios not available

f- Using in-situ brain perfusion to determine fold increase

g- Determined at a single time point post oral dose

h- Determined at 2 time points; here we reported 1 hr after oral dose

i- Determined at 2 time points; here we reported 1 hr after oral dose; B/P ratio in absence of P-gp and Bcrp was not reported

Drug	Target	Wild-type	Substrate Status					References
			P-gp	P-gp B/P ratio	BCRP	BCRP B/P ratio	Combined P-gp/BCRP B/P ratio	
Erlotinib[b]	EGFR	0.14	✓	0.41	✓	0.14	0.58	(de Vries et al., 2012)
Tandutinib[b]	PDGFR, FLT3		✓	~3.2 fold	✓	~0.9 fold	~13.5 fold	(Yang et al., 2010)
Gefitinib[a]	EGFR	0.07 ±0.02	✓		✓		7.3 ±0.5	(Agarwal et al., 2010)
Cediranib[a]	VEGFR	0.25 ± 0.10	✓	5.2± 1.1	✓	0.27± 0.01	6.3 ± 1.2	(Wang et al., 2012)
Sorafenib[a1, d2]	RAF-kinase, VEGFR, PDGFR	[a1]0.094 ±0.007, [d2]5.3 ± 2.7	✓	[a1]0.11 ±0.02, [d2]5.8 ± 2.2	✓	[a1]0.36 ±0.06, [d2]22.6 ± 5.0	[a1]0.91 ±0.29, [d2]49.4 ± 5.2	[a1](Agarwal et al., 2011c) [d2](Lagas et al., 2010)
vandetanib[c]	VEGFR, EGFR	0.21	✓		✓		0.64	(Minocha et al., 2012a)
Pazopanib[c]	VEGFR, PDGFR, c-KIT	0.015	✓		✓		0.041	(Minocha et al., 2012b)
dasatinib[d1, b2]		[1]6.39 ± 1.39 [b2]0.12	✓	[1]22.7 ± 5.41	✓	[1]5.11±0.7	[1]84.3±13.3, [b2]0.93	[1](Lagas et al., 2009) [2](Agarwal et al., 2012)
sunitinib[d1, a2]	VEGFR, PDGFR, c-KIT	1.6 ± 1.0 [a2] 0.51 ± 0.26	✓	2.8 ±0.8, [a2] 2.33 ± 0.56	✓	2.4 ± 0.9, [a2] 0.73 ± 0.44	42.4±10.7, [a2] 17.44 ± 5.08	[d1](Tang et al., 2012) [a2](Oberoi et al., 2013)

Table 2.1 Continued…

Drug	Target	Wild-type	Substrate Status					References
			P-gp	P-gp B/P ratio	BCRP	BCRP B/P ratio	Combined P-gp/BCRP B/P ratio	
imatinib[e1, g2, f3]	BCR-ABL, PDGFR, c-KIT		✓	~2.73 fold[e1], ~3.6 fold[g2], ~5.5 fold[f3]		~2.5 fold[e2]		[e1](Dai et al., 2003) [g2](Breedveld et al., 2005) [f3](Bihorel et al., 2007)
Lapatinib[a]	EGFR	0.03±0.01	✓	0.09 ± 0.02	✓	0.04±0.01	1.2 ±0.42	(Polli et al., 2009)
Everolimus[b]	mTOR		✓	~1.3 fold				(Chu et al., 2009)
GNE-317[i]	Dual PI3K/ mTOR	1.01 ± 0.05	x	x	x			(Salphati et al., 2012a)
GDC-0980[h]	Dual PI3K/ mTOR	0.082 ± 0.008	✓		✓		1.0 ± 0.20	(Salphati et al., 2012b)
GDC-0941[G]	PI3K		✓	~2.24 fold	x	~1.05 fold	~29.42 fold	(Salphati et al., 2010)
PALOMID 529	Dual PI3K/ mTOR	x	x		x			(Lin et al., 2013)
Axitinib[d]	VEGFR-1,2-3	94.8 ± 27	✓	643.6 ±183.2	✓	47.7 ± 12.7	1315 ± 375	(Poller et al., 2011)

2.3.2.1 STRUCTURAL REFINEMENT TO ALLOW PASSIVE DIFFUSION OF DRUGS

An emerging understanding of the molecular aberrations in GBM, the propensity of the disease to invade well beyond the tumor core and the delivery challenges presented by active efflux and tight junctions at the BBB, have stimulated several researchers and pharmaceutical companies to attempt to discover drug candidates that have favorable BBB penetrating properties. For instance, Genentech has synthesized molecularly-targeted dual PI3K/mTOR inhibitors, GNE-317 and GDC-0084, which have been structurally modified using appropriate structural-activity relationships (SAR) such that they show less affinity to active efflux by P-gp and BCRP at the BBB (Heffron et al., 2012). Similarly, BKM120, a Novartis pan-PI3K inhibitor with good BBB penetrating activity has shown promising results in several GBM cell lines *in vivo.* (Wen et al., 2012). The use of computational models to alter the physicochemical properties of the drug has allowed development of compounds that pass BBB by passive diffusion.

2.3.2.2 USE OF PHARMACOLOGICAL INHIBITION

Two important and widely investigated active efflux transporters at the BBB are P-glycoprotein (P-gp) and breast cancer resistance protein (BCRP). Several molecularly-targeted agents and anti-cancer drugs have demonstrated substrate affinity to both P-gp and Bcrp at the BBB (**Table 2.1).** The expression of efflux transporters has also been reported in glioma cells (Demeule et al., 2001; Fattori et al., 2007). This is critical to understand as the presence of active efflux transporters not only presents a functional

barrier on the BBB but also on the brain-tumor cell. Earlier Agarwal et al. have reviewed the role of the BBB and brain-tumor cell barrier in restricting brain penetration of molecularly targeted agents (Agarwal et al., 2011b). These two sequential barriers restrict delivery of chemotherapeutics into the intracellular space of the glioma cell.

One approach to modulate active efflux is by administration of pharmacological inhibitors of P-gp and Bcrp. Elacridar is a commonly used dual P-gp and Bcrp inhibitor investigated both preclinically and clinically. Several researchers have reported higher brain concentrations of molecularly-targeted agents, e.g., including gefitinib (Agarwal et al., 2010), vandetanib (Minocha et al., 2012a) and sunitinib (Tang et al., 2012; Oberoi et al., 2013) on co-administration of elacridar in non-tumor bearing wild-type mice (see Table 2.1). In addition, Agarwal et al. reported higher brain concentrations on administration of erlotinib with elacridar in a U87 orthotopic rat xenograft model of glioma (Agarwal et al., 2013).

Earlier reports of clinical experience with efflux transport inhibitors have shown interesting results. In 2005, Sasongko et al. observed enhanced brain penetration of 11C-verapamil on co-administration of a P-gp inhibitor, cyclosporine A in healthy volunteers (Sasongko et al., 2005; Hsiao et al., 2006). Wagner and colleagues reported similar results using another inhibitor of P-gp, tariquidar, in healthy volunteers (Wagner et al., 2009). Although administration of specific or dual efflux modulators is a strategy worth exploring to enhance the brain accumulation of drugs, this approach has one major

limitation. It is important to consider that concurrent administration of P-gp and Bcrp inhibitors could lead to changes in systemic pharmacokinetics of the drug which could result in increased systemic toxicity.

2.3.3 LOCAL DELIVERY STRATEGIES

2.3.3.1 CONVECTION-ENHANCED DELIVERY (CED)

CED is an invasive local delivery method where the distribution of large and small molecular weight compounds into the brain tissue is driven by positive hydrostatic pressure from a prolonged slow infusion in the brain parenchyma **(Groothuis et al., 1999).** First developed in 1994 (Bobo et al., 1994), CED directly delivers the drug into the intracerebral tumor tissue, which results in drug distribution into the peritumoral tissue by bulk flow, thereby achieving a relatively constant drug concentration over a somewhat predictable distance from the site of infusion; and sparing regions of the brain far from the infusion source (Dickinson et al., 2008; Ding et al., 2010; Serwer and James, 2012).

This method has been extensively evaluated for delivery of therapeutic proteins, oligonucleotides, liposomes and viral-mediated therapies. Notably, delivery of high molecular weight therapeutic proteins such as Pseudomonas aeruginosa exotoxin (PE) such as IL4-PE (PRX321) and IL13-PE38QQR (cintredekin besudotox) have been extensively evaluated in phase I and II trials, with acceptable safety profiles, but did not

reach efficacy standards to obtain FDA approval (Serwer and James, 2012). Cintredekin besudotox was evaluated in a phase III trial (the PRECISE trial, 2011) but failed to show superiority compared to use of Gliadel wafers. Trabedersen (AP-12009), an antisense-oligonucleotide that targets TGFβ-2, showed significant benefit for the 14-month tumor control rate in an anaplastic astrocytoma subgroup compared to chemotherapy alone (temozolomide or procarbazine/lomustine/vincristine) in phase II studies but no significant difference in median survival was observed compared to chemotherapy group (Bogdahn et al., 2011). Combination strategies of PE fusion proteins (MR1-1) with anti-EGFR fragment antibodies showed promising results in preclinical studies, but comparisons with existing therapies need to be established (Ding et al.)**.**

The technique is highly dependent on catheter placement, which can influence geographic distribution of the drug and can also influence induction of adverse effects such as chemical meningitis (Serwer and James, 2012). Moreover, lack of proper drug distribution and efficacy can result due to leakage of infusate into subarachnoid (pressure drives infusate up the needle track) and intravascular space (Sampson et al., 2007). Other factors that can influence drug distribution by CED include parameters such as pH, osmolarity and ionic composition, and the solubility of the drug. These factors can limit the use of convection-enhanced strategy (Groothuis, 2000). Furthermore, there is heterogeneity in spatial distribution of the drug in the brain. Bobo et al. studied the distribution of small molecule [14C]-sucrose and large molecule [111In]-transferrin in cat brain using CED (Bobo et al., 1994). The authors observed that even though sucrose

diffused farther than transferrin, both molecules showed differences in distribution wherein higher drug concentrations were observed closer to the site of catheter tip. This is critical for the treatment of an invasive tumor such as GBM. Such a targeted regional delivery could spare the infiltrated growing edge of the tumor and the invasive glioma cells at distant sites, such as the contralateral hemisphere. Nonetheless, for large molecules that are unable to cross BBB, CED may provide a therapeutically useful delivery tool.

2.3.3.2 OTHER LOCAL DELIVERY STRATEGIES

Other invasive local delivery methods include bolus injection of chemotherapeutics by intracranial (IC) delivery, intracerebro-ventricular (ICV) delivery and intrathecal delivery. Drug administration by these methods bypasses the BBB by locally introducing the drug into the brain parenchyma, ventricles or lumbar puncture into the subarachnoid space of the spinal cord. Other methods make use of biodegradable, cytotoxic drug impregnated wafers (such as Gliadel® wafers (carmustine)) which are placed locally after surgical resection in the tumor cavity (Duntze et al., 2013) and intrathecally placed implantable pumps such as SynchroMed® (Medtronic) and Codman® 3000 (Codman) (Bhatia et al., 2013). Although the major advantage of these methods is that they are not limited by the size of drug molecule (small and large molecules), the main pharmacological limitation lies in that the drug concentration decreases exponentially as the diffusion distance increases due to the sink effect of the brain vasculature. Moreover, the constant flow and drainage of the brain interstitial fluid can have implications on local

drug concentration, which is cleared from the brain parenchyma through this route. This process can limits CNS accumulation of many drugs (Abbott, 2004).

Intranasal delivery is another approach that is being extensively investigated as it provides a noninvasive alternative approach to bypass BBB. The olfactory receptor cells are present at the boundary of both the nasal cavity and the CNS (Uraih and Maronpot, 1990) and this neuronal pathway constitutes a direct connection to the brain parenchyma through paracellular route (Mathison et al., 1998). The major advantage of this route is that it not only circumvents the BBB, but drugs administered through this route also bypass the hepatic first-pass effect and degradation by enzymes such as peptidases in the blood (Dufes et al., 2003; Zhu et al., 2012). This method has been employed to study brain delivery of several peptides and proteins, which are prone to degradation (e.g., insulin, vasoactive intestinal peptide, insulin-like growth factor-1). Factors such as pH and osmolality of the drug are important determinants for effective brain delivery of peptides and proteins. Despite low brain uptake reported due to changes in pH, the nasal route of brain drug delivery provides an interesting alternative to deliver peptides to the CNS.

2.3.4 NANOPARTICLE DRUG CARRIERS

Recent advances in nanotechnology allow delivery of drugs as nanoparticles which are otherwise poorly distributed to the tissues such as the brain. Conventionally, nanocarriers and nanovectors are polymer-based systems that can carry multiple drugs. These carrier

systems enhance delivery of drugs by entrapping or encapsulating the drug in the core, or chemically conjugating or grafting a targeting peptide/ligand on its surface, thus increasing drug solubility and stability. These systems include dendrimers, polymeric micelles, nanoparticles and solid-lipid nanoparticles (SLNs). These carrier systems cross the BBB by utilizing transcellular pathways such as receptor-mediated endocytosis at the BBB (Herve et al., 2008).

A major advantage of SLNs is that their high lipid solubility physically stabilizes the nanoparticle, thereby increasing drug loading capacity and resulting in a controlled rate of drug release (Blasi et al., 2007). Two cytotoxic drugs, doxorubicin and camptothecin, encapsulated in pegylated SLNs exhibited efficient transport across the brain capillary endothelial cells when formulated as pegylated SLNs (Yang et al., 1999; Zara et al., 1999).

Although nanoparticles and lipid-based formulations have shown to increase systemic circulation times and increased tumor retention by enhanced permeation and retention (EPR) effect, their major limiting factor is the rapid clearance from the blood circulation by the reticuloendothelial system (RES). They are mostly limited to regions adjacent to the blood vessels, such that the areas far from the tumor core which constitute the aggressive, infiltrated tumor cells are spared from drug therapy. Moreover, presence of multi-drug resistant proteins on the tumor cells reduces the therapeutic benefit from drugs released from these carrier systems in the vicinity of the tumor (Chavanpatil et al., 2006).

NPs carrying both an efflux transporter inhibitor and an anticancer drug (Song et al., 2010) have been tried in the past and were found to efficiently overcome resistance mediated by active efflux transporters. However, combination strategy has not been very successful due to adverse effects resulting from altered distribution of the drug systemically (Li and Huang, 2008). Furthermore, presence of an intact BBB on the invasive glioma cells and high interstitial fluid pressure, may limit passive targeting of nanoparticles (Boucher et al., 1997; Rich and Bigner, 2004).

2.3.5 PEPTIDE-BASED DRUG DELIVERY

Peptide-like macromolecules are transported into the cells via adsorption- or receptor-based transcytosis processes (Scherrmann, 2002). In this method, the drug is chemically conjugated by a linker to a targeting moiety, which is then taken up by a specific receptor and undergoes endocytosis. These vector-based methods can improve delivery for drugs that are otherwise relatively low or not penetrant into the brain. Small peptides such as AngioPep-2, have been shown to enhance delivery of small molecules into the BBB parenchyma via low-density lipoprotein receptor-related protein (LRP1) (Vlieghe and Khrestchatisky, 2013). ANG1005/GER1005, designed using AngioChem's novel platform technology, consists of three molecules of paclitaxel and one molecule of AngioPep-2 vector (a 19-amino acid vector) was shown to increase brain penetration of paclitaxel in rat brain via in-situ brain perfusion (Takasato et al., 1984). Currently ANG1005 has shown promising results in two Phase I trials for recurrent glioma and metastatic brain tumors (Gabathuler, 2010). Wu and colleagues have engineered a

peptide by phage display, with a sequence of VTWTPQAWFQWV (VTW). They showed that this peptide had higher binding affinity to human glioma cell lines in-vitro and weaker binding affinity to human astrocytes and other cell lines (Wu et al., 2008). Using this peptide sequence, Wang and colleagues developed a PEI/DNA nanoparticles conjugated with VTW and demonstrated selective targeting to tumor cells using U87 human glioblastoma cell line (Wang et al., 2013).

2.3.6 PRODRUG/INFLUX TRANSPORT MODIFICATIONS

The BBB not only is formed by tight junctions and active efflux transporters, but it also expresses a number of influx carrier systems such as amino acid carriers and nutrient transporters that actively play a role in translocating nutrients from the blood to the brain.

A prodrug approach is an important strategy that has been explored to increase brain penetration of drugs across the BBB. A prodrug is essentially a bioreversible derivative of a drug molecule, which undergoes enzymatic or biochemical transformation in the systemic circulation to release the drug (Ettmayer et al., 2004; Rautio et al., 2008; Vlieghe and Khrestchatisky, 2013). Derivatization of the drug molecule could include addition of a lipophilic group to a more polar functional group of the drug or addition of a carrier to the drug. Modification of drug properties by attaching moieties such as amino acids, fatty acids, glycerides or phospholipids, not only alters pharmaceutical properties but also pharmacokinetics and biodistribution of the drug (Patel et al., 2009). Depending

upon structural modifications, translocation of prodrug occurs by processes such as receptor mediated endocytosis, large neutral amino acid transporter (LNAT) and glucose transporter (GLUT) thereby achieving higher drug concentrations in the brain (Stenehjem et al., 2009). Large amino acid transport system, member 1 (LAT1) is the major LNAT transporter and transports drugs that include α-methyldopa, melphalan and gabapentin (Cornford et al., 1992; Gynther et al., 2008). Other similar transport systems at the BBB include cationic amino acid transporter for basic amino acids and monocarboxylate transporter, which transports drugs such as probenecid (Patel et al., 2009). Presence of organic anion transporting polypeptides (OATPs) has been reported in several tissues including the BBB, although the exact localization on the brain endothelial cells is still not confirmed.

The prodrug strategy is a potential option to increase penetration of drug molecules across the BBB by altering the drug design and delivery process.

2.4 CONCLUSIONS AND FUTURE PERSPECTIVES

The BBB influences delivery of several drugs to the brain. This review describes anatomical and functional factors that restrict brain penetration of chemotherapeutics for the treatment of gliomas. In addition, we have also described the influence of glioma microenvironment and heterogeneity in BBB disruption on brain distribution of anti-cancer drugs. Understanding these factors related to the location of the tumor and the tumor characteristics will help guide the development of techniques and approaches for effective drug delivery to the tumors.

This review discusses the current strategies for enhancing brain penetration of drugs for the treatment of GBM. One of the major challenges to effective treatment of gliomas is obtaining sufficient concentrations of these agents in brain beyond the tumor core. During the past decade, several strategies have been employed to improve brain drug delivery, which include techniques to chemically or physically disrupt the tight junctions, use pharmacological inhibitors to overcome multi-drug efflux at the brain capillary endothelial cell and to use drug conjugates, nanoparticles, lipid-based formulations or peptide based delivery methods to enhance transit of drugs across the BBB. In addition, efforts are in progress to develop molecules with optimized brain penetration (such as GNE-317) and no liability to P-gp and Bcrp at the BBB. Most of these strategies have shown promising results in the preclinical setting, however, the results in the clinical trials are disappointing. This may be, in part, due to the invasive nature of glioma where the tumor cells infiltrate into the normal brain. Hence, delivery of therapeutic agents to all regions of the brain is the key to achieve success in the clinical trials. This will be key in refining therapies for GBM, where the reason for failure can be either the lack of adequate delivery of an effective drug, or insufficient activity of the drug at the target, or a lack of both delivery and efficacy.

CHAPTER III

SUNITINIB LC-MS/MS ASSAY IN MOUSE PLASMA AND BRAIN TISSUE: APPLICATION IN CNS DISTRIBUTION STUDIES

This chapter has been published as a manuscript in Chromatographia. 2013 Dec 1;76(23-24).

Sunitinib malate is a multi-targeted tyrosine kinase inhibitor, currently in clinical trials for glioma. Previously developed methods for preclinical studies in species such as mice have either employed HPLC or did not describe a detailed analytical method, which could be employed by other preclinical laboratories. In this paper, we have developed and validated a simple, sensitive high-performance liquid chromatography tandem mass-spectrometric method (LC-MS/MS) for the determination of sunitinib concentration in mouse plasma and brain tissue homogenate using dasatinib free base as the internal standard. A single step liquid-liquid extraction method was used for both the matrices. Since sunitinib exhibits light-induced E/Z isomerism, all sample preparation was done in light-protected conditions. Separation was performed on a ZORBAX Eclipse XDB C18 column 4.6 x 50 mm, 1.8 µm. The mobile phase consisted of 20mM ammonium formate (with 0.1% formic acid): acetonitrile (70:30, v/v) pumped isocratically at a flow rate of 0.25 mL/min with a total run time of 13 minutes. The retention times of sunitinib and dasatinib were 7.8 and 5.5 minutes, respectively. The calibration curve was linear over the range from 1.95 ng/mL to 500 ng/mL in both plasma and brain tissue homogenate with 1.95 ng/mL as the LLOQ for both the matrices. Inter- and intra-day accuracy and precision was <15% for low QC, med QC and high QC and <20% for LLOQ. The method was applied to a pharmacokinetic study in FVB-wild-type mice to determine the plasma and brain concentrations after a single oral sunitinib malate dose of 20 mg/kg.

3.1 INTRODUCTION:

Glioma is a solid neoplasm that originates in the glial cells of the brain. However, drug therapy for diseases of the brain is limited by the presence of the blood brain barrier (BBB) (Mellinghoff et al., 2011). The first step in defining the distribution of a drug to any target organ is via pharmacokinetic studies done in preclinical species. Though the FDA requires preclinical studies to be done in a variety of rodent and non-rodent species, the mouse remains one of the most studied species.

Sunitinib malate (N-(2-diethylaminoethyl)-5-[(Z)-(5-fluoro-2-oxo-1H-indol-3-ylidene)methyl]-2,4-dimethyl-1H-pyrrole-3-carboxamide, SU011248) is an orally active multi-targeted tyrosine-kinase inhibitor (TKI) with potent anti-angiogenic and antitumor activity. In addition, it also inhibits other tumor growth pathway receptors such as PDGFR-α and -β, stem cell factor receptor (c-KIT), basic fibroblast-growth factor receptor (bFGF), FMS-related tyrosine kinase 3 (FLT-3), a proto-oncogene RET and colony stimulating factor receptor (CSF 1-R) (Faivre et al., 2007). Its potent antitumor activity has been reported both *in-vitro* and *in-vivo* in several tumor cell lines and preclinical xenograft models, including brain tumor models (Faivre et al., 2007; Zhou and Gallo, 2009). The FDA approved sunitinib malate for the treatment of metastatic renal cell carcinoma and gastrointestinal stromal tumors in May 2006 (Goodman et al., 2007). Currently, there are many ongoing clinical trials to test the efficacy of sunitinib in glioma, a primary brain tumor, as a single agent and as a combination with other anti-cancer drugs. However, due to the anatomical structure of the blood brain barrier, the brain

delivery of sunitinib is limited and this could potentially impact its pharmacological action in glioma patients.

Sunitinib is an analog of SU5416 (semaxinib) and exhibits light-induced isomerization due to the presence of a double bond between 2-oxindol and the pyrrole ring. Rotation around this double bond leads to the existence of two isomers, the E-isomer and Z-isomer [9]. The powder form exists as the Z-isomer, which is also the thermodynamically stable form of the drug. However, when put into solution in light, it isomerizes and forms the E-isomer, which is an inactive form of sunitinib (de Bruijn et al., 2010). Furthermore, the E-isomer is not available as an analytical standard, and therefore a method for quantifying it cannot be developed. The amount of conversion of Z- to E-isomer depends upon how long the sample solution has been exposed to the light. Sunitinib is an extensively studied drug with regard to development of an assay method but most of these methods are deficient in some respect related to light-sensitivity, the type of method employed (HPLC vs LC-MS/MS) or information with regard to its stability under laboratory conditions or the effect of matrix employed. Gotze et al. reported that the formation ratio of E:Z was 1:4 (Gotze et al., 2012) and used the second peak (Z-isomer) for quantitation while Haouala et al. reported ratio of 1:2 (Haouala et al., 2009) and used summation of both the peak areas for calibration purposes. Such variability in results suggests that the isomer ratio is dependent on many factors in addition to the duration of time the samples have been exposed to light. Several papers have been published on the LC-MS/MS method validation of sunitinib in human plasma (Haouala et al., 2009; Honeywell et al., 2010; de

Bruijn et al., 2010; Rodamer et al., 2011; Bouchet et al., 2011; Gotze et al.; Lankheet et al., 2013), but have failed to mention the light-sensitive phenomenon (Minkin et al., 2008). Baratte et al. reported an analytical method for sunitinib and its metabolite in several tissues, including the brain. However, this method employed monkey tissues, which is not a routinely used laboratory animal (Baratte et al., 2004). Earlier attempts have been made to develop a LC-MS/MS assay for sunitinib where samples have been prepared under light-protected conditions. Zhou et al reported a LC-MS/MS method for determination of sunitinib in mouse plasma and normal and tumor brain tissue (Zhou and Gallo). However, their report did not discuss the stability of sunitinib under laboratory conditions such as sample preparation time stability (bench top) or long term stability for samples frozen from pharmacokinetic studies. In addition, their report also lacked any mention of the effect of matrix on the extraction of sunitinib. Considering these deficiencies in published literature, there is a need to develop a stable and a reliable analytical method for preclinical purposes in an animal that is routinely used for brain distribution studies. Thus, the main purpose of the current study was to develop and validate an LC-MS/MS method in mouse plasma and brain homogenate, which could effectively describe preclinical systemic disposition and brain distribution of sunitinib. To minimize the E-to-Z isomerism, all the experiments in this study were performed in strict light-protected conditions.

3.2 MATERIALS AND METHODS

3.2.1 CHEMICALS

Sunitinib malate salt (**Figure 3.1A**) and internal standard dasatinib (**Figure 3.1B**; IS) were purchased from LC laboratories (Woburn, MA, USA). Acetonitrile (ACN), methanol (MeOH), ethyl acetate and dimethyl sulfoxide (DMSO) were procured from Fisher Scientific (Fair Lawn, NJ, USA). Ammonium formate, formic acid, bovine serum albumin (BSA; > 96% pure from agarose gel electrophoresis) was obtained from Sigma Aldrich (St. Louis, MO, USA). Drug-free mouse plasma was obtained from Valley Biomedicals (Catalog # AP3054, Winchester, VA, USA). The mobile phase was vacuum-filtered through a 0.45um filter (Millipore, Milford, MA, USA).

3.2.2 PREPARATION OF STOCK SOLUTION, CALIBRATION STANDARDS AND QUALITY CONTROLS

All preparation was done in light-protected conditions. Individual stock solutions of sunitinib malate (in black polypropylene tubes) and the IS were prepared at a concentration of 1 mg/mL in DMSO.

Dilutions from the stock solutions were made in methanol to yield a working stock solution of 100 μg/mL to then generate two 10 μg/mL working solutions of sunitinib malate and one 10 μg/mL working solution of the IS. One 10 μg/mL working solution of sunitinib malate was used to prepare a series of eight non-zero calibration standards ranging from 1.95 ng/mL to 500 ng/mL in amber-colored glass vials. 10 μg/mL working

solution of IS was diluted to get a final working concentration of 2 μg/mL. The stock solution, sub-stocks, and the calibration standards were stored in the dark at -80°C.

A separate 10 μg/mL working solution of sunitinib was used to obtain 1 μg/mL sub-stock solution. Quality control samples were prepared independently from this sub-stock solution which to obtain 250 ng/mL (High QC; HQC), 62.5 ng/mL (Medium QC; MQC), 3.9 ng/mL (Low QC; LQC) and 1.95 ng/mL (lower limit of quantification; LLOQ). The QC samples were stored in the dark at -80°C.

3.2.3 SAMPLE PREPARATION

The blank brain homogenate was prepared by homogenizing drug-free mouse brains using a tissue homogenizer (PowerGen 125, Fisher Scientific, Pittsburgh, PA) and diluting it with 3 volumes of ice-cold 5% (w/v) BSA in phosphate-buffer saline (PBS) solution. Drug-free plasma was commercially obtained (see Materials).

Microcentrifuge tubes containing 100 μL of the IS and 100 μL of each calibration standard prepared in triplicate or the QC samples prepared in six replicates were dried under a gentle stream of nitrogen. Then, 100 μL of drug-free plasma or 200 μL of blank brain homogenate was added. This was followed by a single step liquid-liquid extraction, by adding 1 mL of ice-cold ethyl acetate and the tubes were vigorously shaken on a vortex-mixer for 10 minutes, followed by centrifugation at 7500 rpm for 15 minutes at 4 °C (SORVALL LEGEND RT, Kendro). Eight hundred microliters of the supernatant

consisting of the organic solvent was transferred to a fresh set of polypropylene micro centrifuge tubes and dried under nitrogen.

The dried samples were reconstituted in 100 μL of the mobile phase (30:70:0.1, ammonium formate:acetonitrile:formic acid, %v/v) and transferred to the autosampler inserts in amber-colored glass vials for injection. A volume of 5 μL of each sample was injected for analysis by LC-MS/MS.

3.2.4 INSTRUMENTATION AND MASS-SPECTROMETRIC CONDITIONS

The LC system consisted of an Agilent 1200 series binary pump (Santa Clara, CA, USA) and analytical separation was achieved using a ZORBAX Eclipse XDB C18 column 4.6 x 50 mm, 1.8 μm (Agilent Technologies, Santa Clara). The mobile phase consisted of 20 mM ammonium formate buffer (containing 0.1% formic acid) and acetonitrile (70:30; v/v) and was delivered at a flow rate of 0.25 ml/min and the total run time was 13 minutes.

A TSQ Quantum triple quadrupole mass spectrometer (Thermo Finnigan, San Jose, CA, USA) using Selected-Reaction-Monitoring (SRM) mode and an electrospray ionization source (ESI) in positive ion mode was utilized to obtain mass spectra at a voltage of 4500V. The sheath gas pressure and auxillary gas pressure was maintained at 50 and 20 arbitrary units, respectively. The capillary temperature was maintained at 300°C

throughout the run. The collision energy for the analyte and IS was 28eV and 16eV, respectively. Data acquisition and analysis were performed using Xcalibur software, Version 2.0.7. The precursor to product ion transition (Q1 → Q3) for quantitation (m/z) of sunitinib and dasatinib were programmed in the spectrometer at (399.26 → 282.98) and (488.00 → 401.03), respectively, to obtain the optimum parameters.

3.2.5 CALIBRATION CURVE

The linear calibration curve of sunitinib was estimated by using the peak area ratio of the analyte to the IS, employing a weighting factor of $1/y^2$ (where, y= peak area ratio). Parameters obtained from the calibration curve were used to determine the concentration of the unknown samples by back-calculation.

3.3 METHOD VALIDATION: ASSAY CHARACTERISTICS

The developed method was validated for accuracy, precision, stability, linearity, matrix effect, and extraction recovery.

3.3.1 INTER-ASSAY AND INTRA-ASSAY VARIABILITY. Method validation for accuracy and precision in the mouse plasma and brain was performed on three separate days as three batches. Each batch comprised of three replicates of eight non-zero calibration standards and six replicates of each QC sample, including the LLOQ. Inter- and intra-day accuracy and precision was determined by obtaining the plasma and brain

concentrations of sunitinib malate and calculating the relative standard error (%RSE) and percentage coefficient of variation (%CV).

3.3.2 LIMIT OF QUANTIFICATION. According to the FDA guidance for bioanalytical method validation (FDA, 2001; www.fda.org, 2001), the LLOQ is the lowest calibration standard and is selected on the basis that the variability in the accuracy and precision should be less than 20% and the signal-to-noise ratio greater than 5. The signal-to-noise ratio is obtained from the peak area ratio of the LLOQ and the background noise obtained from drug-free plasma and brain homogenate run in the same time window.

3.3.3 MATRIX EFFECTS (IONIZATION EFFICIENCY). The effect of matrix interference caused by endogenously present substances in plasma and brain homogenate on the ionization efficiency was evaluated by determining the ratio as ((ratio of absolute peak area of post-extracted spiked sample/absolute peak area of non-extracted samples reconstituted in the mobile phase)-1)*100. Matrix effect on the ionization efficiency of the IS was also determined in a similar way (Wang et al., 2011).

The post-extracted spiked samples were prepared as follows: three replicates (n=3 each matrix) of 100 μL of the drug-free plasma and 200 μL of drug-free brain homogenate were extracted by liquid-liquid extraction using 1 mL of ice-cold ethyl acetate. Eight hundred microliters of the supernatant was transferred to a microcentrifuge tube and dried

under nitrogen. To the dried residue, 100 μL of the analyte at three concentration levels (HQC, MQC and LQC) and 100 μL of the IS were added and dried again under nitrogen. The dried samples were reconstituted in 100 μL of the mobile phase and were injected into the LC-MS/MS for analysis.

3.3.4 EXTRACTION RECOVERY. A liquid-liquid extraction method was employed to efficiently extract the drug from the biological matrices, plasma and brain. Three replicates (n=3) at three concentration levels (HQC, MQC and LQC) for the analyte and the working concentration of the IS were studied. Extraction recovery was evaluated by comparing the absolute peak areas of the extracted and post-extracted spiked samples reconstituted in mobile phase. The processed samples consist of samples extracted from plasma and brain as mentioned earlier.

Extraction recovery was determined by (ratio of processed samples/ post-extracted spiked samples in mobile phase)*100.

3.3.5 STABILITY. Stability of sunitinib malate was evaluated in five replicates at three concentration levels (HQC, MQC and LQC) in both plasma and brain homogenate. Analysis was performed for short-term, long-term, freeze-thaw, auto-sampler and stock-solution stability.

For short-term or bench-top stability, samples were kept for 5 h at ambient temperature

(room temperature) in light-protected conditions. The time period was chosen on the basis of the maximum time the samples will be exposed to room temperature during sample preparation.

Three freeze-thaw cycles were performed to assess stability. Samples were prepared and thawed unassisted at the bench on day one, then frozen again at -80 °C. This cycle was repeated three times and then the samples were extracted on day three.

Long-term stability was assessed by storing the samples at -80 °C for two months (60 days) followed by extraction on day 61.

Auto-sampler stability of the samples was determined for the extracted and re-constituted QC samples by re-injecting the third day validation run samples, which were additionally stored at 4 °C for 48 h and compared to freshly prepared QC samples.

Since we had prepared the stock solution of all calibration standards and QC's, and stored them at -80 °C, we also determined the stock solution stability by preparing fresh QC's on the day of the experiment and analyzing them with the QC's stored in -80 °C for 6 months. Stock solution stability was determined only in non-extracted neat samples.

All stability studies were determined by comparing the peak area of freshly prepared samples and stability samples expressed as percent recovery.

3.4 METHOD APPLICATION

The LC-MS/MS assay was applied to an oral pharmacokinetic study of sunitinib malate in FVB wild-type mice. Plasma and brain concentration profiles were determined following an oral dose of sunitinib at 20 mg/kg administered as a 1% CMC (carboxymethyl cellulose) suspension via oral gavage in 24 mice. All mice were between 8-10 weeks old at the time of the experiment and the average weight was ~30 grams. The experiment was conducted in accordance with the University of Minnesota (UMN) Institutional Animal Care and Use Committee (IACUC). Animals were euthanized at various time points 0.5, 1, 2, 4, 6, 11 and 16 h post-dose (n=4 at each time point). Blood was collected via cardiac puncture (~500 μL) and immediately transferred into microcentrifuge tubes containing 20 μL (100 units/mL) of heparinized saline. Plasma was separated by centrifuging the blood at 7500 rpm at 4 °C for 15 min. Whole brain was immediately removed and rinsed with ice-cold saline to remove extraneous blood and blot-dried. Brain was snap-frozen in liquid nitrogen and stored in pre-weighted and labeled vials at -80 °C until analysis. On the day of analysis, all brain samples were thawed and weighed to obtain the brain weight expressed as the difference between the pre- and post-vial weights. The brains were homogenized with 3 volumes of 5% BSA using a tissue homogenizer. Pharmacokinetic parameters were calculated using non-compartmental analysis by Phoenix WinNonlin Version 6.3. (Pharsight, CA).

3.5 RESULTS AND DISCUSSION

3.5.1 CHROMATOGRAPHY AND MASS-SPECTROMETRIC CONDITIONS

Dasatinib belongs to the same class of tyrosine-kinase inhibitors as sunitinib and was chosen as the IS due to its similar chromatographic behavior. We chose not to use deuterated sunitinib malate as the IS in part because we did not want to have the complication of interfering peaks due to isomerism for the IS. Moreover, at the time we began our experiments; deuterated sunitinib was not readily available and was very expensive. Therefore, we wanted to use an IS, which is readily available for laboratory purposes. Even though all experiments were done in light-protected conditions, still we could not totally avoid the Z-to-E isomerism of sunitinib. The Z-isomer is the stable form of sunitinib and the E-isomer formed is too small in peak area to account for any significant effect. However, we have determined that after a light exposure time of 5 to 6 hours, equal peak areas of E- and Z-isomer were obtained (1:1 ratio; data not shown). Optimal resolution for analyte and IS was achieved with 70 volumes of aqueous buffer and 30 volumes of acetonitrile, when run isocratically at 0.25 mL/min.

Mass spectrometric conditions were optimized to obtain the maximum stable response of the parent analyte and the product ion. Three product ions were obtained for sunitinib with m/z of 326, 283 and 238. We have chosen the product ion with m/z of 283 as it gave the highest percentage fragmented. The use of Selected Reaction Monitoring (SRM) over Selected Ion Monitoring (SIM), afforded a better advantage in reducing interference and increasing sensitivity. The retention time achieved for E-isomer and Z-isomer of sunitinib

and dasatinib was 2,7 minutes, 7.8 minutes and 5.5 minutes, respectively. Low background noise from the biological matrix showed good selectivity of the method. Typical chromatograms of HQC, LLOQ and IS in both plasma (**Figure 3.2**) and brain (**Figure 3.3**) are shown.

Figure 3.1: Chemical structures of (A) sunitinib and (B), internal standard, dasatinib

(A) Chemical structure of sunitinib malate

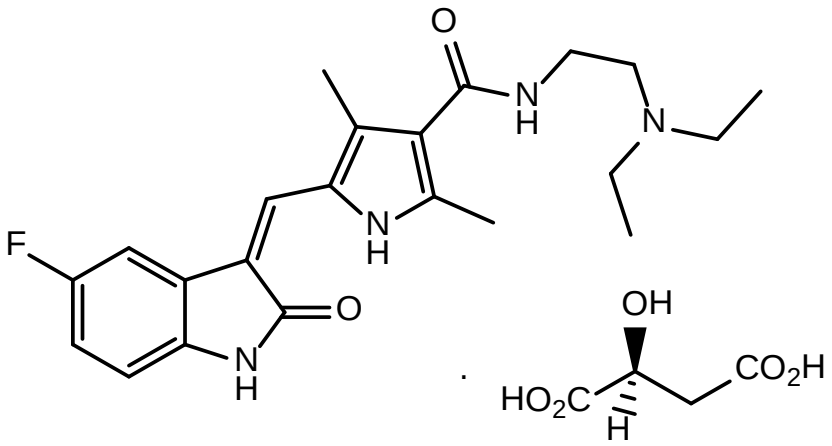

(B) Chemical structure of dasatinib (IS)

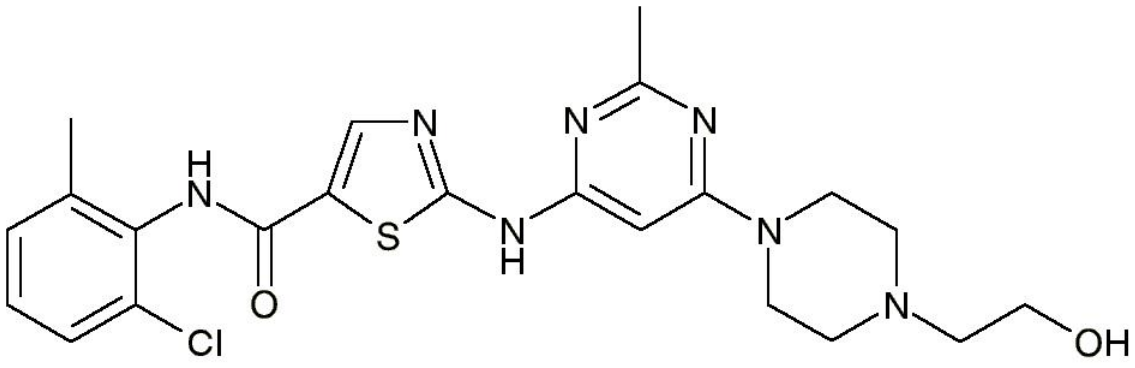

Figure 3.2: Representative HPLC-MS/MS chromatograms of high QC (250 ng/mL), LLOQ (1.95 ng/mL) and IS (dasatinib, 2 μg/mL) in plasma extracts. Two peaks observed for sunitinib in the high QC sample indicate E-isomer (2.7 minutes) and Z-isomer (7.8 minutes).

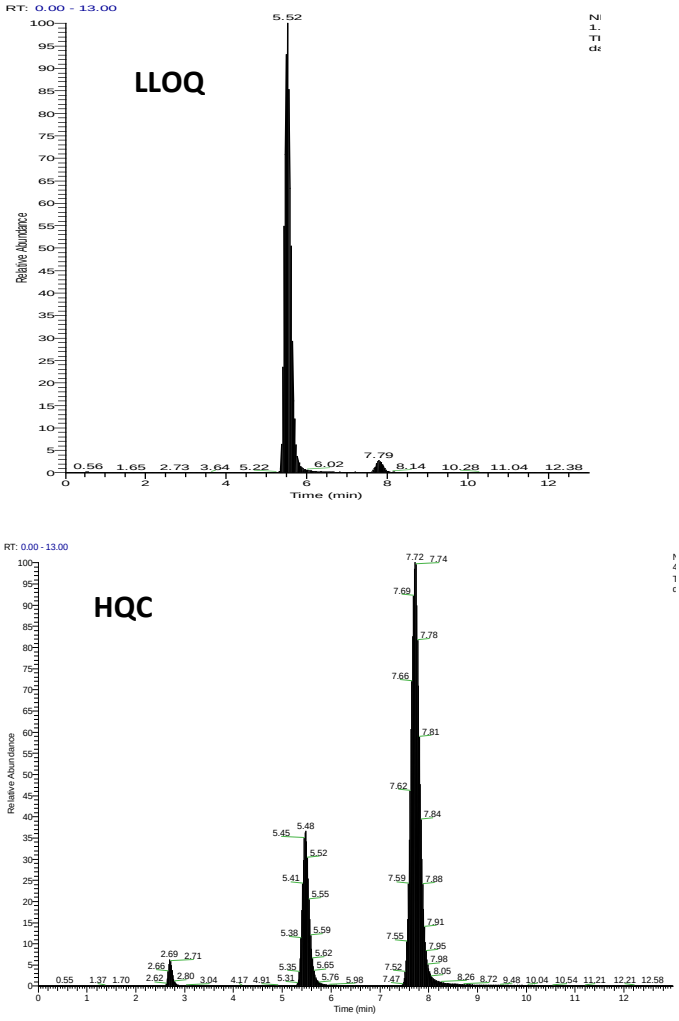

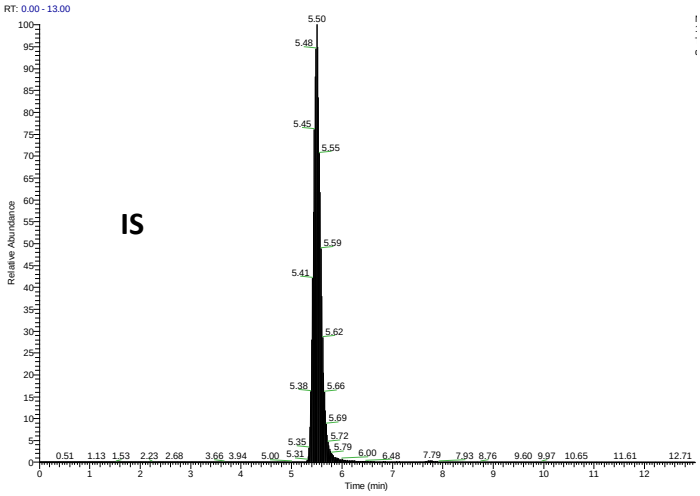
RT: 0.00 - 13.00
IS
Relative Abundance
Time (min)
5.50
5.48
5.45
5.55
5.59
5.41
5.62
5.38
5.66
5.69
5.72
5.79
5.35
5.31
6.00
6.48
7.79
7.93
8.76
9.60
9.97
10.65
11.61
12.71
0.51
1.13
1.53
2.23
2.68
3.66
3.94
5.00

Figure 3.3: Representative HPLC-MS/MS chromatograms of high QC (250 ng/mL), LLOQ (1.95 ng/mL) and IS (dasatinib, 2μg/mL) in brain tissue homogenate extracts. Two peaks observed for sunitinib in the high QC sample indicate E-isomer (2.7 minutes) and Z-isomer (7.8 minutes).

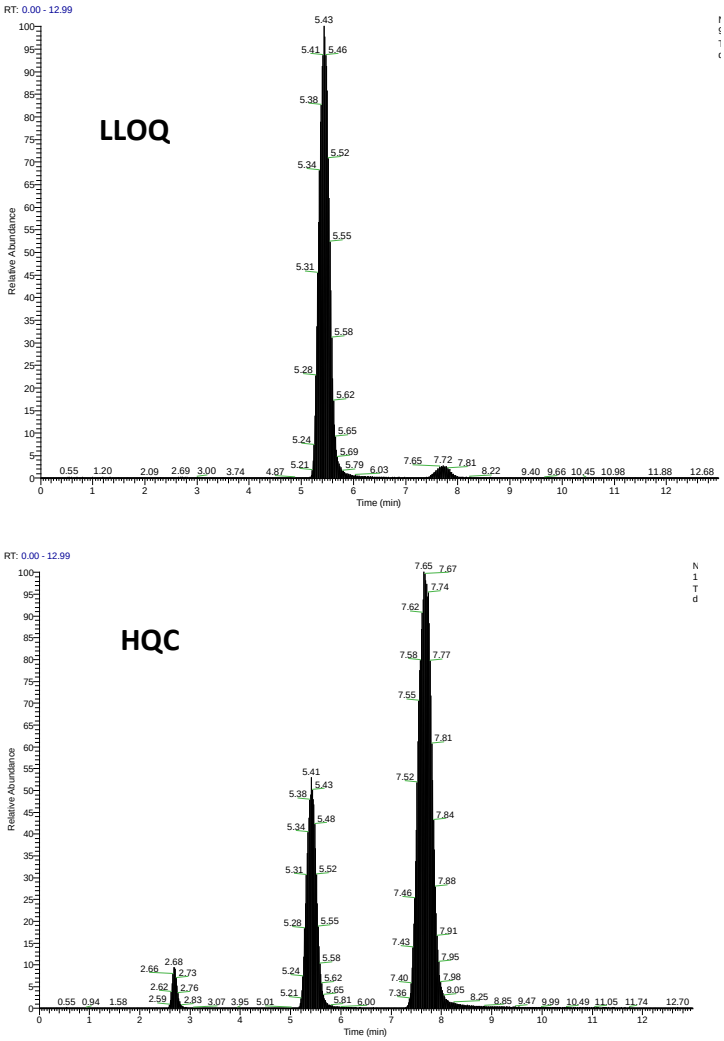

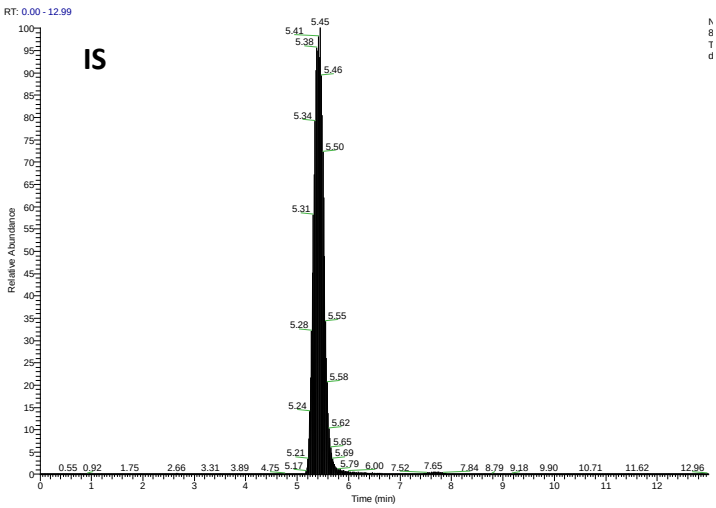
RT: 0.00 - 12.99
IS
Relative Abundance
Time (min)
5.45
5.41
5.38
5.46
5.34
5.50
5.31
5.55
5.28
5.58
5.24
5.62
5.65
5.21
5.69
5.17
5.79
6.00
0.55
0.92
1.75
2.66
3.31
3.89
4.75
7.52
7.65
7.84
8.79
9.18
9.90
10.71
11.62
12.96

3.5.2 LINEARITY, ACCURACY, PRECISION AND LLOQ. The assay was found to be linear over the calibration range from 1.95 ng/mL to 500 ng/mL for both plasma and brain homogenate using a weighting scheme of $1/y^2$ (y= peak area ratio). Selection of the weighting scale was based on the best estimation of coefficient of determination (r^2) and deviation of back-calculated concentrations from calibrators expressed as % difference. The calibration curves for sunitinib in plasma and brain had coefficients of determination (r^2) of about 0.99 and 0.97 for plasma and brain, respectively (n=3 in each run) **(Table 3.1).**

Table 3.1: Precision and accuracy of calibration standards of sunitinib in mouse plasma and brain tissue homogenate

Conc (ng/mL)	Brain		Plasma	
	RE%	CV%	RE%	CV%
1.95	12.9	6.15	-0.076	3.08
3.9	-12	3.5	1.4	3.6
15.6	-1.72	1.92	0.572	1.21
31.25	1.870	3.980	8.365	3.083
62.5	6.54	8.67	-0.858	2.53
125	-4.52	1.50	-1.78	0.640
250	1.09	3.49	-13.2	12.2
500	-1.07	2.38	-0.867	1.94

Inter- and intra-assay variability at four different concentrations, HQC (250 ng/mL), MQC (62.5 ng/mL), LQC (3.9 ng/mL) and LLOQ (1.95 ng/mL) was determined in plasma and brain with six replicates on each day for three separate days. Inter- and intra-assay bias (%CV) and precision (%RE) were within ±15% for all QC's, except at LLOQ (±20%), which is in agreement with FDA guidelines. This indicates that this assay is suitable in terms of accuracy and precision. The detailed results for inter-assay accuracy and precision in plasma and brain and intra-assay accuracy and precision in plasma and in brain are summarized (**Table 3.2).**

Table 3.2: Inter-assay and intra-assay accuracy and precision of sunitinib in mouse plasma and brain tissue homogenate

Matrix	Conc (ng/ml)	Intra-day (N=6)		Inter-day (N=18)	
		RE%	CV%	RE%	CV%
Plasma	LLOQ_1.953 ng/ml	-4.38	4.15	-4.83	4.94
	Low QC_3.906 ng/ml	1.41	2.88	-0.12	8.63
	Med QC_62.5 ng/ml	-5.92	5.17	-3.87	5.84
	High QC_250 ng/ml	-8.72	7.86	-8.97	1.33
Brain	LLOQ_1.953 ng/ml	11.81	10.73	9.05	5.91
	Low QC_3.906 ng/ml	-12.85	5.39	-7.66	7.45
	Med QC_62.5 ng/ml	-1.43	3.27	3.53	5.44
	High QC_250 ng/ml	-6.46	4.35	0.05	5.82

3.5.3 RECOVERY. Recovery was calculated by comparing the absolute peak area of the processed samples at 3.9, 62.5 and 250 ng/mL, using the extraction method described earlier, with those of post-extracted samples at the same concentrations in mobile phase, expressed as a percentage. Extraction recovery of the IS was also determined at 2 μg/mL using the same procedure. Average recovery for sunitinib in plasma and brain was 112.3% and 94.3%, respectively. The recovery results are summarized in **Table 3.3.**

3.5.4 MATRIX EFFECTS. Effect of endogenous substances in the biological matrix was evaluated at three different concentrations, 3.9, 62.5 and 250 ng/mL for sunitinib and at a single concentration of 2 μg/mL for the IS. The suppression of ionization in both plasma and brain homogenate was highest in medium QC (approx. -44%) and lowest for the high QC (approx. -34%). Plasma extracts enhanced the ionization of the IS by ~ 0.04%, but was decreased by -1.7% in the brain homogenate extracts. These results suggest that plasma and brain homogenate interfered with the ionization of the analyte (**Table 3.3**).

Table 3.3: Matrix effect of plasma and brain homogenate on the ionization efficiency of sunitinib and IS and extraction recovery of sunitinib and IS in mouse plasma and brain homogenate.

	Conc (ng/mL)	Matrix Effect, Mean (%)±SD (%) N=3	Extraction Efficiency, Mean (%)±SD (%) N=3
Plasma	Low QC_3.9	-38.1 ± 5.4	126 ± 0.1
	Med QC_62.5	-43.8 ± 4.3	119 ± 0.1
	High QC_250	-33.5 ± 3.5	92 ± 0.1
	Dasatinib (IS)_2000	0.04 ± 0.03	79 ± 0.02
Brain	Low QC_3.9	-43 ± 2.4	113 ± 0.1
	Med QC_62.5	-45 ± 2.6	102 ± 0.1
	High QC_250	-34.1 ± 3.1	68 ± 0.04
	Dasatinib (IS)_2000	-1.7 ± 0.9	72 ± 0.02

3.5.5 STABILITY. Five replicates of HQC, MQC and LQC were used to assess the stability of sunitinib under various conditions. The results are summarized in **Table 3.4**. Results from bench-top stability suggest that the sample preparation time of 5 h did not lead to significant degradation of sunitinib in both the plasma and the brain samples (< ±15%). Results from auto-sampler, freeze-thaw and long-term stability indicate that the degradation of sunitinib might occur under these conditions and therefore determining reliable concentrations from such samples must take this into consideration. Storing the samples after an experiment for long-term (>= 60 days) under frozen conditions (-80C) can lead to deterioration of the drug. It is thus advisable to analyze the samples as soon as possible. Furthermore, results from auto-sampler stability suggest that it is not ideal to use re-constituted samples for determination of sunitinib concentrations if they are kept for more than 48 h in the auto-sampler. With the given run-time in this assay, we were able to analyze up to 120 samples overnight without observing degradation of the analyte. The standard stock solution was found to be stable over the time period of storage (6 months). This is important as it avoids the need to make fresh standards everyday. (**Table 3.5**).

Table 3.4: Stability of analyte and IS under various conditions examined

Matrix	Concentration (ng/mL)	Bench-Top[#] (% recovery) N=5	Freeze-thaw[##] (% recovery) N=5	Auto-sampler[###] (% recovery) N=5	Long-Term[####] (% recovery) N=6
		Mean ± SD	Mean ± SD	Mean ± SD	Mean ± SD
Plasma	3.9	94.79 ± 4.04[*]	84.37 ± 7.38	98.4 ± 6.05[*]	112 ± 21.64
	62.5	91.8 ± 9.74	85.6 ± 9.69	68.66 ± 8.92	67.42 ± 13.80
	250	82.74 ± 20.08	100.73 ± 5.16	100.5 ± 6.13	70.19 ± 5.91
Brain	3.9	95.26 ± 9.84	71.68 ± 5.73	121.08 ± 8.88	122.26 ± 12.14
	62.5	96.35 ± 3.16	82.42 ± 9.88	119.08 ± 8.44	111.62 ± 11.47
	250	98.79 ± 5.05	92.62 ± 4.15	102.18 ± 9.02	107.59 ± 16.11

[*]no. of replicates = 4

[#]At least 5 h at room temperature

[##]At least three freeze-thaw cycles

[###]At least 48 h at 4°C

[####]At least 2 months (60 days) at -80 ± 5°C

Table 3.5: Stock solution stability of the analyte

Nominal Conc (ng/mL)	% recovery Mean ± SD
Low QC_3.9	102.3 ± 0.61
Medium QC_62.5	103.51 ± 0.22
High QC_250	99.54 ± 3.57

3.6 METHOD APPLICATION

The established method was successfully used to determine pharmacokinetic parameters in plasma and brain following a single oral dose of 20 mg/kg sunitinib administered as a 1% CMC suspension in FVB wild-type mice. Plasma and brain samples were collected at predetermined time points and analyzed using this assay. The assay was found to be sensitive in determining sunitinib concentrations in both plasma and brain. A non-compartmental analysis approach yielded a terminal half-life of 1.8 h in plasma and 2 h in brain. All measured concentrations were above the LLOQ. The plasma and brain area under the curve from time zero to infinity (AUC0-∞) was 1.85 hr-μg/mL and 0.77 hr-μg/mL, respectively, and AUC brain-to-plasma ratio was 0.42, i.e., 42% of the drug in plasma reaches the brain, suggesting limited delivery of sunitinib into the brain (measured as the total sunitinib concentrations, **Figure 3.4**). The peak concentration, Cmax, was 320 ng/mL and 127 ng/mL in both plasma and brain, respectively.

Figure 3.4: Plasma and brain sunitinib concentration-time profiles in FVB-wild type mice after a single oral dose of 20 mg/kg.

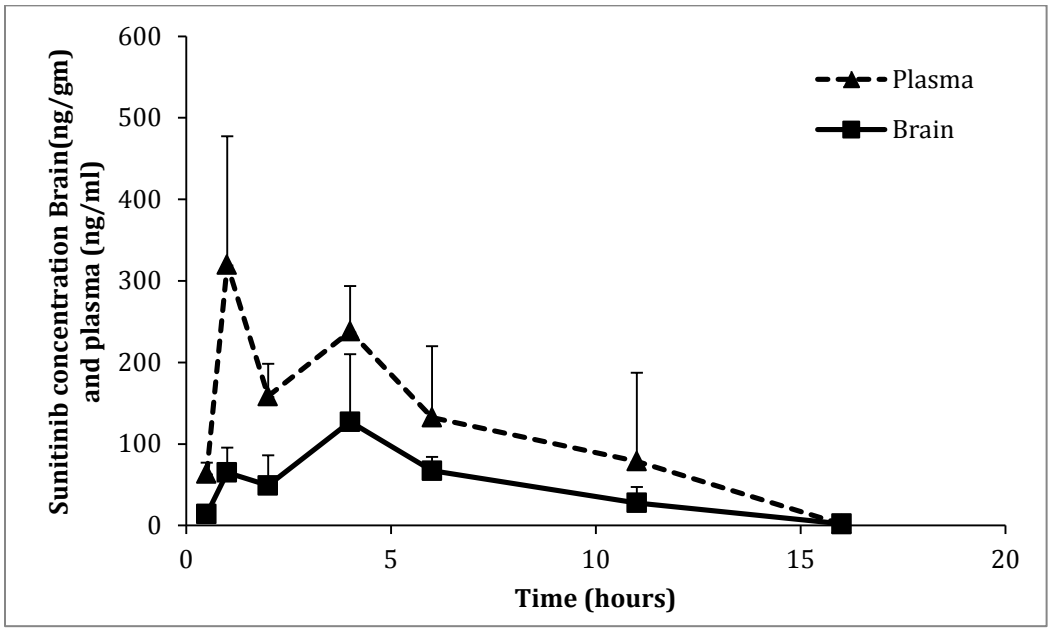

3.7 CONCLUSION

In conclusion, we have developed and validated a robust, sensitive and reproducible LC-MS/MS method for analysis of sunitinib in mouse plasma and brain tissue homogenate. This study reports a validated method for sunitinib analysis in mouse plasma and brain considering its light-sensitive nature and has been successfully employed for pre-clinical pharmacokinetic investigations in mice. High extraction efficiency using a liquid-liquid extraction method in this assay is simple to apply and does not involve the need for an

additional protein precipitation step. The described method was found to be linear over a wide range, from 1.95 ng/mL to 500 ng/mL. This method requires only small amount of sample (100 μL for plasma and 200 μL for brain homogenate), therefore it is also feasible for analysis of sunitinib from in-vitro cell culture studies and using this assay we have determined sunitinib from cellular accumulation studies in our lab.

3.8 FOOTNOTES

We would like to thank Dr. Tianli Wang and Dr. Sagar Agarwal for their valuable discussions. This work was supported by grants, CA 138437, NS 077921 and CA 108961.

CHAPTER IV

PHARMACOKINETIC ASSESSMENT OF EFFLUX TRANSPORT IN SUNITINIB DISTRIBUTION TO THE BRAIN

This chapter has been published as a manuscript in Journal of Pharmacology and Experimental Therapeutics, Dec 2013;347(3):755-64.

This study quantitatively assessed transport mechanisms that limit the brain distribution of sunitinib, and investigated adjuvant strategies to improve its brain delivery for the treatment of glioblastoma multiforme (GBM). Sunitinib has not shown significant activity in GBM clinical trials, despite positive results seen in preclinical xenograft studies. We performed *in vivo* studies in transgenic FVB mice: wild-type, *Mdr1a/b(-/-)*, *Bcrp1(-/-)* and *Mdr1a/b(-/-)Bcrp1(-/-)* genotypes were examined. The brain-to-plasma AUC ratio after an oral dose (20 mg/kg) was similar to steady-state tissue distribution coefficient (Kp), indicating linear distribution kinetics in mice over this concentration range. Furthermore, the distribution of sunitinib to the brain increased after administration of selective P-glycoprotein (P-gp) or breast cancer resistance protein (Bcrp) pharmacological inhibitors, and a dual inhibitor, elacridar, comparable to that of the corresponding transgenic genotype. The brain-to-plasma ratio after co-administration of elacridar in wild-type was ~12, compared to ~17.3 in *Mdr1a/b(-/-)Bcrp1(-/-)* mice. Overall, these findings indicate that there is a co-operation at the BBB in restricting the brain penetration of sunitinib and brain delivery can be enhanced by administration of a dual inhibitor. These data indicate that the presence of cooperative efflux transporters, P-gp and Bcrp, in an intact BBB, can protect invasive glioma cells from chemotherapy. Thus, one may consider the use transporter inhibition as a powerful adjuvant in the design of future clinical trials for the targeted delivery of sunitinib to GBM.

4.1 INTRODUCTION

Glioblastoma multiforme (GBM) is an aggressive tumor with a median survival of 12.6 months with treatment (Louis et al., 2007). Progression of glioma is dependent on a rich blood supply accomplished by angiogenesis (Brem et al., 1992; Tuettenberg et al., 2006), a process mediated by vascular endothelial growth factor receptor (VEGFR), platelet-derived growth factor receptor (PDGFR), basic fibroblast growth factor (bFGF) and epidermal-derived growth factor receptor (EGFR) (Tuettenberg et al., 2006; Wong et al., 2009). Anti-angiogenic therapy is an important treatment option for GBM, in addition to cytotoxic therapy with temozolomide. Bevacizumab (Avastin®), an anti-VEGF monoclonal antibody, was approved in May 2009 for GBM (Cohen et al., 2009). Since then, several targeted agents such as tyrosine-kinase inhibitors (TKIs) have been tested in clinical trials, alone and in combination with other anti-cancer therapies. None of these treatment regimens have shown significant efficacy in GBM patients (di Tomaso et al., 2011; Wick et al., 2011), leaving several unresolved questions remaining; such as whether or not the drugs themselves are ineffective, or if the delivery of a possibly effective drug is inadequate, or both.

Effective delivery of drugs for the treatment of brain disorders has always been a challenging task due to the presence of the blood-brain barrier (BBB). The BBB is comprised of endothelial cells annealed by tight-junctions, which is further complicated by the presence of active efflux transporters. The ATP-Binding Cassette (ABC) family of transporters, include P-glycoprotein (P-gp, ABCB1) and breast cancer resistance protein

(BCRP, ABCG2), two major efflux transporters present in the luminal side of the BBB. These transporters work in tandem to restrict delivery of several therapeutics into the brain (Gottesman et al., 2002; Fletcher et al., 2010) .

The microvasculature within a brain tumor is heterogeneous. The tumor core has some degree of necrosis and is highly permeable (Horowitz et al., 1983), while the brain adjacent to the core may have a slightly higher permeability than normal brain (Levin et al., 1975). The core, visualized by MRI, is often removed during resection; however the tumor cells adjacent to the core, are found in regions with a relatively intact BBB, and are capable of causing the tumor recurrence. Furthermore, some tumor cells infiltrate into distant sites of the brain to form a sanctuary of tumor cells, thus making GBM, in essence, a "whole brain" disease (Agarwal et al., 2011a). The tumor and BBB characteristics work in tandem to present a real challenge in achieving adequate drug delivery throughout the brain, which would yield a treatment that will be most likely to result in a longer progression-free survival in GBM (Agarwal et al., 2011a).

Sunitinib (N-(2-diethylaminoethyl)-5-[(Z)-(5-fluoro-2-oxo-1H-indol-3-ylidene)methyl]-2,4-dimethyl-1H-pyrrole-3-carboxamide); SU112468; Sutent, MW: 532.561223 g/mol MF: C26H33FN4O7) is an orally active TKI with activity against VEGFR1-3 and PDGFR-α/β receptors, which are over-expressed in gliomas (Faivre et al., 2007). Preclinical studies have shown significant anti-tumor and anti-angiogenic activity of sunitinib (Zhou et al., 2008; Zhou and Gallo, 2009). However, recent clinical

trials have been disappointing (Neyns et al., 2011; Pan et al., 2012)**.** One possibility for these conflicting results could be due to the lack of adequate drug delivery, mediated by the efflux transporters at the BBB. Sunitinib is known to interact with P-gp and Bcrp at the BBB (Dai et al., 2009; Hu et al., 2009; Shukla et al., 2009)**.**

Recently, Tang et al. reported that sunitinib is transported in-vitro by human ABCB1 (MDR1) and ABCG2 (BCRP) and murine ABCG2 (Bcrp), but not by human ABCC2 (MRP2) (Tang et al., 2012). They showed that single knockout of efflux transporters, P-gp or Bcrp, did not result in a profound increase in the brain accumulation of sunitinib when given as a single oral dose of 10 mg/kg; however, absence of both the transport systems (*Abcb1a/1b/Abcg2*$^{-/-}$*)* resulted in a 23-fold increase in brain penetration. Furthermore, administration of a high dose of an inhibitor of both P-gp and Bcrp, elacridar, resulted in 12-fold increase in brain accumulation of sunitinib, comparable to the levels observed in *Abcb1a/1b/Abcg2*$^{-/-}$ mice, when examined at a single time point (Tang et al., 2012).

Therefore, the primary aim of this investigation was to study the interaction of sunitinib with P-gp and Bcrp at the BBB and quantitatively assess using pharmacokinetic principles, the true brain partitioning. We further proposed strategies to improve the brain distribution of sunitinib. We determined how assessment of brain partitioning at any single time point can lead to misinterpretation of the influence of efflux mechanisms; however, this assessment can be achieved at transient steady state. A novel aspect of this

study is the inhibition of remaining P-gp and Bcrp in Bcrp knockout and P-gp knockout mice, respectively. This is important, especially for a tumor such as glioma, which is highly invasive in nature and has a greater tendency to infiltrate into the normal regions of the brain. Thus sub-therapeutic concentrations in the regions where BBB has intact tight junctions, in conjunction with efflux transporters, can lead to decreased delivery, and hence efficacy of the targeted therapeutic agent.

4.2 MATERIALS

4.2.1 CHEMICALS AND REAGENTS

Sunitinib malate and dasatinib free base were purchased from LC Labs (Woburn, MA). Elacridar [GF120918; **N**-(4-[2-(6,7-dimethoxy-3,4-dihydro-1**H**-isoquinolin-2-yl)ethyl]-5-methoxy-9-oxo-10**H**-acridine-4-carboxamide] and Ko143 [(3S,6S,12aS)-1,2,3,4,6,7,12,12aoctahydro-

9-methoxy-6-(2-methylpropyl)-1,4-dioxopyrazino(1',2':1,6) pyrido(3,4-b)indole-3-

propanoic acid 1,1-dimethylethyl ester] were purchased from Toronto Research Chemicals, Inc. (North York, ON, Canada). Zosuquidar [LY335979; (R)-4-((1aR,6R,10bS)-1,2-difluoro-1,1a,6,10btetrahydrodibenzo-

(a,e)cyclopropa(c)cycloheptan-6-yl)-α-((5-quinoloyloxy) methyl)-1-piperazine ethanol, trihydrochloride] was a gift from Eli Lilly & Co. (Indianapolis, IN). All other reagents and chemicals were of HPLC grade and were purchased from Sigma (St. Louis, MO).

4.2.2 ANIMALS

In-vivo studies were performed in the FVB mouse strain of either sex, wild-type and transgenic mice that have the gene for P-gp knocked out (*Mdr1a/b(-/-)* knockout mice), Bcrp (*Bcrp1(-/-)* knockout mice) and both P-gp and Bcrp (*Mdr1a/b(-/-)Bcrp1(-/-)* or "triple-knockout" mice) obtained from Taconic Farms (Germantown, NY). All mice were 8-10 weeks old and were maintained under temperature-controlled conditions with 12-hr dark/12-hr light cycle. Mice were handled according to the guidelines set by the National Institute for Health (NIH) and all experiments were conducted in accordance with the Institutional Animal care and Use Committee (IACUC) of the University of Minnesota.

4.2.3 PLASMA AND BRAIN PHARMACOKINETICS AFTER ORAL ADMINISTRATION

The sunitinib dosing solutions for all in-vivo studies were prepared as a stable suspension in 1% carboxymethylcellulose on the day of the experiment. All mice were administered 20 mg/kg by oral gavage were euthanized using a carbon-dioxide chamber at the desired time point. Since sunitinib exhibits light-sensitive diastereoisomerism (de Bruijn et al., 2010)**,** all experiments and sample analyses were performed in light-protected conditions.

In the oral dosing study, wild-type, *Mdr1 a/b (-/-)*, *Bcrp1(-/-)* and *Mdr1 a/b (-/-)*, *Bcrp1(-/-)* mice were administered 20 mg/kg sunitinib suspension via oral gavage. Blood and brain were harvested at pre-determined time points, i.e., 0.5, 1, 2, 4, 6, 11, 16 and 22

hours post-dose (n=3 to 4 at each time point). Following euthanasia, blood was collected via cardiac puncture and immediately transferred to tubes containing 20 µL of 100 units/mL heparinized saline. Plasma was obtained by centrifugation at 4^0C at 3500 rpm for 15 minutes. Whole brain was rapidly removed, rinsed with ice-cold buffer and blotted with tissue paper to remove superficial blood vessels, followed by flash freezing in liquid nitrogen. Brains were transferred to pre-weighed tubes and plasma and brain samples were stored at -80^0C until analysis.

On the day of the analysis, brain samples were thawed at room temperature and brain weights were determined. Brains were homogenized using 3 volumes of ice-cold 5% bovine serum albumin (BSA) prepared in phosphate-buffered saline (pH= 7.4) using a tissue homogenizer (PowerGen 125, Fisher Scientific, Pittsburgh, PA)

Previously, we have determined that the brain vascular space in FVB mice is 1.4% of the whole brain volume (Dai et al., 2003)**,** therefore we used this value to correct all brain concentrations for the residual drug in the brain vasculature.

4.2.4 STEADY-STATE BRAIN DISTRIBUTION OF SUNITINIB

The steady-state brain-to-plasma ratio or the "tissue partition coefficient" (Kp) was determined for sunitinib by measuring the plasma and brain concentrations in wild-type, *Mdr1(-/-), Bcrp1(-/-)* and *Mdr1a/b(-/-)Bcrp1(-/-)* mice using Alzet osmotic minipumps (Durect Corporation, Cupertino, CA) as described previously for sunitinib (Dudek et al.,

2013). In brief, 30 mg of sunitinib was dissolved in 1 mL of DMSO and osmotic minipumps (model 1003D) were loaded with 100 µL. The pumps were equilibrated by immersing them overnight in saline at 37^0C in light-protected conditions. On the day of the experiment, mice were anesthetized with isoflurane (Boynton Health Service Pharmacy, University of Minnesota, Minneapolis, MN) and the primed pumps were surgically implanted in the peritoneal cavity of the mice, after which the mice were allowed to recover on a heated pad. Each minipump is designed to operate at a flow rate of 1 µL/hr, which, in this case, yields a constant intraperitoneal infusion rate of 30 µg/hr. After 48 h (approximately 24 half-lives), animals were euthanized and brain and blood were harvested as described earlier. A 48 hr infusion was sufficient to achieve steady state as both the plasma and brain half-lives were approximately 2 hrs. Plasma and brain samples were stored in -80^0C until the day of analysis. On the day of the analysis, brains were prepared for analysis as described above.

4.2.5 INHIBITION OF P-gp AND/OR Bcrp1

The influence of selective or dual pharmacological inhibition of P-gp and Bcrp on the brain distribution of sunitinib was examined by pre-treating FVB wild-type mice with selective inhibitors of P-gp (zosuquidar, LY335979) (Dantzig et al., 2001), Bcrp (Ko-143) (Allen et al., 2002) and a dual inhibitor of P-gp/Bcrp (elacridar, GF120918) (Maliepaard et al., 2001; Hubensack et al., 2008). Zosuquidar was administered at a dose of 25 mg/kg and both Ko-143 and elacridar were administered at doses of 10 mg/kg

(vehicle: 40% DMSO, 40% propylene glycol, 20% saline). All inhibitors were administered via intravenous route, 30 minutes prior to sunitinib dosing (20 mg/kg) via oral gavage. Mice were sacrificed 1 hour post sunitinib dosing, and blood and brain specimens were collected and prepared for analysis as described above. To further delineate the role of P-gp and Bcrp in regulating the brain distribution of sunitinib at the mouse BBB, we studied the effect of selective pharmacological inhibitors in transgenic mice, therefore, P-gp knockout mice (*Mdr1a/b(-/-)*) were administered a Bcrp-selective inhibitor, Ko-143 (10mg/kg) and Bcrp knockout mice (*Bcrp1(-/-)*) were administered a P-gp selective inhibitor, zosuquidar (25 mg/kg) and FVB wild-type mice were administered both zosuquidar and Ko-143 intravenously 30 minutes prior to the sunitinib oral dose (20 mg/kg). Mice were sacrificed 1 hour after sunitinib dosing and blood and brain specimens were collected and stored at -80^0C until analysis.

Further, we compared the brain concentrations and brain-to-plasma concentration ratios at the 1-hour time point following pharmacological inhibition with those obtained at 1-hour time point in genetically altered mice, i.e., the *Mdr1a/b(-/-), Bcrp1(-/-)* and *Mdr1a/b(-/-)Bcrp1(-/-)* mice after oral administration. Moreover, given that these brain distribution data are often reported in the literature at a single time-point post dose, these experiments allow us to compare single time point brain distribution (brain-to-plasma concentration ratios at a single time point) with the steady-state concentration ratios and the AUC ratios from time zero to infinity.

4.2.6 DATA ANALYSIS

Estimation of pharmacokinetic parameters and metrics was accomplished using Phoenix WinNonlin version 6.3 employing non-compartmental estimation methods (Pharsight, Mountain View, CA). C_{max} and T_{max} were direct measurements obtained as the maximum observed concentration and the time to reach C_{max}, respectively. The area under the concentration time profile (AUC) was calculated up to the last measured concentration using log-linear trapezoidal approximation ($AUC_{0\text{-}tlast}$), with an area extrapolation to time infinity in the terminal phase by adding C_{last}/λ_z, where λ_z is the terminal rate constant of the drug from plasma or brain, that was calculated from the last three to five data points of the respective concentration-time profiles. An extension of Nedelman and Jia's method was employed to analyze data using a sparse sampling method, and to estimate variance on area under the concentration time profile from time 0 to the last measurable time point (Nedelman and Jia, 1998)**.** The percentage of extrapolated AUC was less than 2% for all the four groups for both plasma and brain. In addition, we assessed the transient steady-state kinetics of sunitinib. A transient steady state occurs when the brain concentration is at maximum, $C_{max,\ brain}$. At that time, the rate of change of drug concentration in the brain is zero. That is, a transient steady state is determined by the ratio of maximum observed brain concentration (C_{max}) to the corresponding plasma concentration at that time point. The 'AUC' brain-to-plasma ratio and the 'transient' steady-state ratio were compared to the 'steady-state' brain-to-plasma ratio obtained after a continuous intraperitoneal infusion lasting 48 hours. We also determined brain-to-plasma concentration ratios at all measured time points in all genotypes. Furthermore, a drug-targeting index (DTI) of

sunitinib was determined for both the efflux transporters as AUC brain-to-plasma ratios of the "treatment" groups (Pgp knockout, Bcrp knockout or triple knockout) divided by the AUC brain-to-plasma ratios of the control group, in this case the AUC brain-to-plasma ratio in FVB wild-type mice, written as

$$DTI = [AUC_{brain}/AUC_{plasma}]_{,\ knockout} / [AUC_{brain}/AUC_{plasma}]_{,\ wild\text{-}type}$$

4.2.7 LC-MS/MS ANALYSIS

Quantitative determination of sunitinib concentrations in mouse plasma and brain tissue homogenate was done using high performance liquid chromatography-tandem mass spectrometry (LC-MS/MS) according to the method previously described (Oberoi RK, 2013). In brief, on the day of the analysis, samples were thawed at room temperature, protected from light. Brain samples were homogenized with 3 volumes of 5% ice-cold bovine serum albumin in phosphate buffered saline (pH=7.4). 100 µL of plasma and 200 µL of brain homogenate were transferred to micro centrifuge tubes containing 100 µL of internal standard, dasatinib (2000 ng/mL). Samples were extracted by adding 1 mL of ice-cold ethyl acetate and vigorously shaken for 5 minutes, followed by centrifugation at 4^0C at 7500 rpm for 10 minutes. 750µL of the supernatant was transferred to microcentrifuge tubes and dried under a gentle stream of nitrogen. Dried samples were re-constituted in 100 µL of mobile phase (70:30:0.1, v/v %, 20 mM ammonium formate, pH 3.5: acetonitrile: formic acid) and transferred to amber colored glass vials. 5 µL of the

sample was injected into LC-MS/MS. The chromatographic system consisted of Agilent Technologies model 1200 separation system. Separation of the analyte was achieved on ZORBAX XDB Eclipse C_{18} column (4.6 x 50 mm, 1.8um, Agilent Technologies). The LC-system was interfaced with TSQ Quantum triple quadrupole mass spectrometer (Thermo Finnigan, San Jose, CA) equipped with selected reaction monitoring (SRM) mode by electrospray ionization source (ESI) operated in positive ion mode at a spray voltage of 4000V. The mobile phase flow rate was 0.25 mL/min and the total run time was 13 min. Data acquisition and analysis was performed using the Xcalibur software, version 2.0.7. The mass-to-charge transitions programmed in the spectrometer were (399→283) and (488→401) for analyte sunitinib and internal standard, dasatinib, respectively.

4.2.8 STATISTICAL ANALYSIS

Unpaired two-sample t-tests were used to test for statistical significance between two groups. One-way ANOVA, followed by Bonferroni's test, was employed to test for significance among multiple groups. Significance was declared at $p < 0.05$ for all tests. (GraphPad Prism 5.01, San Diego, CA, USA).

4.3 RESULTS

4.3.1 SUNITINIB PHARMACOKINETICS IN PLASMA AND BRAIN AFTER ORAL ADMINISTRATION

Sunitinib plasma and brain concentration-time profiles were determined in wild-type, *Mdr1a/b(-/-), Bcrp1(-/-)* and *Mdr1a/b(-/-)Bcrp1(-/-)* mice after a single oral dose of 20 mg/kg sunitinib. The plasma and brain concentrations in the wild-type mice at the 22 hr time-point were below the limit of quantification (LLOQ, 1.95 ng/mL) and therefore were not considered in the pharmacokinetic analyses.

Plasma concentrations (and hence the AUCs in plasma) were not statistically different among the four genotypes. This suggests that absence of P-gp and/or Bcrp does not influence the systemic pharmacokinetics of sunitinib. The apparent oral clearances (CL/F) observed amongst the genotypes were similar. The apparent oral clearance of sunitinib in wild-type, *Mdr1a/b(-/-), Bcrp1(-/-)* and *Mdr1a/b(-/-)Bcrp1(-/-)* was 4.6 mL/min, 4.1 mL/min, 5.1 mL/min and 6.5 mL/min, respectively. This is reflected in similar areas under the plasma concentration-time profiles among each group (AUC plasma) **(Figure 4.1 (a), Table 4.1).** However, the brain concentrations varied greatly amongst the genotype groups. In the wild-type mice, the brain concentrations were lower than the plasma concentrations at all the measured time points, indicating limited delivery of sunitinib into the brain. Brain concentration-time profiles in Bcrp knockout mice and P-gp knockout mice closely followed concentrations corresponding in the plasma. This indicates that Bcrp or P-gp alone do not dramatically affect the brain distribution of sunitinib. However, the brain concentrations in the triple knockout mice were

significantly greater than the plasma concentrations at all measured time points ($p < 0.05$), indicating that like many other TKIs, sunitinib brain distribution is influenced by both P-gp and Bcrp acting in concert at the BBB **(Figure 4.1 (b))** (Chen et al., 2009; Lagas et al., 2009; Polli et al., 2009; Poller et al., 2011)**.** Non-compartmental analysis of all four concentration-time profiles indicated that the terminal half-life in plasma was similar to the terminal half-life in the brain within each group. The half-life in plasma ranged from 1.8 hrs to 3.0 hrs while the half-life in the brain ranged from 2.0 hr to 3.2 hrs **(Table 4.1)**. Although the AUC in plasma was not different between groups, significant differences, however, were observed in the brain AUCs ($AUC_{0\text{-}tlast}$) in all knockout mice compared to the wild-type mice. This indicates that the efflux transporters influence sunitinib brain distribution between groups; a slight difference in the P-gp and BCRP knockout animals, but with a much more pronounced effect in the triple-knockout animals. The maximum observed concentration in the brain ($C_{max\ brain}$) was also significantly different between all groups of mice. The $C_{max\ brain}$ in the wild-type (0.13 ±0.04 µg/gm) was lower than that observed in *Bcrp1 (-/-)* mice (0.20 ± 0.02 µg/gm), *Mdr1a/b(-/-)* mice (0.52 ± 0.14 µg/gm) and *Mdr1a/b(-/-)Bcrp1(-/-)* (4.9 ± 0.7 µg/gm) mice. The area under the brain concentration time profile (AUC 0-∞, brain) was 37.4-fold higher in *Mdr1a/b(-/-)Bcrp1(-/-)* mice compared to wild-type mice, whereas the AUC brain in *Mdr1a/b(-/-)* mice was 4.75-fold higher and in Bcrp1(-/-) mice was 2.08-fold higher, compared to the wild-type mice (**Table 4.1).**

The resulting AUC brain-to-plasma ratio, also known as tissue Kp (brain-to-plasma partition coefficient), was 0.42 in the wild-type mice, suggesting that sunitinib has,

compared to many other TKIs (Agarwal et al., 2011b; Minocha et al., 2012b; Minocha et al., 2012a), a greater partitioning into the brain. However, in the absence of both P-gp and Bcrp (*Mdr1a/b(-/-)Bcrp1(-/-)*) mice, the AUC brain-to-plasma ratio is 20.5, whereas in *Mdr1a/b(-/-)* and *Bcrp1(-/-)* mice, the AUC brain-to-plasma ratio was 1.61 and 0.88, respectively. These results indicate that the both P-gp and Bcrp work in cooperation to efflux sunitinib out of the brain. This could impact the drug levels in the brain for treatment of brain tumors, both primary and metastatic. The drug-targeting index (DTI) of sunitinib was calculated as the ratio of AUC brain-to-plasma ratios, in the transgenic mice divided by the same ratio in the control group, which in this case are the wild-type mice. Based on the mean AUC0-∞ values, the observed DTI values were 3.8 for *Mdr1a/b(-/-)*, 2.4 for *Bcrp1(-/-)* and 55.5 for *Mdr1a/b(-/-)Bcrp1(-/-)*. This indicates a great influence of the efflux transporters in limiting the brain targeting of sunitinib **(Table 4.1).** These results closely follow the pattern previously observed for several TKIs, where a greater than additive effect of P-gp and Bcrp is observed (Lagas et al., 2009; Polli et al., 2009). Our results indicate that the efflux activity with *Mdr1a/b(-/-)* mice and *Bcrp1(-/-)* mice is a combined effect since we determined that P-gp efflux activity (DTI for *Mdr1a/b(-/-)* mice) was 3.8-fold and Bcrp efflux activity (DTI for *Bcrp1(-/-)* mice) was 2.4-fold. Therefore, it is hard to conclusively say whether either P-gp or Bcrp has a greater contribution to the *in vivo* efflux clearance of sunitinib from the brain. Nevertheless, it is clear that both transporters work in tandem at the BBB to efflux sunitinib from the brain, and the action of both transporters must be inhibited to significantly improve the distribution of sunitinib to the brain.

The brain-to-plasma concentration ratios vs. time of all genotypes are shown in **Figure 4.1 (c).** In all the mouse genotypes, these ratios showed an increase before reaching a plateau, when a pseudo-distributional equilibrium had been attained.

Table 4.1: Plasma and brain pharmacokinetic parameters determined by non-compartmental analysis after the administration of a single oral dose of sunitinib (20 mg/kg) in wild-type, Mdr1a/b(−/−), Bcrp1(−/−), and Mdr1a/b(−/−)Bcrp1(−/−) mice.

Results are expressed as mean ± S.D. n = 3 - 4.

PLASMA				
Parameter (units)	FVB-wild type	*Mdr1a/b(-/-)*	*Bcrp1(-/-)*	*Mdr1a/b(-/-)Bcrp1(-/-)*
Cmax (ug/mL)	0.32 ± 0.08	0.42 ± 0.13	0.225 ± 0.09	0.38 ± 0.04
Half-life (hr)	1.8	2.1	3.0	2.8
Tmax (hr)	1	0.5	2	2
CL/F (mL/min)	4.6	4.1	5.1	6.5
AUC (0-tlast) (hr-ug/mL)	1.85 ± 0.36	2.26 ± 0.26	1.81 ± 0.20	1.39 ± 0.12
AUC (0-inf) (hr-ug/mL)	1.85	2.27	1.83	1.40
BRAIN				
Cmax (ug/mL)	0.13 ± 0.04	0.52 ± 0.14	0.20 ± 0.02	4.92 ± 0.74
Half-life (hr)	2.0	2.5	3.2	3.0
Tmax (hr)	4	4	6	2
AUC (0-tlast) (hr-ug/mL)	0.76 ± 0.11	3.63 ± 0.15	1.58 ± 0.15	28.43 ± 3.10
AUC (0-inf) (hr-ug/mL)	0.77	3.65	1.61	28.8
BRAIN/PLASMA RATIO				
AUC_{Brain}/ AUC_{Plasma}	0.42	1.61	0.88	20.53
DTI		3.9	2.1	48.9

Cmax, maximum observed concentration; half-life (hr), time taken to reach one-half of its steady-state value; AUC, area under the concentration-time profile curve; DTI, drug targeting index

Figure 4.1 (a): Plasma concentration-time profiles of sunitinib after a single oral dose (20 mg/kg) in FVB wild-type, Mdr1a/b(-/-), Bcrp1(-/-) and Mdr1a/b(-/-)Bcrp1(-/-) mice

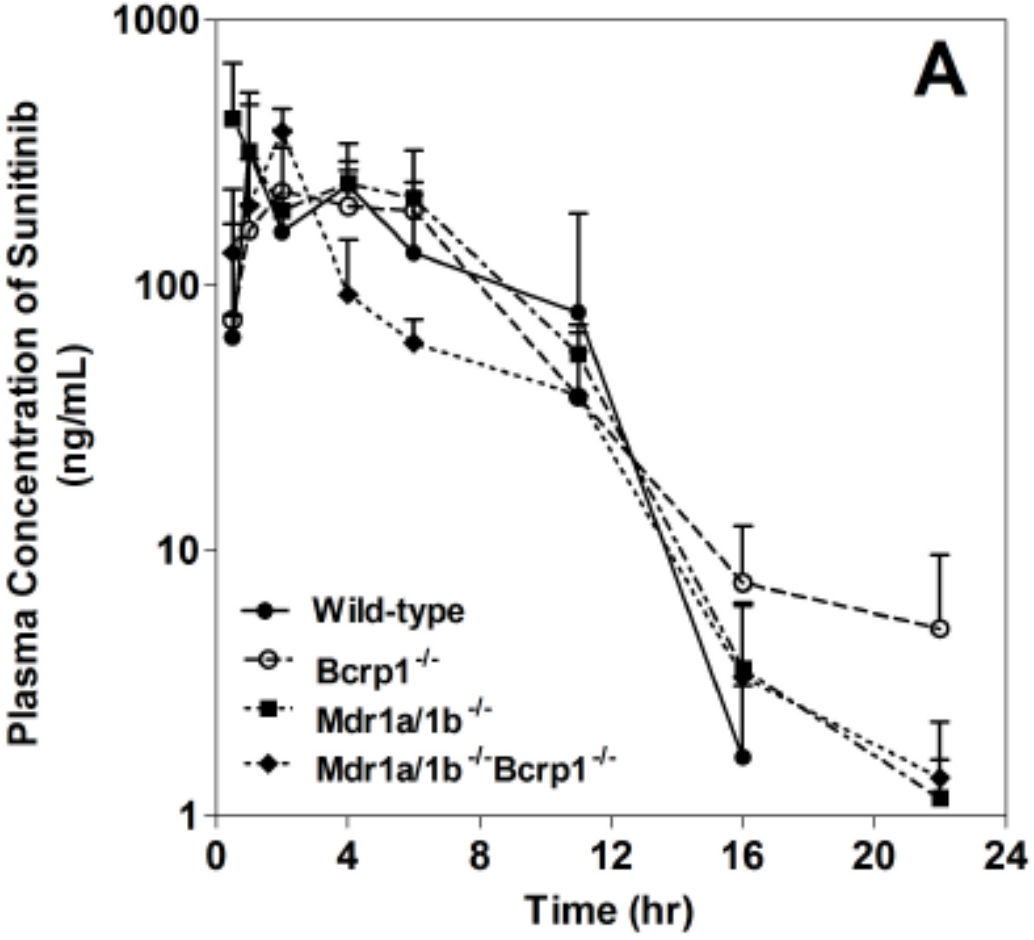

Figure 4.1 (b): corresponding brain concentration-time profiles of sunitinib after a single oral dose (20 mg/kg) in FVB wild-type, Mdr1a/b(-/-), Bcrp1(-/-) and Mdr1a/b(-/-)Bcrp1(-/-) mice

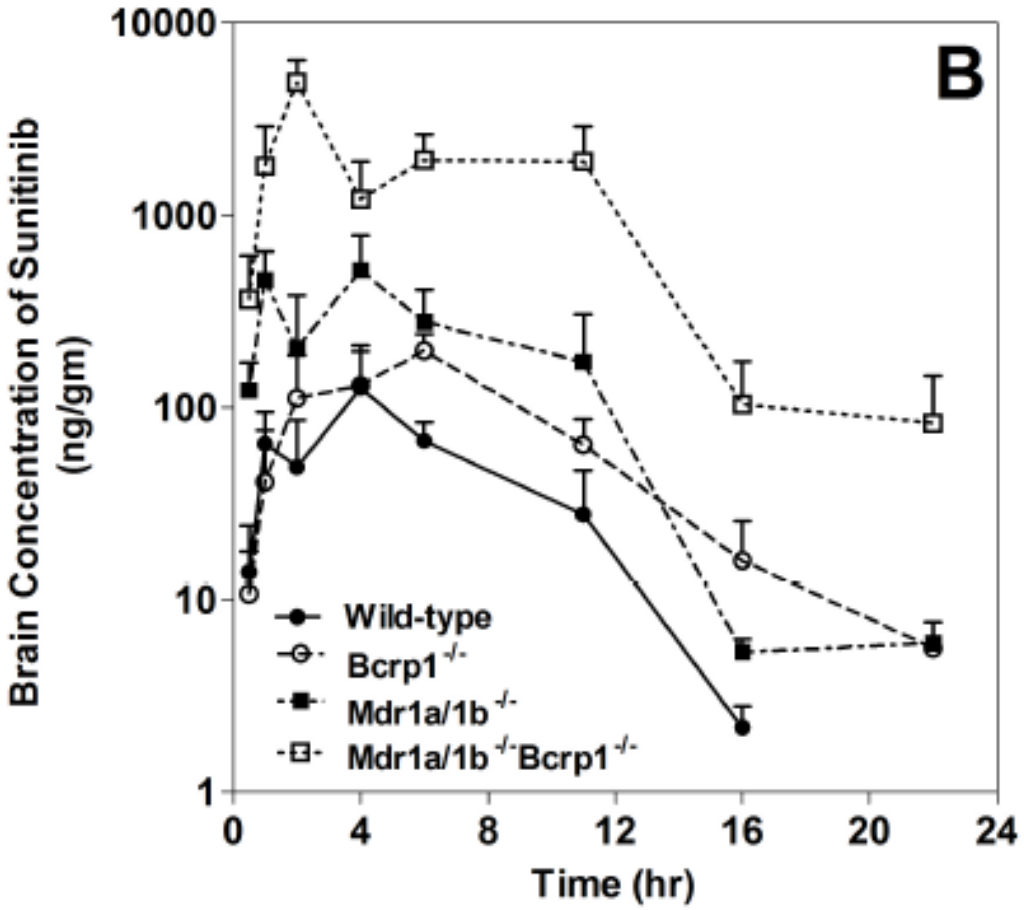

Figure 4.1 (c): Brain-to-plasma ratios with time in wild-type, Mdr1a/b(-/-), Bcrp1(-/-) and Mdr1a/b(-/-)Bcrp1(-/-) mice

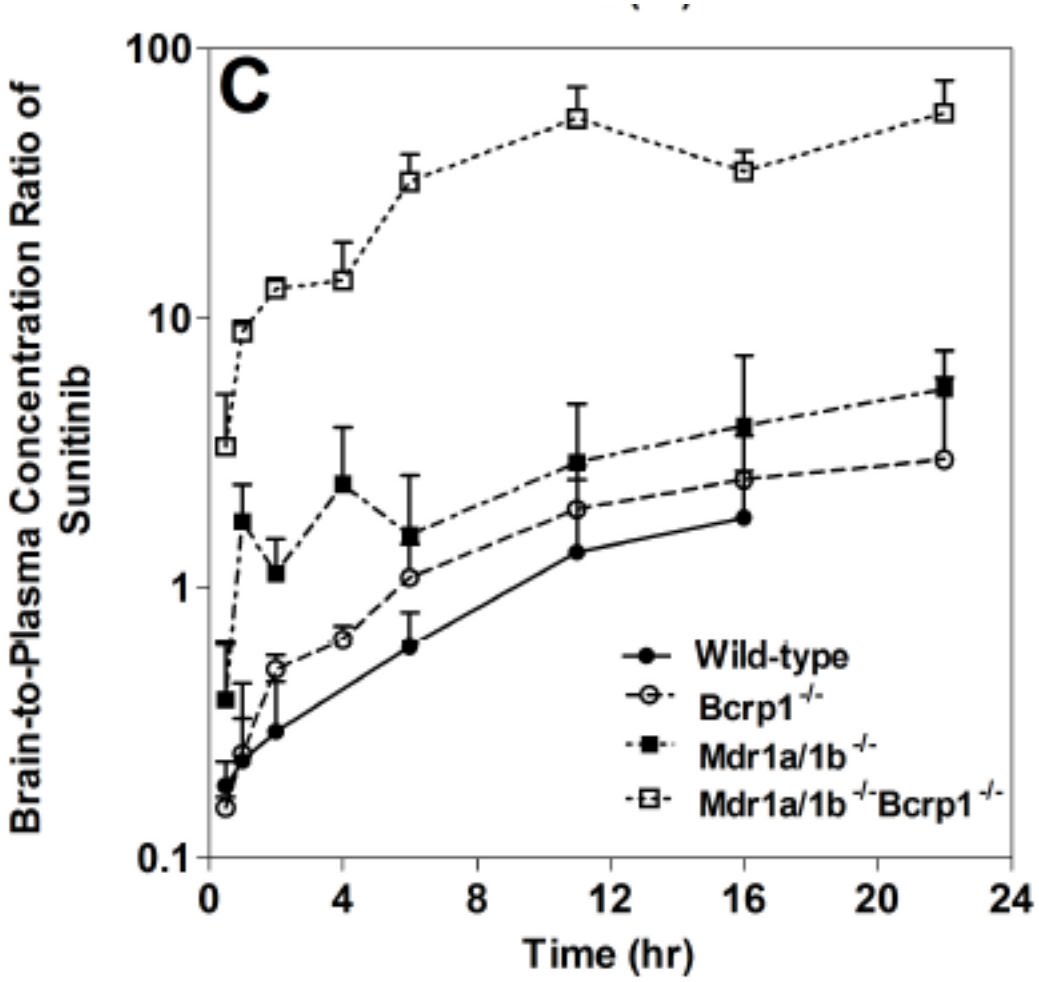

4.3.2 STEADY STATE PLASMA AND BRAIN DISTRIBUTION OF SUNITINIB

An intraperitoneal infusion was employed to clearly elucidate the influence of active efflux by P-glycoprotein and Bcrp on the BBB penetration of sunitinib at steady state. In a system that exhibits linear distribution characteristics, the steady-state tissue-to-plasma concentration ratio should be equivalent to the tissue-to-plasma AUC ratio. The infusion was administered at a constant rate of 30 µg/hr and the plasma and brain concentrations were determined 48 hours (15-20 half-lives) after the start of infusion in wild-type, *Mdr1a/b(-/-)* mice, *Bcrp1(-/-)* mice and *Mdr1a/b(-/-)Bcrp1(-/-)* mice. The steady-state plasma concentrations were not significantly different from each other in the four genotypes, and ranged from 0.195 ± 0.186 µg/mL to 0.264 ± 0.086 µg/mL; another indication that P-gp and Bcrp do not influence the apparent clearance of sunitinib from plasma (**Figure 4.2 (a)).** This is in agreement with the single oral dose study where the apparent clearance of sunitinib is also not altered by active efflux. However, the steady-state brain concentration in the wild-type mice was significantly lower (0.09 ± 0.07 µg/gm) than that observed in the triple knockout mice (4.46 ± 1.66 µg/gm) ($p < 0.05$). When compared to wild-type mice, the brain steady-state concentrations were not different in the *Bcrp1(-/-)* mice (0.09 ± 0.04 µg/gm), but were 4.3-fold higher in *Mdr1a/b(-/-)* mice (0.39 ± 0.36 µg/gm, $p < 0.05$) (**table 4.2, Figure 4.2 (b))**. The steady-state brain-to-plasma ratio was 2.33 ± 0.56 in *Mdr1a/b(-/-)* mice and 0.73 ± 0.44 in *Bcrp1(-/-)* mice, whereas, in the *Mdr1a/b(-/-)Bcrp1(-/-)* mice it was 17.44 ± 5.08, a 34-fold increase in sunitinib brain distribution when both of the transporters are absent. These steady-state data indicate that a single deletion of either P-gp or Bcrp does not

impact sunitinib brain distribution to a great extent, however deletion of both transporters result in a significant increase in sunitinib brain distribution (**figure 4.2 (c)**).

Table 4.2: Steady state plasma and brain concentrations of sunitinib in wild-type, Mdr1a/b(−/−), Bcrp1(−/−), and Mdr1a/b(−/−)Bcrp1(−/−) mice after a constant intraperitoneal infusion of sunitinib at a rate of 30 µg/hr for 48 hrs (n =4 each group). *Data presented as mean ± S.D., #P < 0.005 compared to wild-type.

Genotype	*Plasma Css (µg/ml)	*Brain Css (µg/gm)	Brain-to-plasma ratio
FVB-wild type	0.19 ± 0.16	0.09 ± 0.06	0.51 ± 0.26
Mdr1a/b(-/-)	0.18 ± 0.15	0.39 ± 0.36	2.33 ± 0.56#
Bcrp1(-/-)	0.19 ± 0.19	0.09 ± 0.04	0.73 ± 0.44
Mdr1a/b(-/-)Bcrp1(-/-)	0.26 ± 0.09	4.46 ± 1.66#	17.44 ± 5.08#

Figure 4.2: (a) steady-state plasma concentrations of sunitinib after a continuous intraperitoneal infusion at 30 µg/hr for 48 hrs in wild-type, Mdr1a/b(-/-), Bcrp1(-/-) and Mdr1a/b(-/-)Bcrp1(-/-) mice; (b) corresponding steady-state brain concentrations of sunitinib in wild-type, Mdr1a/b(-/-), Bcrp1(-/-) and Mdr1a/b(-/-)Bcrp1(-/-) mice; (c) steady-state brain-to-plasma ratios of sunitinib

Data represented as Mean ± S.D.

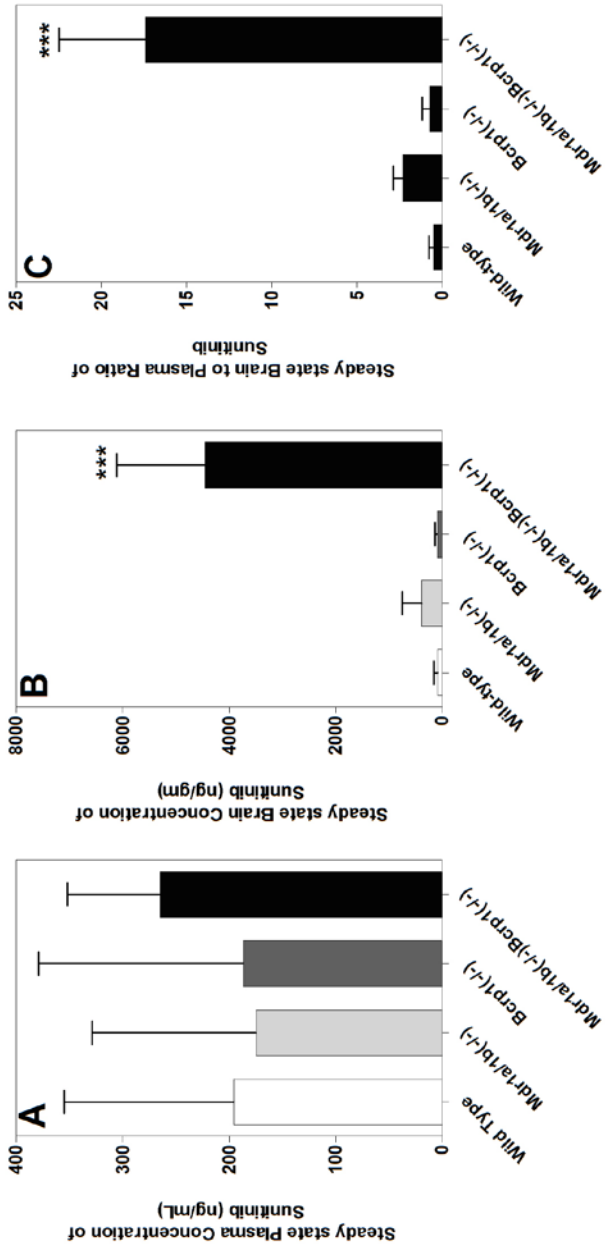

These results are in agreement with the previous report by Tang et al. (Tang et al., 2012)**.** The authors reported sunitinib brain distribution across the same genotypes of mice at a single time point (6 hr post oral dose). Since the efflux clearance from brain depends on the relevant efflux transporters available [i.e., present (WT) vs. absent (transgenic knockout mice)], determination of brain-to-plasma ratio at a single time point may lead to significant errors, depending on the time point and the distribution kinetics of the drug (Wang, 2011). Further, if the chosen time point does not represent a steady state, then the brain-to-plasma ratio will change with time until pseudo-distributional equilibrium is achieved in the terminal phase **(see Figure 4.1 (c)).** However, it is important to note that, after a single dose or intermittent multiple dosing, the steady-state condition for brain distribution can be approximated by a transient steady state in the brain, which will occur at a specific time that corresponds to the maximum concentration in the brain (peak brain concentration) relative to the plasma concentration at that same time (Tmax of drug in brain). Determination of tissue distribution at a single time point can however, be done at transient steady-state, that is, when the drug concentration in the target tissue is at maximum ($C_{max,\ tissue}$). At this point, the rate of change of drug concentration in the target tissue, which in this case, is the brain, is equal to zero, implying that the rate into the brain is at pseudo-distributional equilibrium with the rate out of the brain. In our results, we observed that the steady-state brain-to-plasma concentration ratio ($C_{ss\ brain}/C_{ss\ plasma}$) in all four genotypes was similar to the corresponding brain-to-plasma partition coefficient (Kp) observed after oral dose (AUC_{brain}/AUC_{plasma}), which in turn was comparable to that obtained at transient steady-state ($C_{brain,\ max}/C_{plasma}$), and at 1 hr post oral dose ($C_{brain,\ 1\ hr}$

po/C_{plasma}, 1 hr po) in all genotypes. **(Table 4.3).**

Table 4.3: Brain-to-plasma ratios of sunitinib in all genotypes after a single oral dose (20 mg/kg), steady state concentration ratios after a continuous intraperitoneal infusion (rate equal to 30 µg/hr), at transient steady state (calculated as the maximum brain concentration to the corresponding plasma concentration in each genotype) and concentration ratios determined at 1 hr post oral dose (20 mg/kg) in each genotype. Data presented as mean ± S.D.

Genotype	AUC_0^{∞} p.o.	C_{ss} steady-state i.p.	Transient steady-state	Ratio at 1 hr
FVB-wild type	0.42	0.51 ± 0.26	0.66 ± 0.17	0.42 ± 0.09
Mdr1a/b(-/-)	1.61	2.33 ± 0.56	2.42 ± 1.42	1.76 ± 0.65
Bcrp1(-/-)	0.88	0.73 ± 0.44	1.09 ± 0.38	0.24 ± 0.20
Mdr1a/b(-/-)Bcrp1(-/-)	20.53	17.44 ± 5.08	12.83 ± 1.26	8.14 ± 3.47

4.3.3 INHIBITION OF P-GP AND BCRP INFLUENCES THE BRAIN DISTRIBUTION OF SUNITINIB

In the past, many research groups have employed two approaches to delineate the contribution of efflux transporters in drug delivery to the CNS: 1) a genetic approach with the use of genetically knockout transgenic mice, and 2) pharmacological inhibition of P-gp and Bcrp at blood-brain barrier (Wang et al., 2012)**.**

In this study, we have compared the above approaches by comparing the brain-to-plasma concentration ratio at 1 hr (plasma Tmax in wild-type, **Table 4.1**) after an oral dose of 20 mg/kg sunitinib in genetically knockout mice (*Mdr1a/b(-/-), Bcrp1(-/-)* and *Mdr1a/b(-/-)Bcrp1(-/-)*) to the wild-type mice that were administered pharmacological inhibitors of these two efflux transporters. Genetic deletion of transporters resulted in a drug targeting index at a single time point, 1 hr of 0.5 in Bcrp knockout mice, 3.7-fold in P-gp knockout mice and 17.3-fold in triple knockout mice. Administration of pharmacological inhibitors did not influence the plasma concentration of sunitinib at this time point (**Figure 4.3 (a)),** however significant differences were observed in the brain concentrations (**Figure 4.3 (b)).** A specific Bcrp inhibitor (Ko-143, 10 mg/kg) and a specific P-gp inhibitor (zosuquidar, LY335979, 25 mg/kg) resulted in brain targeting of 0.9-fold and 3.5-fold, respectively. In addition, a 12-fold increase in brain targeting of sunitinib was observed on administration of the dual P-gp/Bcrp inhibitor (elacridar, GF120918, 10 mg/kg). The brain targeting of sunitinib using these pharmacological inhibitors was comparable to that observed with the transgenic mice **(Figure 4.3 (c)).**

Figure 4.3 (a): plasma concentrations of sunitinib at 1 hr post oral dose (20 mg/kg) in wild-type mice after administration of selective P-gp inhibitor (LY335979 (25 mg/kg)), selective Bcrp inhibitor (Ko-143 (10 mg/kg)), both LY335979 and Ko143, and dual P-gp/Bcrp inhibitor (elacridar (10 mg/kg)), selective P-gp inhibitor in Bcrp1(-/-) and selective Bcrp inhibitor in Mdr1a/b(-/-) mice. The plasma concentrations with pharmacological inhibition are compared at 1 hr in transgenic transporter-deficient mice

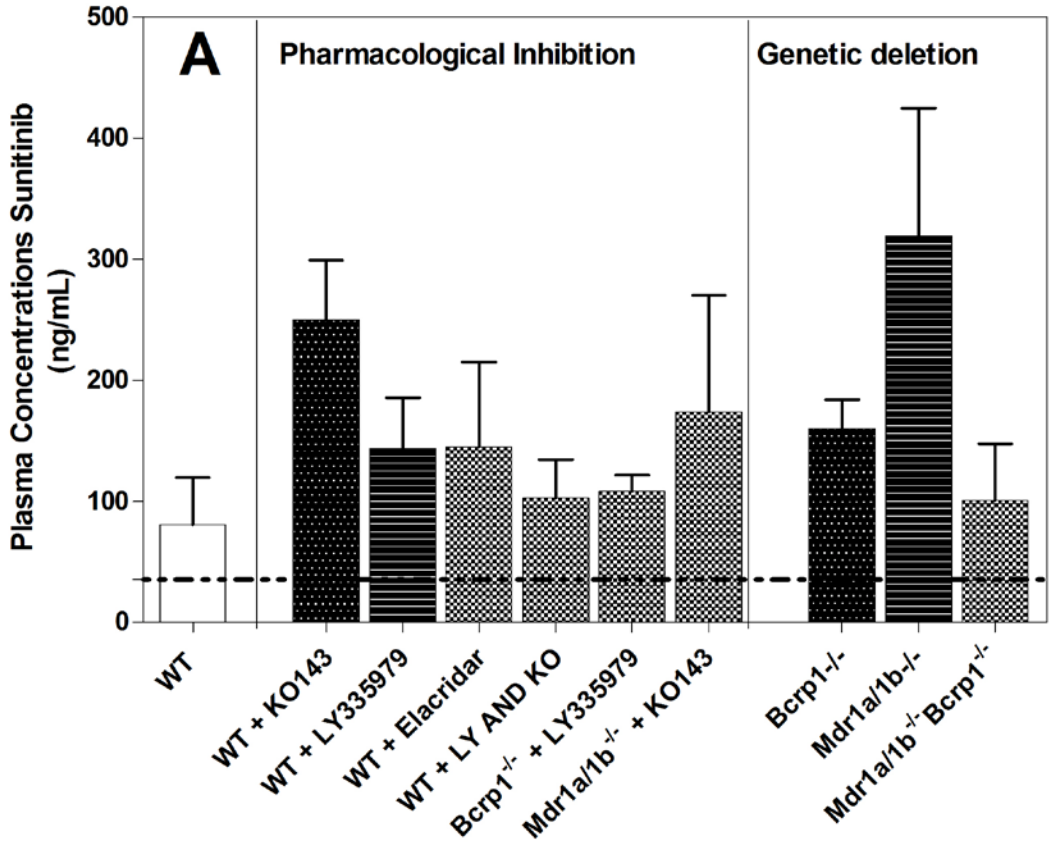

Figure 4.3 (b): Corresponding brain concentrations of sunitinib in the treatment group at 1 hr post oral dose (20 mg/kg) in wild-type mice after administration of selective P-gp inhibitor (LY335979 (25 mg/kg)), selective Bcrp inhibitor (Ko-143 (10 mg/kg)), both LY335979 and Ko143, and dual P-gp/Bcrp inhibitor (elacridar (10 mg/kg)), selective P-gp inhibitor in Bcrp1(-/-) and selective Bcrp inhibitor in Mdr1a/b(-/-) mice. The brain concentrations with pharmacological inhibition are compared at 1 hr in transgenic transporter-deficient mice

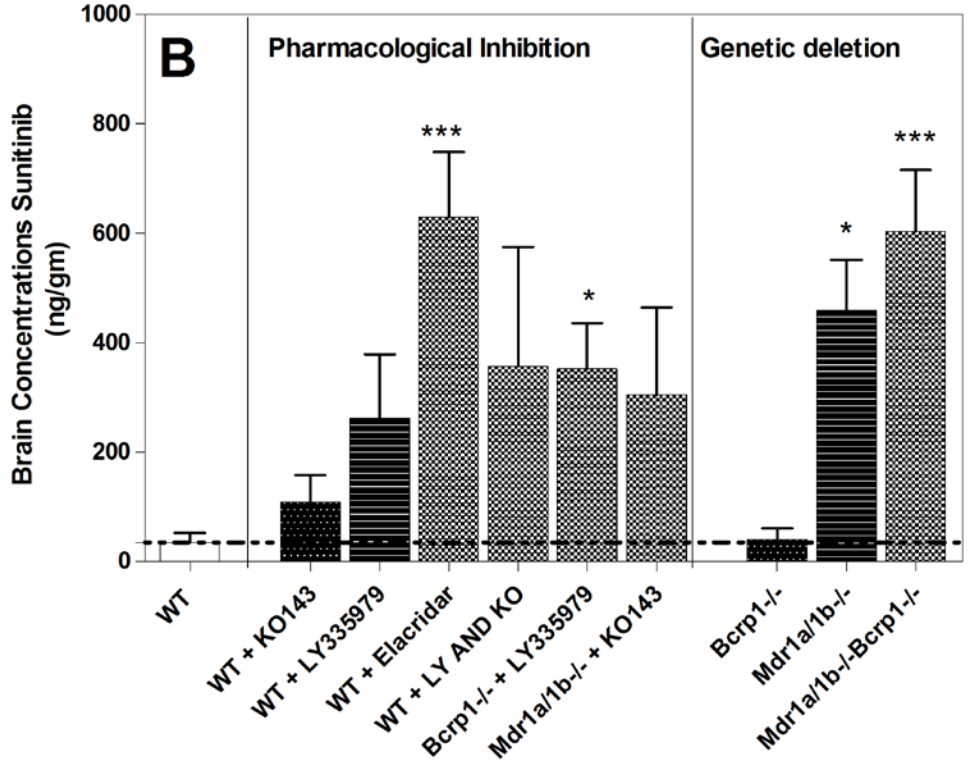

Figure 4.3 (c) corresponding brain-to-plasma ratios of sunitinib at 1 hr post oral dose (20 mg/kg) in wild-type mice after administration of selective P-gp inhibitor (LY335979 (25 mg/kg)), selective Bcrp inhibitor (Ko-143 (10 mg/kg)), both LY335979 and Ko143, and dual P-gp/Bcrp inhibitor (elacridar (10 mg/kg)), selective P-gp inhibitor in Bcrp1(-/-) and selective Bcrp inhibitor in Mdr1a/b(-/-) mice.

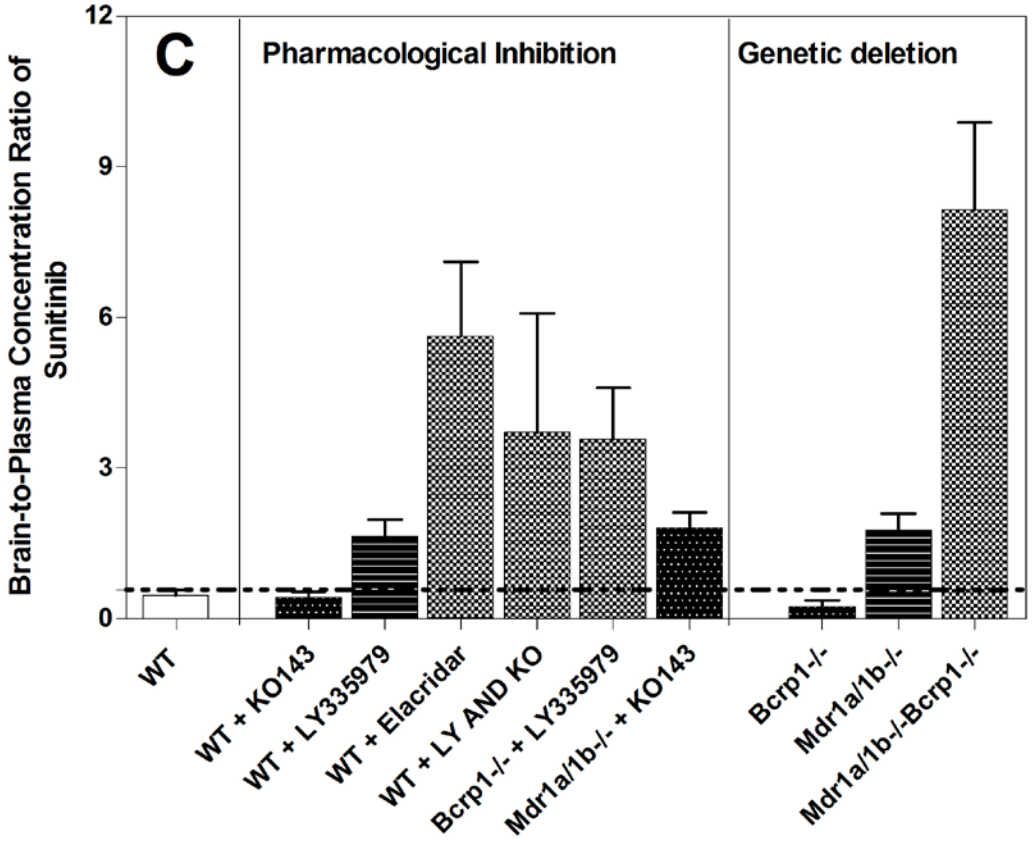

Importantly, the current study examines the effect of the specific P-gp inhibitor, zosuquidar, in *Bcrp1(-/-)* mice, and the specific Bcrp inhibitor, Ko-143, in *Mdr1a/b(-/-)* mice on sunitinib brain distribution. Further, simultaneous inhibition of P-gp and BCRP was achieved by administration of both zosuquidar and Ko-143 to the FVB wild-type mice. The plasma and brain concentrations from these mice were determined at 1 hr post oral dose of 20 mg/kg sunitinib. The brain-to-plasma ratio was 1.8 in *Mdr1a/b(-/-)* mice who received Ko-143, while the brain-to-plasma ratio in *Bcrp1(-/-)* mice who received zosuquidar was 3.6. However, the cohort of wild-type mice that received both zosuquidar and Ko-143 had a brain-to-plasma ratio of 3.7, where the group that received elacridar and *Mdr1a/b(-/-)Bcrp1(-/-)* mice, had a brain-to-plasma ratio of 5.6 and 8.1, respectively **(Figure 4.3, table 4.4)**.

These results show the correlation between the use of selective and non-selective pharmacological transport inhibitors and specific genetic deletion of transporters in the brain distribution of sunitinib. This agreement between the two approaches also indicates that, for sunitinib, it is likely that Ko143 and LY335979 are truly selective for the inhibition of Bcrp and P-gp, respectively. Moreover, in this regard, we have previously determined (Agarwal et al., 2012) via quantitative proteomics approach that genetic deletion of P-gp and Bcrp does not influence the expression of several transport systems at the BBB and P-gp or Bcrp do not compensate for the loss of one another by up-regulation of the other's expression in the BBB.

Table 4.4: Comparison of brain-to-plasma ratio of sunitinib in transgenic transporter deficient mice and in FVB-wild type treated with specific P-gp and/or Bcrp inhibitors.

Pharmacological Inhibition		**Genetic Deletion**	
	Mean ± SD		Mean ± SD
Wild-type	0.47 ± 0.18	Wild-type	0.47 ± 0.18
Wild-type+ LY335979	1.64 ± 0.57	*Mdr1a/b(-/-)*	1.76 ± 0.65
Wild-type + Ko-143	0.42 ± 0.24	*Bcrp1(-/-)*	0.24 ± 0.20
Wild-type + elacridar	5.63 ± 2.33		
Wild-type + LY335979 + Ko143	3.71 ± 2.37	*Mdr1a/b(-/-)Bcrp1(-/-)*	8.14 ± 3.47
Mdr1a/b(-/-) + Ko143	1.81 ± 0.59		
Bcrp1(-/-) + LY335979	3.56 ± 2.08		

4.4 DISCUSSION

The objective of this study was to investigate and pharmacokinetically assess mechanisms that limit brain distribution of sunitinib for the treatment of glioblastoma multiforme (GBM). Gliomas are fatal brain tumors characterized by high degree of microvascular proliferation with endothelial cell migration. A highly invasive tumor, the cells have a strong tendency to migrate in other parts of the brain and hide beneath an intact BBB (Agarwal et al., 2011a)**.** It is therefore important to achieve adequate drug concentrations across the BBB, in the brain parenchyma, to target the tumor cells that reside in the growing edge of the tumor as well as in the distant sites of the brain. Previous preclinical investigations have suggested that efflux transporters, P-gp and Bcrp, limit the delivery of several anti-cancer agents into the brain. In the current study, we have examined the influence of P-gp and Bcrp, in restricting the brain distribution of sunitinib in the FVB strain; wild type, *Mdr1a/b(-/-)*, *Bcrp1(-/-)*and *Mdr1a/b(-/-)Bcrp1(-/-)* mice using novel pharmacokinetic tissue distribution assessment methods, and proposed strategies to improve its delivery across BBB based on efflux transport inhibition.

Sunitinib is a multi-targeted tyrosine kinase inhibitor with activity against VEGFR 1-3 and PDGFR-α/β, in addition to other regulators of tumor growth and angiogenesis (Christensen, 2007). As a pan-inhibitor of VEGFR, particularly VEGFR2, sunitinib represents an attractive treatment option as an anti-angiogenic drug in the therapy of glioma. However, clinical trials using sunitinib (Neyns et al., 2011; Pan et al., 2012) and several molecularly targeted agents (e.g., cediranib, pazopanib, vandetanib) have shown

to be unsuccessful in GBM therapy (Batchelor et al., 2010; Iwamoto et al., 2010; Kreisl et al., 2012)**.** This may be due in part to the limited delivery of these agents across BBB (Minocha et al., 2012a; Wang et al., 2012).

To quantify the influence of efflux transporters, P-gp and Bcrp, on the brain distribution of sunitinib, we performed oral pharmacokinetic studies in FVB mice, wild-type, *Mdr1a/b(-/-), Bcrp1(-/-)* and *Mdr1a/b(-/-), Bcrp1(-/-)*. Plasma and brain concentration-time profiles were determined in all the four groups. $AUC_{0-\infty,\ plasma}$ were not different amongst all four genotypes; however, $AUC_{0-\infty,\ brain}$ were different amongst all groups. Although sunitinib showed substantial partitioning into the brain (Kp = 0.42), deletion of both P-gp and Bcrp resulted in an AUC brain-to-plasma ratio of 20.5. Single deletion of P-gp or Bcrp had a little influence on the brain distribution of sunitinib; however, a notable difference was observed in the absence of both these transporters. This suggest that both P-gp and Bcrp act in a concerted fashion to limit the brain distribution of sunitinib **(Table 4.1, Figure 4.1).** The drug targeting index (DTI) of sunitinib for the brain was 3.9 in *Mdr1a/b(-/-)* mice and 2.1 in *Bcrp1(-/-)* mice. The DTI in *Mdr1a/b(-/-)Bcrp1(-/-)* mice was 48.9, indicating a significant role of both P-gp and Bcrp on sunitinib's brain distribution.

Further, to examine the penetration of sunitinib across the BBB, we determined the steady state brain-to-plasma ratios ($C_{ss,\ brain}/C_{ss,\ plasma}$) in wild type and transgenic transporter-deficient mice using a continuous intraperitoneal infusion lasting 48 hours.

Although, the plasma concentrations at steady state were not different among all groups, suggesting that the systemic distribution of sunitinib is not influenced by active efflux via P-gp and Bcrp, the steady-state brain concentrations were significantly greater in the group that lacked both P-gp and Bcrp ($p < 0.05$) **(Figure 4.2, Table 4.2).** The steady state brain-to-plasma ratios in wild type, *Mdr1a/b(-/-), Bcrp1(-/-)* and *Mdr1a/b(-/-)Bcrp1(-/-)* mice were 0.51 ± 0.26, 2.33 ± 0.56, 0.73 ± 0.44 and 17.44 ± 5.08, respectively. These ratios are comparable to the corresponding AUC brain-to-plasma ratios determined after a single oral dose **(Table 4.3).**

Earlier, Tang et al. reported the influence of P-gp and Bcrp on the brain distribution of sunitinib (Tang et al., 2012) across the transporter-deleted genotypes of mice, at 6 hr post single oral dose. Estimation of true drug partitioning into a tissue at a single time point can misguide interpretation of the effect of efflux transport on tissue distribution, depending on the chosen time point and the differences in the distributional kinetics of the drug under investigation. Characterization of brain distribution at a transient steady state can be considered to be an estimate of the steady-state tissue partitioning since it is at that point in time when the rate of drug entry into the brain is equal to the rate out of the brain **(Table 4.3).** Estimation of the brain-to-plasma distribution using a single time point before or after attainment of $C_{max\ brain}$ can lead to an under- or over-estimation of the true tissue (brain) partition coefficient. Therefore, determining brain distribution at only one time point may be misleading depending on when the brain/plasma concentration ratio is determined, which is dependent on when the brain is sampled. Riad et al. have

earlier studied this “transient steady state” approach for carbamazepine metabolites in humans (Riad et al., 1993)**.** In our study, we found that the AUC brain-to-plasma ratio after single oral dose was similar to both the steady-state brain-to-plasma ratio and the brain-to-plasma ratio at a transient steady state **(Table 4.3).**

Besides using transporter knockout mice, we also studied the effect of administering specific P-gp or Bcrp inhibitors and a dual inhibitor of P-gp and Bcrp on the plasma and brain concentration of sunitinib at 1 hr post oral dose of sunitinib. Results from this study indicated that plasma concentrations were not different at 1 hr in all treatment groups **(Figure 4.3 (a))** and brain concentrations were not different in the cohorts that received specific P-gp inhibitor, zosuquidar, and specific Bcrp inhibitor, Ko-143. However, a ~12 fold increase in the brain-to-plasma ratio was observed in the group of mice that received dual P-gp and Bcrp inhibitor, elacridar. These findings were comparable to that observed with the knockout mice **(Figure 4.3 (b) and (c), Table 4.4).**

The results from this study warranted further investigation on the potential role of P-gp and Bcrp in mediating the active efflux of sunitinib from brain. To examine this, we administered specific P-gp inhibitor to *Bcrp1(-/-)* mice and specific Bcrp inhibitor to *Mdr1a/b(-/-)* mice. Additionally, we also administered both zosuquidar and Ko-143 to wild type mice and determined plasma and brain concentrations of sunitinib at 1 hr. To the best of our knowledge, this is the first time that such an approach has been employed to understand the role of P-gp and Bcrp in the distribution of sunitinib. The results from

this study confirmed our results from the single oral dose study and steady-state distributional kinetics, i.e., that sunitinib is actively effluxed by both P-gp and Bcrp at the BBB. It is important to note here that the brain-to-plasma concentration ratio of sunitinib in the groups of mice receiving pharmacological inhibitors for both P-gp and Bcrp were not significantly different from the single knockout mice receiving specific P-gp or Bcrp inhibitor and the corresponding transgenic mice **(Figure 4.3 (c)).** The concordance between these approaches (use of transgenic mice vs. pharmacological inhibitors) to determine the impact of efflux transport via P-gp and Bcrp on the brain distribution of sunitinib suggests that pharmacological inhibition can be used as an effective tool to improve the brain distribution of sunitinib for the treatment of glioma. Recently, Kunimatsu and colleagues reported a similar phenomenon on greater accumulation in the brain on dual inhibition of efflux transport in rats (Kunimatsu et al., 2013)**.** This is important since tailored-chemotherapy with sunitinib in an anaplastic meningioma patient expressing PDGFR-β failed to show desirable efficacy (Yoshikawa et al., 2012). It is therefore important to understand that in addition to the intended molecular target, issues related to effective drug delivery are pertinent in treatment of brain tumor.

In conclusion, we have shown that sunitinib has limited penetration into the brain due to the presence of active efflux mediated by both P-gp and Bcrp at the BBB. Single deletion of P-gp or Bcrp does not play a significant role as compared to dual P-gp and Bcrp deletion, indicating a simple functional compensation between these two transporters at the BBB in restricting the brain distribution of sunitinib. We also showed here that the

tissue partition coefficient obtained after single oral dose calculated by the AUC brain-to-plasma ratio is similar to the brain-to-plasma steady-state concentration ratios, which would be expected for non-saturable, linear distributional kinetics. Furthermore, determination of the extent of brain distribution of sunitinib can be determined at a single time point, provided that at the chosen time point, is the time in which a transient steady state is attained between the plasma and the brain. This will occur at a time when the brain concentration reaches a maximum following a single dose. Relying on a single time point not at this transient steady state to determine the brain partition coefficient can lead to significant errors, and complicate the comparison of several studies. Moreover, administration of selective inhibitors of active efflux as well as dual inhibitor of efflux transporters resulted in enhanced brain penetration of sunitinib; in concordance with that observed in transgenic mice. These results can be of clinical significance to improve the brain delivery of sunitinib to areas of tumor cells that lie hidden beneath an intact BBB that has active P-gp and Bcrp transport systems.

4.5 FOOTNOTES

This work was supported by National Institutes of Health Cancer grants CA138437 and NS077921) and the Ronald J. Sawchuk Fellowship in Pharmacokinetics, Department of Pharmaceutics, University of Minnesota (to R.K.O).

CHAPTER V

NON-LINEAR MIXED EFFECT MODELING OF SERIAL SACRIFICE DATA: SENSITIVITY ANALYSIS OF SAMPLE SIZE AND BETWEEN SUBJECT VARIABILITY FOR BRAIN DISTRIBUTION STUDIES

Preclinical pharmacokinetic studies in rodents are often limited by the number of samples that can be withdrawn to one sample (plasma and corresponding tissue) per subject. In this one point per animal design, a naïve-pooled approach is often used to estimate AUCs in tissue and plasma and the AUC ratio is used to estimate distribution coefficients (Kp). Such ratios ignore within-animal correlations; in addition, they are not associated with any statistical certainty. The goals of this study were: (1) to determine the uncertainty associated with ratios of exposure, Kp; (2) examine bias and precision in evaluating the influence of between- subject variability (BSV) and sample size at each time point on estimation of Kp. We used a model drug, sunitinib, to study this approach.

Model: NONMEM VII was used for estimations. Sunitinib has restricted delivery into the brain via efflux mechanisms mediated by P-glycoprotein (P-gp) and breast cancer resistance protein (Bcrp). However, uncertainty in Kp values was not obtained using conventional trapezoidal method for estimation of area under the concentration-time curve from time 0 to infinity ($AUC_{0-\infty}$). Datasets consisted of plasma (Cpl) and brain (Cbr) concentrations after single oral dose (20 mg/kg) and steady-state concentrations (obtained after a continuous intraperitoneal infusion at a rate of 30 µg/hr) of sunitinib. A one-compartment model described Cpl which was used as forcing function to describe Cbr. BSV was fixed to 20% for all parameters. *Simulations:* PsN was used for all simulations. Influence of sample size at each time point (n = 2, 3, 4, 8, 12) and BSV (10%, 20%, 40%) on bias and precision of Kp was evaluated.

The predicted plasma and brain concentrations from the model adequately described the observed values. The Kp ratios were found to be comparable to naïve-pooled method. The values of Kp were relatively insensitive to assumptions regarding BSV. Bias was <1% for levels of BSV and sample size tested. Precision improved with sample size.

Population-based approach for serial-sacrifice data provides variability on AUC-based parameters for statistical evaluation. Assumptions' regarding magnitude of BSV and sample size does not influence parameter estimates but affects precision.

5.1 INTRODUCTION

Preclinical pharmacokinetic and toxicokinetic studies are an essential part of the early drug discovery stage and are usually conducted with a set of guidelines in a homogenous population of animals, both rodent and non-rodent species. The goal is to investigate the disposition of the drug with the primary motive being able to determine its exposure. In large non-rodent species (e.g., monkeys and dogs), serial sampling allows for collection of more than one sample per subject. However, this is not the case in rodents (e.g., rats and mice). Usually, the number of samples that can be obtained is limited to one sample per time point per subject. This kind of sampling procedure is called as a serial-sacrifice design or 'quantic' design (Ette et al., 1995a). A major disadvantage of this procedure is that intra-individual concentration-time course data are not available; hence, estimation of inter-animal variability is a challenge. Conventionally, to determine exposure as the area under the concentration time curve (AUC), concentrations are averaged at each time point and an AUC is calculated using the trapezoidal rule. This is called the naïve data averaging approach and is commonly conducted using a non-compartmental analysis (NCA).

In a tissue distribution study, the primary goal is to determine the tissue distribution coefficient (commonly referred to as $K_{p,\ tissue}$). K_p is determined by obtaining the ratio of $AUC_{0\text{-}inf}$ in tissue and the plasma $AUC_{0\text{-}inf}$. In a serial sacrifice design, one set of paired plasma and tissue concentrations are contributed from each animal. The analysis of this type of data becomes statistically complicated because the within-animal correlation in

the data is ignored when data are averaged in the naïve data pooling approach. Another shortcoming of this method is that a measure of uncertainty associated with the tissue distribution coefficient is not readily calculated. This leads to an inability to statistically compare treatments or groups of animals. A third drawback of this method is that we are unable to estimate inter-animal variability, as we do not obtain intra-individual concentration-time profiles.

Non-linear mixed effect modeling (NLME) approaches have gained wide acceptance as a useful tool to determine population pharmacokinetic (PopPK) and pharmacodynamic (PD) parameters for sparse data. In the past, attempts have been made to analyze 'quantic' data using these approaches (Hing et al., 2001) and comparisons have been made with the noncompartmental analysis approach. It has been reported and shown through simulations that the NLME approach offers a more robust method for estimation of population PK parameters (eg., CL and V) (Ette et al., 1995b). Most of the earlier analyses focused on modeling the plasma concentration-time profile data, with exception of a few that considered analysis of both plasma and tissue, although separately. In NLME, variability or randomness in parameter estimates is partitioned into between-subject variability (BSV, or inter-animal variability) and residual-unexplained variability (RUV, a pooled measure of remaining variability, e.g., analytical variability and model misspecification error). In a serial-sacrifice design, it is not possible to distinguish both types of variability because deviation between an observed and predicted concentration could be due to either BSV or RUV and probably both. Hence, the value of one type is

assumed known and fixed, allowing estimation of the other (Hing et al., 2001). It is of concern to understand the sensitivity of NLME when variability of one type is assumed known vs. the other type. In previous attempts, RUV has often been assumed constant to a value (10% (Hing et al., 2001) or 15% (Ette et al., 1995a)) often close to the lowest limit of quantification of the analytical assay method or slightly higher, implying that RUV is primarily determined by assay error, while BSV was estimated. While this approach does have merit, the situation becomes more complicated with two types of outputs (e.g., drug and metabolite or plasma and brain concentrations, or concentration and effect) being measured. While it is obvious that each type of measurement might have different analytical errors associated with it, it is not clear how to ascribe RUV when the two types of measurements also includes different extents of model misspecification. The limitations of currently employed analysis methods (e.g., NCA) and assumptions from previous methods (e.g., fixing RUV while estimating BSV in NLME) led us to seek answers to key questions pertaining to the need for and implications of obtaining variability around a point estimate.

The current investigation was motivated by the results obtained from the brain distribution study of sunitinib in FVB-wild type, *Mdr1a/b(-/-)* (P-gp knockout), *Bcrp1(-/-)* (Bcrp knockout) and *Mdr1a/b(-/-)Bcrp1(-/-)* (triple knockout) (Oberoi et al., 2013). Previously we have conducted this study to evaluate the influence of efflux transporters on the brain distribution of sunitinib by estimation of the brain-tissue distribution coefficient for each genotype. In our model, between-subject variability (inter-animal

variability) was assumed constant and residual unexplained variability was estimated. Further, we examined the influence of the assumed magnitude of BSV at three levels (low, medium, high) and the sample size at each time point (small to large) on the estimation of the tissue distribution coefficient for each genotype by stochastic simulations and estimations *(see methods section)*.

5.2 METHODS

Model development was performed by nonlinear mixed effects modeling using NONMEM® software (version 7.2, Icon Development Solutions, Ellicott City, MD, USA) in conjunction with Visual Fortran compiler (Professional Edition for Windows 11.1, Intel®) and PdxPop (Version 5.1, ICON Development Solutions). Additionally, stochastic simulations and estimations were performed using Perl speaks NONMEM® (version 3.5.3, http://psn.sourceforge.net/) and Pirana® (version 2.5.0, http://www.pirana-software.com/). R-Studio® (version 2.15.0, http://r-project.org/) was used for graphical presentation.

5.2.1 MOTIVATING EXAMPLE

The objective of this study was to determine uncertainty associated with the tissue partition coefficient (*in this case, the tissue is the brain; hence, the brain partition coefficient)* in a serial sacrifice design and compare our proposed method to the approach

traditionally employed, that is, naïve-data averaging approach or noncompartmental analysis (NCA).

Briefly, the data set consisted of plasma and brain concentrations of sunitinib from two separate studies conducted in FVB-wild type, *Mdr1(-/-)*, *Bcrp1(-/-)* and *Mdr1a/b(-/-)Bcrp1(-/-)* mice.

Study 1 consisted of plasma and brain concentrations obtained after a single oral dose of 20 mg/kg. Mice were sacrificed at pre-determined time intervals 0.5, 1, 2, 4, 6, 11, 16 and 22 hours (n=3 or 4 at each time point). Study 2 consisted of plasma and brain concentrations obtained after a continuous intraperitoneal infusion at a rate of 30 μg/hr for 48 hours (n=4 in each group). Therefore, each animal contributed one plasma and corresponding brain concentration. Brain distribution coefficient, Kp, was incorporated as a parameter into the model.

From the given data set, plasma and brain concentrations at each time point were averaged to obtain a mean value. Using trapezoidal rule, area under the concentration time profile from time 0 to time infinity ($AUC_{0\text{-}inf}$) was obtained. This method resulted in a single value of AUC plasma and AUC brain. Kp, the distribution coefficient, was obtained as the ratio of $AUC_{0\text{-}inf}$ brain-to-plasma. This approach is also called as naïve data-averaging approach and results in a single estimate of Kp, without an estimate of variability.

Non compartmental analysis of these data have been reported previously (Oberoi et al., 2013) and the results are summarized in Table 5.1.

5.2.2 PHARMACOKINETIC AND STATISTICAL MODEL

A pharmacokinetic model (**Figure 5.1**) with first order rate of absorption was specified to simultaneously explain the plasma and brain concentration-time course data. The PK model consisted of two inputs, one as a single oral dose and another as a continuous intraperitoneal infusion. The brain concentration-time course was modeled using the plasma concentrations as a forcing function, thus maintaining within-animal correlations.

The plasma concentration time course after a single oral dose and intraperitoneal infusion was explained by a set of differential equations *(see appendix)*. Here, C(p) = plasma concentration and C(br)= brain concentrations. CL/F and V/F are apparent oral clearance and apparent oral volume of distribution and follows normal distribution with variance σ^2, ~N(CL/F, $\sigma^2_{CL/F}$) and ~N(V/F, $\sigma^2_{V/F}$). F is the relative oral bioavailability determined relative to i.p. infusion. A common absorption rate constant, K_a, was assumed for the model. Since our goal was to determine the brain distribution coefficient, we incorporated K_p as a parameter in our model where K_p followed normal distribution with variance σ^2, ~N(K_p, σ^2_{Kp}). CL_{out} was parameterized in terms of K_p and CL_{in}. The PK model was built using NONMEM subroutine ADVAN6 and differential equations were written to

simultaneously model plasma and brain concentrations. A complete schematic of the model is provided in **Figure 5.1.**

A first order conditional estimation method (FOCE) was utilized to obtain population parameter estimates. Between-subject variability (BSV) in parameters ($Ø_I$) was modeled using exponential error model following normal distribution with mean zero and variance σ^2 as shown below:

$$Ø_I = TVØ*\exp(eta); \quad eta \sim N(0, \omega^2_{theta}),$$

where TVØ is the typical value of the parameter in the population. The variance (ω^2) was fixed to 20% for all the parameters in the current model.

Figure 5.1: Schematic representation of the hybrid-population pharmacokinetic model with first order rate of absorption from the gut and peritoneum to simulatenously describe plasma and brain concentration-time profile. Plasma concentrations were defined as a one-compartment model and were used as a forcing function to explain the brain concentrations. The brain distribution coefficient (K_p) is defined as CL_{in}/CL_{out}.

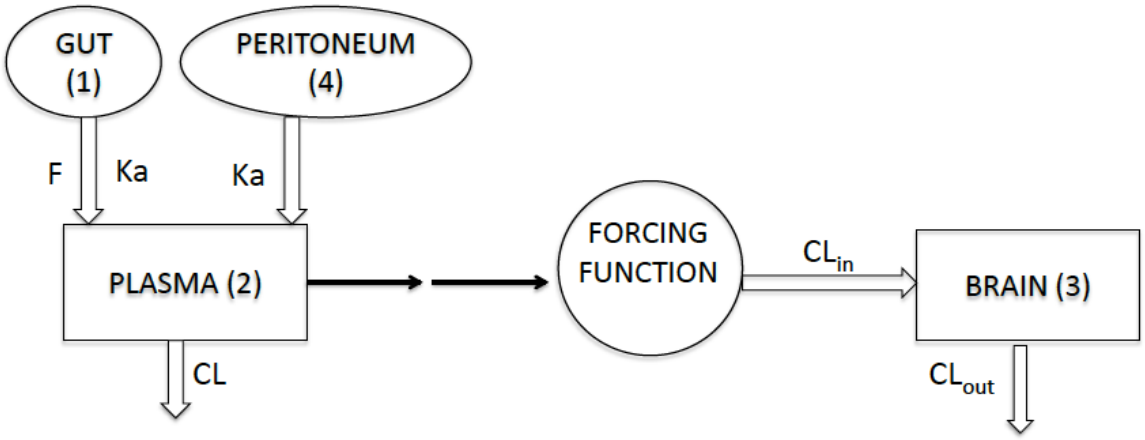

***Error model*:**

Plasma and brain concentrations were modeled separately using proportional error model for each tissue such that observed concentration C_{obs} is given by

$$C_{obs} = C_{pred} * \exp(\varepsilon)$$

Where ε is assumed to follow normal distribution with mean zero and variance σ^2.

5.2.3 DATA ANALYSIS USING NONMEM

We had 127 each plasma and brain concentrations. Non-linear mixed effects modeling approach was implemented in NONMEM (ADVAN6, TRANS1, TOL5, FOCE-estimation method) to simultaneously model sunitinib plasma and brain concentrations. A one-compartment model with a common first order rate of absorption from gut and peritoneum with first order rate of elimination from the central compartment was employed to model plasma concentrations. Brain concentrations were defined by a CL_{in} and a CL_{out} of the brain compartment. The plasma concentration was the driving force for the rate into the brain compartment. The model was parameterized in terms of apparent oral clearance (CL/F_{abs}), apparent volume of distribution (V/F_{abs}), a clearance in (CL_{in}), relative bioavailability (F_{rel}) and brain-partition coefficient (Kp). Variability in the PK parameters was modeled as

$$\Theta = TV\Theta * \exp(\eta_{\Theta}),$$

where TVΘ is the typical value of the parameter and $\eta \sim N(0, \omega^2)$.

We investigated the effect of genotype on K_p, by performing a step-wise covariate analysis where the covariate was the genotype. With prior knowledge that plasma and brain concentrations were obtained from four genotypes, wild-type, *Mdr1(-/-)*, *Bcrp1(-/-)* and *Mdr1(-/-)Bcrp1(-/-)*, we performed our analysis by removing each group one at a time with wild-type as reference and observing the increase in OFV (> 10.83 at p-value < 0.001). *(a)* In the first step, the OFV of the final model (four genotypes as covariates on Kp) was estimated. Subsequently, the effect of genotype was analyzed using following procedure: *(b)* all the knockout animals (*Mdr1(-/-)Bcrp1(-/-), Bcrp1(-/-)* and *Mdr1a/b(-/-)*) were combined into one group and estimated as a single Kp vs. the wild-type, *(c)* in the third step, K_p values for *Mdr1a/b(-/-)* and wild-type were estimated while (*Mdr1(-/-)Bcrp1(-/-) and Bcrp1(-/-)* were combined into one group, *(d)* then K_p values for *Bcrp1(-/-)* and wild type were estimated while (*Mdr1(-/-)Bcrp1(-/-) and Mdr1a/b(-/-)* were combined into one group, *(e)* in the last step, a single K_p was estimated for wild-type, *Bcrp1(-/-) and Mdr1a/b(-/-)* vs. the K_p of *Mdr1a/b(-/-)Bcrp1(-/-)*.

Our final model consisted of genotype added as a covariate on Kp. One of the assumptions we made was that all the animals are from the same homogenous population, therefore, inter-animal variability (BSV) is likely to be less than 50%. The residual unexplained variability (RUV) included not only different analytical errors for plasma and brain concentrations, but also differences in the extent of model misspecification.

Therefore, in this model, BSV was fixed to 20% and RUV was estimated for both plasma and brain concentrations. In order to assess our assumption on fixing BSV = 20%, we performed a sensitivity analysis for BSV from 2.5% to 40%. The effect of BSV on parameter estimates (accuracy and precision given by the point estimate and confidence interval, respectively) was determined. The results of Kp estimation obtained using NONMEM were compared to the values obtained using non-compartmental analysis method (Oberoi et al.).

5.2.4 MODEL EVALUATION

Model evaluation was performed using goodness of fit plots (prediction-based diagnostics and residual-based diagnostics) and simulation-based diagnostics (visual predictive check (VPC)). VPC was implemented within PsN. 500 new datasets were generated through simulations of the final model that described the central tendency and the variability in the observed data obtained through 10^{th} and 90^{th} percentile range. Furthermore, VPC plots were stratified according to genotype and compartment, plasma or brain.

5.3 SIMULATIONS

The purpose of the simulations was to answer two key questions; one, how does the magnitude of assumed between-subject variability influence estimation of brain partition

coefficient (Kp), and second, how does the sample size, that is, number of animals sacrificed at each time point influence estimation of Kp. In the current study, the model used was a one-compartment open model based on the PK model described above.

Individual parameter values for CL, V, CL_{in} and K_p were randomly generated by sampling from the population distribution for eta~ $N(0, \omega^2_{theta})$. The simulation study consisted of a data simulation model and a data analysis model. For the data simulation model, sample size at each time point (n= 2, 3, 4, 8, 12) was evaluated assuming BSV fixed at 20%. The data analysis model was evaluated for 3 levels of BSV (10%, 20%, 40%), that is, the simulated data was estimated as 3 levels of BSV.

The simulations were performed in Pirana using PsN employing stochastic simulations and estimations mode (SSE). SSE is a method that is employed for model comparison and hypothesis testing and gives insight to our models and model performance. In this study, we used SSE as a tool to evaluate model performance and our assumptions for BSV. We performed simulations on the input PK model with BSV fixed at 20% and then estimated all the simulated data sets for each sample size by varying the model paramaters for BSV to 10%, 20% or 40%.

Varying sample size at each time point

The simulated data set was generated at BSV=20% and each animal supplied one plasma and corresponding tissue observation. The number of animals studied at each time point

varied from low to high (n=2, 3, 4, 8, 12). The simulated data set was re-estimated for parameters at BSV=10%, 20% and 40%, thus making total of 15 scenarios that were investigated. The effect of sample size and inter-animal variability on estimation of bias (accuracy) and precision was investigated.

5.4 ANALYSIS

Since the value of the 'true' parameter was known in the simulations, bias and a metric of precision were estimated relative to the known true value.

Bias was calculated as the mean prediction error (MPE) given as the relative difference between the known 'true' value and the 'predicted' value obtained from re-estimation of the simulated data for each scenario. Bias was reported as

$$MPE = (predicted - true)/true$$

A metric for precision was defined as a measure of error that could be tolerated in estimation of the parameter. We determined this metric of precision as the number of times the bias values were within ±5%, ±10% and ±20% of the known 'true' value and plotted for different sample sizes and BSV for each genotype.

5.5 RESULTS

5.5.1 CASE STUDY

We have previously applied NCA approach to assess the brain distribution of sunitinib to the brain (Oberoi et al., 2013). To determine whether P-gp and/or Bcrp play a significant

role in the brain disposition of sunitinib, statistical evaluation between these Kp values needed to be evaluated. The objective of the current investigation was to determine the uncertainty associated with AUC-derived parameters such as the brain partition coefficient (K_p) in a serial sacrifice design. To achieve this goal, we employed a non-linear mixed effect modeling approach to destructively sampled data. A hybrid pharmacokinetic model was applied to simultaneously explain plasma and brain concentration-time profile in all four genotypes. This method ensured that within-animal correlations were maintained. **Table 5.1** displays the AUC brain-to-plasma ratios obtained from NCA and population analysis method. No measures of uncertainty around the estimates of Kp were obtained from NCA whereas the estimates of Kp from the population analysis method had associated estimates of precision. All parameter estimates obtained using NONMEM had relative standard error (RSE) % less than 20% and the values of point estimates were similar to those determined using NCA. These model-based results also suggest that both P-gp and Bcrp play a significant role in influencing the brain distribution of sunitinib.

Table 5.1: Final parameter estimates of the brain distribution coefficient determined by noncompartmental analysis (NCA) and population based approach. RSE% = percent relative standard error, C.I.= 95% confidence interval = estimate ± 1.96*(standard error of estimate) (Oberoi et al., 2013).

Model parameters	Population estimate (%RSE)	95% C.I.	Parameter estimate (NCA)
Kp wild type	0.402 (17)	0.27, 0.53	0.42
Kp *Mdr1a/b(-/-)*	2.02 (17)	1.36, 2.68	1.61
Kp *Bcrp1(-/-)*	0.88 (16)	0.604, 1.15	0.88
Kp *Mdr1a/b(-/-) Bcrp1(-/-)*	17.6 (12)	13.3, 21.9	20.53
Residual variability			
Proportional error- plasma	73.8%		NA
Proportional error- brain	59.6%		NA

We also evaluated our assumption of fixing the BSV to 20% in the model for evaluation of Kp using sensitivity analysis, wherein the BSV was tested across range from 2.5 % to 40%. **Table 5.2** displays the results from sensitivity analysis of varying BSV on the point estimate of Kp. The values obtained for Kp were similar across the range of BSV values tested with no clear trend in values as BSV increased. These results suggest that BSV has little impact on estimation of Kp in a serial sacrifice design.

Table 5.2: Sensitivity analysis of varying between-subject variability on point estimate of brain distribution coefficient, K_p determined by population-based approach. The estimates were compared to the values obtained by noncompartmental analysis (NCA). (Oberoi et al., 2013).

	NCA	2.5%	5%	20%	30%	40%
Kp- Wild type	*0.42*	0.394	0.394	0.402	0.382	0.35
Kp- P-gp Knockout	*1.61*	2.1	2.11	2.02	1.87	1.56
Kp- Bcrp Knockout	*0.88*	0.853	0.852	0.878	0.874	0.831
Kp- Bcrp/P-gp knockout	*20.53*	16.9	17	17.6	17.4	16.5
Proportional error-plasma (%)		84.3	82.4	73.8	67.5	41
Proportional error-brain (%)		74.5	73.1	59.6	49	40

5.5.2 MODEL EVALUATION

The goodness of fit plots are shown in **Figure 5.2.** The model predicted plasma and brain concentrations in all four genotypes reasonably fit the observed data. **Figure 5.2 (a)** shows observed concentrations vs. model predicted concentrations. The individually observed plasma and brain concentrations, stratified by genotype indicated by color, do not deviate substantially from model predicted individual and population predicted concentrations **(Figure 5.2 (b) and (c)).**

The conditional weighted residuals (CWRES) vs. time which is a weighted difference between observed and predicted suntinib concentrations, were randomly distributed around zero and were within 2 units from the zero-ordinate, indicating that the structural model plausibily fits the observed data.

Figure 5.2 (a): Shows model predicted and observed concentrations in the plasma and brain of all four genotypes, wild-type, Mdr1a/b(-/-), Bcrp1(-/-) and Mdr1a/b(-/-)Bcrp1(-/-).

The black and red dots represent observed plasma and brain concentrations and the solid black and red lines indicate model predicted plasma and brain concentration-time profile.

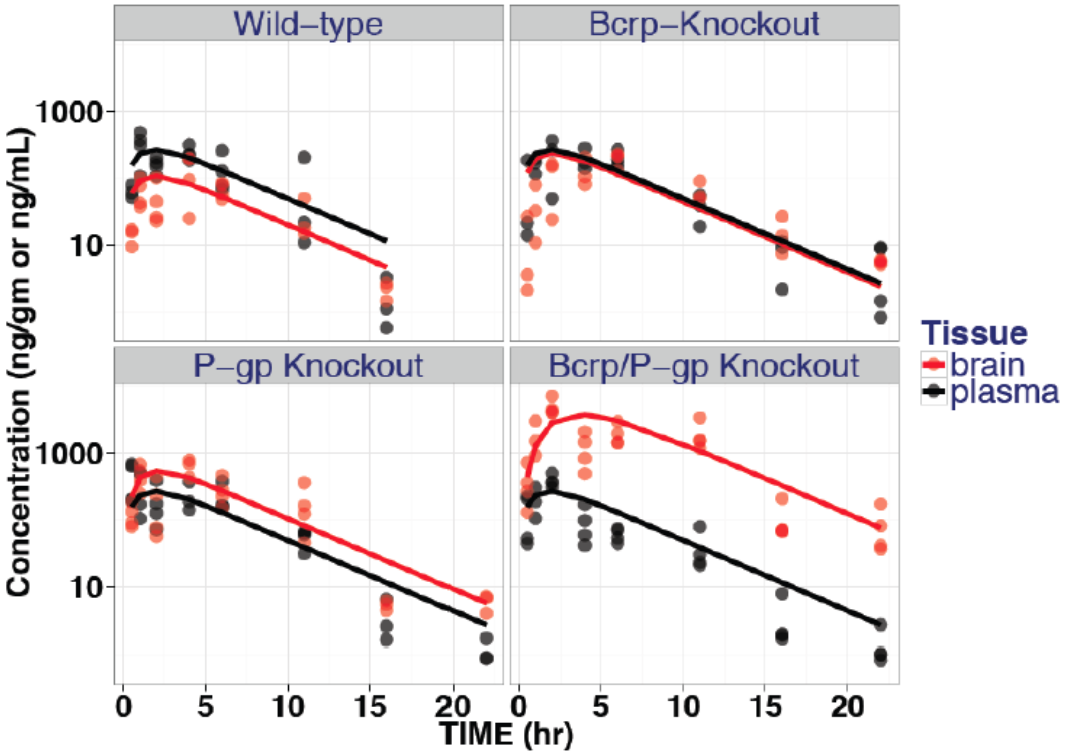

Figure 5.2 (b): Goodness-of-fit plots for the final hybrid pharmacokinetic model for plasma stratified (color-coded) by genotypes

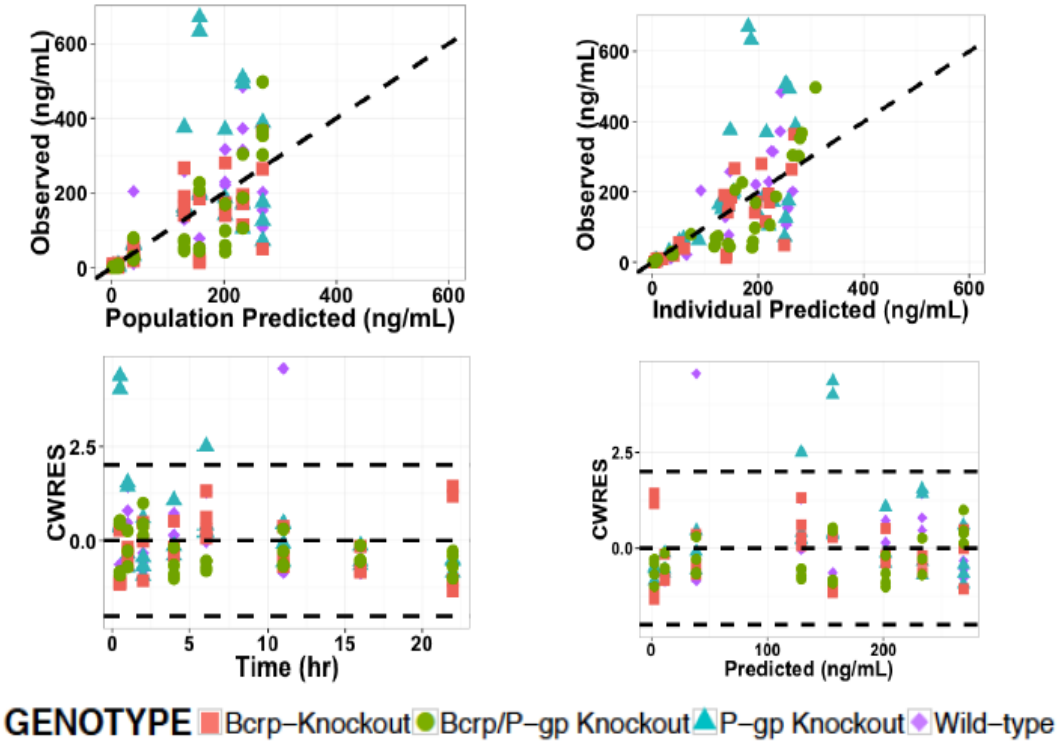

Figure 5.2 (c): Goodness-of-fit plots for the final hybrid pharmacokinetic model for brain stratified (color-coded) by genotypes

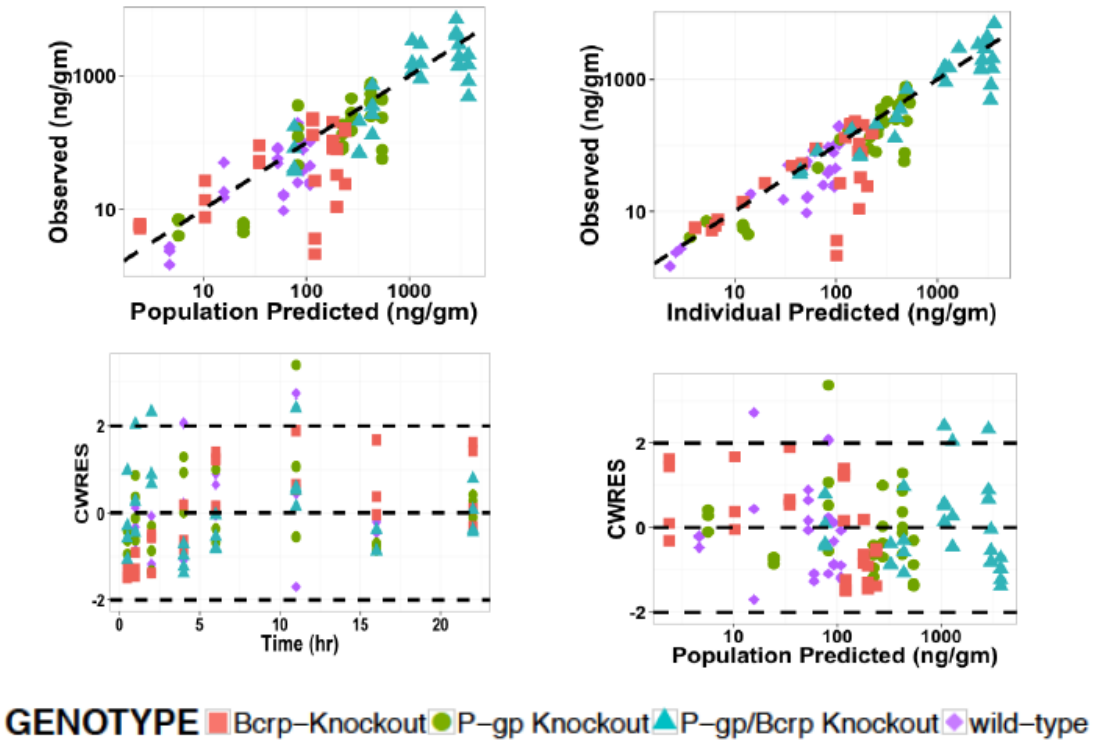

For the VPC, the observed data for all genotypes was simulated to form 500 new datasets using the same experimental design and parameter estimates. The 10^{th} and 90^{th} percentile of the simulated data were calculated and plotted against the observed concentrations. The 50^{th} percentile of the median of the observed data and simulated data were plotted and compared as shown in **figure 5.3.**

The visual predictive checks were stratified by tissue and genotypes. The lower bound predictions for the wild-type plasma showed a negative trend indicating that the lower tail of normal distribution predict concentrations that are below the lowest limit of quantification of the analytical method. Log-transformation of plasma data, use of exponential error model or restricting the predicted plasma concentrations to the lowest standard value are alternatives that have been suggested previously. However, we think such a modification could introduce bias in interpretation. The estimate of residual proportional error for plasma and brain are ~74% and 60%, respectively. Negative predictions of concentrations could also have been caused by high estimates of RUV. Since we fixed BSV to 20%, the remaining error not explained by the model was pooled into RUV, which could attribute to the high estimates of RUV for both plasma and brain.

Figure 5.3 (a-d) Concentration-time profile of sunitinib in plasma and brain stratified by genotypes. Observed concentrations (grey dots), median of observed concentrations (solid red line), population predicted concentrations by simulations (median = black solid line), 10th and 90th percentile (black dotted line) are depicted for each genotype.

(a) Wild-type

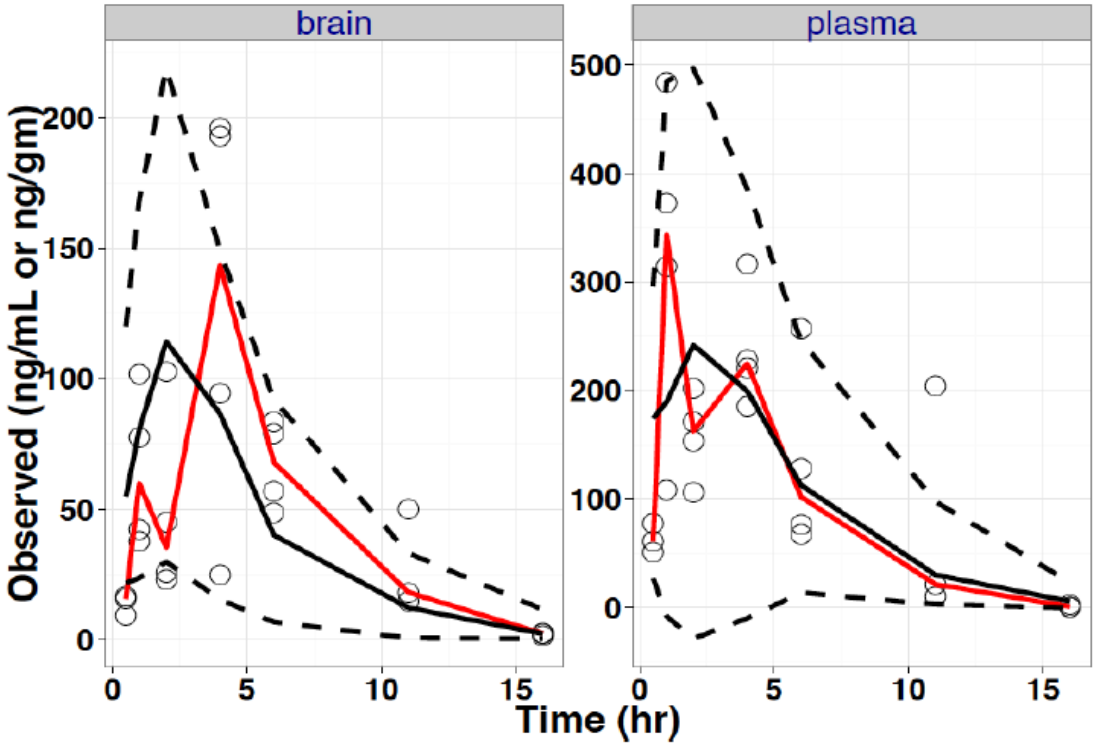

(b) *Mdr1a/b(-/-)* (P-gp knockout)

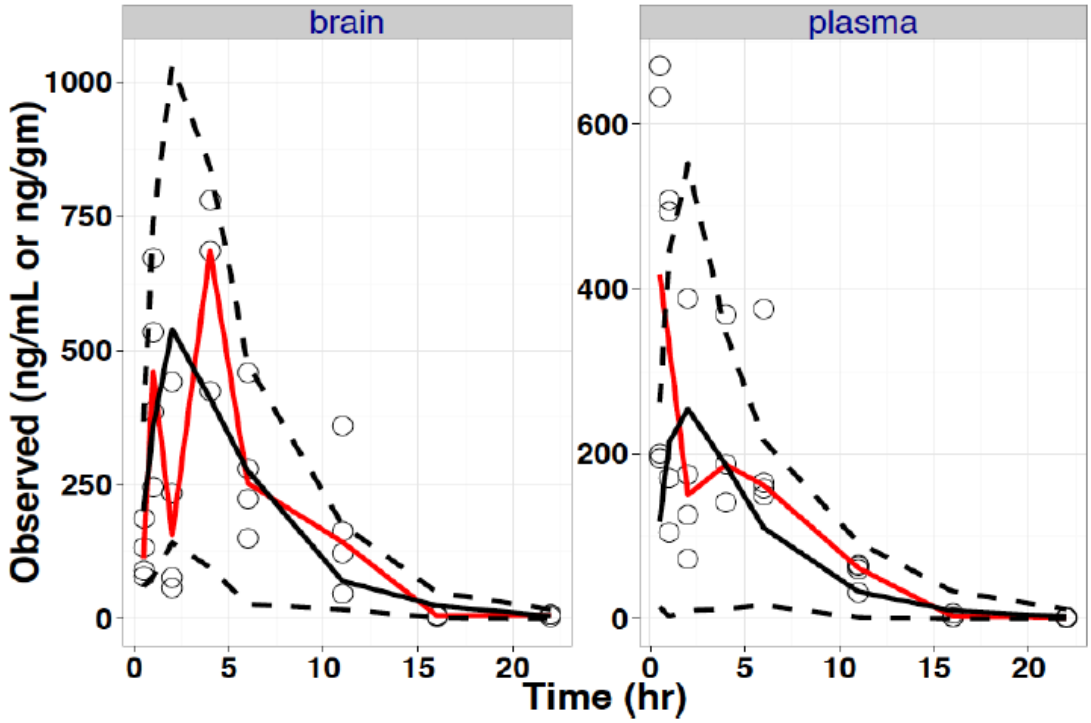

(c) *Bcrp1(-/-)* (Bcrp-knockout)

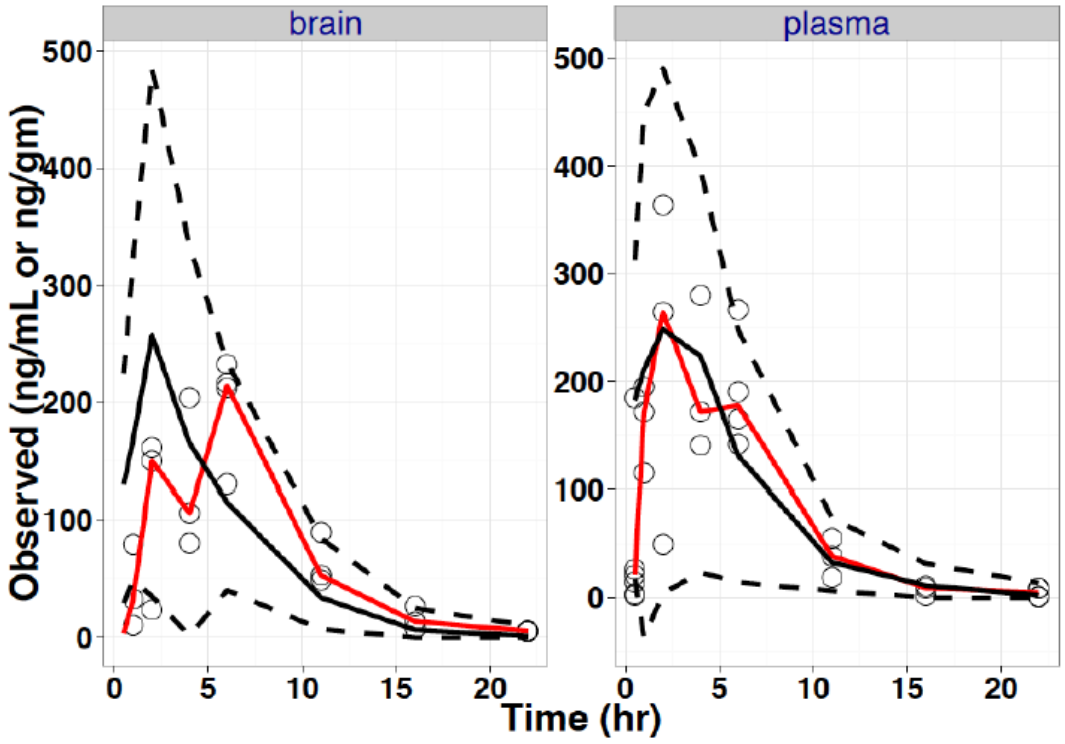

(d) *Mdr1a/b(-/-)Bcrp1(-/-)* (P-gp/Bcrp- knockout or 'triple' knockout)

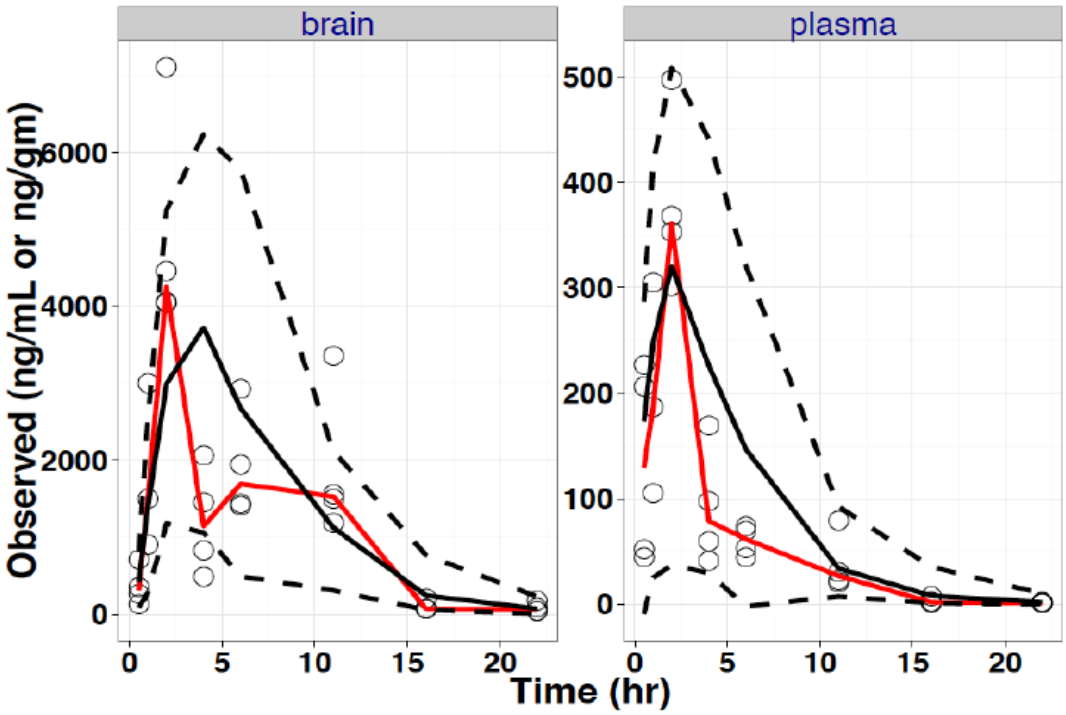

5.5.3 EVALUATION OF STUDY DESIGN ELEMENTS USING SIMULATIONS

We assessed model performance and sensitivity of brain distribution coefficient, Kp, using simulations wherein the sample size at each time point was varied and the resulting simulated datasets were estimated at 3 levels of BSV (10%, 20% or 40%).

Briefly, 1000 new data sets were simulated for each sample size (n= 2, 3, 4, 8 and 12) using the parameter estimates from the PK-model with BSV fixed at 20%. Each of the simulated data set was estimated at 3 levels of BSV (10%, 20% or 40%). Since the 'true' value of the parameter estimates was known in the simulation, we were able to determine bias and a measure of precision in the study.

Table 5.3 summarizes the results from the estimation of bias as the number of animals at each time point increase. Irrespective of the number of animals used at each time point, bias was < 2-3% for all simulation scenarios tested. BSV had no influence over estimation of bias in a serial sacrifice deisgn. Earlier, Wang et al. reported similar findings on the effect of BSV using a bayesian approach to NCA (Wang et al., 2014).

Precision was evaluated for each sample size using a novel approach by estimating the fraction of Kp-estimates within 5%, 10% and 20% of the estimate of bias obtained using the known parameter values. As the number of animals at each time point increased, estimates of Kp became closer to the true value. Overall, these estimates were not

substantially affected by the magnitude of between animal variability. At BSV= 10%, 20% and 40%, similar trends were observed for precision in estimation of Kp as shown in **figure 5.4.**

Table 5.3: median (25^{th} and 75^{th} quantile) of estimate of bias determined as ((predicted-true)/true) from 1000 simulations and re-estimations for brain distribution coefficient, K_p.

Inter-animal variability	Sample size	Bcrp-knockout	P-gp Knockout	P-gp/Bcrp Knockout	Wild-type
10%	2	-0.001 (-0.15, 0.17)	-0.016 (-0.16, 0.17)	-0.037 (-0.18, 0.14)	-0.028 (-0.15, 0.14)
	3	-0.02 (-0.15, 0.14)	-0.014 (-0.14, 0.14)	-0.015 (-0.15, 0.14)	-0.008 (-0.13, 0.13)
	4	-0.001 (-0.15, 0.12)	-0.003 (-0.12, 0.14)	-0.005 (-0.12, 0.12)	-0.006 (-0.11, 0.13)
	8	-0.002 (-0.15, 0.09)	-0.010 (-0.10, 0.09)	0.006 (-0.08, 0.10)	0.007 (-0.08, 0.10)
	12	0.007 (-0.15, 0.09)	-0.0004 (-0.08, 0.08)	0.014 (-0.05, 0.10)	0.009 (-0.06, 0.07)
20%	2	-0.004 (-0.15, 0.16)	-0.010 (-0.16, 0.18)	-0.03 (-0.18, 0.15)	-0.023 (-0.15, 0.15)
	3	-0.011 (-0.15, 0.14)	-0.012 (-0.14, 0.14)	-0.02 (-0.15, 0.13)	-0.002 (-0.14, 0.14)
	4	-0.008 (-0.12, 0.11)	-0.006 (-0.13, 0.13)	-0.02 (-0.13, 0.10)	-0.006 (-0.11, 0.14)
	8	-0.008 (-0.09, 0.09)	-0.014 (-0.10, 0.08)	-0.01 (-0.09, 0.08)	-0.003 (-0.08, 0.09)
	12	-0.001 (-0.07, 0.08)	-0.003 (-0.08, 0.07)	-0.008 (-0.07, 0.06)	-0.002 (-0.07, 0.07)
40%	2	-0.001 (-0.15, 0.17)	-0.006 (-0.15, 0.17)	-0.025 (-0.17, 0.14)	-0.012 (-0.15, 0.15)
	3	-0.016 (-0.14, 0.12)	-0.009 (-0.13, 0.13)	-0.02 (-0.14, 0.12)	-0.005 (-0.13, 0.13)
	4	-0.018 (-0.11, 0.11)	-0.002 (-0.11, 0.10)	-0.022 (-0.12, 0.09)	-0.002 (-0.11, 0.11)
	8	-0.013 (-0.09, 0.08)	-0.014 (-0.09, 0.07)	-0.011 (-0.09, 0.07)	-0.006 (-0.08, 0.07)
	12	-0.012 (-0.07, 0.06)	-0.012 (-0.07, 0.06)	-0.010 (-0.07, 0.54)	-0.008 (-0.07, 0.06)

Figure 5.4: Fraction of 1000 replicate simulations giving an estimate of Kp within 5%, 10% and 20% of the true value. The analysis evaluated the influence of sample size at each time point and between-subject variability in precisely estimating Kp under the given model.

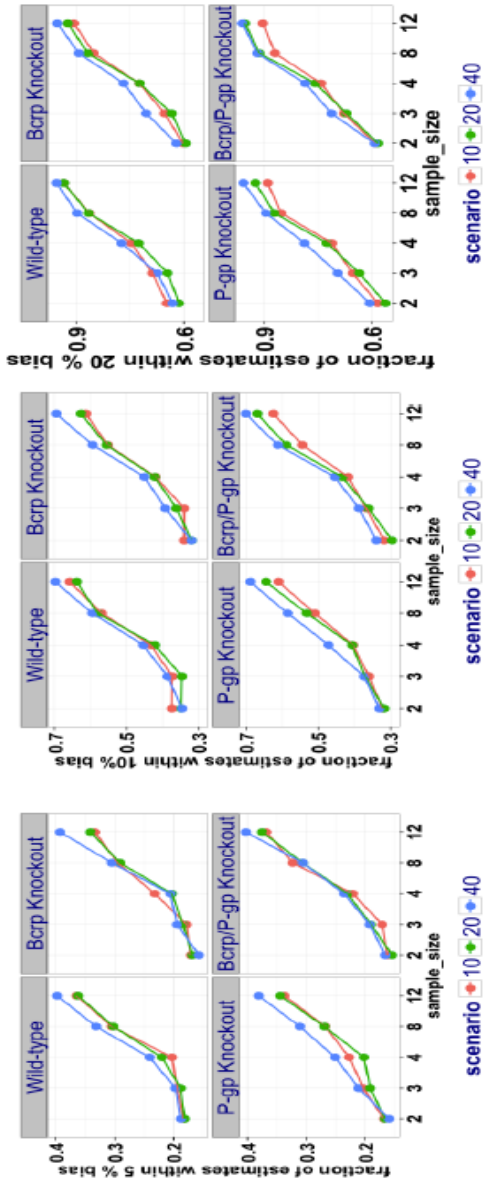

5.6 DISCUSSION

Rodents such as mice and rats are among the most commonly used animals for pharmacokinetic and toxicokinetic studies. The size of the animals limits the number of samples that can be withdrawn in a time-course study, therefore, often groups of animals are sacrificed at specified time points to obtain plasma and tissues. This design is called a 'serial sacrifice design' or destructively sampled design. However, in tissue distribution studies the goal is to determine the tissue partition coefficient. This is traditionally done by averaging concentrations at each time point to obtain a mean value. This approach, however, has its disadvantages. First, we lose correlation in the structure of the data by averaging the concentrations at each time point for both plasma and tissue. This also results in loss of information for each animal because each animal supplies two concentrations, plasma and tissue (Ette et al., 1995a). Second, we do not obtain variability around the partition coefficient so it is difficult to ascertain any statistical significance of genotype (in this case) or treatment or group effect.

The objective of this study was to statistically assess variability in the brain distribution coefficient in a serial sacrifice design. We have proposed a mixed effect modeling (MEM) approach over the commonly used naïve-data averaging method for estimating population parameters and uncertainty associated with brain distribution coefficient, Kp. In the past, the MEM method has been investigated for determination of plasma PK parameters such as Cl and Vd for quantic data (Hing et al., 2001). Ette et al. compared

the traditional NCA approach to resampling based approaches - random sampling (RS) and pseudo-profile based bootstrap (PpbB) methods to estimate tissue/plasma AUC ratios. The authors also evaluated the effect of correlation between plasma and tissue concentrations using paired and unpaired data in estimating tissue/plasma AUC ratios (Chu and Ette, 2005). The authors observed that the RS approach was more robust than the PpbB method.

Our approach is an alternative approach to random sampling and does not rely on any resampling assumptions and multi-step approach to determine the tissue distribution coefficient. In this study, plasma and brain concentrations were simulatenously modeled using a hybrid pharmacokinetic model wherein the plasma concentrations were modeled as a forcing function for the corresponding brain concentrations. This approach ensured that within animal correlations in the data were maintained. In the MEM method, the variability in parameter estimates is influenced by BSV and RUV. In our analysis, we assumed that all animals belong to the same homogenous population and therefore we fixed the between subject variability fixed at 20% and estimated RUV. Our approach was motivated by the results obtained from the brain distribution of sunitinib (Oberoi et al., 2013).

Results from the case study show that the point estimates of K_p obtained from NCA were comparable to the K_p ratios obtained using MEM method. In addition, we also obtained uncertainty around the point estimates of AUC brain/plasma ratio for all genotypes.

Based on these results and the uncertainty associated with the Kp ratios, we found that both P-gp and Bcrp significantly limit the brain distribution of sunitinib. We also found that the model predicted plasma and brain concentrations described the observed concentrations reasonably well. Furthermore, we also performed a sensitivity analysis to test the assumptions on fixing BSV to 20% in the model. We found that varying the BSV from 2.5% to 40% did not influence estimates of K_p for all genotypes. Therefore, BSV did not appear as a sensitive parameter in the model.

The second objective of this investigation was to examine the influence of BSV (10%, 20% and 40%) and sample size (low to high) at each time point on tissue partition coefficient in a serial sacrifice design. We studied the effect of study design features using stochastic simulation and estimation (SSE) method using PsN. 1000 simulated data sets were generated using known parameter estimates and BSV =20% for each sample size (n=2, 3, 4, 8, 12). Each of the simulated data sets were then estimated assuming BSV =10% or 20% or 40%. Bias and precision were determined. Under the conditions studied, the model parameters were estimated irrespective of the value of between subject variability. The accuracy of parameter estimates was unaffected by varying either BSV or sample size at each time point. Bias was less than 2-3% in all scenarios studied. Precision was determined by the fraction of estimates of Kp that were within 5%, 10% or 20% of the known 'true' value. We observed that as the number of animals at each time point increased from low to high, higher fraction of estimates were within 20% of the true value. 5% and 10% difference in bias (difference of estimated Kp value from simulations

and given parameter values for simulation) were stringent conditions as only 40% and 70% of the time the estimates were within 5% and 10%, respectively, of true value when the number of animals per time point was 12. More commonly, 3-4 animals are grouped at each time point in a destructively sampled design. When 20% difference in bias was acceptable, 80%-85% of the time, the parameter estimates were precisely estimated. Therefore, as the number of animals sampled at each time point increases, precision in estimation of Kp increases while accuracy remains unaffected. However, assumptions regarding the magnitude of between subject variability in a serial sacrifice design are relatively unimportant.

The results obtained in this study are comparable to those obtained by Ette et al. (Ette et al., 1995b). The authors reported that with BSV between 15% and 30%, CL and V were precisely estimated with 4 - 15 animals/time point. The authors assumed that a substantial fraction of RUV was due to assay error and fixed intraindividual variability (RUV) to 15%, an approach previously employed by several researchers previously (Ette et al., 1995b). They observed that varying RUV significantly increased the magnitude in bias. Other groups have also assumed that errors in measurement of concentration contribute significantly to error associated with structural model parameters. Our approach differs from this in that we estimated RUV as a measure of model misspecification error or error in data collection that would appear as random and unexplainable with little emphasis on analytical assay error.

One criticism for using the NLME based approach is that assumptions regarding the magnitude of between subject variability and residual unexplained variability are subjective. However, under the assumtpions of the current model, we have shown that varying the magnitude of BSV does not influence the estimates of tissue distribution coefficient. Obtaining a duplicate assay for each sample would provide more information to adequately define the analytical component of RUV. In the simulation studies, we obtained plasma concentrations that were below the limit of quantification. The concentrations in the tail of a normal-distributed data are plausible when one type of variability is fixed (in this case, BSV) as all the remaining error in the model is lumped into another type (RUV, in this case).

In summary, we have demonstrated that an NLME based approach provides estimates of precision and standad error associated with derived pharmacokinetic parameters (for example, tissue distribution coefficient) following destructive sampling under certain conditions. This approach is an alternative to noncompartmental based approaches such as random sampling, pseudo-profile based bootstrap approach and bayesian approach that have been investigated previously to determine variability with PK parameters.

CHAPTER VI

INFLUENCE OF ACTIVE EFFLUX AT THE BLOOD BRAIN BARRIER ON THE PHARMACOKINETIC-PHARMACODYNAMIC ANALYSIS OF DUAL PI3K/mTOR INHIBITORS

6.1 INTRODUCTION

Glioblastoma multiforme (GBM) is an invasive and the most malignant form of primary brain tumor with an average median survival of 14.6 months with the current standard of care, surgery, radiation and chemotherapy (Grossman et al., 2010; Stupp et al., 2005). Despite multimodal treatment options comprising of surgery, radiotherapy and chemotherapy, GBM remains incurable and recurrence of the disease is inevitable resulting in death. Several molecularly targeted agents have been evaluated in clinical trials but the results have been disappointing (Agarwal et al., 2011b; Akhavan et al., 2010; Huang et al., 2009).

Often the failure in clinical trials is attributed to resistance mechanisms such as the up-regulation of alternative tumor growth pathways via redundancy, drug efflux mechanisms, decrease in sensitivity of pro-apoptotic ligands to their cell surface receptors, an ineffective drug or an ineffective target (Haar et al., 2012; Schmalz et al., 2011). Unfortunately, there is little emphasis on drug delivery issues. The brain is surrounded by a complex anatomical and functional barrier, the blood brain barrier (BBB) that restricts the penetration of xenobiotics from the peripheral circulation into the brain parenchyma. This limited penetrance is mediated by a combination of the endothelial tight junctions and active efflux (Pardridge, 2005). ATP-binding cassette (ABC) transporters such as P-glycoprotein (P-gp) and breast cancer resistance protein (BCRP) are the two of the most important active efflux transporters expressed on the luminal side of the BBB (Schinkel and Jonker, 2003). These transporters have been

regarded as the ‘gatekeepers’ that have restricted brain penetration of several anticancer drugs (Agarwal et al., 2011a). Previous studies have shown that many molecularly targeted agents are substrates for both P-gp and BCRP (Tamaki et al., 2011). Some researchers have argued that the BBB is leaky in the tumor core; hence drug delivery is not an issue for GBM treatment (Hofer and Frei, 2007). Recent studies have also shown high drug concentrations in the tumor core compared to the areas surrounding the core (Agarwal et al., 2013; Michaud et al., 2010). Although the core is surgically removed, there is mounting evidence that recurrence of GBM can be attributed to the residual cells that migrate centimeters away from the tumor core forming a niche of tumor cells (Berens and Giese, 1999). Recent imaging techniques have been enabled researchers to identify this population of cells. Bulk tumor cells are visible on T1- contrast enhanced MRI and to a larger extent on ^{18}F-DOPA PET images while invasive cells become more readily apparent on T2-FLAIR images (Pafundi et al., 2013). This highly infiltrative nature of the tumor further complicates the treatment of GBM. Presence of intact BBB in these regions can significantly limit brain distribution of chemotherapeutics (Agarwal et al., 2011b). Therefore, restricted delivery of drugs to the invasive glioma cells could be one of the reasons for failure in GBM clinical trials.

Researchers have experimentally investigated and shown that BBB disruption is not homogenous within the tumor mass as the core is heterogeneously disrupted than the rim and the contralateral hemisphere (Choucair et al., 1986); (Levin et al., 1975). In order to fully assess the brain distribution and efficacy in preclinical models, the ideal animal

model should not only represent GBM in tumor biology and histopathology but should also mimic the invasiveness and angiogenic potential of GBM progression (Newcomb and Zagzag, 2009). Use of an inappropriate preclinical GBM model to investigate drug delivery could also be one of the reasons for inefficacy observed in clinical trials for several anti cancer drugs. Previously investigators have employed flank models or more traditional models such as U87MG glioma cell line model. The flank models fail to mimic the glioma microenvironment and the BBB characteristics in limiting brain penetration. On the other hand, the U87 human glioma cell line model fails to recapitulate the true nature of human GBM invasiveness and heterogeneity in BBB disruption. The U87 model was derived from a patient in 1968 but current neurooncological and neurosurgical standards would not classify the U87 tumor as a GBM today (Ponten and Macintyre, 1968). Despite these dissimilarities to glioblastoma, this model has been used in more than 1,700 publications (Clark et al., 2010). The tumor cells grow as a ball of cells with a sharply defined tumor boundary, much unlike the human counterpart (Newcomb and Zagzag, 2009). Preclinical results based on such models can lead to misleading interpretations, as one would believe that the BBB is not an impediment in drug delivery. Use of green fluorescent protein (GFP) enhanced tumors can help differentiate the brain regions into the core, the brain around the core and the contralateral hemisphere. Previously our lab has demonstrated the importance of BBB in limiting brain penetration of erlotinib and dasatinib using spontaneous and xenograft models, respectively (Agarwal et al., 2013; Agarwal et al., 2012). These studies showed that the brain concentrations in the core were significantly higher than in the rim and the

contralateral hemisphere and provided a plausible explanation that inadequate drug delivery to the normal and tumor brain could be the likely mechanism for failure of molecularly targeted agents in clinical trials.

PI3K (phosphatidylinositol-3-kinase)/Akt/mTOR (mammalian target of rapamycin) pathway (PI3K/AKT/mTOR) is one of the most deregulated pathways in GBM (Akhavan et al., 2010). It is the downstream signaling pathway for several receptor tyrosine kinases such as epidermal derived growth factor receptor (EGFR), vascular endothelial growth factor receptor (VEGFR), platelet-derived growth factor receptor (PDGFR) and insulin-growth factor receptor (IGFR) (Knobbe and Reifenberger, 2003). PI3K deregulation has been detected in more than 86% GBM samples and is known to play an important role in gliomagenesis (2008; Jiang and Liu, 2009; Karar and Maity, 2011). Therefore, inhibition of PI3K pathway represents an attractive target for therapeutic intervention in GBM. mTOR, the downstream target of this pathway is critical to GBM progression by regulating cell proliferation, survival, migration and angiogenesis via two multi-protein complexes, mTORC1 and mTORC2 (Guertin and Sabatini, 2007; Gulati et al., 2009). Activation of mTORC1 results in phosphorylation and activation of translation (S6) and initiation factor that control cell growth (Kim et al., 2002) while mTORC2 activates AKT in a PI3K-independent manner resulting in cell survival, proliferation and metabolism (Sarbassov et al., 2005). First generation mTOR inhibitors such as rapamycin and rapamycin analogs (Rapalogs such as temsirolimus and everolimus) predominantly and selectively inhibit mTORC1 and have been extensively studied in GBM clinical trials.

Unfortunately, these compounds have failed to show any therapeutic efficacy, potentially due to limited drug targeting of mTORC1 or compensatory upregulation of alternative signaling pathways such as MAP-kinase pathway (Carracedo et al., 2008; Galanis et al., 2005; Rodon et al., 2013). Second generation mTOR inhibitors such as dual mTORC1/2 complex inhibitors or dual PI3K/mTOR inhibitors are being currently investigated in several cancers including GBM (Rodon et al., 2013; Sabbah et al., 2011).

In this study, we have investigated the role of blood-brain barrier in limiting brain distribution and efficacy of PI3K/mTOR inhibitors in three GBM models: GL261 syngeneic model, GBM10 patient-derived xenograft model and U87 human glioma cell line derived model. GNE-317 and GDC-0980 are dual PI3K/mTOR inhibitors with potent activity against PI3K and both mTORC1 and mTORC2 **(Figure 6.1).** GNE-317 was custom synthesized to penetrate the BBB (Salphati et al., 2012a) while GDC-0980 is liable to active efflux at the BBB (Salphati et al., 2012b). The objective of this study was to investigate (a) heterogeneity in BBB disruption in preclinical glioma models, (b) the role of intact BBB in the area around the tumor core in restricting delivery of molecularly targeted agents intracellularly and (c) whether there is a need of not only effective delivery but also an effective drug to target the tumor cells.

Figure 6.1: Structures of (a) GDC-0980 and (b) GNE-317. Both are dual PI3K/mTOR inhibitors with a similar backbone except for difference in the side chain (highlighted here in the figure).

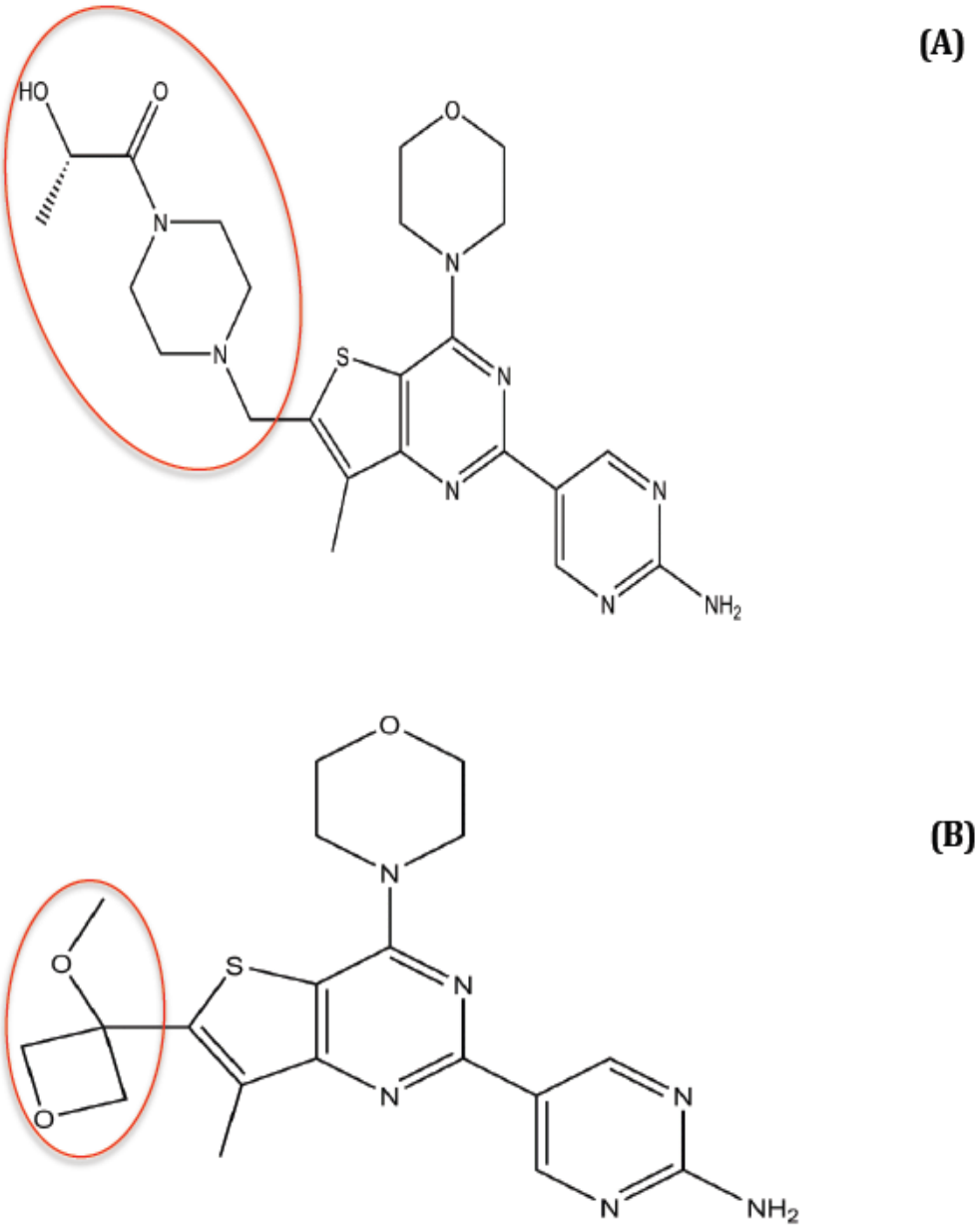

6.2 MATERIALS AND METHODS

6.2.1 CHEMICALS AND REAGENTS

GNE-317 and GDC-0980 were obtained from Genentech (San Francisco, CA). Ammonium formate and acetonitrile were HPLC grade and were procured from Sigma-Aldrich (St. Louis, MO). Texas Red Dextran 3000 MW (TRD) was purchased from Molecular Probes (Invitrogen).

6.2.2 GLIOBLASTOMA ANIMAL MODELS

Three glioma models were used for in-vivo tumor studies: GL261 mouse model (a syngeneic murine model), GBM10 (a patient-derived glioblastoma multiforme xenograft model obtained from Mayo Clinic, Rochester, MN) and U87 (a patient-derived glioblastoma multiforme cell line purchased from American Type Culture Collection, Manasass, VA, USA). Studies in GL261 model were conducted in collaboration with Dr. David Largaespada, Department of Neuroscience, University of Minnesota, MN, USA and studies with GBM10 and U87 were conducted in collaboration with Dr. Jann Sarkaria, Mayo Clinic, Rochester, MN, USA.

6.2.2.1 GL261 ORTHOTOPIC SYNGENEIC MODEL OF GLIOMA

GL261 cells transfected with luciferase and GFP (green fluorescent enhanced protein) were obtained from Dr. David Largaespada lab at the University of Minnesota. Cells were cultured in Dulbecco's modified Eagle's medium (DMEM) supplemented with 10% fetal bovine serum albumin, penicillin (100 U/ml), streptomycin (100 μg/ml), G418

(4mg/mL) and Puromycin (4 mg/mL). All supplements were obtained from Sigma-Aldrich. Cells were maintained in 5% oxygen conditions. For inoculations, cells were harvested using TrypLE (Life Technologies, NY, USA) and suspended in PBS at a concentration of 30,000 cells/μl. Female C57BL/6 mice (6-8 weeks) were obtained from Jackson Laboratories (Wilmington, MA). Mice were anesthetized with ketamine/xylazine cocktail solution (53.7 mg/ml ketamine, 9.26 mg/ml xylazine) delivered at 1 ml/kg. 1 μl of the cell solution containing 3 x 10^4 GL261-luc-GFP (enhanced green fluorescent protein) labeled cells were injected intracranially and stereotactically into the right ventral striatum (0.5 mm anterior, 2.5 mm lateral, 3.0 mm depth from the surface). The tumor was allowed to grow for 1 week before further studies.

6.2.2.2 GBM10 PATIENT-DERIVED AND U87 CELL-LINE XENOGRAFT MODEL

GBM10 is a serially passaged glioblastoma cell line derived from the tumor of a patient. Molecular genetic aberrations and histopathology of the tumor has already been described previously (Yang et al., 2008). The cells were grown as flank tumors in immunocompromised mice and harvested and grown in short-term cell cultures (5-14 days) as described previously (Carlson et al., 2011) in Dulbecco's modified Eagle's medium supplemented with 10% fetal bovine serum albumin, penicillin (100 U/ml) and streptomycin (100 μg/ml). U87 is a glioma cell line maintained in Dulbecco's modified Eagle's medium supplemented with 10% fetal bovine serum albumin and 10mM HEPES,

penicillin (100 U/ml) and streptomycin (100 μg/ml).

Briefly, the following procedure was followed for both GBM10 and U87 models. Female athymic nude mice (Ncr-*nu/nu*, National Cancer Institute) (5-6 weeks old) were maintained as flank tumor passages. The flank tumor cells obtained from these animals was mechanically disaggregated to form a cell suspension and maintained in DMEM with 2.5% fetal calf serum. Following trypsinization, the cells were re-suspended in phosphate buffered saline (PBS) at 10^5 cells/μL. Using a stereotaxic frame (ASI Instruments, Houston, TX) GBM10 cells and U87 cells were suspended at a concentration of 3 x 10^5 cells and injected into the right basal ganglia (3 μL) (1mm right lateral and 2mm anterior to the bregma). For *in-vivo* brain distribution studies, GFP-labeled GBM10 and GFP-labeled U87 cells were used.

6.2.3 REGIONAL BREAKDOWN OF THE BBB

6.2.3.1 GL261 SYNGENEIC MODEL

Cohorts of GL261-luc-GFP labeled tumor-bearing C57BL/6 mice were injected with Texas Red dextran (1.5 mg/animal body weight, molecular weight= 3000 Da) via tail vein. To investigate the degree of BBB disruption during tumor progression, the animals were grouped into four categories according to their signal strength as determined by luciferase imaging ($5x10^{-5}$, $5x10^{-6}$, $5x10^{-7}$, $5x10^{-8}$ p/sec/cm^2/sr). After 10 minutes, the animals were perfused with a brief cardiac washout for 30 seconds at a rate of 10 mL/minute. Following perfusion, brains were harvested and flash frozen in isopentane (-

80°C). Brains were then sectioned (20- micron slices) using a cryostat and mounted on charged glass slides. After preparation, slices were imaged using the fluorescence filters of a Leica DMI 6000B microscope. Images were acquired in grayscale using a Retiga 2000R camera at a variety of exposure times to allow visualization of signal in the smaller tumor-bearing slices and to prevent signal saturation in the larger tumor-bearing slices. The individual images were acquired using QImaging QCapture Pro v 6.0 software, compiled using Microsoft Image Composite Editor and then color was synthetically applied using Adobe Photoshop.

6.2.3.2 GBM10 AND U87 XENOGRAFT MODEL

GBM10 and U87 cells used for BBB integrity studies were not GFP-enhanced tumors. TRD (1.5 mg/animal) was administered via tail vein. After allowing circulation for 10 minutes, the animal was perfused with extracellular fluid buffer (ECF buffer) at a rate of 10 mL/min. Following perfusion, whole brains were harvested and frozen in ice-cold isopentane at -80C. Brains were then sectioned (20-micron) into slices and mounted on glass slides. Brains were imaged for Texas Red and Brightfield. The extent of tumor growth was confirmed by cresyl violet staining. Briefly, the glass slides were fixed in 4% paraformaldehyde in PBS for 10 minutes and immersed in 0.1% cresyl violet acetate for 15 minutes. The sections were then processed for dehydration and cleaning in 70% ethanol for 15 seconds and 90% ethanol for 10 seconds. Bright field images were then captured using Retiga 2000R camera (Leica DMI 6000B microscope).

6.2.4 CYTOTOXICITY STUDIES

Cytotoxicity studies were conducted in all 3 cell lines; GL261, GBM10 and U87.

6.2.4.1 GL261 AND U87 CELL LINE

GNE-317 and GDC-0980 were added to cells (75% confluent) in 96-well plate in increasing concentrations (0.0001-1000 μM, <0.05% DMSO). The plates were incubated at 37°C for 48 hours. Following incubation, tumor growth potential was determined using MTS cytotoxicity assay (Promega, Madison, WI). 40 μL of tetrazolium dye was added to each well and further incubated for 2 hrs. Plates were analyzed for colorimetric changes and optical density was read at an absorbance of 490 nm using Synergy 2 microplate reader and Gen5 v 2.04 software. Plates were read to determine the degree of cell survival. Numerical values from treated wells were normalized to the values of vehicle-treated wells to gain percent survival.

6.2.4.2 GBM10 CELL LINE

GNE-317 and GDC-0980 were tested for cytotoxicity in GBM10 cells. Cells were seeded in 96-well plates at a cell density of 5000 cells per well (n=3 plates for each drug) and incubated for 24 hours to allow cell attachment. The cells were then incubated for 48 hours with increasing concentrations of GNE-317 or GDC-0980 (0.015uM to 100uM), DMSO control and vehicle control. Following incubation, cells were washed with PBS and 40uL of MTT reagent (3-(4, 5-dimethylthiazol-2-yl)-2, 5-diphenyl tetrazolium bromide) (Alfa Chemical Corp.) at a concentration of 5 mg/mL was added to each well.

After an additional 3 hrs of incubation at 37°C at 60 rpm, 100µL of DMSO was added to each well. The plates were continuously agitated on an orbital shaker for 1 hr at 60 rpm, 37°C. The absorbance of each well was determined using a plate reader at a wavelength of 570 nM. Viability was determined as the amount of purple formazan produced. The percent survival was normalized to the percentage of absorbance of cells treated with DMSO control. The percentage of DMSO was less than 0.01% for all drug solutions.

6.2.5 *IN-VIVO* STUDIES

Mice were handled according to the guidelines set by the National institute of Health (NIH) and experiments were conducted in accordance with the Institutional Animal care and Use Committee (IACUC) at the University of Minnesota or the Mayo Institutional Animal Care and Use Committee.

Single oral dose brain distribution studies and steady-state brain distribution studies for both GNE-317 and GDC-0980 were conducted in non-tumor bearing Friend Leukemia virus strain B (FVB) mouse of either sex in wild-type and in transgenic mice "triple-knockout" mice (TKO), mice lacking both P-gp and Bcrp (*Mdr1a/b(-/-)Bcrp1(-/-)*) (8-10 weeks old). Mice were obtained from Taconic farms (Germantown, NY) and maintained under temperature controlled conditions with 12 hour dark-12 hour light cycle and unlimited access to food and water.

Tumor distribution studies and survival studies were conducted in GL261 syngeneic model (C57BL/6 mice, female (~7 weeks old purchased from Jackson Labs), GBM10 patient-derived xenograft model and U87 cell line derived xenograft model (athymic nude mice).

6.2.5.1 PLASMA AND BRAIN DISTRIBUTION OF GNE-317 AND GDC-0980 IN FVB MICE

GNE-317 (30 mg/kg) and GDC-0980 (7.5 mg/kg) drug solutions were prepared freshly on the day of the experiment as a suspension in 0.5% methylcellulose and 0.2% tween 80. All mice were administered the drugs simultaneously in two separate syringes by oral gavage and euthanized using carbon-dioxide chamber at desired time points, i.e., 1, 4, 6 or 8 and 16 hrs after dose (n=3-4 at each time point). Following euthanasia, blood was collected by cardiac puncture and transferred to tubes containing 20μL of 100 units/mL heparinized saline. Plasma was separated by centrifugation at 3500 rpm at 4°C for 15 minutes. Brain was harvested, rinsed with ice-cold buffer and flash frozen in liquid nitrogen. Brain samples were transferred to pre-weighed tubes. Plasma and brain samples were stored in -80°C until analysis by LC-MS/MS.

At the time of analysis, brain samples were thawed at room temperature and brain weights were obtained. Brains were homogenized with 3 volumes of 5% bovine serum albumin (BSA) prepared in phosphate buffer saline (PBS) (pH=7.4) using a tissue

homogenizer (PowerGen 125, Fisher Scientific, Pittsburgh, PA). Brain concentrations were determined by correcting for the brain vascular space in FVB mice (1.4 % of the whole brain volume (Dai et al.).

Noncompartmental analysis was performed using Phoenix WinNonlin 6.1 (Pharsight, Mountain View, CA). The area under the concentration time curve till the last measured time point ($AUC_{0\text{-}tlast}$) was calculated for both plasma and brain concentration time profiles using the log-linear trapezoidal approximation method. In addition, we determined the brain partition coefficient, Kp, given by the AUC ratio of brain to plasma for both wild-type and TKO mice. We also examined the drug targeting index (DTI) which is given by the AUC brain-to-plasma ratio in TKO mice divided by the AUC brain-to-plasma ratio in the wild-type mice, written as,

$$DTI = AUC_{brain/Plasma\ (TKO)}/AUC_{brain/Plasma\ (wild\text{-}type)}$$

6.2.5.2 PLASMA AND BRAIN STEADY-STATE PHARMACOKINETICS OF GNE-317 AND GDC-0980 IN FVB MICE

The steady state brain-to-plasma ratio (Kp) for both GNE-317 and GDC-0980 were determined in mice using Alzet osmotic minipumps (Durect Corporation, Cupertino, CA). A 5 mg/ml solution of GNE-317 and 10 mg/ml solution of GDC-0980 was prepared in dimethylsulfoxide and osmotic minipumps (model 1003D) were filled with 100 µL of either drug solution. The pumps were allowed to equilibrate overnight by soaking them in

a sterile saline solution at 37^0C. On the day of the experiment, mice were anesthetized with 5% isoflurane (Boynton Health Service Pharmacy, University of Minnesota, Minneapolis, MN) and maintained under anesthesia with 2% isoflurane in oxygen during surgery. The primed pumps were surgically implanted in the peritoneal cavity of the mice, after which the mice were allowed to recover on a heated pad. Each pump operates at a rate of 1 µL/hr, which yielded a constant intraperitoneal infusion of 5 µg/hr for GNE-317 or 10 µg/hr for GDC-0980. All animals were euthanized 48 hrs post surgery and blood was collected via cardiac puncture and whole brain was harvested. Blood and brain were processed as described above. On the day of the analysis, brain samples were prepared as described above. Steady state brain-to-plasma ratios were determined for both GNE-317 and GDC-0980 in wild-type and TKO mice.

6.2.6 REGIONAL BRAIN DISTRIBUTION OF GNE-317 AND GDC-0980 IN GLIOBLASTOMA MOUSE MODELS

6.2.6.1 GL261 MODEL

Presence of GFP in tumor cells aided in dissecting the brain into three parts - the tumor core, the brain around the core and the contralateral hemisphere as illustrated in **Figure 6.2.** Tumor-bearing mice were randomly assigned to one of the three groups (n=6 per group), (a) control (vehicle treated), (b) GDC-0980 (7.5 mg/kg) and (c) GNE-317 (30 mg/kg). Drug solutions were prepared in 0.5% methylcellulose with 0.2% tween 80. All mice were administered one of the three treatments orally for 3 consecutive days. All

mice were sacrificed either 1hr after the last dose or 6hr after the last dose, following which brain and plasma were harvested. Brains were sectioned into three regions: the tumor core, the brain around the tumor and the contralateral hemisphere. Brain samples were prepared as described previously. Tissue specimens from each group were analyzed for drug concentrations using LC-MS/MS.

Figure 6.2: GFP-enhanced GL261 mouse brain

Qualitative figure showing the dissection of the tumor core, rim and the contralateral hemisphere in a GL261 mouse glioma model. The tumor cells are enhanced green by GFP and dissected using GFP-goggles.

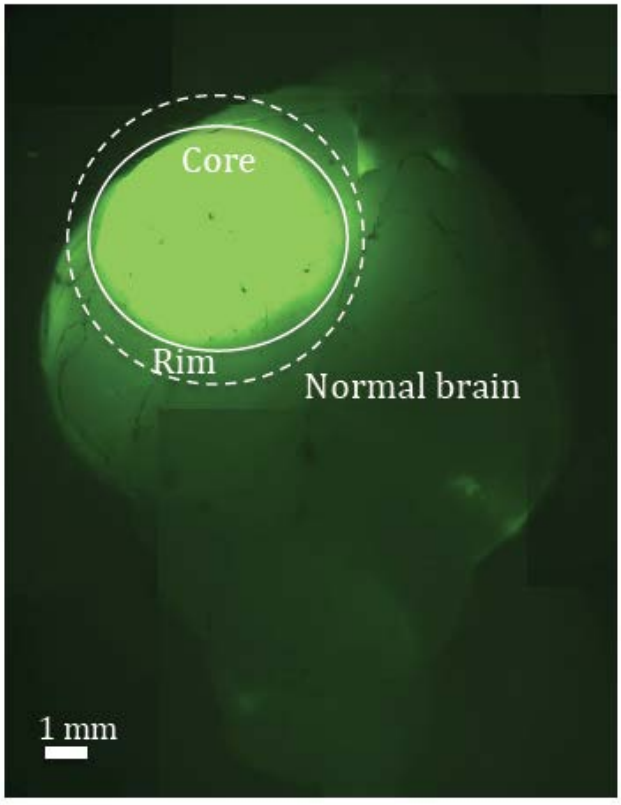

6.2.6.2 GBM10 AND U87 MODEL

Female athymic nude mice (Ncr-*nu/nu*) bearing GFP-labeled GBM10 (n=3) and GFP-labeled U87 (n=5) tumor were treated with both GNE-317 (30 mg/kg) and GDC-0980 (7.5 mg/kg) simultaneously. Drug solutions were prepared in 0.5% methylcellulose and 0.2% tween 80. Mice were sacrificed 1 hr after the dose and plasma and brains were harvested. GFP-labeling aided in dissecting the brain into three parts – the core, the brain around the tumor core and the contralateral hemisphere. For GBM10-treated group, plasma samples were not collected.

6.2.7 QUANTIFICATION OF GNE-317 AND GDC-0980 IN MOUSE BRAIN AND PLASMA BY LC-MS/MS

The plasma and brain concentrations of GNE-317 and GDC-0980 were determined using high-performance liquid chromatography-tandem mass spectrometry (LS-MS/MS). On the day of the analysis, frozen brain samples were thawed at room temperature. Brain weights were determined as described above and samples were homogenized using 3 volumes of 5% ice-cold bovine serum albumin prepared in phosphate-buffer saline (PBS) (pH= 7.4).

Drug concentrations in GNE-317 alone or GDC-0980 alone treated groups were analyzed as follows: 100 μL of plasma or 200 μL of brain homogenate sample were taken in microcentrifuge tubes containing 10 μL of 2 μg/mL of internal standard (GNE-317:

AG1478 (4-[3-chloroanilino]-6,7-dimethoxyquinazoline) and GDC-0980: dasatinib, free base) and extracted via vigorous vortexing with 500 μL of ice-cold ethyl acetate. Following centrifugation at 7500 rpm for 15 minutes at 4°C, 400 μL of the supernatant was transferred to microcentrifuge tubes and dried under nitrogen. Dried samples were re-constituted with 100 μL of mobile phase for GNE-317 (60:40:0.1, v/v%, 20 mM ammonium formate, pH 3.5: acetonitrile: formic acid) or GDC-0980 (72:28:0.1, v/v%, 20 mM ammonium formate, pH 3.5: acetonitrile: formic acid) and transferred to glass autosampler vials. 5 μL of the sample was injected into LC-MS/MS. Chromatographic system consisted of Agilent Technologies model 1200 separation system (Santa Clara, CA). Separation of the analyte was achieved using Agilent ZORBAX XDB Eclipse C_{18} column (4.6 x 50 mm, 1.8 μm). The LC-system was linked to TSQ Quantum triple quadrupole mass spectrometer (Thermo Finnigan, San Jose, CA) and data analysis was performed using Xcalibur software, version 2.0.7. The instrument was equipped with selected reaction monitoring (SRM) mode with an electrospray ionization source (ESI) operated in positive ion mode at a spray voltage of 5000 V for both GNE-317 and GDC-0980. The mobile phase flow rate was 0.25 mL/min. The mass-to-charge transitions were programmed for GNE-317 (415.11 → 385.13) and internal standard, AG1478 (317.03 → 300.98) and GDC-0980 (499.24 → 340.98) and internal standard dasatinib (499→ 401). The total run time was 10 minutes and 12 minutes for GNE-317 and GDC-0980, respectively. The assay was linear over a range of 1.9 ng/ml to 1000 ng/ml with a coefficient of variation lower that 20% throughout the entire range.

Dual GNE-317 and GDC-0980 quantification method

For groups treated with both GNE-317 and GDC-0980 simultaneously, quantification of GNE-317 and GDC-0980 was performed using the dual gradient method as follows: 100 μL of plasma sample and 200 μL of brain homogenate was spiked with 10 μL of 2 μg/mL internal standard, AG1478 (4-[3-chloroanilino]-6,7-dimethoxyquinazoline) and extracted using 500 μL of ice-cold ethyl acetate. Samples were shaken vigorously at 7500 rpm at 4°C for 15 minutes, following which 400 μL of the supernatant was transferred to another tube and dried under a gentle stream of nitrogen. Samples were reconstituted in 100μL of mobile phase (72:28:0.1, v/v%, 20mM ammonium formate, pH=3.5 (A): acetonitrile (B): formic acid (A)) and transferred to glass autosampler vials. 5uL of the sample was injected into LC-MS/MS. The LC-system and TSQ Quantum triple quadrupole mass spectrometer system similar as described above. A gradient elution method was used starting at 28% B for 5 minutes (0.25 mL/min), followed by 100% B for 2.5 minutes (0.25 mL/min). A linear gradient was applied from 7.9 -11.5 minutes (28% B) at a flow rate of 0.5 mL/min. The total run time was 11 minutes. The mass-to-charge (m/z) transitions were 499.24 → 340.98, 499.24 → 340.98 and 317.03 → 300.98 for GDC-0980, GNE-317 and AG1478, respectively. The assay was linear over a range of 1.9 ng/ml to 1000 ng/ml with a coefficient of variation lower that 20% throughout the entire range.

6.2.8 PHARMACODYNAMIC EFFECTS OF GNE-317 AND GDC-0980 USING IMMUNOHISTOCHEMISTRY IN GL261-LUC-GFP LABELED GLIOMA MODEL

To determine efficacy of dual PI3K/AKT/mTOR inhibitors, GNE-317 and GDC-0980, GL261-luc-GFP labeled tumor bearing mice ($5*10^7$ photons/sec/cm^2/Sr) were randomized into three groups (n=5-6 per group), (a) control (vehicle treated), (b) GDC-0980 (7.5 mg/kg) and (c) GNE-317 (30 mg/kg). Drug solutions were prepared in 0.5% methylcellulose with 0.2% tween 80. Mice were administered one of the three treatments orally for 3 consecutive days, following which all mice were sacrificed either 1hr after the last dose or 6hr after the last dose. Brains were harvested as described previously and perfused with 30 mL PBS buffer. Brains were stored in 10% buffered formalin for 24 hours and then switched to 70% ethanol. Standard processing was used to paraffin embed tissues for slicing onto charged glass slides. Using a microtome, brains were sectioned into 5-μm slices. Formalin-fixed, paraffin-embedded tissue sections were deparaffinized with xylene, rinsed with ethanol and rehydrated. Immunohistochemistry (IHC) staining was performed using the following antibodies: Akt (1:200, Cell Signaling), p-Akt ^{Ser473} (1:50, Cell Signaling), S6 (1:100, Cell Signaling), pS6 $^{Ser235/236}$ (1:100, Cell Signaling), 4EBP1 (1:1000, Cell Signaling) and, p4EBP1$^{Thr37/46}$ (1:1000, Cell Signaling). Non-specific binding of antibody was achieved using 3% bovine serum albumin. The universal secondary protocol and DAB MAP kit (Vector Laboratories, Burlingame, CA) was used to detect the signal with one exception; we used a biotinylated secondary antibody followed by the application of VectaStain Elite ABC for

enhancement/amplification of signal. We also performed a brief 30-second hematoxylin staining to provide background for antibody staining. The tissues were dehydrated and mounted using Permount (Fisher Scientific). Darker staining of the tumor cells when treated with antibody corresponds to relative overexpression of the target. The slides were imaged using Nikon AZ100 Macrofluorescence microscope and associated NIS elements software was used to automatically stitch individual pictures and analyze horseradish peroxidase (HRP) staining intensity.

6.2.9 EFFICACY STUDIES IN GLIOMA MODELS

In-vivo efficacy studies were conducted in all three glioma models, GL261, GBM10 and U87-tumor bearing mice. All mice were randomized into three groups; (1) placebo (vehicle control), (2) GNE-317 (30 mg/kg) and (3) GDC-0980 (7.5 mg/kg) (n=10 mice/per group) and received one of the three treatments via oral gavage once daily with experimental end point being death or moribund state of mice. Drug solutions were prepared in 0.5% methylcellulose and 0.2% tween 80.

6.2.10 BIOLUMINESCENCE IMAGING

Animals bearing GFP-luc-GL261 tumors were monitored for tumor growth and effect of treatment with GNE-317 and GDC-0980. Bioluminescence imaging was based on the conversion of luciferin to light-emitting oxyluciferin by an enzyme, luciferase. Mice were

intraperitoneally injected with 100 μL of D-luciferin (28.5 mg/mL, Gold Bio), a substrate for luciferase enzyme. After 10 minutes, mice were anesthetized with 5% isoflurane using nosecones within the imager and placed in IVIS Xenogen 50 imager (Perkin Elmer). After the end of exposure period (1 second), a grey-scale image was obtained which was overlaid with a 5-minute luminescent exposure taken with the imager's Xenogen camera. Luciferase activity was analyzed using Living Image Software according to the manufacturer's instructions (Perkin Elmer, USA). All measurements were performed under the same experimental settings of camera. The signals were quantified and plotted as radiance (photons/sec/cm2/sr) with respect to the time, starting 7 days after surgery on the first day of treatment (GNE-317 or GDC-0980) or no treatment (placebo).

6.2.11 STATISTICAL ANALYSIS

The unpaired two-sample t-test was used to compare between two groups. One-way ANOVA, followed by Bonferroni's test was conducted to test for significance among multiple groups. Significance was declared at $p<0.05$ for all tests. All tests were done using GraphPad Prism 5.01, San Diego, CA. Survival probabilities were estimated using Kaplan Meier survival curves. The treatment groups were compared using log-rank test.

6.3 RESULTS

6.3.1 REGIONAL BREAKDOWN OF THE ENDOTHELIAL TIGHT JUNCTIONS IN THE BLOOD-BRAIN BARRIER

Heterogeneity in blood-brain barrier (BBB) disruption was evaluated using a permeability marker, Texas Red 3kDa dextran (TRD). TRD is an intravascular marker which can permeate through a disrupted membrane only. The normal permeability of the BBB is restricted to molecules <500 Da, therefore, a molecule such as TRD (molecular weight = 3000 Da) would only permeate when the tight junctions are disrupted. After i.v. administration, TRD was allowed to circulate for 10 minutes following which the mouse was anaesthetized, given rapid perfusion of ECF buffer and brain was harvested. Brain penetration of TRD was analyzed in 20-micron thick sections of the whole brain. For GL261-luc-GFP model, the TRD staining was visualized at four different time points ($5x10^{-5}$, $5x10^{-6}$, $5x10^{-7}$ and $5x10^{-8}$ p/sec/cm^2/sr) as assessed by bioluminescent imaging. At all signal strengths, heterogeneity in BBB disruption was apparent. As the tumor progressed ($5x10^{-8}$ p/sec/cm^2/sr), characteristic features of GBM became more visible. These features included absence of a clear tumor boundary and heterogeneity in BBB disruption in the tumor brain compared to the normal brain. Representative qualitative images showing Texas Red dextran accumulation in GL261 mouse brain from four different animals that had different signal strengths is shown in **figure 6.3 (a)**. Results from this analysis suggest that GL261 mouse model resembles spatial heterogeneity in BBB breakdown similar to that observed in human GBM.

Figure 6.3 (a): BBB permeability in GL261, GBM10 and U87 is visualized using Texas Red dextran. We used TRD is a permeability marker. Presence of the tumor region was detected using GFP in GL261 and cresyl violet and bright field in GBM10 and U87.

(a) GFP-luc-GL261 tumor bearing mice were assessed for different signal strengths using luciferase imaging. Representative images show heterogeneity in accumulation of TRD. Green represents GFP-enhanced tumor region. These images show higher accumulation of TRD in tumor region compared to non-tumor region. Within the tumor regions, there is heterogeneity in TRD accumulation suggesting heterogeneous breakdown of BBB in GL261, comparable to human GBM.

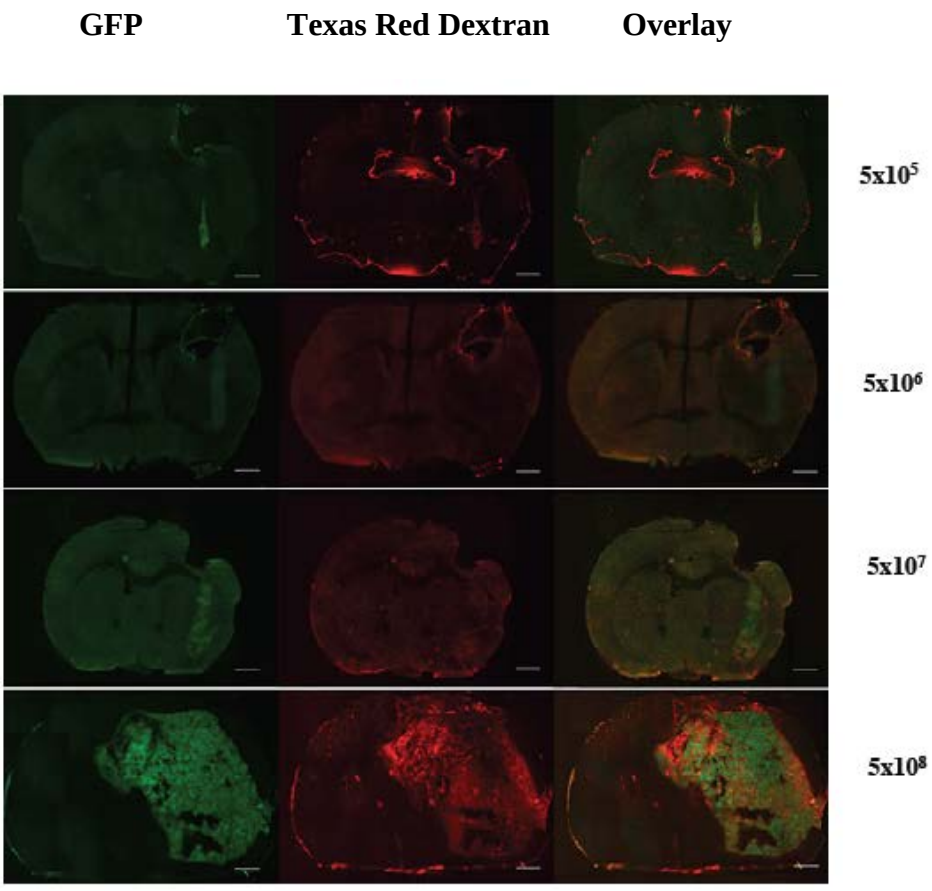

Figure 6.3 (b) BBB disruption in GBM10 and U87. GBM10 shows heterogeneity in BBB disruption, unlike in U87, which shows a homogenous breakdown of BBB. Also shown are Cresyl violet staining of the tumors and TRD accumulation in GBM10 and U87 with corresponding brightfield images of the tumor.

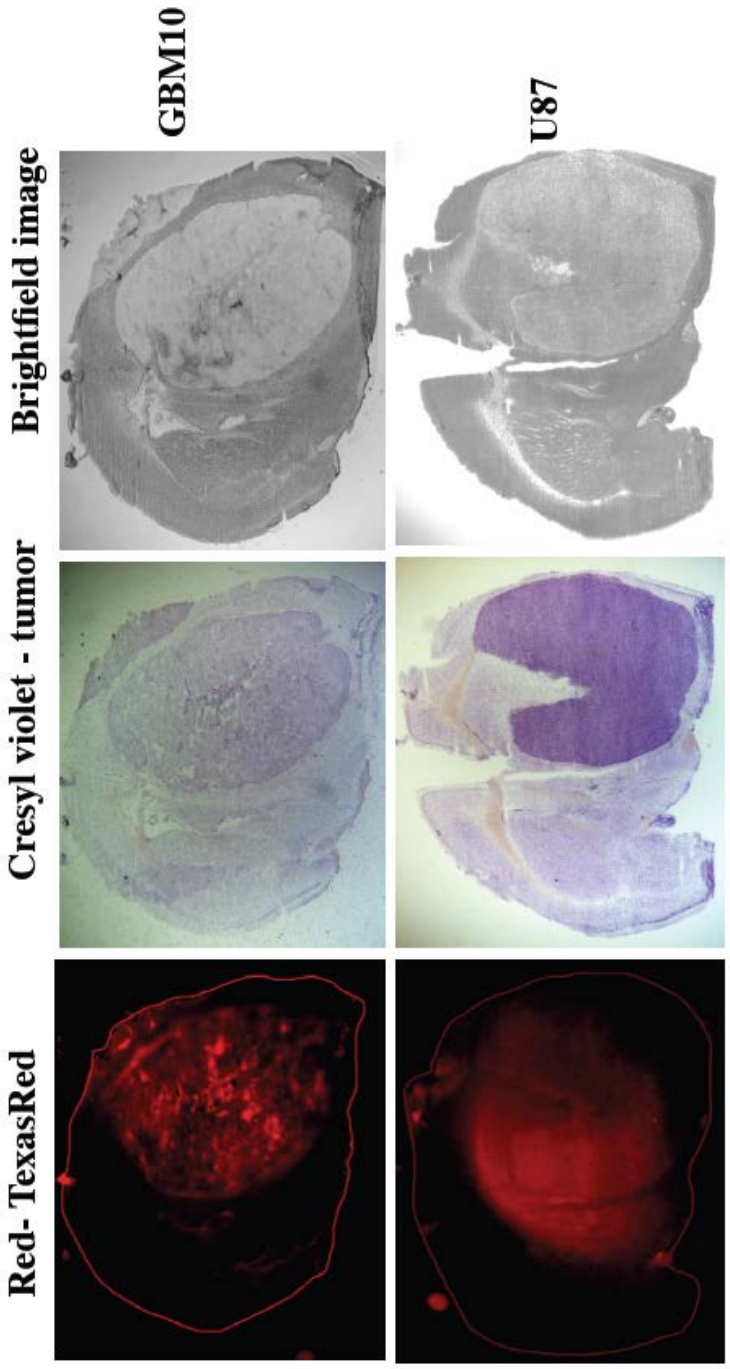

Similarly in GBM10, microscopic examination of TRD brain penetration revealed areas of heterogeneity within the brain tumor core and less accumulation of TRD in the growing edge of the tumor **(Figure 6.3 (b)).** On the other hand, TRD accumulation in U87 micro-dissected tumors did not reveal heterogeneity in BBB disruption. The disruption of BBB as shown by TRD brain penetration suggested a homogenous breakdown of the barrier **(figure 6.3 (c)).** There was significant background for TRD in U87. However, tumors in U87 glioma model had sharply demarcated edge of the tumor separated from the adjacent brain, unlike the tumors in GL261 and GBM10 model. It is critical to understanding and evaluate the heterogeneity in BBB breakdown as it can mislead interpretation of drug concentrations in the core vs. the adjacent brain as different brain-to-plasma ratios will be observed in these regions of the brain.

6.3.2 CYTOTOXICITY ASSAY

In-vitro efficacy of GNE-317 and GDC-0980 was determined in all three cell lines. Similar trends were observed across all three glioma models. Treatment with GNE-317 and GDC-0980 *in-vitro* resulted in a dose dependent inhibition of tumor cells as measured by the MTS and MTT assays. Both the drugs showed similar efficacy in *in-vitro* as observed by similar IC50's **(Table 6.1 and Figure 6.4).** IC50 in this case was defined as the concentration that results in 50% of maximal inhibition.

Table 6.1: Cytotoxicity results

	GNE-317 (µM)	GDC-0980 (µM)
GL261 cells	0.46	0.70
GBM10 cells	0.4	0.9
U87 cells	0.77	1.1

Figure 6.4 Cytotoxicity studies of GNE-317 and GDC-0980 in GL261, GBM10 and U87 cells in in-vitro

Figures (a-c) show percent viability curves of GNE-317 and GDC-0980 in all three glioma cell lines. The IC50s are shown in the figure. The figure shows similar trend of GNE-317 and GDC-0980 in all three cell lines suggesting both drugs have similar potency in-vitro.

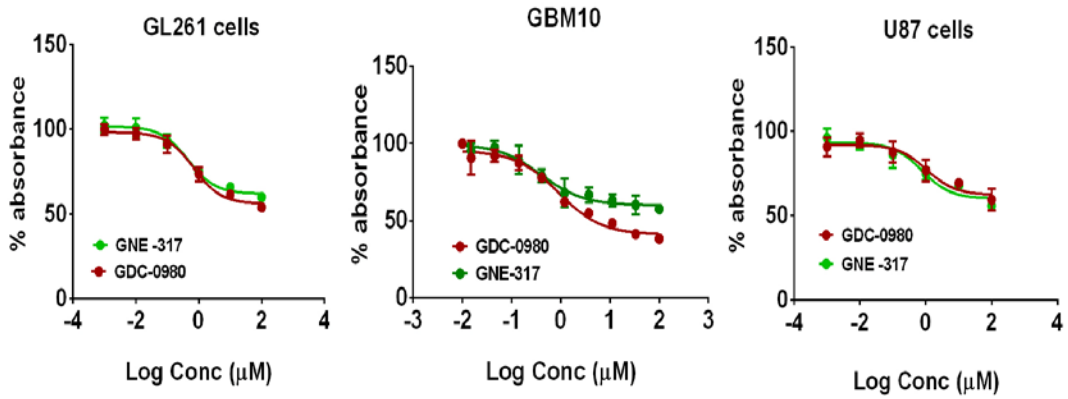

6.3.3 PLASMA AND BRAIN DISTRIBUTION OF GNE-317 AND GDC-0980 AFTER SINGLE ORAL DOSE IN FVB MICE

GNE-317 and GDC-0980 pharmacokinetics were determined after a single oral administration of both drugs in FVB-wild type and TKO mice. The brain and plasma concentration time profiles of GNE-317 and GDC-0980 in FVB-wild type and TKO mice are shown in **Figure 6.5.**

The brain concentrations of GNE-317 closely followed plasma concentrations in both wild-type and TKO mice, suggesting that both P-gp and Bcrp do not influence brain distribution of GNE-317 **(Figure 6.5 (a) and (b)).** The maximum plasma concentrations were observed at 1 hr in both wild-type and TKO mice. The brain-to-plasma concentration ratios were ~1 at all measured time points in both strains of mice **(Figure 6.5 (c)).** The area under the concentration time curve to the last measured time point (AUC_{0-t}) in both plasma and brain of the wild-type mice were 10.59 ± 0.81 h-µg/mL and 10.06 ± 0.9 h-µg/mL respectively. In the absence of P-gp and Bcrp, the AUC_{0-t} was 11.99 ± 1.65 h-µg/ml and 12.80 ± 1.24 h-µg/ml in the plasma and brain, respectively. Similar AUCs in plasma and brain in both wild-type and TKO mice indicate that GNE-317 brain distribution is not restricted by active efflux at the blood brain barrier. The brain partition coefficient, K_p, given by the AUC ratio in brain to AUC ratio in plasma was ~1 (0.95 in wild type and 1.07 in TKO), implying that there is equal partitioning in the brain as in the plasma. The observed drug targeting index value for GNE-317 was 1.13. This indicates

that both P-gp and Bcrp do not play a role in restricting the brain distribution of GNE-317.

On the other hand, brain concentrations of GDC-0980 were significantly lower than the corresponding plasma concentrations in wild-type mice at all measured time points ($p<0.05$), whereas, brain concentrations in TKO mice were greater than the plasma concentrations, indicating that both P-gp and Bcrp limit brain distribution of GDC-0980 **(figure 6.5 (d) and (e)).** The brain-to-plasma ratio vs. time graph showed an increase before reaching a plateau, suggesting that a pseudo-distributional equilibrium has been achieved **(figure 6.5 (f)).** The $AUC_{0\text{-}tlast}$ in the wild-type plasma (10.56 ± 1.47 h-µg/ml) and TKO plasma (4.51 ± 1.15 h-µg/mL) were significantly different from each other, although the plasma concentrations at all measured time points except 16 hr were not significantly different **(Table 6.2).** The brain distribution coefficient of GDC-0980 in wild type was 0.05 and increased by a drug targeting index of ~35 fold to 1.75 in the TKO mice.

These results are comparable to those observed by Salphati and colleagues in two separate publications on GNE-317 (Salphati et al., 2012a) and GDC-0980 (Salphati et al., 2012b) suggesting that the difference in targeting potential of GNE-317 is due to its higher brain permeability compared to drugs of similar class such as GDC-0980 that are liable to active efflux by P-gp and Bcrp at the BBB.

Figure 6.5 (a-c): plasma and brain concentration-time profiles of GNE-317 (30 mg/kg) and GDC-0980 (7.5 mg/kg) in FVBn wild-type and TKO mice after a single simultaneous oral dose

Plasma and brain concentration time profiles of GNE-317 in wild type (a) and TKO mice (b). Corresponding brain-to-plasma ratio with respect to time is shown in (c) for both wild type and TKO mice.

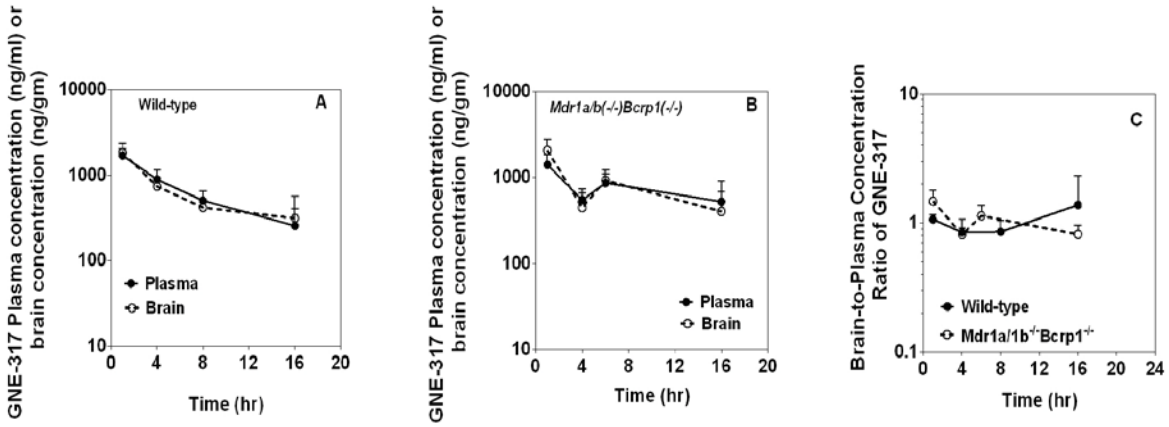

Figure 6.5 (d-f): plasma and brain concentration-time profiles of GNE-317 (30 mg/kg) and GDC-0980 (7.5 mg/kg) in FVBn wild-type and TKO mice after a single simultaneous oral dose Panel (d) and (e) show plasma and brain concentration time profiles of GDC-0980 in wild type and TKO mice, respectively. Corresponding brain-to-plasma ratios with time are shown in (f). Data represent mean ± S.D. (n= 3-4 at each time point).

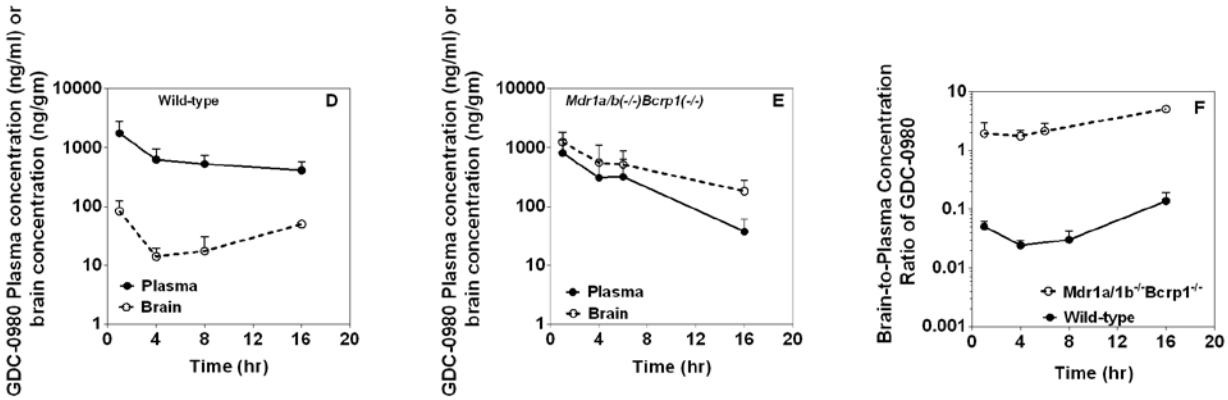

Table 6.2: Plasma and brain pharmacokinetic parameters determined by non-compartmental analysis after simultaneous administration of a single oral dose of GNE-317 (30 mg/kg) and GDC-0980 (7.5 mg/kg) in wild-type and Mdr1a/b(−/−)Bcrp1(−/−) mice. Results are expressed as mean ± S.D. n = 3 – 4 at each time point.

		GNE-317		**GDC-0980**	
	Parameter (units)	Wild-type	*Mdr1a/b(-/-)Bcrp1(-/-)*	Wild-type	*Mdr1a/b(-/-)Bcrp1(-/-)*
Plasma	C_{max} (µg/mL)	1.7 ± 0.20	1.41 ± 0.21	1.76 ± 0.58	0.81 ± 0.27
	T_{max} (hr)	1	1	1	1
	$AUC_{0\text{-}tlast}$ (h.µg/mL)	10.59 ± 0.81	11.99 ± 1.65	10.56 ± 1.47	4.51 ± 1.15
Brain	C_{max} (µg/mL)	1.84 ± 0.29	2.07 ± 0.36	0.083 ±0.023	1.25 ± 0.27
	T_{max} (hr)	1	1	1	1
	$AUC_{0\text{-}tlast}$ (h.µg/mL)	10.06 ± 0.9	12.80 ± 1.24	0.52 ± 0.06	7.91 ± 1.44
	K_p = AUC_{brain} /AUC_{plasma}	0.95	1.07	0.05	1.75
	DTI	1.13		35	

6.3.4 PLASMA AND BRAIN DISTRIBUTION OF GNE-317 AND GDC-0980 AFTER STEADY-STATE IN FVB MICE

The influence of P-gp and Bcrp on brain distribution of GNE-317 and GDC-0980 was determined by studying the steady state plasma and brain distribution in FVB-wild type and TKO mice. A continuous intraperitoneal infusion was administered at a constant rate of 5 μg/hr for GNE-317 or 10 μg/hr for GDC-0980 lasting 48 hrs. The steady-state plasma and brain concentrations for GNE-317 were not significantly different between wild type and TKO mice. The mean steady-state plasma concentrations for GNE-317 in the wild type and TKO mice were 3.12 ± 1.39 ng/mL and 3.81 ± 2.32 ng/mL, respectively and the corresponding steady-state brain concentrations were 2.69 ± 2.00 ng/gm and 2.98 ± 1.89 ng/gm, respectively **(Figure 6.6 (a) and (b)).** The resulting brain-to-plasma ratios were comparable between wild-type and TKO mice (0.81±0.28 (WT) vs. 0.98 ± 0.78 (TKO)). These results suggest that both P-gp and Bcrp do not play a significant role in altering the systemic clearance as well as brain distribution of GNE-317 **(figure 6.6 (c)).**

The mean steady-state plasma concentrations for GDC-0980 did not differ significantly between the wild type (25.99 ± 9.5 ng/mL) and TKO mice (58.42 ± 24.9 ng/mL) indicating that both P-gp and Bcrp do not influence the systemic clearance of GDC-0980 **(Figure 6.6 (d)).** However, the steady-state brain concentration in the wild-type mice (2.5 ± 0.70 ng/gm) was significantly lower than the TKO mice (58.06 ± 19.4 ng/gm) ($p<0.05$) **(figure 6.6 (e)).** The corresponding steady-state brain-to-plasma ratio was 0.1 ± 0.02 in

wild-type mice and increased to 1.03 ± 0.27 in TKO mice, a ~10-fold increase in brain distribution when both P-gp and Bcrp are absent **(figure 6.6 (f) and table 6.3).**

These results are in agreement with the previous reports by Salphati et al. for both GNE-317 (Salphati et al., 2012a) and GDC-0980 (Salphati et al., 2012b).The authors showed in two separate investigations that GNE-317 is not liable to active efflux at the BBB whereas GDC-0980 has limited distribution to the brain due to active efflux by both P-gp and Bcrp at the BBB.

Figure 6.6 (a-c): Steady state (a) plasma concentrations and (b) brain concentrations of GNE-317 in FVBn wild-type and TKO mice after a continuous intraperitoneal infusion at a rate of 5 µg/hr for 48 hours; (c) corresponding steady-state brain-to-plasma concentration ratio. Values are represented as mean ± S.D. (n= 4 per group)

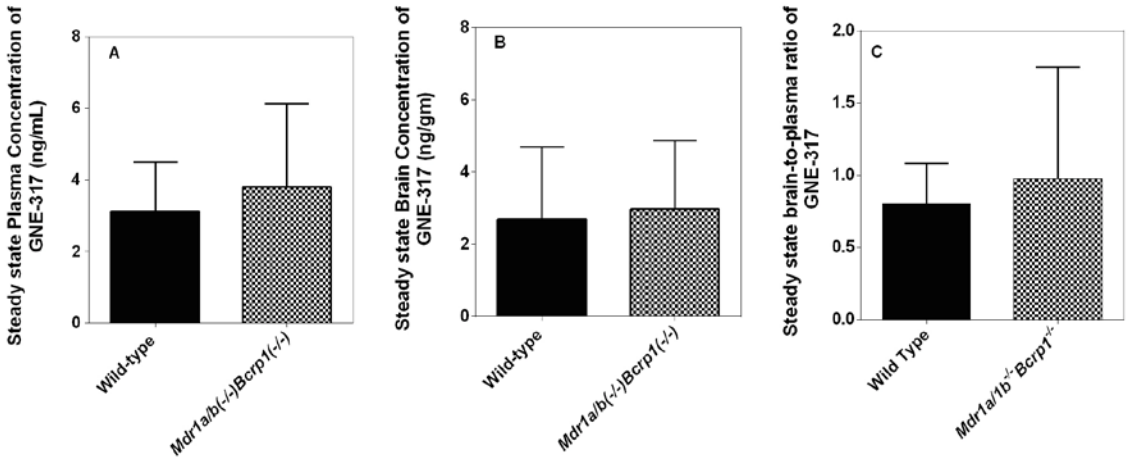

Figure 6.6 (d-f): Steady state (d) plasma concentrations and (e) brain concentrations of GDC-0980 in FVBn wild-type and TKO mice after a continuous intraperitoneal infusion at a rate of 10 µg/hr for 48 hours; (f) corresponding steady-state brain-to-plasma concentration ratio. Values are represented as mean ± S.D. (n= 4 per group), ***p<0.05 compared to wild-type.

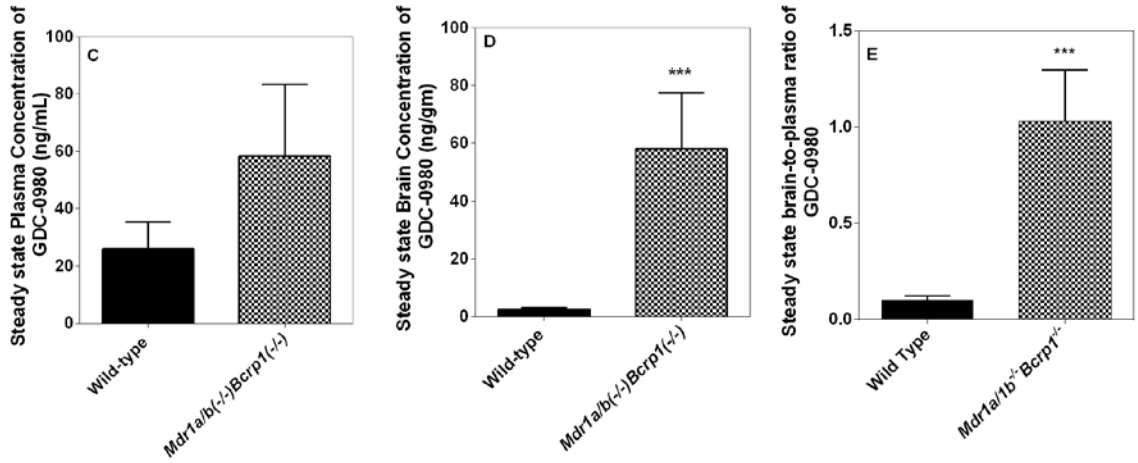

Table 6.3: Steady state plasma and brain concentrations of GNE-317 and GDC-0980 in wild-type and Mdr1a/b(−/−)Bcrp1(−/−) mice after a constant intraperitoneal infusion of GNE-317 at a rate of 5 µg/hr or GDC-0980 at a rate of 10 µg/hr for 48 hrs (n =4 each group). *Data presented as mean ± S.D., $^{\#}P < 0.005$ compared to wild-type.

	GNE-317		**GDC-0980**	
	Wild-type	*Mdr1a/b(-/-) Bcrp1(-/-)*	Wild-type	*Mdr1a/b(-/-) Bcrp1(-/-)*
Plasma C_{ss} (ng/mL)	3.12 ± 1.38	3.81 ± 2.32	25.99 ± 9.45	58.42 ± 24.9
Brain C_{ss} (ng/gm)	2.69 ± 2.00	2.98 ± 1.89	2.53 ± 0.7	58.06 ± 19.4
Brain/Plasma ratio	0.81 ± 0.28	0.98 ± 0.77	0.1 ± 0.02	$1.03 \pm 0.27^{\#}$

6.3.5 DIFFERENTIAL BRAIN DISTRIBUTION OF GNE-317 AND GDC-0980 IN GLIOMA MODELS

We assessed the ability of the BBB to restrict the brain distribution of molecularly targeted agents to different regions of a tumor brain in all three glioma models guided by GFP-labeled tumor cells. This was achieved using two dual PI3K/mTOR inhibitors, GNE-317 and GDC-0980. Each of these drugs has different liabilities for active efflux by P-gp and Bcrp at the BBB. GFP-guided tumor dissection allowed the tumor brain to be divided into three sections - the tumor core, the brain around the tumor ("rim") and the contralateral hemisphere ("normal brain") **(Figure 6.2).**

6.3.5.1 GL261-LUC-GFP LABELED MICE

Mice were either administered vehicle, GNE-317 or GDC-0980 once daily for three consecutive days and plasma and brain were harvested at 1 hr or 6 hr after the last oral dose. Comparison of brain concentrations in the tumor core vs. the rim vs. the contralateral hemisphere suggests that there is significant heterogeneity in brain distribution due to the tumor and the accompanying changed in BBB disruption.

As shown in **figure 6.7 (a),** after 1 hr and 6 hr post last oral dose, the brain concentrations in the tumor core vs. the rim vs. the normal brain were not significantly different for GNE-317. The corresponding brain-to-plasma ratios at both 1hr and 6 hr for the three regions of the brain suggest that active efflux by both P-gp and Bcrp does not influence

brain penetration of GNE-317 **(figure 6.7 (b) and table 6.4).**

On the contrary, brain concentrations for GDC-0980 were significantly different amongst the different regions of the brain. The mean GDC-0980 brain concentrations in the tumor core at 1 hr after the last oral dose was 0.72 ± 0.28 μg/gm and decreased to 0.16 ± 0.10 μg/gm in the rim and 0.078 ± 0.037 μg/gm in the contralateral hemisphere at 1 hr post last oral dose. Similar trend was observed at 6 hours post dose. The mean brain concentrations in the tumor core (0.20 ± 0.11 μg/gm) were higher than in the brain around the tumor (0.04 ± 0.02 μg/gm) and the contralateral hemisphere (0.07 ± 0.04 μg/gm) **(figure 6.7 (c) and table 6.4).**

The corresponding brain-to-plasma concentration ratio at 1 hr and 6 hr post oral dose was 0.59 ± 0.17 and 0.33 ± 0.22, respectively in the tumor core and decreased significantly in the tumor rim and contralateral hemisphere ($p<0.05$). At both 1 hr and 6 hr, the brain-to-plasma ratios in the tumor rim (0.12 ± 0.04 and 0.05 ± 0.02) and in the contralateral hemisphere (0.05 ± 0.01 and 0.12 ± 0.08) were not significantly different **(figure 6.7 (d)).** These results indicate that although BBB integrity is disrupted in the tumor core and drug can penetrate this region, the intact BBB in the regions beyond the core (the tumor rim and the contralateral hemisphere) restricts delivery of drugs.

Figure 6.7 (a-b): Regional brain distribution of GNE-317 (30 mg/kg) in GFP-luc-GL261 syngeneic mouse glioma model. (a) Brain concentrations of GNE-317 were not significantly different from each other in the core, brain around the core and the contralateral hemisphere. The brain concentrations closely followed plasma concentrations at both 1 hr and 6 hr after the last oral dose. The corresponding brain-to-plasma ratios are shown in (b .) Data represented as Mean ± S.D. (n=6 per time point per drug).

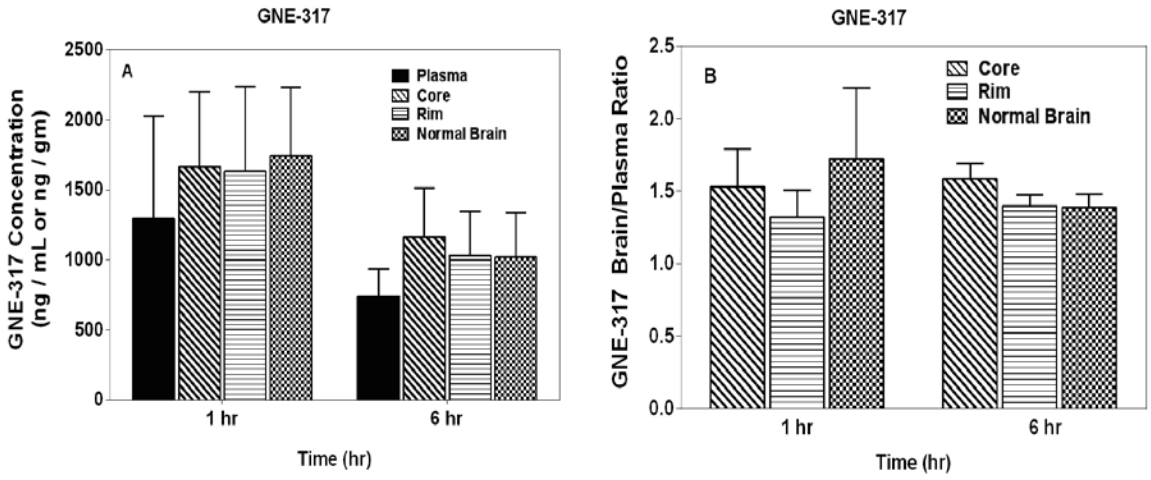

Figure 6.7 (c-d): Regional brain distribution of GNE-317 (30 mg/kg) and GDC-0980 (7.5 mg/kg) in GFP-luc-GL261 syngeneic mouse glioma model. (c) brain concentrations of GDC-0980 were significantly higher than the brain concentrations in the rim and the contralateral hemisphere at both 1 hr and 6 hr after the last oral dose. The corresponding brain-to-plasma ratios are shown in (d). All values are represented as mean ± S.D. (n= 6 at each time point per drug). *p<0.05 compared to concentrations in the core, #p<0.05 compared to plasma concentrations

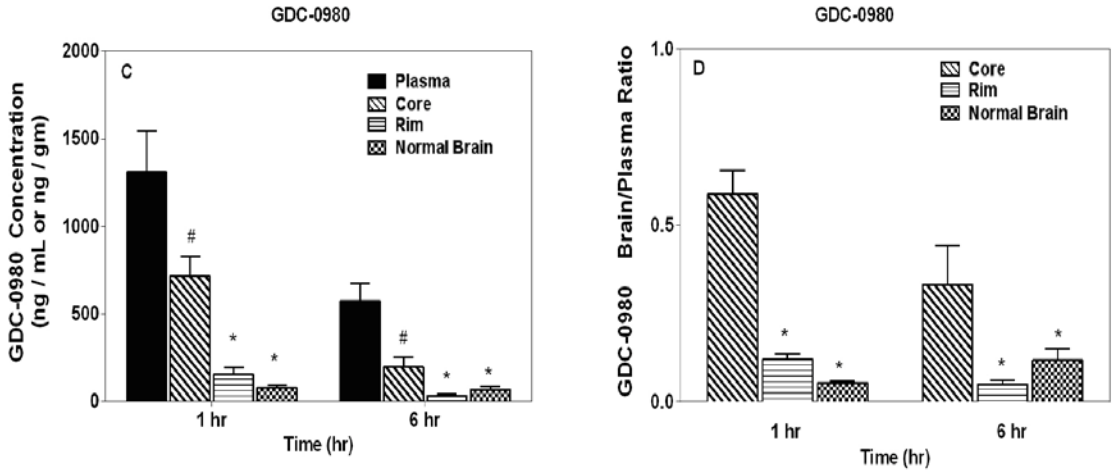

Table 6.4: plasma and brain concentrations of GNE-317 (30 mg/kg) and GDC-0980 (7.5 mg/kg) after 3 consecutive doses once daily in GFP-luc-GL261 mouse glioma model. Values represent mean ± S.D. (n= 6 per time point pretreatment).

NB= normal contralateral hemisphere

GDC-0980							
	Concentrations				**B/P ratio**		
	Plasma (µg/mL)	**Core (µg/gm)**	**Rim (µg/gm)**	**NB (µg/gm)**	**Core (µg/gm)**	**Rim (µg/gm)**	**NB (µg/gm)**
1 hr	1.3 ± 0.58	0.72 ± 0.28	0.16 ± 0.10	0.08 ± 0.04	0.6 ± 0.2	0.12 ± 0.04	0.05 ± 0.01
6 hr	0.58 ± 0.22	0.20 ± 0.11	0.04 ± 0.02	0.07 ± 0.04	0.33 ± 0.22	0.05 ± 0.02	0.12 ± 0.08
GNE-317							
1 hr	1.3 ± 0.74	1.8 ± 0.53	1.7 ± 0.58	1.7 ± 0.44	1.58 ± 0.59	1.45 ± 0.46	1.73 ± 1.08
6 hr	0.74 ± 0.19	1.2 ± 0.35	1.0 ± 0.32	1.0 ± 0.32	1.58 ± 0.26	1.40 ± 0.19	1.39 ± 0.23

6.3.5.2 GFP-LABELED GBM10 AND GFP-LABELED U87 MODEL

Mice were administered a single oral dose of GNE-317 (30 mg/kg) and GDC-0980 (7.5 mg/kg) simultaneously and plasma and brain were harvested 1 hr after the dose. For GBM10 glioma model, we did not harvest plasma. Drug concentrations were determined in brain core vs. rim vs. contralateral hemisphere as described previously. **Figure 6.8** shows plasma and brain concentrations of GNE-317 and GDC-0980 in U87 and GBM10 glioma model. The brain concentrations of GNE-317 in the core, rim and contralateral hemisphere were not significantly different to each other and to plasma in the U87 model (**figure 6.8 (a)).** The brain concentrations for GDC-0980 in the core were higher than the brain concentrations in the rim and the contralateral hemisphere for U87 model, but they were not significantly different to each other. GDC-0980 brain concentrations in the core were significantly less than the corresponding plasma concentrations, suggesting limited brain penetration of GDC-0980 in the core. Similar trend was observed in GBM10 orthotopic xenograft model **(Figure 6.8 (c) and table 6.5).** The brain concentrations of GNE-317 were ~1 in all the three regions of the brain. However, for GDC-0980, although brain concentrations were higher in the core compared to the rim and contralateral hemisphere, these concentrations were not significantly different from each other. The corresponding brain-to-plasma ratios for GNE-317 and GDC-0980 in U87 model are shown in **Figure 6.8 (b)**.

Figure 6.8 (a-b): Regional brain distribution of GNE-317 (30 mg/kg) and GDC-0980 (7.5 mg/kg) in U87 orthotopic xenograft model of glioblastoma after a single simultaneous oral dose. Brain and plasma concentrations of GNE-317 and GDC-0980 are shown in (a) U87 model and (b) corresponding brain-to-plasma ratio at 1 hr after a single oral dose. Values are represented as mean ± S.D. (n=5 for U87). $^{\#}$p-value <0.05 compared to plasma

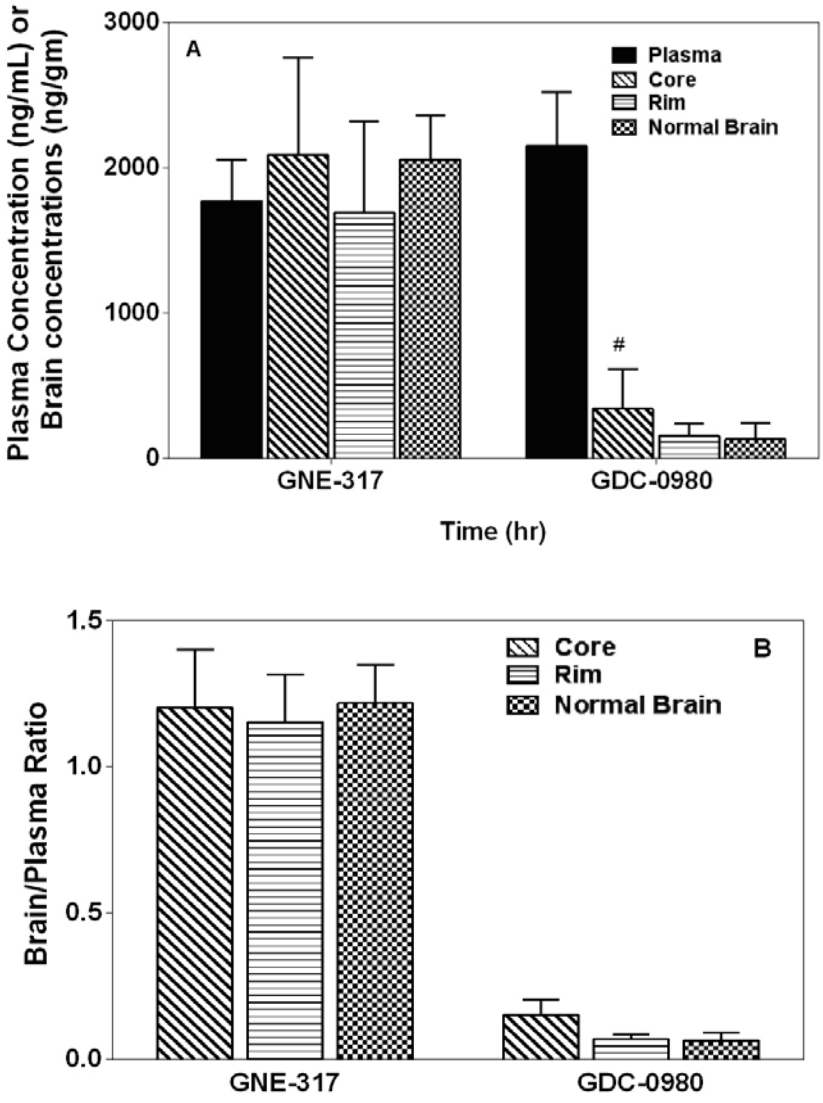

Figure 6.8 (c): Regional brain distribution of GNE-317 (30 mg/kg) and GDC-0980 (7.5 mg/kg) in GBM10 orthotopic xenograft model of glioblastoma after a single simultaneous oral dose at 1 hr post dose. Plasma concentrations are not shown, as plasma samples were not obtained. Values are represented as mean ± S.D. (n= 3 for GBM10).

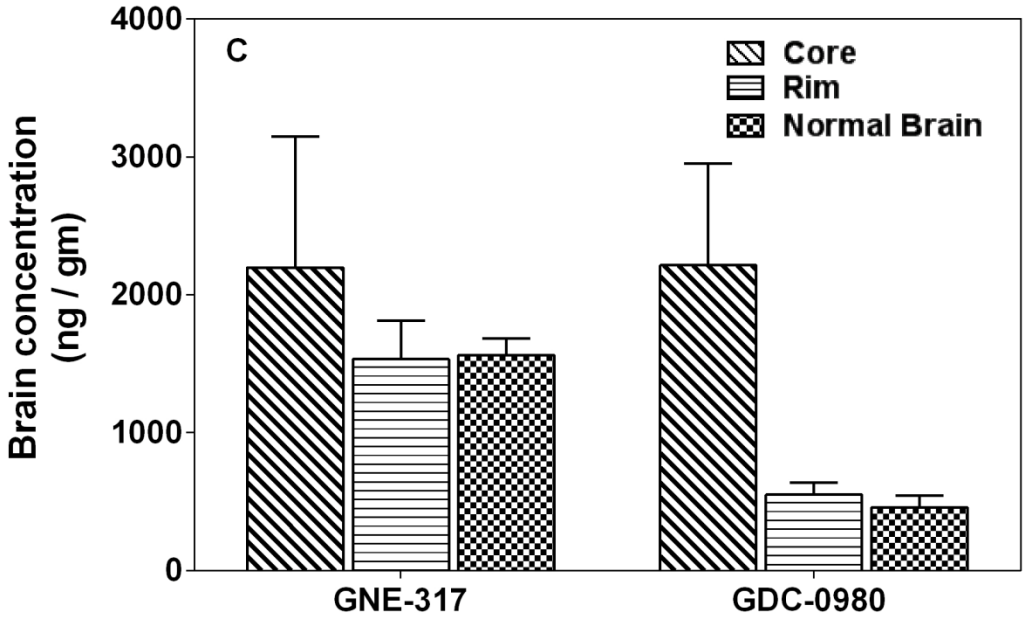

Table 6.5: Plasma and brain concentrations of GNE-317 (30 mg/kg) and GDC-0980 (7.5 mg/kg) at 1 hr after a single simultaneous oral dose in GBM10 and U87 orthotopic xenograft models of glioblastoma. Values represent mean ± S.D. (n= 3 for GBM10 and n=5 for U87)

GDC-0980							
	Concentrations				**B/P ratio**		
	Plasma (µg/mL)	**Core (µg/gm)**	**Rim (µg/gm)**	**NB (µg/gm)**	**Core (µg/gm)**	**Rim (µg/gm)**	**NB (µg/gm)**
GBM10	NA	2.2 ± 1.3	0.55 ± 0.16	0.45 ± 0.15	NA	NA	NA
U87	2.1 ± 0.37	0.34 ± 0.27	0.15 ± 0.09	0.13 ± 0.11	0.15 ± 0.12	0.07 ± 0.03	0.06 ± 0.05
GNE-317							
GBM10	NA	2.2 ± 1.6	1.5 ± 0.48	1.6 ± 0.21	NA	NA	NA
U87	1.8 ± 0.29	2.1 ± 0.67	1.7 ± 0.63	2.1 ± 0.30	1.2 ± 0.4	0.99 ± 0.45	1.2 ± 0.26

6.3.6 PHARMACODYNAMIC EFFICACY OF GNE-317 AND GDC-0980 IN THE BRAIN

To determine the influence of drug delivery on targeting potential, GL261-luc-GFP labeled mice were randomized into three groups and dosed with (a) placebo (vehicle), (b) GNE-317 (30 mg/kg), or (c) GDC-0980 (7.5 mg/kg) for 3 consecutive days. Mice were euthanized 1 h **(Figure 6.9 (a))** or 6 h **(Figure 6.9 (b))** after the third dose and brain was harvested. IHC was performed on 5μM thick sections for (phosphorylated) p-Akt, pS6 and p4EBP1 and total-AKT, S6 and 4EBP4. Based on staining for specific antibodies, we observed by visual inspection that there was a decrease in the expression of pS6 and p4EBP1 on treatment with GNE-317 and GDC-0980 at both 1 hr and 6 hr after the last oral dose compared to control (no treatment group) in the core and the rim. There appears to be a greater decrease in staining of tissues treated with GNE-317 compared to GDC-0980 treated group. No difference was observed in p-AKT and AKT expression in the control vs. the treated groups. The total levels of AKT, S6 and 4EBP1 did not change with treatment **(Figure 6.9 (c) and (d)).** Whole brain slices scale at 100 μm and inset scale at 15 μm.

Figure 6.9 (a): Immunohistochemistry of phosphorylated antibodies upregulated in GL261-luc-GFP syngeneic mouse model for (a) no treatment, (b) GDC-0980 alone and (c) GNE-317 alone at 1 hr after the last oral dose. Brown stain indicates presence of respective protein in the tissues.

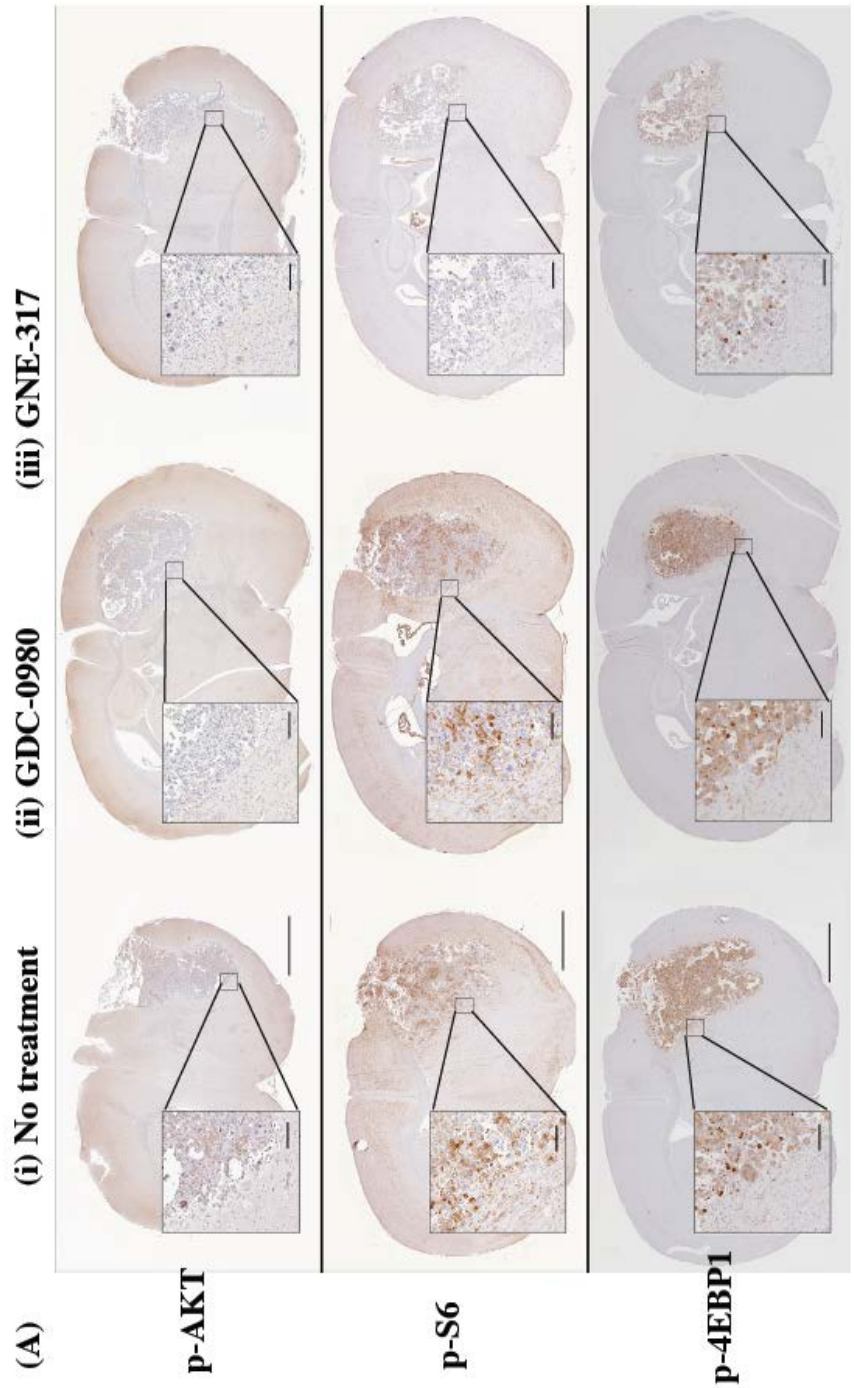

Figure 6.9 (b): Immunohistochemistry of phosphorylated antibodies upregulated in GL261-luc-GFP syngeneic mouse model for (a) no treatment, (b) GDC-0980 alone and (c) GNE-317 alone at 6 hr after the last oral dose. Brown stain indicates presence of respective protein in the tissues.

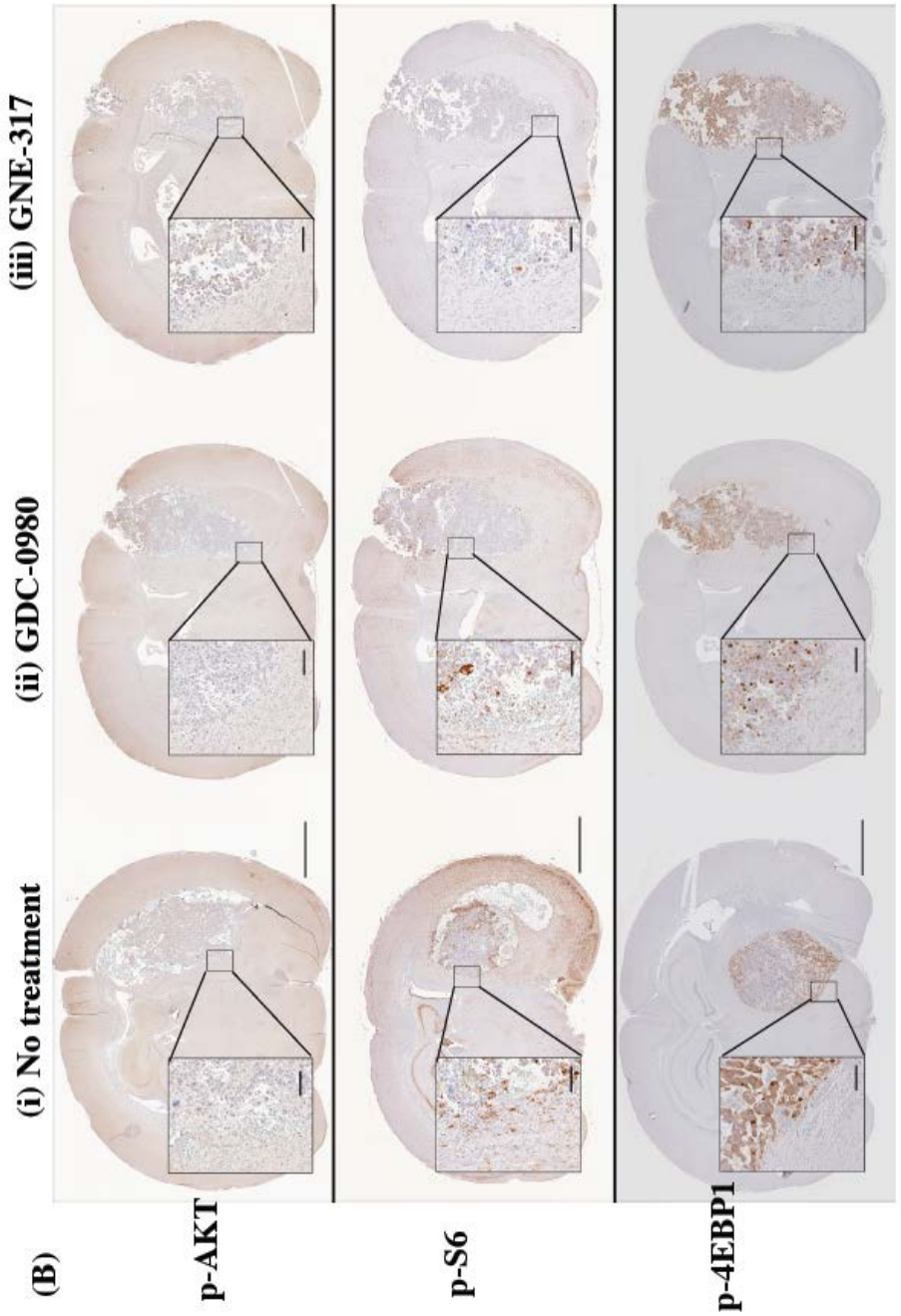

Figure 6.9 (c): Immunohistochemistry of total levels of intracellular targets in GL261-luc-GFP syngeneic mouse model for (a) no treatment, (b) GDC-0980 alone and (c) GNE-317 alone at 1 hr after the last oral dose. Brown stain indicates presence of respective protein in the tissues.

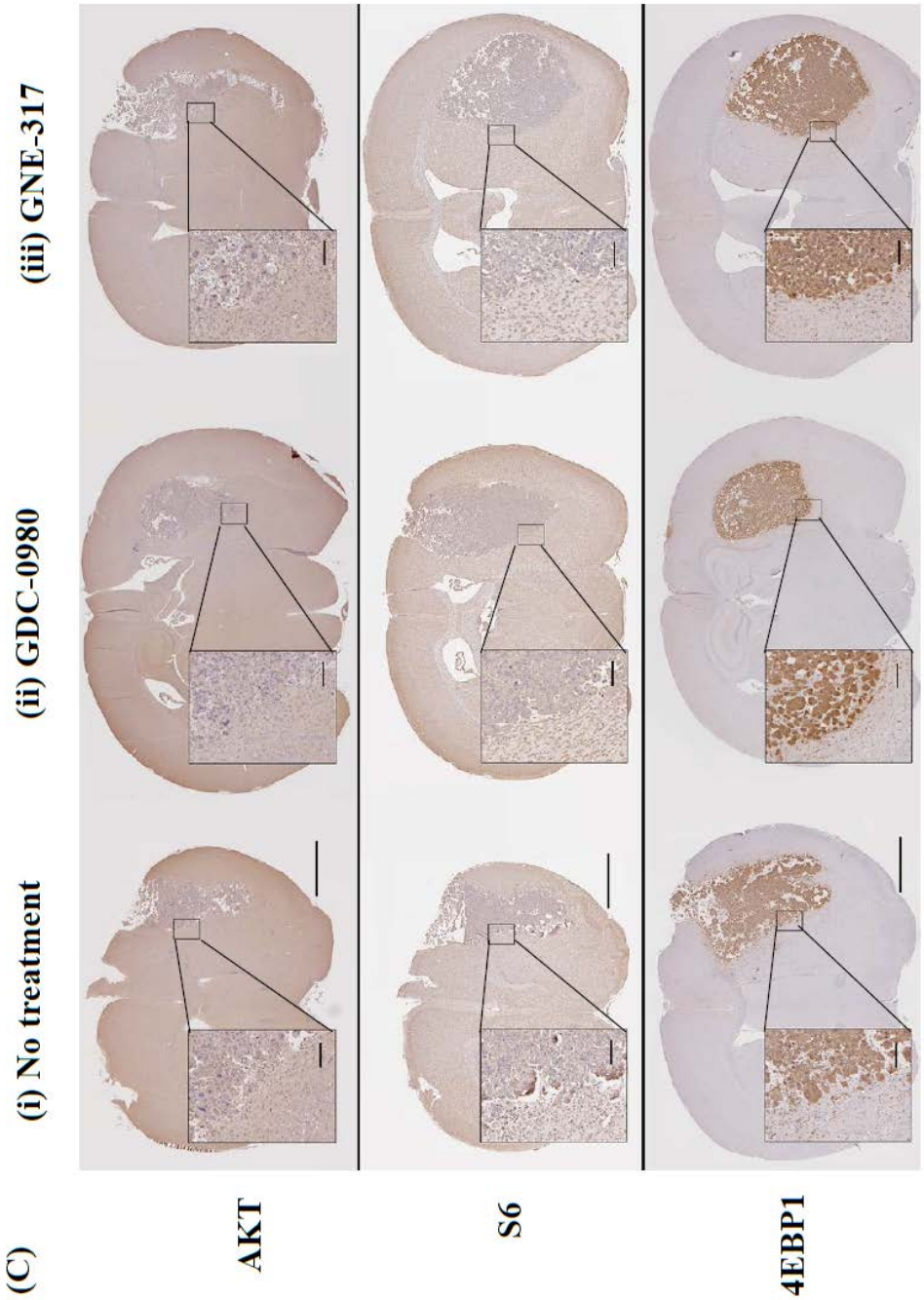

Figure 6.9 (d): Immunohistochemistry of total levels of intracellular targets in GL261-luc-GFP syngeneic mouse model for (a) no treatment, (b) GDC-0980 alone and (c) GNE-317 alone at 6 hr after the last oral dose. Brown stain indicates presence of respective protein in the tissues.

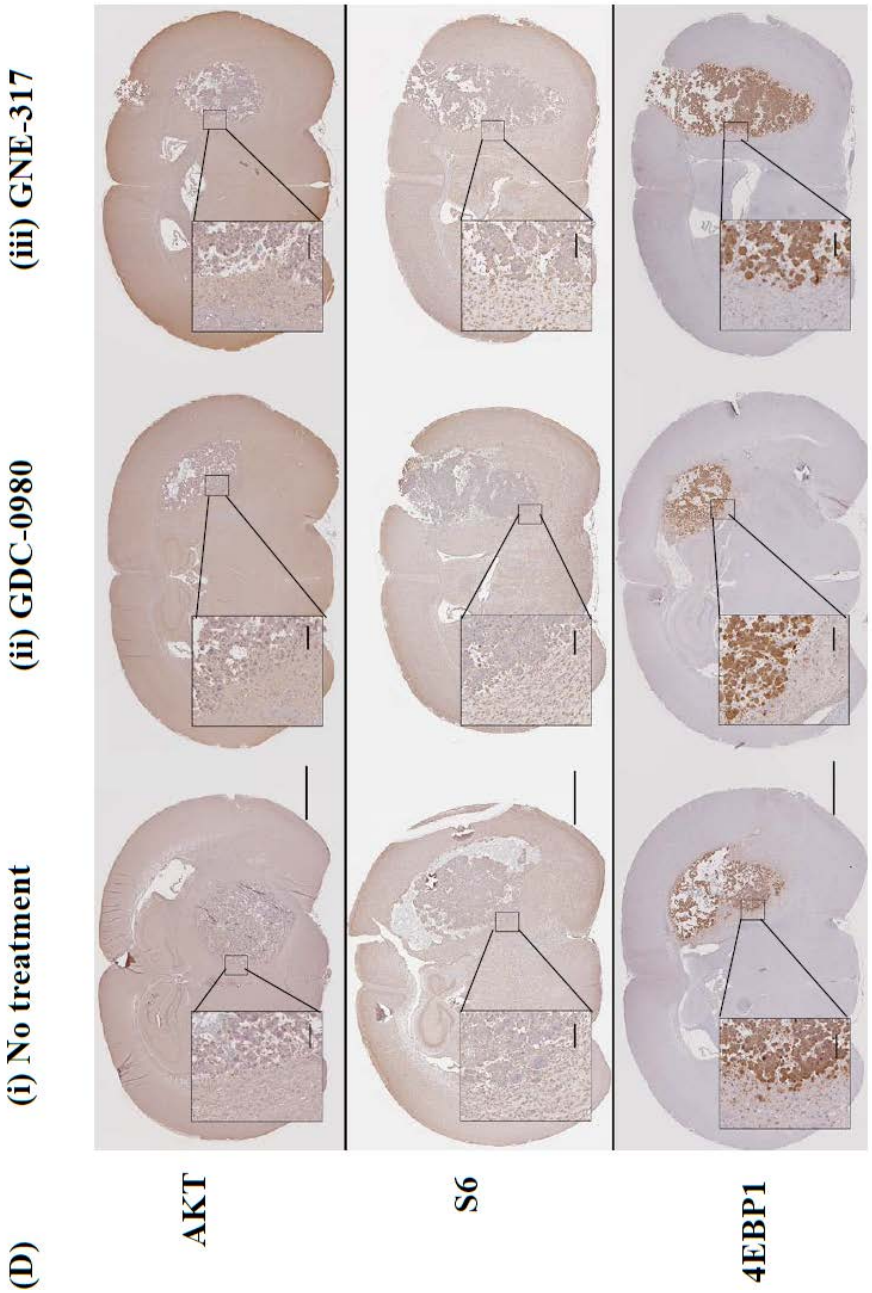

6.3.7 SURVIVAL BENEFIT IN GLIOMA MODELS

Therapeutic efficacy of both GNE-317 and GDC-0980 was studied in all three glioma models where mice were treated with control (vehicle) or GNE-317 (30 mg/kg) or GDC-0980 (7.5mg/kg) until moribund or dead. Survival studies in U87 glioma model showed no difference in survival in GNE-317 treated group vs. GDC-0980 treated group ($p=0.12$), but both treatments were significantly different from placebo ($p<0.0005$) **(figure 6.10 (a)).**

Figure 6.10: Survival efficacy of GNE-317 and GDC-0980 in (a) U87, (b) GBM10 and (c) GL261 mouse glioma models. Mice were randomized into three groups, placebo (vehicle control), GNE-317 (30 mg/kg) and GDC-0980 (7.5 mg/kg). Survival is represented as a cumulative survival of 10 mice in each group. Time scale indicates time from the first day of treatment.

(a) U87

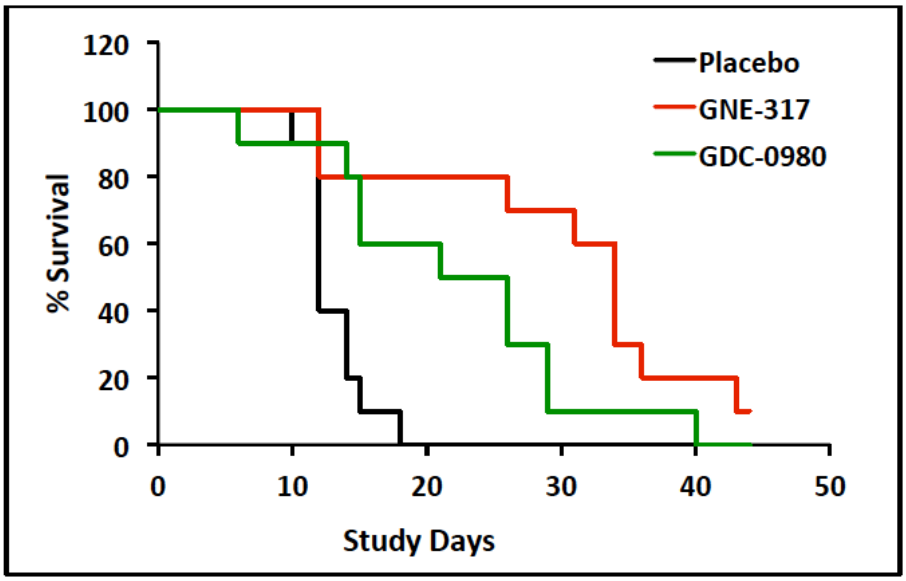

Survival in GBM10 xenografts also showed similar trend wherein there was no significant difference in survival between GNE-317 and GDC-0980 treated groups (p=0.071) but both treatments dramatically extended survival compared to placebo vehicle control (placebo vs. GNE <0.0001 and placebo vs. GDC <0.035) **(figure 6.10 (b)).**

Figure 6.10 (b): Survival efficacy of GNE-317 and GDC-0980 in GBM10

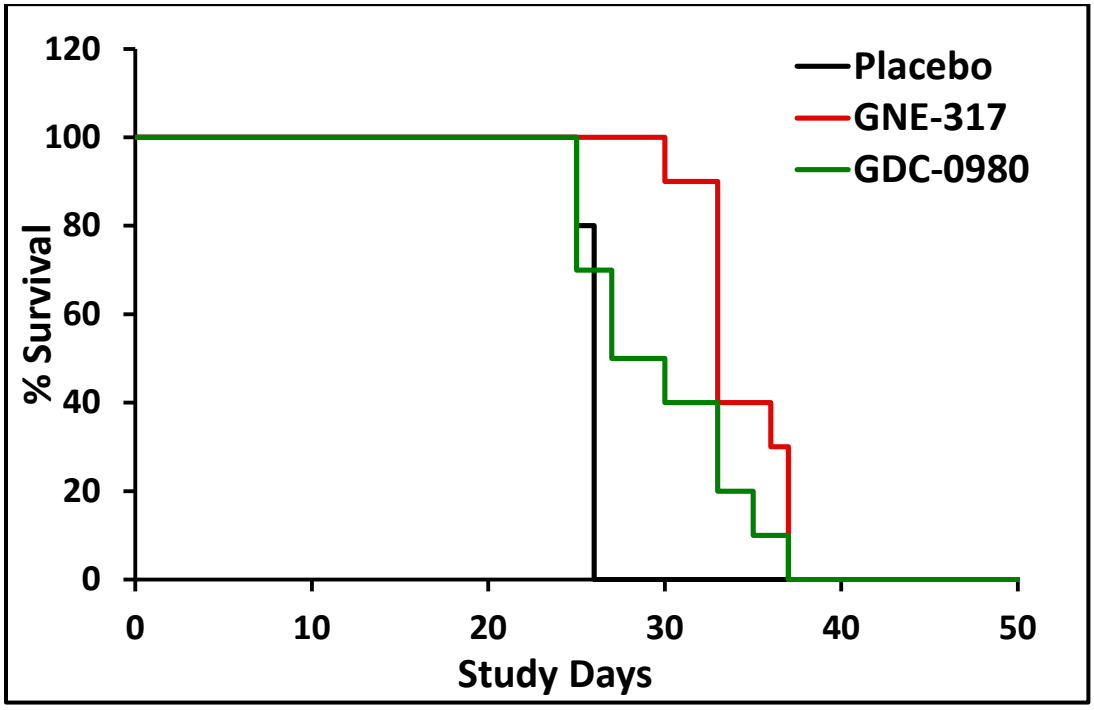

On the other hand, results in GL261 model showed that there was no difference in survival in any of the treatment groups **(figure 6.10 (c) and table 6.6).** The GDC-0980 treated group showed earlier deaths compared to GNE-317 treated group. The median bioluminescence values were similar across all groups (**Figure 6.10 (d))**. This suggested that the tumor burden was not affected by treatment and earlier deaths in GDC-0980 treated group could be attributed to toxicity in GL261 model over once daily dosing regimen **(figure 6.10 (d)).** Results from GL261 model require further investigation. It appears that although both GNE-317 and GDC-0980 have similar potency *in-vitro* (similar IC50s), none of the drugs showed improvement in efficacy when administered *in-vivo*. This could be attributed to differences in dosing, as both the drugs were given at the maximally tolerated dose (as suggested by Genentech). It is also likely that the GL261 tumor is less sensitive to PI3K driven pathway.

Figure 6.10 (c): Survival efficacy of GNE-317 and GDC-0980 in GL261

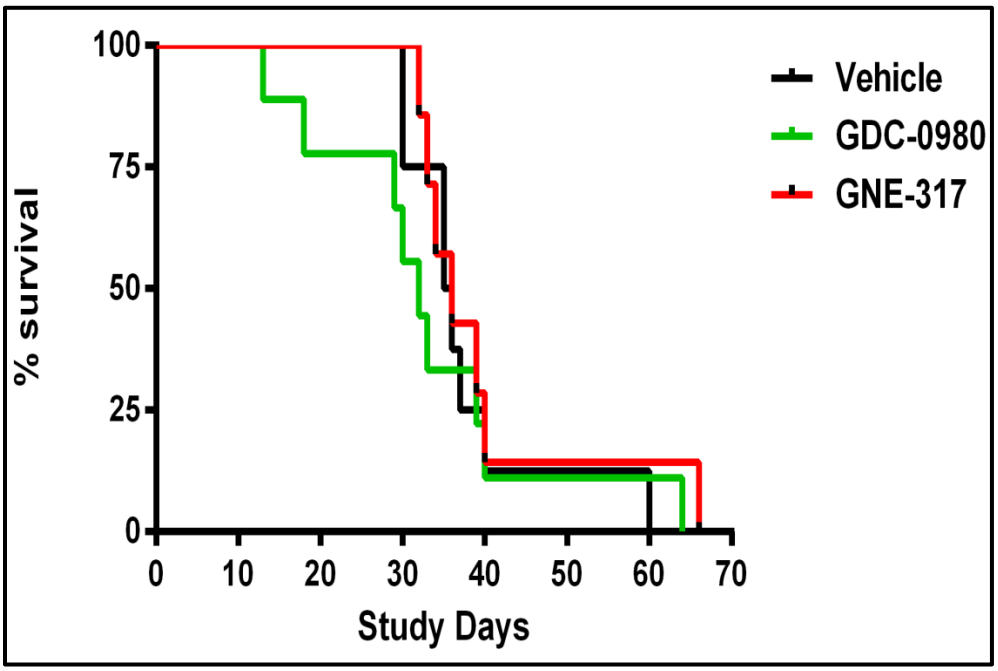

Figure 6.10 (d): shows the corresponding tumor burden as measured by bioluminescence in GFP-luc-GL261 mouse model. The figure shows that there was no decrease in the tumor burden on treatment with GNE-317 or GDC-0980 compared to no treatment (placebo) suggesting that GNE-317 and GDC-0980 were not effective against GL261 model.

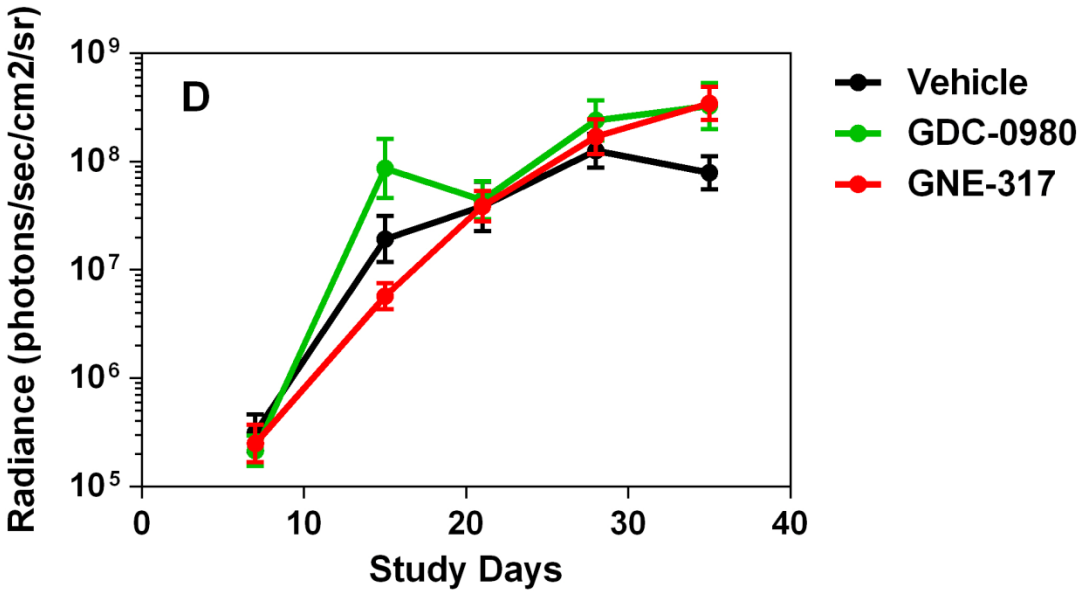

Table 6.6: Survival probabilities of GNE-317 and GDC-0980 in U87, GBM10 and GL261 mouse model of glioblastoma.

P-value vs. Placebo by log-rank test				
Treatment	**N**	**U87**	**GBM10**	**GL261**
GNE-317	10	<0.0003	< 0.0001	<0.64
GDC-0980	10	<0.0004	< 0.035	<0.72
GNE-317 vs. GDC-0980	10	=0.12	= 0.071	=0.27

The results from survival study show that both GNE-317 and GDC-0980 are therapeutically effective in improving survival compared to placebo in GBM10 and U87 xenografts but these drugs were not different from each other. The failure of these drugs to show difference in efficacy compared to each other could be due to limited single agent efficacy of GNE-317 compared to GDC-0980, despite better BBB permeability. Both GNE-317 and GDC-0980 did not show any survival benefit in GL261 syngeneic model suggesting that these drugs may not be efficacious in this model.

6.4 DISCUSSION

Glioblastoma multiforme (GBM) is a grade IV astrocytoma with poor prognosis and median survival of 12-15 months despite multi-model treatment options. The infiltrative nature of the disease makes it particularly challenging to treat the tumor cells that lie in areas centimeters away from the tumor core. Drug delivery-related issues have often not been considered a plausible explanation because high drug concentrations are observed in the tumor core, indicating a disrupted BBB. The objective of this study was (a) to investigate whether the BBB is heterogeneously disrupted in GL261, GBM10 and U87 mouse models of glioma, which recapitulates the pathology of human GBM. This is important to fully understand the influence of BBB in drug delivery to GBM, (b) although the BBB is disrupted in the tumor core, presence of an intact BBB in the area around the tumor core and in the contralateral hemisphere, can severely restrict delivery of molecularly targeted agents intracellularly and (c) there is a need of not only effective delivery but also an effective drug to target the tumor cells.

GBM is a highly aggressive and invasive brain tumor and in order to assess success of therapy it is important to identify appropriate models that share the same invasive and heterogeneity properties as human GBM. GL261 is a syngeneic model that closely mimics GBM in invasiveness and angiogenic properties (Newcomb and Zagzag, 2009). Newcomb and Zagzag have shown that similar to the human GBM, the GL261 murine model also demonstrates an irregularly shaped heterogeneous mass with disrupted BBB (Newcomb and Zagzag, 2009; Zagzag et al., 2000). There are several studies that have

shown that drug concentrations in the resected tumor core are higher comparable to the concentrations in the regions non-enhanced on contrast imaging. In a seminal study by Blakeley and colleagues, the authors showed that methotrexate concentrations in the tumor core were ten-fold higher than in the regions beyond the core (Blakeley et al., 2009). Similar results have been reported for other anti-cancer agents such as paclitaxel (Fine et al., 2006) and temozolomide (Rosso et al., 2009). Previously our group has reported similar results for erlotinib (Agarwal et al., 2013) and dasatinib (Agarwal et al., 2012) in both, a spontaneous and a xenograft glioma model. We have demonstrated that the lack of efficacy and overall survival were related to the presence of Bcrp/P-gp in the intact BBB in areas away from the tumor core in the wild type tumor bearing mice compared to P-gp/Bcrp knockout mice.

PI3K/mTOR/AKT is one of the most frequently dysregulated pathways in GBM. Some drugs targeting this pathway have shown limited distribution across the BBB due to activity of the efflux transporters, P-gp and Bcrp (Chu et al., 2009; Salphati et al., 2010). To fully evaluate the role of active efflux at the BBB, we conducted brain distribution studies in non-tumor bearing (FVBn) and tumor bearing syngeneic (GL261-luc-GFP) glioma model and xenograft models (GBM10 and U87) using two structurally related dual PI3K/AKT/mTOR inhibitors, GNE-317 and GDC-0980, with different substrate affinities for active efflux transporters, P-gp and Bcrp.

Our studies show that the BBB is disrupted in the tumor core. The accumulation of Texas

Red dextran (TRD), a vascular marker, varied in the brain with higher accumulation in the tumor core and no accumulation in the contralateral hemisphere. Such differences in BBB disruption suggests that the drug concentrations observed in the tumor core do not fully represent the true whole brain concentrations and this could mislead our interpretation for inadequacy in drug delivery. The brain distribution studies in non-tumor and tumor bearing mice indicate that GNE-317 has better brain delivery than GDC-0980. The steady-state brain-to-plasma concentration ratio of GNE-317 was similar in FVBn-wild type (0.81 ± 0.28) vs. TKO mice (0.98 ± 0.77). However, the steady-state brain-to-plasma concentration ratio of GDC-0980 was ~10 fold higher in TKO mice (0.1 ± 0.02 (Wild-type) vs. 1.03 ± 0.27 (TKO)). The steady-state brain-to-plasma ratios for both GNE-317 and GDC-0980 obtained after administering both drugs separately in mice were comparable to the brain partition coefficient (Kp) obtained after a single oral dose of both drugs administered simultaneously in wild-type and TKO mice. This suggests linear distribution kinetics of both GNE-317 and GDC-0980 and clarifies potential for any pharmacokinetic interaction between the two drugs when administered simultaneously.

Tumor brain distribution studies show that brain concentrations of GNE-317 are similar in the core vs. the brain around the core vs. the contralateral hemisphere. Thus, the brain-to-plasma ratio is ~1 across all regions of the brain in U87 and GL261 model. We could not determine brain-to-plasma ratios for GBM10 as we did not obtain plasma specimens. However, the brain concentrations of GDC-0980 in the core were higher compared to the

regions beyond the core (rim and the contralateral hemisphere) in all the three glioma models studied. The difference in brain concentrations was significant in GL261 mouse model but not in GBM10 and U87 mouse models. Thus the brain-to-plasma ratios of GDC-0980 vary across all regions of the brain. These results demonstrate the functional importance of active efflux on an intact BBB in the tumor periphery, which harbors invasive tumor cells. Results from the tumor distribution studies in glioma mouse models suggest that brain distribution of GNE-317 is not limited by active efflux at the BBB whereas GDC-0980 has restricted brain penetration in the areas around the tumor core and in the contralateral hemisphere.

However, differences in tumor distribution of GNE-317 and GDC-0980 did not affect efficacy *in-vivo* between the two groups in all glioma mouse models investigated (GL261 syngeneic mouse model, patient-derived xenograft GBM10 and cell-line derived U87 mouse model). In both GBM10 and U87, although both treatment groups were significantly different from placebo and improved survival, we did not see a significant difference in efficacy of GNE-317 vs. the GDC-0980 treated group. This discrepancy in efficacy of GNE-317 vs. GDC-0980 in GBM10 and U87 suggest that GNE-317 may not have sufficient single agent activity against PI3K and mTORs (mTORC1 and mTORC2). There could also be issues related to the intestinal absorption and bioavailability of GNE-317 compared to GDC-0980 due to differences in dosing, although both GNE-317 and GDC-0980 had equivalent AUCs in plasma. We administered maximal tolerated dose for both GNE-317 and GDC-0980 in all the studies as suggested by Genentech. In GL261

mouse model there was no effect of either drug in improving the survival of mice. Despite similar targeting potential of these drugs *in-vitro,* and reduction in expression of targets such as p-S6 and p-EBP41 in immunohistochemical analysis, we did not observe any efficacy in *in-vivo.* A plausible explanation for this could be that GL261 tumor is not a PI3K driven tumor and hence these drugs did not show expected pharmacodynamic effects on improving survival *in-vivo*. These studies indicate that although the blood brain barrier is an impediment to drug delivery, it is also important to consider a drug with right efficacy and targeting potential. Moreover, in order to better understand these aspects of drug delivery, it is critical that we use an appropriate animal model that will help us delineate the role of a targeted agent against a pathway. One alternative is to use spontaneous glioma models which are driven by a particular gene such as *PTEN*($^{-/-}$) driven tumor bearing mice.

6.5 CONCLUSIONS

In summary, this study underlines the importance of the BBB in restricting delivery of anti-cancer agents to the tumor cells for treatment of GBM. The heterogeneity in BBB integrity in GL261 and GBM10 model illustrates accurate representation of an invasive tumor like GBM. Disruption of BBB in the tumor core vs. the tumor periphery and the contralateral hemisphere emphasizes the fact that drug concentrations measured in the tumor core do not represent true brain concentrations and believing that the BBB is not an impediment to drug delivery for GBM is misleading. This could be one of the

plausible reasons for failure of several drugs in clinical trials and higher rates of tumor recurrence.

6.6 FOOTNOTES

I would like to thank Dr. David Largaespada (Department of Genetics, Cell Biology and Development) and Chani Becker (graduate student, Department of Neuroscience) at the University of Minnesota and Dr. Jann N. Sarkaria and Jenny Pokorny (Mayo Clinic) for their collaboration on this project. I would also like to thank Joey McFarren and Daniel M. Muldoon (undergraduate students, Department of Neuroscience, University of Minnesota) for helping with imaging and IHC in this project.

CHAPTER VII

RECAPITULATION

Glioblastoma multiforme (GBM) is a devastating and incurable primary brain tumor. Despite advances in treatments such as surgery, radiation and chemotherapy, recurrence of the tumor is inevitable leading to patient death. The median overall survival in GBM patients is 12-18 months and after recurrence, the survival is 5-7 months. With advances in research, several new molecularly-targeted agents have been evaluated in GBM patients, but they have shown limited clinical benefit in prolonging overall survival. Treatment of GBM becomes challenging due to two major factors; (a) the invasive growth pattern of GBM that results in infiltration of tumor cells to areas centimeters away from the tumor core, resulting in formation of satellite lesions in the brain which are capable of tumor regrowth; (b) the presence of intact blood brain barrier (BBB) in the areas surrounding the tumor core that shield the tumor cells from chemotherapy. The blood-brain barrier such as, through a combination of endothelial tight junctions and active efflux transporters, P-glycoprotein (P-gp) and breast cancer resistance protein (BCRP), acts as a protective barrier that limits therapeutic efficacy of many chemotherapeutic drugs.

The most important aspect of GBM treatment lies in understanding the fact GBM is a highly invasive and infiltrative tumor wherein the tumor cells reside behind an intact BBB in areas away from the bulk tumor mass. It is important to acknowledge that although the BBB is disrupted in the tumor core, presence of intact BBB in the brain around the core (“rim”) and the normal contralateral hemisphere makes GBM a disease of the whole brain and this makes the need to effectively deliver drugs across the BBB

imperative. The heart of this thesis project is to investigate the role of active efflux transporters in brain distribution of molecularly-targeted agents in non-tumor bearing and glioma-tumor bearing mice.

The first part of this project dealt with development and validation of an analytical assay for determination of mouse plasma and brain tissue concentrations of sunitinib, an anti-VEGFR inhibitor, using liquid chromatography tandem mass spectrometry (LC-MS/MS) **(chapter 2).** Consequently, this assay was utilized to determine sunitinib concentrations in FVB mice **(chapter 3).** Earlier our lab and several other researchers have reported and demonstrated that P-gp and Bcrp limit brain distribution of molecularly-targeted agents such as sorafenib, gefitinib, erlotinib, imatinib, cediranib and dasatinib. In this project we pharmacokinetically examined the role of active efflux by P-gp and Bcrp on the brain distribution of sunitinib in FVB-wild type, *Mdr1a/b(-/-), Bcrp1(-/-)* and *Mdr1a/b(-/-)Bcrp1(-/-)* mice. We compared the brain partition coefficient of sunitinib in all four genotypes after a single oral dose and at steady state after continuous intraperitoneal infusion. These brain-to-plasma ratios, called as brain partition coefficient (Kp) were compared to the transient steady state ratios for all genotypes. The transient steady state is defined as the point in time, after a single dose, at which the rate of drug entry into the brain is equal to the rate of exit from the brain. For a system that follows linear distribution kinetics, these ratios will be similar. Results from these studies indicated that both absence of both P-gp and Bcrp increased brain penetration of sunitinib resulting in a drug targeting index (DTI) of ~49 fold. This suggests that both P-gp and Bcrp play a role

in restricting the brain distribution of sunitinib into the brain. We further evaluated the influence of administering pharmacological inhibitors of active efflux transporters. We observed that dual inhibition of P-gp/Bcrp1 via administration of elacridar (GF120918) resulted in similar brain-to-plasma ratio at 1 hr post oral dose of sunitinib (~12 fold increase) as observed in *Mdr1a/b(-/-)Bcrp1(-/-)* mice at 1 hr post oral dose (~17.3 fold increase).

In an one-point-per-animal study designs, a naïve-pooled approach is used to estimate AUCs in plasma and the tissue and the AUC ratio is used to estimate the brain partition coefficient (Kp). Kp is obtained as a point estimate and such ratios ignore within-animal correlations; in addition, they are not associated with any statistical certainty. We proposed a novel statistical analysis approach method using a non-linear mixed effect modeling approach (NONMEM) **(chapter 4)** to estimate variability in the brain partition coefficient for brain distribution studies in a serial-sacrifice design. In this chapter, we used the sunitinib study reported in chapter 3 as a model case study. We developed a pharmacokinetic model to simultaneously depict plasma and brain concentrations, thus maintaining within-animal correlations. Our results indicate that the predicted plasma and brain concentrations closely followed the observed values in all four genotypes. Additionally, the Kp ratios obtained from the model were comparable to the Kp ratios obtained from the NCA analysis. Furthermore, we evaluated bias and precision in estimation of Kp under the influence of study design elements such as between-animal variability and sample size at each time point using a stochastic simulation and estimation

method (SSE). Our results suggest that the assumptions regarding the magnitude of bias and sample size do not influence Kp, but precision is affected by sample size.

The final chapter of this thesis project examined the role of active efflux in glioma tumor bearing mice using two dual PI3K/mTOR inhibitors with different BBB permeability characteristics **(chapter 5)**. GNE-317 is designed to evade active efflux and penetrate the BBB, while GDC-0980 has limited brain permeability due to active efflux by P-gp and Bcrp. We used a GL261-luc-GFP labeled syngeneic mouse model, a patient-derived GBM10 orthotopic xenograft mouse model, and a cell-line derived U87 orthotopic xenograft mouse model. We showed that the BBB is heterogeneously disrupted within the tumor core and this could mislead our interpretation for drug distribution into the tumor. Using GFP-labeled tumor models we investigated the brain distribution of GNE-317 and GDC-0980 in the tumor core, the rim (brain around the tumor), and the contralateral brain tissue. The results showed that the brain distribution of GNE-317 was similar in the three regions of the brain. On the other hand, for GDC-0980, higher drug concentrations were observed in the tumor core compared to the areas surrounding the tumor core, that is, the rim and contralateral hemisphere. This indicated that the BBB is intact in areas away from the core, thereby limiting brain distribution of drugs with limited permeability across the brain capillary endothelial cells. We further examined the influence of drug efflux mechanisms on the efficacy of GNE-317 and GDC-0980 in all three glioma models. Results from GBM10 and U87 study suggested that both GNE-317 and GDC-0980 improved survival compared to placebo, although both treatments were

not significantly different from one another. However, in GL261, there was no difference between the treatment groups and placebo. These results suggest that for treating an invasive tumor such as GBM, it is critical to not only acknowledge the importance of effective drug delivery but also to use a drug that is effective once it engages the target.

Future work on this project will examine the influence of anti-angiogenic therapy (AAT) on the tumor delivery of concomitantly administered drugs for treatment of GBM. An anti-angiogenic therapy may be considered a paradox as it could restore the low permeability characteristics of the BBB via vessel normalization. This AAT-mediated restoration of BBB integrity could influence the delivery of drugs with low BBB permeability such as GDC-0980. It would be interesting to investigate the influence of the dual PI3K/mTOR inhibitors themselves on BBB integrity, as it has been reported that this class of drugs also exhibits anti-angiogenic properties.

BIBLIOGRAPHY

CHAPTER I

Abbott NJ (2000) Inflammatory mediators and modulation of blood-brain barrier permeability. *Cell Mol Neurobiol* **20**:131-147.

Abbott NJ (2002) Astrocyte-endothelial interactions and blood-brain barrier permeability. *J Anat* **200**:629-638.

Abbott NJ, Patabendige AA, Dolman DE, Yusof SR and Begley DJ (2010) Structure and function of the blood-brain barrier. *Neurobiol Dis* **37**:13-25.

Abbott NJ, Ronnback L and Hansson E (2006) Astrocyte-endothelial interactions at the blood-brain barrier. *Nat Rev Neurosci* **7**:41-53.

Abounader R and Laterra J (2005) Scatter factor/hepatocyte growth factor in brain tumor growth and angiogenesis. *Neuro Oncol* **7**:436-451.

Agarwal S, Hartz AM, Elmquist WF and Bauer B (2011a) Breast cancer resistance protein and P-glycoprotein in brain cancer: two gatekeepers team up. *Curr Pharm Des* **17**:2793-2802.

Agarwal S, Manchanda P, Vogelbaum MA, Ohlfest JR and Elmquist WF (2013) Function of the blood-brain barrier and restriction of drug delivery to invasive glioma cells: findings in an orthotopic rat xenograft model of glioma. *Drug Metab Dispos* **41**:33-39.

Agarwal S, Sane R, Gallardo JL, Ohlfest JR and Elmquist WF (2010) Distribution of gefitinib to the brain is limited by P-glycoprotein (ABCB1) and breast cancer resistance protein (ABCG2)-mediated active efflux. *J Pharmacol Exp Ther* **334**:147-155.

Agarwal S, Sane R, Oberoi R, Ohlfest JR and Elmquist WF (2011b) Delivery of molecularly targeted therapy to malignant glioma, a disease of the whole brain. *Expert Rev Mol Med* **13**:e17.

Agarwal S, Uchida Y, Mittapalli RK, Sane R, Terasaki T and Elmquist WF (2012) Quantitative proteomics of transporter expression in brain capillary endothelial cells isolated from P-glycoprotein (P-gp), breast cancer resistance protein (Bcrp), and P-gp/Bcrp knockout mice. *Drug Metab Dispos* **40**:1164-1169.

Albert FK, Forsting M, Sartor K, Adams HP and Kunze S (1994) Early postoperative magnetic resonance imaging after resection of malignant glioma: objective evaluation of residual tumor and its influence on regrowth and prognosis. *Neurosurgery* **34**:45-60; discussion 60-41.

Andre T and Chibaudel B (2013) [Aflibercept (Zaltrap((R))) approved in metastatic colorectal cancer]. *Bull Cancer* **100**:1023-1025.

Armstrong AJ, Shen T, Halabi S, Kemeny G, Bitting RL, Kartcheske P, Embree E, Morris K, Winters C, Jaffe T, Fleming M and George DJ (2013) A phase II trial of temsirolimus in men with castration-resistant metastatic prostate cancer. *Clin Genitourin Cancer* **11**:397-406.

Bai RY, Staedtke V and Riggins GJ (2011) Molecular targeting of glioblastoma: Drug discovery and therapies. *Trends Mol Med* **17**:301-312.

Beckner ME, Jane EP, Jankowitz B, Agostino NR, Walter KA, Hamilton RL and Pollack IF (2007) Tumor cells from ultrasonic aspirations of glioblastomas migrate and form spheres with radial outgrowth. *Cancer Lett* **255**:135-144.

Begley DJ (2004) Delivery of therapeutic agents to the central nervous system: the problems and the possibilities. *Pharmacol Ther* **104**:29-45.

Begley DJ and Brightman MW (2003) Structural and functional aspects of the blood-brain barrier. *Prog Drug Res* **61**:39-78.

Berens ME and Giese A (1999) "...those left behind." Biology and oncology of invasive glioma cells. *Neoplasia* **1**:208-219.

Betz AL, Firth JA and Goldstein GW (1980) Polarity of the blood-brain barrier: distribution of enzymes between the luminal and antiluminal membranes of brain capillary endothelial cells. *Brain Res* **192**:17-28.

Bota DA, Desjardins A, Quinn JA, Affronti ML and Friedman HS (2007) Interstitial chemotherapy with biodegradable BCNU (Gliadel) wafers in the treatment of malignant gliomas. *Ther Clin Risk Manag* **3**:707-715.

Brandes AA, Ermani M, Turazzi S, Scelzi E, Berti F, Amista P, Rotilio A, Licata C and Fiorentino MV (1999) Procarbazine and high-dose tamoxifen as a second-line

regimen in recurrent high-grade gliomas: a phase II study. *J Clin Oncol* **17**:645-650.

Breedveld P, Pluim D, Cipriani G, Wielinga P, van Tellingen O, Schinkel AH and Schellens JH (2005) The effect of Bcrp1 (Abcg2) on the in vivo pharmacokinetics and brain penetration of imatinib mesylate (Gleevec): implications for the use of breast cancer resistance protein and P-glycoprotein inhibitors to enable the brain penetration of imatinib in patients. *Cancer Res* **65**:2577-2582.

Brem H, Piantadosi S, Burger PC, Walker M, Selker R, Vick NA, Black K, Sisti M, Brem S, Mohr G and et al. (1995) Placebo-controlled trial of safety and efficacy of intraoperative controlled delivery by biodegradable polymers of chemotherapy for recurrent gliomas. The Polymer-brain Tumor Treatment Group. *Lancet* **345**:1008-1012.

Brem S (1976) The role of vascular proliferation in the growth of brain tumors. *Clin Neurosurg* **23**:440-453.

Brem S, Cotran R and Folkman J (1972) Tumor angiogenesis: a quantitative method for histologic grading. *J Natl Cancer Inst* **48**:347-356.

Busaidy NL, Farooki A, Dowlati A, Perentesis JP, Dancey JE, Doyle LA, Brell JM and Siu LL (2012) Management of metabolic effects associated with anticancer agents targeting the PI3K-Akt-mTOR pathway. *J Clin Oncol* **30**:2919-2928.

Chen Y, Agarwal S, Shaik NM, Chen C, Yang Z and Elmquist WF (2009) P-glycoprotein and breast cancer resistance protein influence brain distribution of dasatinib. *J Pharmacol Exp Ther* **330**:956-963.

Cheng CK, Fan QW and Weiss WA (2009) PI3K signaling in glioma--animal models and therapeutic challenges. *Brain Pathol* **19**:112-120.

Christensen JG (2007) A preclinical review of sunitinib, a multitargeted receptor tyrosine kinase inhibitor with anti-angiogenic and antitumour activities. *Ann Oncol* **18 Suppl 10**:x3-10.

Cloughesy TF, Yoshimoto K, Nghiemphu P, Brown K, Dang J, Zhu S, Hsueh T, Chen Y, Wang W, Youngkin D, Liau L, Martin N, Becker D, Bergsneider M, Lai A, Green R, Oglesby T, Koleto M, Trent J, Horvath S, Mischel PS, Mellinghoff IK and

Sawyers CL (2008) Antitumor activity of rapamycin in a Phase I trial for patients with recurrent PTEN-deficient glioblastoma. *PLoS Med* **5**:e8.

Cordon-Cardo C, O'Brien JP, Casals D, Rittman-Grauer L, Biedler JL, Melamed MR and Bertino JR (1989) Multidrug-resistance gene (P-glycoprotein) is expressed by endothelial cells at blood-brain barrier sites. *Proc Natl Acad Sci U S A* **86**:695-698.

Czabanka M, Bruenner J, Parmaksiz G, Broggini T, Topalovic M, Bayerl SH, Auf G, Kremenetskaia I, Nieminen M, Jabouille A, Mueller S, Harms U, Harms C, Koch A, Heppner FL and Vajkoczy P (2013) Combined temozolomide and sunitinib treatment leads to better tumour control but increased vascular resistance in O6-methylguanine methyltransferase-methylated gliomas. *Eur J Cancer* **49**:2243-2252.

D'Amico R, Lei L, Kennedy BC, Sisti J, Ebiana V, Crisman C, Christensen JG, Gil O, Rosenfeld SS, Canoll P and Bruce JN (2012) The addition of Sunitinib to radiation delays tumor growth in a murine model of glioblastoma. *Neurol Res* **34**:252-261.

Darefsky AS, King JT, Jr. and Dubrow R (2012) Adult glioblastoma multiforme survival in the temozolomide era: a population-based analysis of Surveillance, Epidemiology, and End Results registries. *Cancer* **118**:2163-2172.

de Vries NA, Zhao J, Kroon E, Buckle T, Beijnen JH and van Tellingen O (2007) P-glycoprotein and breast cancer resistance protein: two dominant transporters working together in limiting the brain penetration of topotecan. *Clin Cancer Res* **13**:6440-6449.

Decleves X, Fajac A, Lehmann-Che J, Tardy M, Mercier C, Hurbain I, Laplanche JL, Bernaudin JF and Scherrmann JM (2002) Molecular and functional MDR1-Pgp and MRPs expression in human glioblastoma multiforme cell lines. *Int J Cancer* **98**:173-180.

Delbaldo C, Faivre S, Dreyer C and Raymond E (2012) Sunitinib in advanced pancreatic neuroendocrine tumors: latest evidence and clinical potential. *Ther Adv Med Oncol* **4**:9-18.

Demeule M, Regina A, Jodoin J, Laplante A, Dagenais C, Berthelet F, Moghrabi A and Beliveau R (2002) Drug transport to the brain: key roles for the efflux pump P-glycoprotein in the blood-brain barrier. *Vascul Pharmacol* **38**:339-348.

Doyle LA, Yang W, Abruzzo LV, Krogmann T, Gao Y, Rishi AK and Ross DD (1998) A multidrug resistance transporter from human MCF-7 breast cancer cells. *Proc Natl Acad Sci U S A* **95**:15665-15670.

Duda DG, Jain RK and Willett CG (2007) Antiangiogenics: the potential role of integrating this novel treatment modality with chemoradiation for solid cancers. *J Clin Oncol* **25**:4033-4042.

Eilers M, Roy U and Mondal D (2008) MRP (ABCC) transporters-mediated efflux of anti-HIV drugs, saquinavir and zidovudine, from human endothelial cells. *Exp Biol Med (Maywood)* **233**:1149-1160.

Ellis L, Ku SY, Ramakrishnan S, Lasorsa E, Azabdaftari G, Godoy A and Pili R (2013) Combinatorial antitumor effect of HDAC and the PI3K-Akt-mTOR pathway inhibition in a Pten defecient model of prostate cancer. *Oncotarget* **4**:2225-2236.

Ette EI, Howie CA, Kelman AW and Whiting B (1995) Experimental design and efficient parameter estimation in preclinical pharmacokinetic studies. *Pharm Res* **12**:729-737.

Fan QW and Weiss WA (2012) Inhibition of PI3K-Akt-mTOR signaling in glioblastoma by mTORC1/2 inhibitors. *Methods Mol Biol* **821**:349-359.

Franceschi E, Cavallo G, Lonardi S, Magrini E, Tosoni A, Grosso D, Scopece L, Blatt V, Urbini B, Pession A, Tallini G, Crino L and Brandes AA (2007) Gefitinib in patients with progressive high-grade gliomas: a multicentre phase II study by Gruppo Italiano Cooperativo di Neuro-Oncologia (GICNO). *Br J Cancer* **96**:1047-1051.

Friden M, Winiwarter S, Jerndal G, Bengtsson O, Wan H, Bredberg U, Hammarlund-Udenaes M and Antonsson M (2009) Structure-brain exposure relationships in rat and human using a novel data set of unbound drug concentrations in brain interstitial and cerebrospinal fluids. *J Med Chem* **52**:6233-6243.

Gadgeel SM, Lew DL, Synold TW, LoRusso P, Chung V, Christensen SD, Smith DC, Kingsbury L, Hoering A and Kurzrock R (2013) Phase I study evaluating the combination of lapatinib (a Her2/Neu and EGFR inhibitor) and everolimus (an mTOR inhibitor) in patients with advanced cancers: South West Oncology Group (SWOG) Study S0528. *Cancer Chemother Pharmacol* **72**:1089-1096.

Gerber HP, Malik AK, Solar GP, Sherman D, Liang XH, Meng G, Hong K, Marsters JC and Ferrara N (2002) VEGF regulates haematopoietic stem cell survival by an internal autocrine loop mechanism. *Nature* **417**:954-958.

Goudar RK, Shi Q, Hjelmeland MD, Keir ST, McLendon RE, Wikstrand CJ, Reese ED, Conrad CA, Traxler P, Lane HA, Reardon DA, Cavenee WK, Wang XF, Bigner DD, Friedman HS and Rich JN (2005) Combination therapy of inhibitors of epidermal growth factor receptor/vascular endothelial growth factor receptor 2 (AEE788) and the mammalian target of rapamycin (RAD001) offers improved glioblastoma tumor growth inhibition. *Mol Cancer Ther* **4**:101-112.

Grepin R and Pages G (2010) Molecular mechanisms of resistance to tumour anti-angiogenic strategies. *J Oncol* **2010**:835680.

Gruber Filbin M, Dabral SK, Pazyra-Murphy MF, Ramkissoon S, Kung AL, Pak E, Chung J, Theisen MA, Sun Y, Franchetti Y, Shulman DS, Redjal N, Tabak B, Beroukhim R, Wang Q, Zhao J, Dorsch M, Buonamici S, Ligon KL, Kelleher JF and Segal RA (2013) Coordinate activation of Shh and PI3K signaling in PTEN-deficient glioblastoma: new therapeutic opportunities. *Nat Med* **19**:1518-1523.

Guertin DA and Sabatini DM (2007) Defining the role of mTOR in cancer. *Cancer Cell* **12**:9-22.

Gupta K and Salunke P (2012) Molecular markers of glioma: an update on recent progress and perspectives. *J Cancer Res Clin Oncol* **138**:1971-1981.

Hammarlund-Udenaes M, Bredberg U and Friden M (2009) Methodologies to assess brain drug delivery in lead optimization. *Curr Top Med Chem* **9**:148-162.

Hammarlund-Udenaes M, Friden M, Syvanen S and Gupta A (2008) On the rate and extent of drug delivery to the brain. *Pharm Res* **25**:1737-1750.

Hermanson M, Funa K, Koopmann J, Maintz D, Waha A, Westermark B, Heldin CH, Wiestler OD, Louis DN, von Deimling A and Nister M (1996) Association of loss of heterozygosity on chromosome 17p with high platelet-derived growth factor alpha receptor expression in human malignant gliomas. *Cancer Res* **56**:164-171.

Hu X, Pandolfi PP, Li Y, Koutcher JA, Rosenblum M and Holland EC (2005) mTOR promotes survival and astrocytic characteristics induced by Pten/AKT signaling in glioblastoma. *Neoplasia* **7**:356-368.

Huang J and Manning BD (2009) A complex interplay between Akt, TSC2 and the two mTOR complexes. *Biochem Soc Trans* **37**:217-222.

Inda MM, Bonavia R, Mukasa A, Narita Y, Sah DW, Vandenberg S, Brennan C, Johns TG, Bachoo R, Hadwiger P, Tan P, Depinho RA, Cavenee W and Furnari F (2010) Tumor heterogeneity is an active process maintained by a mutant EGFR-induced cytokine circuit in glioblastoma. *Genes Dev* **24**:1731-1745.

Jain RK, di Tomaso E, Duda DG, Loeffler JS, Sorensen AG and Batchelor TT (2007) Angiogenesis in brain tumours. *Nat Rev Neurosci* **8**:610-622.

Kim Y, Kim E, Wu Q, Guryanova O, Hitomi M, Lathia JD, Serwanski D, Sloan AE, Weil RJ, Lee J, Nishiyama A, Bao S, Hjelmeland AB and Rich JN (2012) Platelet-derived growth factor receptors differentially inform intertumoral and intratumoral heterogeneity. *Genes Dev* **26**:1247-1262.

Kreisl TN, Lassman AB, Mischel PS, Rosen N, Scher HI, Teruya-Feldstein J, Shaffer D, Lis E and Abrey LE (2009) A pilot study of everolimus and gefitinib in the treatment of recurrent glioblastoma (GBM). *J Neurooncol* **92**:99-105.

Kusuhara H and Sugiyama Y (2001) Efflux transport systems for drugs at the blood-brain barrier and blood-cerebrospinal fluid barrier (Part 1). *Drug Discov Today* **6**:150-156.

Lassen U, Sorensen M, Gaziel TB, Hasselbalch B and Poulsen HS (2013) Phase II study of bevacizumab and temsirolimus combination therapy for recurrent glioblastoma multiforme. *Anticancer Res* **33**:1657-1660.

Lee Titsworth W, Murad GJ, Hoh BL and Rahman M (2014) Fighting fire with fire: the revival of thermotherapy for gliomas. *Anticancer Res* **34**:565-574.

Levin VA, Freeman-Dove M and Landahl HD (1975) Permeability characteristics of brain adjacent to tumors in rats. *Arch Neurol* **32**:785-791.

Liang Y, Li XY, Rebar EJ, Li P, Zhou Y, Chen B, Wolffe AP and Case CC (2002) Activation of vascular endothelial growth factor A transcription in tumorigenic glioblastoma cell lines by an enhancer with cell type-specific DNase I accessibility. *J Biol Chem* **277**:20087-20094.

Lokker NA, Sullivan CM, Hollenbach SJ, Israel MA and Giese NA (2002) Platelet-derived growth factor (PDGF) autocrine signaling regulates survival and mitogenic pathways in glioblastoma cells: evidence that the novel PDGF-C and PDGF-D ligands may play a role in the development of brain tumors. *Cancer Res* **62**:3729-3735.

Louis DN, Ohgaki H, Wiestler OD, Cavenee WK, Burger PC, Jouvet A, Scheithauer BW and Kleihues P (2007) The 2007 WHO classification of tumours of the central nervous system. *Acta Neuropathol* **114**:97-109.

Ma CX, Suman VJ, Goetz M, Haluska P, Moynihan T, Nanda R, Olopade O, Pluard T, Guo Z, Chen HX, Erlichman C, Ellis MJ and Fleming GF (2013) A phase I trial of the IGF-1R antibody Cixutumumab in combination with temsirolimus in patients with metastatic breast cancer. *Breast Cancer Res Treat* **139**:145-153.

Maity A, Pore N, Lee J, Solomon D and O'Rourke DM (2000) Epidermal growth factor receptor transcriptionally up-regulates vascular endothelial growth factor expression in human glioblastoma cells via a pathway involving phosphatidylinositol 3'-kinase and distinct from that induced by hypoxia. *Cancer Res* **60**:5879-5886.

Mangas-Sanjuan V, Gonzalez-Alvarez M, Gonzalez-Alvarez I and Bermejo M (2010) Drug penetration across the blood-brain barrier: an overview. *Ther Deliv* **1**:535-562.

Matheny RW, Jr. and Adamo ML (2009) Effects of PI3K catalytic subunit and Akt isoform deficiency on mTOR and p70S6K activation in myoblasts. *Biochem Biophys Res Commun* **390**:252-257.

Mazure NM, Chen EY, Laderoute KR and Giaccia AJ (1997) Induction of vascular endothelial growth factor by hypoxia is modulated by a phosphatidylinositol 3-kinase/Akt signaling pathway in Ha-ras-transformed cells through a hypoxia inducible factor-1 transcriptional element. *Blood* **90**:3322-3331.

Nazarenko I, Hede SM, He X, Hedren A, Thompson J, Lindstrom MS and Nister M (2012) PDGF and PDGF receptors in glioma. *Ups J Med Sci* **117**:99-112.

Oh DS, Adamson DC and Kirkpatrick JP (2012) Targeted radiotherapy for malignant gliomas. *Curr Drug Discov Technol* **9**:268-279.

Ohr M and Kaiser PK (2012) Intravitreal aflibercept injection for neovascular (wet) age-related macular degeneration. *Expert Opin Pharmacother* **13**:585-591.

Onishi M, Ichikawa T, Kurozumi K and Date I (2011) Angiogenesis and invasion in glioma. *Brain Tumor Pathol* **28**:13-24.

Pardridge WM (2007) Blood-brain barrier delivery. *Drug Discov Today* **12**:54-61.

Parney IF and Chang SM (2003) Current chemotherapy for glioblastoma. *Cancer J* **9**:149-156.

Pierce GF, Mustoe TA, Altrock BW, Deuel TF and Thomason A (1991) Role of platelet-derived growth factor in wound healing. *J Cell Biochem* **45**:319-326.

Polli JW, Olson KL, Chism JP, John-Williams LS, Yeager RL, Woodard SM, Otto V, Castellino S and Demby VE (2009) An unexpected synergist role of P-glycoprotein and breast cancer resistance protein on the central nervous system penetration of the tyrosine kinase inhibitor lapatinib (N-{3-chloro-4-[(3-fluorobenzyl)oxy]phenyl}-6-[5-({[2-(methylsulfonyl)ethyl]amino }methyl)-2-furyl]-4-quinazolinamine; GW572016). *Drug Metab Dispos* **37**:439-442.

Porter KR, McCarthy BJ, Freels S, Kim Y and Davis FG (2010) Prevalence estimates for primary brain tumors in the United States by age, gender, behavior, and histology. *Neuro Oncol* **12**:520-527.

Prasad G, Sottero T, Yang X, Mueller S, James CD, Weiss WA, Polley MY, Ozawa T, Berger MS, Aftab DT, Prados MD and Haas-Kogan DA (2011) Inhibition of PI3K/mTOR pathways in glioblastoma and implications for combination therapy with temozolomide. *Neuro Oncol* **13**:384-392.

Rasheed BK, Wiltshire RN, Bigner SH and Bigner DD (1999) Molecular pathogenesis of malignant gliomas. *Curr Opin Oncol* **11**:162-167.

Reardon DA, Desjardins A, Vredenburgh JJ, Gururangan S, Friedman AH, Herndon JE, 2nd, Marcello J, Norfleet JA, McLendon RE, Sampson JH and Friedman HS (2010) Phase 2 trial of erlotinib plus sirolimus in adults with recurrent glioblastoma. *J Neurooncol* **96**:219-230.

Reardon DA and Wen PY (2006) Therapeutic advances in the treatment of glioblastoma: rationale and potential role of targeted agents. *Oncologist* **11**:152-164.

Reardon DA, Wen PY, Desjardins A, Batchelor TT and Vredenburgh JJ (2008) Glioblastoma multiforme: an emerging paradigm of anti-VEGF therapy. *Expert Opin Biol Ther* **8**:541-553.

Rock EP, Goodman V, Jiang JX, Mahjoob K, Verbois SL, Morse D, Dagher R, Justice R and Pazdur R (2007) Food and Drug Administration drug approval summary: Sunitinib malate for the treatment of gastrointestinal stromal tumor and advanced renal cell carcinoma. *Oncologist* **12**:107-113.

Rodrigus P (2003) Motexafin gadolinium: a possible new radiosensitiser. *Expert Opin Investig Drugs* **12**:1205-1210.

Romanelli P, Conti A, Pontoriero A, Ricciardi GK, Tomasello F, De Renzis C, Innocenzi G, Esposito V and Cantore G (2009) Role of stereotactic radiosurgery and fractionated stereotactic radiotherapy for the treatment of recurrent glioblastoma multiforme. *Neurosurg Focus* **27**:E8.

Rong Y, Durden DL, Van Meir EG and Brat DJ (2006) 'Pseudopalisading' necrosis in glioblastoma: a familiar morphologic feature that links vascular pathology, hypoxia, and angiogenesis. *J Neuropathol Exp Neurol* **65**:529-539.

Salphati L, Pang J, Plise EG, Lee LB, Olivero AG, Prior WW, Sampath D, Wong S and Zhang X (2012) Preclinical assessment of the absorption and disposition of the phosphatidylinositol 3-kinase/mammalian target of rapamycin inhibitor GDC-0980 and prediction of its pharmacokinetics and efficacy in human. *Drug Metab Dispos* **40**:1785-1796.

Sami A and Karsy M (2013) Targeting the PI3K/AKT/mTOR signaling pathway in glioblastoma: novel therapeutic agents and advances in understanding. *Tumour Biol* **34**:1991-2002.

Sarbassov DD, Ali SM and Sabatini DM (2005) Growing roles for the mTOR pathway. *Curr Opin Cell Biol* **17**:596-603.

Schinkel AH and Jonker JW (2003) Mammalian drug efflux transporters of the ATP binding cassette (ABC) family: an overview. *Adv Drug Deliv Rev* **55**:3-29.

Schinkel AH, Smit JJ, van Tellingen O, Beijnen JH, Wagenaar E, van Deemter L, Mol CA, van der Valk MA, Robanus-Maandag EC, te Riele HP and et al. (1994) Disruption of the mouse mdr1a P-glycoprotein gene leads to a deficiency in the blood-brain barrier and to increased sensitivity to drugs. *Cell* **77**:491-502.

Sharom FJ (2008) ABC multidrug transporters: structure, function and role in chemoresistance. *Pharmacogenomics* **9**:105-127.

Siegelin MD, Raskett CM, Gilbert CA, Ross AH and Altieri DC (2010) Sorafenib exerts anti-glioma activity in vitro and in vivo. *Neurosci Lett* **478**:165-170.

Siemann DW, Norris CM, Ryan A and Shi W (2009) Impact of tumor cell VEGF expression on the in vivo efficacy of vandetanib (ZACTIMA; ZD6474). *Anticancer Res* **29**:1987-1992.

Soffietti R, Ruda R and Mutani R (2002) Management of brain metastases. *J Neurol* **249**:1357-1369.

Stefanik DF, Rizkalla LR, Soi A, Goldblatt SA and Rizkalla WM (1991) Acidic and basic fibroblast growth factors are present in glioblastoma multiforme. *Cancer Res* **51**:5760-5765.

Stewart MW (2011) Aflibercept (VEGF-TRAP): the next anti-VEGF drug. *Inflamm Allergy Drug Targets* **10**:497-508.

Stupp R, Mason WP, van den Bent MJ, Weller M, Fisher B, Taphoorn MJ, Belanger K, Brandes AA, Marosi C, Bogdahn U, Curschmann J, Janzer RC, Ludwin SK, Gorlia T, Allgeier A, Lacombe D, Cairncross JG, Eisenhauer E and Mirimanoff RO (2005) Radiotherapy plus concomitant and adjuvant temozolomide for glioblastoma. *N Engl J Med* **352**:987-996.

Summerfield SG, Read K, Begley DJ, Obradovic T, Hidalgo IJ, Coggon S, Lewis AV, Porter RA and Jeffrey P (2007) Central nervous system drug disposition: the relationship between in situ brain permeability and brain free fraction. *J Pharmacol Exp Ther* **322**:205-213.

Sun L, Hui AM, Su Q, Vortmeyer A, Kotliarov Y, Pastorino S, Passaniti A, Menon J, Walling J, Bailey R, Rosenblum M, Mikkelsen T and Fine HA (2006) Neuronal and glioma-derived stem cell factor induces angiogenesis within the brain. *Cancer Cell* **9**:287-300.

Suvasini R, Shruti B, Thota B, Shinde SV, Friedmann-Morvinski D, Nawaz Z, Prasanna KV, Thennarasu K, Hegde AS, Arivazhagan A, Chandramouli BA, Santosh V and Somasundaram K (2011) Insulin growth factor-2 binding protein 3 (IGF2BP3) is a glioblastoma-specific marker that activates phosphatidylinositol 3-kinase/mitogen-activated protein kinase (PI3K/MAPK) pathways by modulating IGF-2. *J Biol Chem* **286**:25882-25890.

Takano S, Yamashita T and Ohneda O (2010) Molecular therapeutic targets for glioma angiogenesis. *J Oncol* **2010**:351908.

van den Bent MJ, Hegi ME and Stupp R (2006) Recent developments in the use of chemotherapy in brain tumours. *Eur J Cancer* **42**:582-588.

Vredenburgh JJ, Desjardins A, Herndon JE, 2nd, Dowell JM, Reardon DA, Quinn JA, Rich JN, Sathornsumetee S, Gururangan S, Wagner M, Bigner DD, Friedman AH and Friedman HS (2007) Phase II trial of bevacizumab and irinotecan in recurrent malignant glioma. *Clin Cancer Res* **13**:1253-1259.

Walker MD, Alexander E, Jr., Hunt WE, MacCarty CS, Mahaley MS, Jr., Mealey J, Jr., Norrell HA, Owens G, Ransohoff J, Wilson CB, Gehan EA and Strike TA (1978) Evaluation of BCNU and/or radiotherapy in the treatment of anaplastic gliomas. A cooperative clinical trial. *J Neurosurg* **49**:333-343.

Wedge SR, Kendrew J, Hennequin LF, Valentine PJ, Barry ST, Brave SR, Smith NR, James NH, Dukes M, Curwen JO, Chester R, Jackson JA, Boffey SJ, Kilburn LL, Barnett S, Richmond GH, Wadsworth PF, Walker M, Bigley AL, Taylor ST, Cooper L, Beck S, Jurgensmeier JM and Ogilvie DJ (2005) AZD2171: a highly

potent, orally bioavailable, vascular endothelial growth factor receptor-2 tyrosine kinase inhibitor for the treatment of cancer. *Cancer Res* **65**:4389-4400.

Wen PY, Lee EQ, Reardon DA, Ligon KL and Alfred Yung WK (2012) Current clinical development of PI3K pathway inhibitors in glioblastoma. *Neuro Oncol* **14**:819-829.

Wolburg H and Lippoldt A (2002) Tight junctions of the blood-brain barrier: development, composition and regulation. *Vascul Pharmacol* **38**:323-337.

Wolburg H, Wolburg-Buchholz K, Kraus J, Rascher-Eggstein G, Liebner S, Hamm S, Duffner F, Grote EH, Risau W and Engelhardt B (2003) Localization of claudin-3 in tight junctions of the blood-brain barrier is selectively lost during experimental autoimmune encephalomyelitis and human glioblastoma multiforme. *Acta Neuropathol* **105**:586-592.

Wong ML, Prawira A, Kaye AH and Hovens CM (2009) Tumour angiogenesis: its mechanism and therapeutic implications in malignant gliomas. *J Clin Neurosci* **16**:1119-1130.

Xu C, Wu X and Zhu J (2013a) VEGF promotes proliferation of human glioblastoma multiforme stem-like cells through VEGF receptor 2. *ScientificWorldJournal* **2013**:417413.

Xu S, Li S, Guo Z, Luo J, Ellis MJ and Ma CX (2013b) Combined targeting of mTOR and AKT is an effective strategy for basal-like breast cancer in patient-derived xenograft models. *Mol Cancer Ther* **12**:1665-1675.

Yao X, Ping Y, Liu Y, Chen K, Yoshimura T, Liu M, Gong W, Chen C, Niu Q, Guo D, Zhang X, Wang JM and Bian X (2013) Vascular endothelial growth factor receptor 2 (VEGFR-2) plays a key role in vasculogenic mimicry formation, neovascularization and tumor initiation by Glioma stem-like cells. *PLoS One* **8**:e57188.

Yi D, Hua TX and Lin HY (2011) EGFR gene overexpression retained in an invasive xenograft model by solid orthotopic transplantation of human glioblastoma multiforme into nude mice. *Cancer Invest* **29**:229-239.

Zhang EY, Knipp GT, Ekins S and Swaan PW (2002) Structural biology and function of solute transporters: implications for identifying and designing substrates. *Drug Metab Rev* **34**:709-750.

Zhang J, Cao R, Zhang Y, Jia T, Cao Y and Wahlberg E (2009) Differential roles of PDGFR-alpha and PDGFR-beta in angiogenesis and vessel stability. *FASEB J* **23**:153-163.

Zhang W, Haines BB, Efferson C, Zhu J, Ware C, Kunii K, Tammam J, Angagaw M, Hinton MC, Keilhack H, Paweletz CP, Zhang T, Winter C, Sathyanarayanan S, Cheng J, Zawel L, Fawell S, Gilliland G and Majumder PK (2012) Evidence of mTOR Activation by an AKT-Independent Mechanism Provides Support for the Combined Treatment of PTEN-Deficient Prostate Tumors with mTOR and AKT Inhibitors. *Transl Oncol* **5**:422-429.

Abbott NJ (2004) Evidence for bulk flow of brain interstitial fluid: significance for physiology and pathology. *Neurochem Int* **45**:545-552.

Agarwal S, Hartz AM, Elmquist WF and Bauer B (2011a) Breast cancer resistance protein and P-glycoprotein in brain cancer: two gatekeepers team up. *Curr Pharm Des* **17**:2793-2802.

Agarwal S, Manchanda P, Vogelbaum MA, Ohlfest JR and Elmquist WF (2013) Function of the blood-brain barrier and restriction of drug delivery to invasive glioma cells: findings in an orthotopic rat xenograft model of glioma. *Drug Metab Dispos* **41**:33-39.

Agarwal S, Mittapalli RK, Zellmer DM, Gallardo JL, Donelson R, Seiler C, Decker SA, Santacruz KS, Pokorny JL, Sarkaria JN, Elmquist WF and Ohlfest JR (2012) Active efflux of Dasatinib from the brain limits efficacy against murine glioblastoma: broad implications for the clinical use of molecularly targeted agents. *Mol Cancer Ther* **11**:2183-2192.

Agarwal S, Sane R, Gallardo JL, Ohlfest JR and Elmquist WF (2010) Distribution of gefitinib to the brain is limited by P-glycoprotein (ABCB1) and breast cancer resistance protein (ABCG2)-mediated active efflux. *J Pharmacol Exp Ther* **334**:147-155.

Agarwal S, Sane R, Oberoi R, Ohlfest JR and Elmquist WF (2011b) Delivery of molecularly targeted therapy to malignant glioma, a disease of the whole brain. *Expert Rev Mol Med* **13**:e17.

Agarwal S, Sane R, Ohlfest JR and Elmquist WF (2011c) The role of the breast cancer resistance protein (ABCG2) in the distribution of sorafenib to the brain. *J Pharmacol Exp Ther* **336**:223-233.

Agnihotri S, Burrell KE, Wolf A, Jalali S, Hawkins C, Rutka JT and Zadeh G (2013) Glioblastoma, a brief review of history, molecular genetics, animal models and novel therapeutic strategies. *Arch Immunol Ther Exp (Warsz)* **61**:25-41.

Alavijeh MS, Chishty M, Qaiser MZ and Palmer AM (2005) Drug metabolism and pharmacokinetics, the blood-brain barrier, and central nervous system drug discovery. *NeuroRx* **2**:554-571.

Alvarez JI, Dodelet-Devillers A, Kebir H, Ifergan I, Fabre PJ, Terouz S, Sabbagh M, Wosik K, Bourbonniere L, Bernard M, van Horssen J, de Vries HE, Charron F and Prat A (2011) The Hedgehog pathway promotes blood-brain barrier integrity and CNS immune quiescence. *Science* **334**:1727-1731.

Aryal M, Arvanitis CD, Alexander PM and McDannold N (2014) Ultrasound-mediated blood-brain barrier disruption for targeted drug delivery in the central nervous system. *Adv Drug Deliv Rev* **72C**:94-109.

Ballabh P, Braun A and Nedergaard M (2004) The blood-brain barrier: an overview: structure, regulation, and clinical implications. *Neurobiol Dis* **16**:1-13.

Barcellos-Hoff MH, Newcomb EW, Zagzag D and Narayana A (2009) Therapeutic targets in malignant glioblastoma microenvironment. *Semin Radiat Oncol* **19**:163-170.

Berens ME and Giese A (1999) "...those left behind." Biology and oncology of invasive glioma cells. *Neoplasia* **1**:208-219.

Bergstrom CA (2005) In silico predictions of drug solubility and permeability: two rate-limiting barriers to oral drug absorption. *Basic Clin Pharmacol Toxicol* **96**:156-161.

Bhatia G, Lau ME, Gulur P and Koury KM (2013) Intrathecal Drug Delivery (ITDD) systems for cancer pain. *F1000Res* **2**:96.

Bihorel S, Camenisch G, Lemaire M and Scherrmann JM (2007) Influence of breast cancer resistance protein (Abcg2) and p-glycoprotein (Abcb1a) on the transport of imatinib mesylate (Gleevec) across the mouse blood-brain barrier. *J Neurochem* **102**:1749-1757.

Blasi P, Giovagnoli S, Schoubben A, Ricci M and Rossi C (2007) Solid lipid nanoparticles for targeted brain drug delivery. *Adv Drug Deliv Rev* **59**:454-477.

Bobo RH, Laske DW, Akbasak A, Morrison PF, Dedrick RL and Oldfield EH (1994) Convection-enhanced delivery of macromolecules in the brain. *Proc Natl Acad Sci U S A* **91**:2076-2080.

Bogdahn U, Hau P, Stockhammer G, Venkataramana NK, Mahapatra AK, Suri A, Balasubramaniam A, Nair S, Oliushine V, Parfenov V, Poverennova I, Zaaroor M, Jachimczak P, Ludwig S, Schmaus S, Heinrichs H and Schlingensiepen KH (2011) Targeted therapy for high-grade glioma with the TGF-beta2 inhibitor trabedersen: results of a randomized and controlled phase IIb study. *Neuro Oncol* **13**:132-142.

Borlongan CV and Emerich DF (2003) Facilitation of drug entry into the CNS via transient permeation of blood brain barrier: laboratory and preliminary clinical evidence from bradykinin receptor agonist, Cereport. *Brain Res Bull* **60**:297-306.

Boucher Y, Salehi H, Witwer B, Harsh GRt and Jain RK (1997) Interstitial fluid pressure in intracranial tumours in patients and in rodents. *Br J Cancer* **75**:829-836.

Breedveld P, Pluim D, Cipriani G, Wielinga P, van Tellingen O, Schinkel AH and Schellens JH (2005) The effect of Bcrp1 (Abcg2) on the in vivo pharmacokinetics and brain penetration of imatinib mesylate (Gleevec): implications for the use of breast cancer resistance protein and P-glycoprotein inhibitors to enable the brain penetration of imatinib in patients. *Cancer Res* **65**:2577-2582.

Brightman MW and Broadwell RD (1976) The morphological approach to the study of normal and abnormal brain permeability. *Adv Exp Med Biol* **69**:41-54.

Burger PC, Dubois PJ, Schold SC, Jr., Smith KR, Jr., Odom GL, Crafts DC and Giangaspero F (1983) Computerized tomographic and pathologic studies of the untreated, quiescent, and recurrent glioblastoma multiforme. *J Neurosurg* **58**:159-169.

Charles NA, Holland EC, Gilbertson R, Glass R and Kettenmann H (2012) The brain tumor microenvironment. *Glia* **60**:502-514.

Chavanpatil MD, Patil Y and Panyam J (2006) Susceptibility of nanoparticle-encapsulated paclitaxel to P-glycoprotein-mediated drug efflux. *Int J Pharm* **320**:150-156.

Chu C, Abbara C, Noel-Hudson MS, Thomas-Bourgneuf L, Gonin P, Farinotti R and Bonhomme-Faivre L (2009) Disposition of everolimus in mdr1a-/1b- mice and after a pre-treatment of lapatinib in Swiss mice. *Biochem Pharmacol* **77**:1629-1634.

Cornford EM, Young D, Paxton JW, Finlay GJ, Wilson WR and Pardridge WM (1992) Melphalan penetration of the blood-brain barrier via the neutral amino acid transporter in tumor-bearing brain. *Cancer Res* **52**:138-143.

Dai H, Marbach P, Lemaire M, Hayes M and Elmquist WF (2003) Distribution of STI-571 to the brain is limited by P-glycoprotein-mediated efflux. *J Pharmacol Exp Ther* **304**:1085-1092.

de Groot JF, Fuller G, Kumar AJ, Piao Y, Eterovic K, Ji Y and Conrad CA (2010) Tumor invasion after treatment of glioblastoma with bevacizumab: radiographic and pathologic correlation in humans and mice. *Neuro Oncol* **12**:233-242.

de Vries HE, Blom-Roosemalen MC, van Oosten M, de Boer AG, van Berkel TJ, Breimer DD and Kuiper J (1996) The influence of cytokines on the integrity of the blood-brain barrier in vitro. *J Neuroimmunol* **64**:37-43.

de Vries NA, Buckle T, Zhao J, Beijnen JH, Schellens JH and van Tellingen O (2012) Restricted brain penetration of the tyrosine kinase inhibitor erlotinib due to the drug transporters P-gp and BCRP. *Invest New Drugs* **30**:443-449.

Demeule M, Shedid D, Beaulieu E, Del Maestro RF, Moghrabi A, Ghosn PB, Moumdjian R, Berthelet F and Beliveau R (2001) Expression of multidrug-resistance P-glycoprotein (MDR1) in human brain tumors. *Int J Cancer* **93**:62-66.

Dickinson PJ, LeCouteur RA, Higgins RJ, Bringas JR, Roberts B, Larson RF, Yamashita Y, Krauze M, Noble CO, Drummond D, Kirpotin DB, Park JW, Berger MS and Bankiewicz KS (2008) Canine model of convection-enhanced delivery of liposomes containing CPT-11 monitored with real-time magnetic resonance imaging: laboratory investigation. *J Neurosurg* **108**:989-998.

Ding D, Kanaly CW, Bigner DD, Cummings TJ, Herndon JE, 2nd, Pastan I, Raghavan R and Sampson JH (2010) Convection-enhanced delivery of free gadolinium with the recombinant immunotoxin MR1-1. *J Neurooncol* **98**:1-7.

Doctrow SR, Abelleira SM, Curry LA, Heller-Harrison R, Kozarich JW, Malfroy B, McCarroll LA, Morgan KG, Morrow AR, Musso GF and et al. (1994) The bradykinin analog RMP-7 increases intracellular free calcium levels in rat brain microvascular endothelial cells. *J Pharmacol Exp Ther* **271**:229-237.

Dufes C, Olivier JC, Gaillard F, Gaillard A, Couet W and Muller JM (2003) Brain delivery of vasoactive intestinal peptide (VIP) following nasal administration to rats. *Int J Pharm* **255**:87-97.

Duntze J, Litre CF, Eap C, Theret E, Debreuve A, Jovenin N, Lechapt-Zalcman E, Metellus P, Colin P, Guillamo JS, Emery E, Menei P, Rousseaux P and Peruzzi P (2013) Implanted carmustine wafers followed by concomitant radiochemotherapy to treat newly diagnosed malignant gliomas: prospective, observational, multicenter study on 92 cases. *Ann Surg Oncol* **20**:2065-2072.

Elliott PJ, Hayward NJ, Dean RL, Blunt DG and Bartus RT (1996) Intravenous RMP-7 selectively increases uptake of carboplatin into rat brain tumors. *Cancer Res* **56**:3998-4005.

Etame AB, Diaz RJ, Smith CA, Mainprize TG, Hynynen K and Rutka JT (2012) Focused ultrasound disruption of the blood-brain barrier: a new frontier for therapeutic delivery in molecular neurooncology. *Neurosurg Focus* **32**:E3.

Ettmayer P, Amidon GL, Clement B and Testa B (2004) Lessons learned from marketed and investigational prodrugs. *J Med Chem* **47**:2393-2404.

Fattori S, Becherini F, Cianfriglia M, Parenti G, Romanini A and Castagna M (2007) Human brain tumors: multidrug-resistance P-glycoprotein expression in tumor cells and intratumoral capillary endothelial cells. *Virchows Arch* **451**:81-87.

Furnari FB, Fenton T, Bachoo RM, Mukasa A, Stommel JM, Stegh A, Hahn WC, Ligon KL, Louis DN, Brennan C, Chin L, DePinho RA and Cavenee WK (2007) Malignant astrocytic glioma: genetics, biology, and paths to treatment. *Genes Dev* **21**:2683-2710.

Gabathuler R (2010) Approaches to transport therapeutic drugs across the blood-brain barrier to treat brain diseases. *Neurobiol Dis* **37**:48-57.

Groothuis DR (2000) The blood-brain and blood-tumor barriers: a review of strategies for increasing drug delivery. *Neuro Oncol* **2**:45-59.

Groothuis DR, Ward S, Itskovich AC, Dobrescu C, Allen CV, Dills C and Levy RM (1999) Comparison of 14C-sucrose delivery to the brain by intravenous, intraventricular, and convection-enhanced intracerebral infusion. *J Neurosurg* **90**:321-331.

Gynther M, Laine K, Ropponen J, Leppanen J, Mannila A, Nevalainen T, Savolainen J, Jarvinen T and Rautio J (2008) Large neutral amino acid transporter enables brain drug delivery via prodrugs. *J Med Chem* **51**:932-936.

Hawkins BT and Davis TP (2005) The blood-brain barrier/neurovascular unit in health and disease. *Pharmacol Rev* **57**:173-185.

Heffron TP, Salphati L, Alicke B, Cheong J, Dotson J, Edgar K, Goldsmith R, Gould SE, Lee LB, Lesnick JD, Lewis C, Ndubaku C, Nonomiya J, Olivero AG, Pang J, Plise EG, Sideris S, Trapp S, Wallin J, Wang L and Zhang X (2012) The design and identification of brain penetrant inhibitors of phosphoinositide 3-kinase alpha. *J Med Chem* **55**:8007-8020.

Herve F, Ghinea N and Scherrmann JM (2008) CNS delivery via adsorptive transcytosis. *AAPS J* **10**:455-472.

Hou LC, Veeravagu A, Hsu AR and Tse VC (2006) Recurrent glioblastoma multiforme: a review of natural history and management options. *Neurosurg Focus* **20**:E5.

Hsiao P, Sasongko L, Link JM, Mankoff DA, Muzi M, Collier AC and Unadkat JD (2006) Verapamil P-glycoprotein transport across the rat blood-brain barrier: cyclosporine, a concentration inhibition analysis, and comparison with human data. *J Pharmacol Exp Ther* **317**:704-710.

Hynynen K (2008) Ultrasound for drug and gene delivery to the brain. *Adv Drug Deliv Rev* **60**:1209-1217.

Hynynen K, McDannold N, Vykhodtseva N, Raymond S, Weissleder R, Jolesz FA and Sheikov N (2006) Focal disruption of the blood-brain barrier due to 260-kHz ultrasound bursts: a method for molecular imaging and targeted drug delivery. *J Neurosurg* **105**:445-454.

Inamura T and Black KL (1994) Bradykinin selectively opens blood-tumor barrier in experimental brain tumors. *J Cereb Blood Flow Metab* **14**:862-870.

Jain RK, di Tomaso E, Duda DG, Loeffler JS, Sorensen AG and Batchelor TT (2007) Angiogenesis in brain tumours. *Nat Rev Neurosci* **8**:610-622.

Kemper EM, Boogerd W, Thuis I, Beijnen JH and van Tellingen O (2004) Modulation of the blood-brain barrier in oncology: therapeutic opportunities for the treatment of brain tumours? *Cancer Treat Rev* **30**:415-423.

Kraemer DF, Fortin D and Neuwelt EA (2002) Chemotherapeutic dose intensification for treatment of malignant brain tumors: recent developments and future directions. *Curr Neurol Neurosci Rep* **2**:216-224.

Kroll RA and Neuwelt EA (1998) Outwitting the blood-brain barrier for therapeutic purposes: osmotic opening and other means. *Neurosurgery* **42**:1083-1099; discussion 1099-1100.

Lagas JS, van Waterschoot RA, Sparidans RW, Wagenaar E, Beijnen JH and Schinkel AH (2010) Breast cancer resistance protein and P-glycoprotein limit sorafenib brain accumulation. *Mol Cancer Ther* **9**:319-326.

Lagas JS, van Waterschoot RA, van Tilburg VA, Hillebrand MJ, Lankheet N, Rosing H, Beijnen JH and Schinkel AH (2009) Brain accumulation of dasatinib is restricted by P-glycoprotein (ABCB1) and breast cancer resistance protein (ABCG2) and can be enhanced by elacridar treatment. *Clin Cancer Res* **15**:2344-2351.

Lamszus K, Laterra J, Westphal M and Rosen EM (1999) Scatter factor/hepatocyte growth factor (SF/HGF) content and function in human gliomas. *Int J Dev Neurosci* **17**:517-530.

Larsson B (1960) Blood vessel changes following local irradiation of the brain with high-energy protons. *Acta Soc Med Ups* **65**:51-71.

Lee SW, Kim WJ, Park JA, Choi YK, Kwon YW and Kim KW (2006) Blood-brain barrier interfaces and brain tumors. *Arch Pharm Res* **29**:265-275.

Li SD and Huang L (2008) Pharmacokinetics and biodistribution of nanoparticles. *Mol Pharm* **5**:496-504.

Liebner S, Fischmann A, Rascher G, Duffner F, Grote EH, Kalbacher H and Wolburg H (2000) Claudin-1 and claudin-5 expression and tight junction morphology are altered in blood vessels of human glioblastoma multiforme. *Acta Neuropathol* **100**:323-331.

Lin F, Buil L, Sherris D, Beijnen JH and van Tellingen O (2013) Dual mTORC1 and mTORC2 inhibitor Palomid 529 penetrates the blood-brain barrier without restriction by ABCB1 and ABCG2. *Int J Cancer* **133**:1222-1233.

Liu HL, Hua MY, Chen PY, Chu PC, Pan CH, Yang HW, Huang CY, Wang JJ, Yen TC and Wei KC (2010) Blood-brain barrier disruption with focused ultrasound enhances delivery of chemotherapeutic drugs for glioblastoma treatment. *Radiology* **255**:415-425.

Mangas-Sanjuan V, Gonzalez-Alvarez M, Gonzalez-Alvarez I and Bermejo M (2010) Drug penetration across the blood-brain barrier: an overview. *Therapeutic delivery* **1**:535-562.

Mathison S, Nagilla R and Kompella UB (1998) Nasal route for direct delivery of solutes to the central nervous system: fact or fiction? *J Drug Target* **5**:415-441.

Michaud K, Solomon DA, Oermann E, Kim JS, Zhong WZ, Prados MD, Ozawa T, James CD and Waldman T (2010) Pharmacologic inhibition of cyclin-dependent kinases 4 and 6 arrests the growth of glioblastoma multiforme intracranial xenografts. *Cancer Res* **70**:3228-3238.

Minocha M, Khurana V, Qin B, Pal D and Mitra AK (2012a) Co-administration strategy to enhance brain accumulation of vandetanib by modulating P-glycoprotein (P-gp/Abcb1) and breast cancer resistance protein (Bcrp1/Abcg2) mediated efflux with m-TOR inhibitors. *Int J Pharm* **434**:306-314.

Minocha M, Khurana V, Qin B, Pal D and Mitra AK (2012b) Enhanced brain accumulation of pazopanib by modulating P-gp and Bcrp1 mediated efflux with canertinib or erlotinib. *Int J Pharm* **436**:127-134.

Nakano S, Matsukado K and Black KL (1996) Increased brain tumor microvessel permeability after intracarotid bradykinin infusion is mediated by nitric oxide. *Cancer Res* **56**:4027-4031.

Oberoi RK, Mittapalli RK and Elmquist WF (2013) Pharmacokinetic assessment of efflux transport in sunitinib distribution to the brain. *J Pharmacol Exp Ther* **347**:755-764.

On NH, Mitchell R, Savant SD, Bachmeier CJ, Hatch GM and Miller DW (2013) Examination of blood-brain barrier (BBB) integrity in a mouse brain tumor model. *J Neurooncol* **111**:133-143.

Onda K, Tanaka R, Takahashi H, Takeda N and Ikuta F (1989) Cerebral glioblastoma with cerebrospinal fluid dissemination: a clinicopathological study of 14 cases examined by complete autopsy. *Neurosurgery* **25**:533-540.

Pafundi DH, Laack NN, Youland RS, Parney IF, Lowe VJ, Giannini C, Kemp BJ, Grams MP, Morris JM, Hoover JM, Hu LS, Sarkaria JN and Brinkmann DH (2013) Biopsy validation of 18F-DOPA PET and biodistribution in gliomas for neurosurgical planning and radiotherapy target delineation: results of a prospective pilot study. *Neuro Oncol* **15**:1058-1067.

Pardridge WM (2002) Targeting neurotherapeutic agents through the blood-brain barrier. *Arch Neurol* **59**:35-40.

Patel MM, Goyal BR, Bhadada SV, Bhatt JS and Amin AF (2009) Getting into the brain: approaches to enhance brain drug delivery. *CNS Drugs* **23**:35-58.

Poller B, Iusuf D, Sparidans RW, Wagenaar E, Beijnen JH and Schinkel AH (2011) Differential impact of P-glycoprotein (ABCB1) and breast cancer resistance protein (ABCG2) on axitinib brain accumulation and oral plasma pharmacokinetics. *Drug Metab Dispos* **39**:729-735.

Polli JW, Olson KL, Chism JP, John-Williams LS, Yeager RL, Woodard SM, Otto V, Castellino S and Demby VE (2009) An unexpected synergist role of P-glycoprotein and breast cancer resistance protein on the central nervous system penetration of the tyrosine kinase inhibitor lapatinib (N-{3-chloro-4-[(3-fluorobenzyl)oxy]phenyl}-6-[5-({[2-(methylsulfonyl)ethyl]amino }methyl)-2-furyl]-4-quinazolinamine; GW572016). *Drug Metab Dispos* **37**:439-442.

Prados MD, Schold SJS, Fine HA, Jaeckle K, Hochberg F, Mechtler L, Fetell MR, Phuphanich S, Feun L, Janus TJ, Ford K and Graney W (2003) A randomized,

double-blind, placebo-controlled, phase 2 study of RMP-7 in combination with carboplatin administered intravenously for the treatment of recurrent malignant glioma. *Neuro Oncol* **5**:96-103.

Rapoport SI (1970) Effect of concentrated solutions on blood-brain barrier. *Am J Physiol* **219**:270-274.

Rapoport SI, Hori M and Klatzo I (1972) Testing of a hypothesis for osmotic opening of the blood-brain barrier. *Am J Physiol* **223**:323-331.

Rautio J, Laine K, Gynther M and Savolainen J (2008) Prodrug approaches for CNS delivery. *AAPS J* **10**:92-102.

Rich JN and Bigner DD (2004) Development of novel targeted therapies in the treatment of malignant glioma. *Nat Rev Drug Discov* **3**:430-446.

Romer JT, Kimura H, Magdaleno S, Sasai K, Fuller C, Baines H, Connelly M, Stewart CF, Gould S, Rubin LL and Curran T (2004) Suppression of the Shh pathway using a small molecule inhibitor eliminates medulloblastoma in Ptc1(+/-)p53(-/-) mice. *Cancer Cell* **6**:229-240.

Salphati L, Heffron TP, Alicke B, Nishimura M, Barck K, Carano RA, Cheong J, Edgar KA, Greve J, Kharbanda S, Koeppen H, Lau S, Lee LB, Pang J, Plise EG, Pokorny JL, Reslan HB, Sarkaria JN, Wallin JJ, Zhang X, Gould SE, Olivero AG and Phillips HS (2012a) Targeting the PI3K pathway in the brain--efficacy of a PI3K inhibitor optimized to cross the blood-brain barrier. *Clin Cancer Res* **18**:6239-6248.

Salphati L, Lee LB, Pang J, Plise EG and Zhang X (2010) Role of P-glycoprotein and breast cancer resistance protein-1 in the brain penetration and brain pharmacodynamic activity of the novel phosphatidylinositol 3-kinase inhibitor GDC-0941. *Drug Metab Dispos* **38**:1422-1426.

Salphati L, Pang J, Plise EG, Lee LB, Olivero AG, Prior WW, Sampath D, Wong S and Zhang X (2012b) Preclinical assessment of the absorption and disposition of the phosphatidylinositol 3-kinase/mammalian target of rapamycin inhibitor GDC-0980 and prediction of its pharmacokinetics and efficacy in human. *Drug Metab Dispos* **40**:1785-1796.

Sampson JH, Brady ML, Petry NA, Croteau D, Friedman AH, Friedman HS, Wong T, Bigner DD, Pastan I, Puri RK and Pedain C (2007) Intracerebral infusate distribution by convection-enhanced delivery in humans with malignant gliomas: descriptive effects of target anatomy and catheter positioning. *Neurosurgery* **60**:ONS89-98; discussion ONS98-89.

Sasongko L, Link JM, Muzi M, Mankoff DA, Yang X, Collier AC, Shoner SC and Unadkat JD (2005) Imaging P-glycoprotein transport activity at the human blood-brain barrier with positron emission tomography. *Clin Pharmacol Ther* **77**:503-514.

Scherrmann JM (2002) Drug delivery to brain via the blood-brain barrier. *Vascul Pharmacol* **38**:349-354.

Serwer LP and James CD (2012) Challenges in drug delivery to tumors of the central nervous system: an overview of pharmacological and surgical considerations. *Adv Drug Deliv Rev* **64**:590-597.

Sheikov N, McDannold N, Vykhodtseva N, Jolesz F and Hynynen K (2004) Cellular mechanisms of the blood-brain barrier opening induced by ultrasound in presence of microbubbles. *Ultrasound Med Biol* **30**:979-989.

Smith QR (2003) A review of blood-brain barrier transport techniques. *Methods Mol Med* **89**:193-208.

Song XR, Zheng Y, He G, Yang L, Luo YF, He ZY, Li SZ, Li JM, Yu S, Luo X, Hou SX and Wei YQ (2010) Development of PLGA nanoparticles simultaneously loaded with vincristine and verapamil for treatment of hepatocellular carcinoma. *J Pharm Sci* **99**:4874-4879.

Stenehjem DD, Hartz AM, Bauer B and Anderson GW (2009) Novel and emerging strategies in drug delivery for overcoming the blood-brain barrier. *Future Med Chem* **1**:1623-1641.

Stupp R, Mason WP, van den Bent MJ, Weller M, Fisher B, Taphoorn MJ, Belanger K, Brandes AA, Marosi C, Bogdahn U, Curschmann J, Janzer RC, Ludwin SK, Gorlia T, Allgeier A, Lacombe D, Cairncross JG, Eisenhauer E and Mirimanoff

RO (2005) Radiotherapy plus concomitant and adjuvant temozolomide for glioblastoma. *N Engl J Med* **352**:987-996.

Takasato Y, Rapoport SI and Smith QR (1984) An in situ brain perfusion technique to study cerebrovascular transport in the rat. *Am J Physiol* **247**:H484-493.

Tamai I and Tsuji A (2000) Transporter-mediated permeation of drugs across the blood-brain barrier. *J Pharm Sci* **89**:1371-1388.

Tang SC, Lagas JS, Lankheet NA, Poller B, Hillebrand MJ, Rosing H, Beijnen JH and Schinkel AH (2012) Brain accumulation of sunitinib is restricted by P-glycoprotein (ABCB1) and breast cancer resistance protein (ABCG2) and can be enhanced by oral elacridar and sunitinib coadministration. *Int J Cancer* **130**:223-233.

Ting CY, Fan CH, Liu HL, Huang CY, Hsieh HY, Yen TC, Wei KC and Yeh CK (2012) Concurrent blood-brain barrier opening and local drug delivery using drug-carrying microbubbles and focused ultrasound for brain glioma treatment. *Biomaterials* **33**:704-712.

Uraih LC and Maronpot RR (1990) Normal histology of the nasal cavity and application of special techniques. *Environ Health Perspect* **85**:187-208.

Vartanian A, Singh SK, Agnihotri S, Jalali S, Burrell K, Aldape KD and Zadeh G (2014) GBM's multifaceted landscape: highlighting regional and microenvironmental heterogeneity. *Neuro Oncol*.

Vick NA, Khandekar JD and Bigner DD (1977) Chemotherapy of brain tumors. *Arch Neurol* **34**:523-526.

Vlieghe P and Khrestchatisky M (2013) Medicinal chemistry based approaches and nanotechnology-based systems to improve CNS drug targeting and delivery. *Med Res Rev* **33**:457-516.

Wagner CC, Bauer M, Karch R, Feurstein T, Kopp S, Chiba P, Kletter K, Loscher W, Muller M, Zeitlinger M and Langer O (2009) A pilot study to assess the efficacy of tariquidar to inhibit P-glycoprotein at the human blood-brain barrier with (R)-11C-verapamil and PET. *J Nucl Med* **50**:1954-1961.

Wang C, Ning L, Wang H, Lu Z, Li X, Fan X, Wang X and Liu Y (2013) A peptide-mediated targeting gene delivery system for malignant glioma cells. *Int J Nanomedicine* **8**:3631-3640.

Wang T, Agarwal S and Elmquist WF (2012) Brain distribution of cediranib is limited by active efflux at the blood-brain barrier. *J Pharmacol Exp Ther* **341**:386-395.

Wen PY, Lee EQ, Reardon DA, Ligon KL and Alfred Yung WK (2012) Current clinical development of PI3K pathway inhibitors in glioblastoma. *Neuro Oncol* **14**:819-829.

Williams PC, Henner WD, Roman-Goldstein S, Dahlborg SA, Brummett RE, Tableman M, Dana BW and Neuwelt EA (1995) Toxicity and efficacy of carboplatin and etoposide in conjunction with disruption of the blood-brain tumor barrier in the treatment of intracranial neoplasms. *Neurosurgery* **37**:17-27; discussion 27-18.

Wu C, Lo SL, Boulaire J, Hong ML, Beh HM, Leung DS and Wang S (2008) A peptide-based carrier for intracellular delivery of proteins into malignant glial cells in vitro. *J Control Release* **130**:140-145.

Yang JJ, Milton MN, Yu S, Liao M, Liu N, Wu JT, Gan L, Balani SK, Lee FW, Prakash S and Xia CQ (2010) P-glycoprotein and breast cancer resistance protein affect disposition of tandutinib, a tyrosine kinase inhibitor. *Drug Metab Lett* **4**:201-212.

Yang SC, Lu LF, Cai Y, Zhu JB, Liang BW and Yang CZ (1999) Body distribution in mice of intravenously injected camptothecin solid lipid nanoparticles and targeting effect on brain. *J Control Release* **59**:299-307.

Zara GP, Cavalli R, Fundaro A, Bargoni A, Caputo O and Gasco MR (1999) Pharmacokinetics of doxorubicin incorporated in solid lipid nanospheres (SLN). *Pharmacol Res* **40**:281-286.

Zhu J, Jiang Y, Xu G and Liu X (2012) Intranasal administration: a potential solution for cross-BBB delivering neurotrophic factors. *Histol Histopathol* **27**:537-548.

CHAPTER III

Baratte S, Sarati S, Frigerio E, James CA, Ye C and Zhang Q (2004) Quantitation of SU1 1248, an oral multi-target tyrosine kinase inhibitor, and its metabolite in monkey tissues by liquid chromatograph with tandem mass spectrometry following semi-automated liquid-liquid extraction. *J Chromatogr A* **1024**:87-94.

Bouchet S, Chauzit E, Ducint D, Castaing N, Canal-Raffin M, Moore N, Titier K and Molimard M Simultaneous determination of nine tyrosine kinase inhibitors by 96-well solid-phase extraction and ultra performance LC/MS-MS. *Clin Chim Acta* **412**:1060-1067.

de Bruijn P, Sleijfer S, Lam MH, Mathijssen RH, Wiemer EA and Loos WJ Bioanalytical method for the quantification of sunitinib and its n-desethyl metabolite SU12662 in human plasma by ultra performance liquid chromatography/tandem triple-quadrupole mass spectrometry. *J Pharm Biomed Anal* **51**:934-941.

Faivre S, Demetri G, Sargent W and Raymond E (2007) Molecular basis for sunitinib efficacy and future clinical development. *Nat Rev Drug Discov* **6**:734-745.

FDA (2001) http://www.fda.gov/downloads/Drugs/Guidances/ucm070107.pdf, in.

Goodman VL, Rock EP, Dagher R, Ramchandani RP, Abraham S, Gobburu JV, Booth BP, Verbois SL, Morse DE, Liang CY, Chidambaram N, Jiang JX, Tang S, Mahjoob K, Justice R and Pazdur R (2007) Approval summary: sunitinib for the treatment of imatinib refractory or intolerant gastrointestinal stromal tumors and advanced renal cell carcinoma. *Clinical cancer research : an official journal of the American Association for Cancer Research* **13**:1367-1373.

Gotze L, Hegele A, Metzelder SK, Renz H and Nockher WA Development and clinical application of a LC-MS/MS method for simultaneous determination of various tyrosine kinase inhibitors in human plasma. *Clin Chim Acta* **413**:143-149.

Haouala A, Zanolari B, Rochat B, Montemurro M, Zaman K, Duchosal MA, Ris HB, Leyvraz S, Widmer N and Decosterd LA (2009) Therapeutic Drug Monitoring of the new targeted anticancer agents imatinib, nilotinib, dasatinib, sunitinib,

sorafenib and lapatinib by LC tandem mass spectrometry. *J Chromatogr B Analyt Technol Biomed Life Sci* **877**:1982-1996.

Honeywell R, Yarzadah K, Giovannetti E, Losekoot N, Smit EF, Walraven M, Lind JS, Tibaldi C, Verheul HM and Peters GJ Simple and selective method for the determination of various tyrosine kinase inhibitors used in the clinical setting by liquid chromatography tandem mass spectrometry. *J Chromatogr B Analyt Technol Biomed Life Sci* **878**:1059-1068.

Lankheet NA, Hillebrand MJ, Rosing H, Schellens JH, Beijnen JH and Huitema AD Method development and validation for the quantification of dasatinib, erlotinib, gefitinib, imatinib, lapatinib, nilotinib, sorafenib and sunitinib in human plasma by liquid chromatography coupled with tandem mass spectrometry. *Biomed Chromatogr*.

Mellinghoff IK, Lassman AB and Wen PY Signal transduction inhibitors and antiangiogenic therapies for malignant glioma. *Glia* **59**:1205-1212.

Minkin P, Zhao M, Chen Z, Ouwerkerk J, Gelderblom H and Baker SD (2008) Quantification of sunitinib in human plasma by high-performance liquid chromatography-tandem mass spectrometry. *J Chromatogr B Analyt Technol Biomed Life Sci* **874**:84-88.

Rodamer M, Elsinghorst PW, Kinzig M, Gutschow M and Sorgel F Development and validation of a liquid chromatography/tandem mass spectrometry procedure for the quantification of sunitinib (SU11248) and its active metabolite, N-desethyl sunitinib (SU12662), in human plasma: application to an explorative study. *J Chromatogr B Analyt Technol Biomed Life Sci* **879**:695-706.

Wang T, Oberoi RK and Elmquist WF (2011) Determination of cediranib in mouse plasma and brain tissue using high-performance liquid chromatography-mass spectrometry. *J Chromatogr B Analyt Technol Biomed Life Sci* **879**:3812-3817.

Zhou Q and Gallo JM Quantification of sunitinib in mouse plasma, brain tumor and normal brain using liquid chromatography-electrospray ionization-tandem mass spectrometry and pharmacokinetic application. *J Pharm Biomed Anal* **51**:958-964.

Zhou Q and Gallo JM (2009) Differential effect of sunitinib on the distribution of temozolomide in an orthotopic glioma model. *Neuro-oncology* **11**:301-310.

CHAPTER IV

Agarwal S, Manchanda P, Vogelbaum MA, Ohlfest JR and Elmquist WF (2013) Function of the blood-brain barrier and restriction of drug delivery to invasive glioma cells: findings in an orthotopic rat xenograft model of glioma. *Drug metabolism and disposition: the biological fate of chemicals* **41**:33-39.

Agarwal S, Sane R, Oberoi R, Ohlfest JR and Elmquist WF (2011a) Delivery of molecularly targeted therapy to malignant glioma, a disease of the whole brain. *Expert reviews in molecular medicine* **13**:e17.

Agarwal S, Sane R, Ohlfest JR and Elmquist WF (2011b) The role of the breast cancer resistance protein (ABCG2) in the distribution of sorafenib to the brain. *The Journal of pharmacology and experimental therapeutics* **336**:223-233.

Agarwal S, Uchida Y, Mittapalli RK, Sane R, Terasaki T and Elmquist WF (2012) Quantitative proteomics of transporter expression in brain capillary endothelial cells isolated from P-glycoprotein (P-gp), breast cancer resistance protein (Bcrp), and P-gp/Bcrp knockout mice. *Drug metabolism and disposition: the biological fate of chemicals* **40**:1164-1169.

Allen JD, van Loevezijn A, Lakhai JM, van der Valk M, van Tellingen O, Reid G, Schellens JH, Koomen GJ and Schinkel AH (2002) Potent and specific inhibition of the breast cancer resistance protein multidrug transporter in vitro and in mouse intestine by a novel analogue of fumitremorgin C. *Molecular cancer therapeutics* **1**:417-425.

Batchelor TT, Duda DG, di Tomaso E, Ancukiewicz M, Plotkin SR, Gerstner E, Eichler AF, Drappatz J, Hochberg FH, Benner T, Louis DN, Cohen KS, Chea H, Exarhopoulos A, Loeffler JS, Moses MA, Ivy P, Sorensen AG, Wen PY and Jain RK (2010) Phase II study of cediranib, an oral pan-vascular endothelial growth factor receptor tyrosine kinase inhibitor, in patients with recurrent glioblastoma. *Journal of clinical oncology : official journal of the American Society of Clinical Oncology* **28**:2817-2823.

Brem S, Tsanaclis AM, Gately S, Gross JL and Herblin WF (1992) Immunolocalization of basic fibroblast growth factor to the microvasculature of human brain tumors. *Cancer* **70**:2673-2680.

Chen Y, Agarwal S, Shaik NM, Chen C, Yang Z and Elmquist WF (2009) P-glycoprotein and breast cancer resistance protein influence brain distribution of dasatinib. *The Journal of pharmacology and experimental therapeutics* **330**:956-963.

Christensen JG (2007) A preclinical review of sunitinib, a multitargeted receptor tyrosine kinase inhibitor with anti-angiogenic and antitumour activities. *Annals of oncology : official journal of the European Society for Medical Oncology / ESMO* **18 Suppl 10**:x3-10.

Cohen MH, Shen YL, Keegan P and Pazdur R (2009) FDA drug approval summary: bevacizumab (Avastin) as treatment of recurrent glioblastoma multiforme. *The oncologist* **14**:1131-1138.

Dai CL, Liang YJ, Wang YS, Tiwari AK, Yan YY, Wang F, Chen ZS, Tong XZ and Fu LW (2009) Sensitization of ABCG2-overexpressing cells to conventional chemotherapeutic agent by sunitinib was associated with inhibiting the function of ABCG2. *Cancer letters* **279**:74-83.

Dai H, Marbach P, Lemaire M, Hayes M and Elmquist WF (2003) Distribution of STI-571 to the brain is limited by P-glycoprotein-mediated efflux. *The Journal of pharmacology and experimental therapeutics* **304**:1085-1092.

Dantzig AH, Law KL, Cao J and Starling JJ (2001) Reversal of multidrug resistance by the P-glycoprotein modulator, LY335979, from the bench to the clinic. *Current medicinal chemistry* **8**:39-50.

de Bruijn P, Sleijfer S, Lam MH, Mathijssen RH, Wiemer EA and Loos WJ (2010) Bioanalytical method for the quantification of sunitinib and its n-desethyl metabolite SU12662 in human plasma by ultra performance liquid chromatography/tandem triple-quadrupole mass spectrometry. *Journal of pharmaceutical and biomedical analysis* **51**:934-941.

di Tomaso E, Snuderl M, Kamoun WS, Duda DG, Auluck PK, Fazlollahi L, Andronesi OC, Frosch MP, Wen PY, Plotkin SR, Hedley-Whyte ET, Sorensen AG,

Batchelor TT and Jain RK (2011) Glioblastoma recurrence after cediranib therapy in patients: lack of "rebound" revascularization as mode of escape. *Cancer research* **71**:19-28.

Dudek AZ, Raza A, Chi M, Singhal M, Oberoi R, Mittapalli RK, Agarwal S and Elmquist WF (2013) Brain metastases from renal cell carcinoma in the era of tyrosine kinase inhibitors. *Clinical genitourinary cancer* **11**:155-160.

Faivre S, Demetri G, Sargent W and Raymond E (2007) Molecular basis for sunitinib efficacy and future clinical development. *Nature reviews Drug discovery* **6**:734-745.

Fletcher JI, Haber M, Henderson MJ and Norris MD (2010) ABC transporters in cancer: more than just drug efflux pumps. *Nature reviews Cancer* **10**:147-156.

Gottesman MM, Fojo T and Bates SE (2002) Multidrug resistance in cancer: role of ATP-dependent transporters. *Nature reviews Cancer* **2**:48-58.

Horowitz M, Blasberg R, Molnar P, Strong J, Kornblith P, Pleasants R and Fenstermacher J (1983) Regional [14C]misonidazole distribution in experimental RT-9 brain tumors. *Cancer research* **43**:3800-3807.

Hu S, Chen Z, Franke R, Orwick S, Zhao M, Rudek MA, Sparreboom A and Baker SD (2009) Interaction of the multikinase inhibitors sorafenib and sunitinib with solute carriers and ATP-binding cassette transporters. *Clinical cancer research : an official journal of the American Association for Cancer Research* **15**:6062-6069.

Hubensack M, Muller C, Hocherl P, Fellner S, Spruss T, Bernhardt G and Buschauer A (2008) Effect of the ABCB1 modulators elacridar and tariquidar on the distribution of paclitaxel in nude mice. *Journal of cancer research and clinical oncology* **134**:597-607.

Iwamoto FM, Lamborn KR, Robins HI, Mehta MP, Chang SM, Butowski NA, Deangelis LM, Abrey LE, Zhang WT, Prados MD and Fine HA (2010) Phase II trial of pazopanib (GW786034), an oral multi-targeted angiogenesis inhibitor, for adults with recurrent glioblastoma (North American Brain Tumor Consortium Study 06-02). *Neuro-oncology* **12**:855-861.

Kreisl TN, McNeill KA, Sul J, Iwamoto FM, Shih J and Fine HA (2012) A phase I/II trial of vandetanib for patients with recurrent malignant glioma. *Neuro-oncology* **14**:1519-1526.

Kunimatsu S, Mizuno T, Fukudo M and Katsura T (2013) Effect of p-glycoprotein and breast cancer resistance protein inhibition on the pharmacokinetics of sunitinib in rats. *Drug metabolism and disposition: the biological fate of chemicals* **41**:1592-1597.

Lagas JS, van Waterschoot RA, van Tilburg VA, Hillebrand MJ, Lankheet N, Rosing H, Beijnen JH and Schinkel AH (2009) Brain accumulation of dasatinib is restricted by P-glycoprotein (ABCB1) and breast cancer resistance protein (ABCG2) and can be enhanced by elacridar treatment. *Clinical cancer research : an official journal of the American Association for Cancer Research* **15**:2344-2351.

Levin VA, Freeman-Dove M and Landahl HD (1975) Permeability characteristics of brain adjacent to tumors in rats. *Archives of neurology* **32**:785-791.

Louis DN, Ohgaki H, Wiestler OD, Cavenee WK, Burger PC, Jouvet A, Scheithauer BW and Kleihues P (2007) The 2007 WHO classification of tumours of the central nervous system. *Acta neuropathologica* **114**:97-109.

Maliepaard M, van Gastelen MA, Tohgo A, Hausheer FH, van Waardenburg RC, de Jong LA, Pluim D, Beijnen JH and Schellens JH (2001) Circumvention of breast cancer resistance protein (BCRP)-mediated resistance to camptothecins in vitro using non-substrate drugs or the BCRP inhibitor GF120918. *Clinical cancer research : an official journal of the American Association for Cancer Research* **7**:935-941.

Minocha M, Khurana V, Qin B, Pal D and Mitra AK (2012a) Co-administration strategy to enhance brain accumulation of vandetanib by modulating P-glycoprotein (P-gp/Abcb1) and breast cancer resistance protein (Bcrp1/Abcg2) mediated efflux with m-TOR inhibitors. *International journal of pharmaceutics* **434**:306-314.

Minocha M, Khurana V, Qin B, Pal D and Mitra AK (2012b) Enhanced brain accumulation of pazopanib by modulating P-gp and Bcrp1 mediated efflux with canertinib or erlotinib. *International journal of pharmaceutics* **436**:127-134.

Nedelman JR and Jia X (1998) An extension of Satterthwaite's approximation applied to pharmacokinetics. *Journal of biopharmaceutical statistics* **8**:317-328.

Neyns B, Sadones J, Chaskis C, Dujardin M, Everaert H, Lv S, Duerinck J, Tynninen O, Nupponen N, Michotte A and De Greve J (2011) Phase II study of sunitinib malate in patients with recurrent high-grade glioma. *Journal of neuro-oncology* **103**:491-501.

Oberoi RK, Mittapalli R, Fisher J, Elmquist WF (2013) Sunitinib LC–MS/MS Assay in Mouse Plasma and Brain Tissue: Application in CNS Distribution Studies. C*hromatographia*.

Pan E, Yu D, Yue B, Potthast L, Chowdhary S, Smith P and Chamberlain M (2012) A prospective phase II single-institution trial of sunitinib for recurrent malignant glioma. *Journal of neuro-oncology* **110**:111-118.

Poller B, Iusuf D, Sparidans RW, Wagenaar E, Beijnen JH and Schinkel AH (2011) Differential impact of P-glycoprotein (ABCB1) and breast cancer resistance protein (ABCG2) on axitinib brain accumulation and oral plasma pharmacokinetics. *Drug metabolism and disposition: the biological fate of chemicals* **39**:729-735.

Polli JW, Olson KL, Chism JP, John-Williams LS, Yeager RL, Woodard SM, Otto V, Castellino S and Demby VE (2009) An unexpected synergist role of P-glycoprotein and breast cancer resistance protein on the central nervous system penetration of the tyrosine kinase inhibitor lapatinib (N-{3-chloro-4-[(3-fluorobenzyl)oxy]phenyl}-6-[5-({[2-(methylsulfonyl)ethyl]amino }methyl)-2-furyl]-4-quinazolinamine; GW572016). *Drug metabolism and disposition: the biological fate of chemicals* **37**:439-442.

Riad LE, Chan KK and Sawchuk RJ (1993) Transient steady-state analysis: application in the determination of the relative formation and elimination clearances of two major carbamazepine metabolites in humans. *Pharmaceutical research* **10**:1090-1092.

Shukla S, Robey RW, Bates SE and Ambudkar SV (2009) Sunitinib (Sutent, SU11248), a small-molecule receptor tyrosine kinase inhibitor, blocks function of the ATP-

binding cassette (ABC) transporters P-glycoprotein (ABCB1) and ABCG2. *Drug metabolism and disposition: the biological fate of chemicals* **37**:359-365.

Tang SC, Lagas JS, Lankheet NA, Poller B, Hillebrand MJ, Rosing H, Beijnen JH and Schinkel AH (2012) Brain accumulation of sunitinib is restricted by P-glycoprotein (ABCB1) and breast cancer resistance protein (ABCG2) and can be enhanced by oral elacridar and sunitinib coadministration. *International journal of cancer Journal international du cancer* **130**:223-233.

Tuettenberg J, Friedel C and Vajkoczy P (2006) Angiogenesis in malignant glioma--a target for antitumor therapy? *Critical reviews in oncology/hematology* **59**:181-193.

Wang T (2011) Mechanisms and analysis of the CNS distribution of cediranib, a molecularly-targeted anti-angiogenic agent, in pp 1 online resource (xi, 225 p.).

Wang T, Agarwal S and Elmquist WF (2012) Brain distribution of cediranib is limited by active efflux at the blood-brain barrier. *The Journal of pharmacology and experimental therapeutics* **341**:386-395.

Wick W, Weller M, Weiler M, Batchelor T, Yung AW and Platten M (2011) Pathway inhibition: emerging molecular targets for treating glioblastoma. *Neuro-oncology* **13**:566-579.

Wong ML, Prawira A, Kaye AH and Hovens CM (2009) Tumour angiogenesis: its mechanism and therapeutic implications in malignant gliomas. *Journal of clinical neuroscience : official journal of the Neurosurgical Society of Australasia* **16**:1119-1130.

Yoshikawa A, Nakada M, Ohtsuki S, Hayashi Y, Obuchi W, Sato Y, Ikeda C, Watanabe T, Kawahara Y, Hasegawa T, Sabit H, Kita D, Nakanuma Y, Terasaki T and Hamada JI (2012) Recurrent anaplastic meningioma treated by sunitinib based on results from quantitative proteomics. *Neuropathology and applied neurobiology* **38**:105-110.

Zhou Q and Gallo JM (2009) Differential effect of sunitinib on the distribution of temozolomide in an orthotopic glioma model. *Neuro-oncology* **11**:301-310.

Zhou Q, Guo P and Gallo JM (2008) Impact of angiogenesis inhibition by sunitinib on tumor distribution of temozolomide. *Clinical cancer research : an official journal of the American Association for Cancer Research* **14**:1540-1549.

Chu HM and Ette EI (2005) A random sampling approach for robust estimation of tissue-to-plasma ratio from extremely sparse data. *AAPS J* **7**:E249-258.

Ette EI, Howie CA, Kelman AW and Whiting B (1995a) Experimental design and efficient parameter estimation in preclinical pharmacokinetic studies. *Pharm Res* **12**:729-737.

Ette EI, Kelman AW, Howie CA and Whiting B (1995b) Analysis of animal pharmacokinetic data: performance of the one point per animal design. *J Pharmacokinet Biopharm* **23**:551-566.

Hing JP, Woolfrey SG, Greenslade D and Wright PM (2001) Is mixed effects modeling or naive pooled data analysis preferred for the interpretation of single sample per subject toxicokinetic data? *J Pharmacokinet Pharmacodyn* **28**:193-210.

Oberoi RK, Mittapalli RK and Elmquist WF (2013) Pharmacokinetic assessment of efflux transport in sunitinib distribution to the brain. *J Pharmacol Exp Ther* **347**:755-764.

Wang T, Baron K, Zhong W, Brundage R and Elmquist W (2014) Bayesian approach to estimate AUC, partition coefficient and drug targeting index for studies with serial sacrifice design. *Pharm Res* **31**:649-659.

2008. Comprehensive genomic characterization defines human glioblastoma genes and core pathways. *Nature* 455:1061-1068.

Agarwal, S., A.M. Hartz, W.F. Elmquist, and B. Bauer. 2011a. Breast cancer resistance protein and P-glycoprotein in brain cancer: two gatekeepers team up. *Curr Pharm Des* 17:2793-2802.

Agarwal, S., P. Manchanda, M.A. Vogelbaum, J.R. Ohlfest, and W.F. Elmquist. 2013. Function of the blood-brain barrier and restriction of drug delivery to invasive glioma cells: findings in an orthotopic rat xenograft model of glioma. *Drug metabolism and disposition: the biological fate of chemicals* 41:33-39.

Agarwal, S., R.K. Mittapalli, D.M. Zellmer, J.L. Gallardo, R. Donelson, C. Seiler, S.A. Decker, K.S. Santacruz, J.L. Pokorny, J.N. Sarkaria, W.F. Elmquist, and J.R. Ohlfest. 2012. Active efflux of Dasatinib from the brain limits efficacy against murine glioblastoma: broad implications for the clinical use of molecularly targeted agents. *Molecular cancer therapeutics* 11:2183-2192.

Agarwal, S., R. Sane, R. Oberoi, J.R. Ohlfest, and W.F. Elmquist. 2011b. Delivery of molecularly targeted therapy to malignant glioma, a disease of the whole brain. *Expert reviews in molecular medicine* 13:e17.

Akhavan, D., T.F. Cloughesy, and P.S. Mischel. 2010. mTOR signaling in glioblastoma: lessons learned from bench to bedside. *Neuro Oncol* 12:882-889.

Berens, M.E., and A. Giese. 1999. "...those left behind." Biology and oncology of invasive glioma cells. *Neoplasia* 1:208-219.

Blakeley, J.O., J. Olson, S.A. Grossman, X. He, J. Weingart, and J.G. Supko. 2009. Effect of blood brain barrier permeability in recurrent high grade gliomas on the intratumoral pharmacokinetics of methotrexate: a microdialysis study. *J Neurooncol* 91:51-58.

Carlson, B.L., J.L. Pokorny, M.A. Schroeder, and J.N. Sarkaria. 2011. Establishment, maintenance and in vitro and in vivo applications of primary human glioblastoma

multiforme (GBM) xenograft models for translational biology studies and drug discovery. *Curr Protoc Pharmacol* Chapter 14:Unit 14 16.

Carracedo, A., L. Ma, J. Teruya-Feldstein, F. Rojo, L. Salmena, A. Alimonti, A. Egia, A.T. Sasaki, G. Thomas, S.C. Kozma, A. Papa, C. Nardella, L.C. Cantley, J. Baselga, and P.P. Pandolfi. 2008. Inhibition of mTORC1 leads to MAPK pathway activation through a PI3K-dependent feedback loop in human cancer. *J Clin Invest* 118:3065-3074.

Choucair, A.K., V.A. Levin, P.H. Gutin, R.L. Davis, P. Silver, M.S. Edwards, and C.B. Wilson. 1986. Development of multiple lesions during radiation therapy and chemotherapy in patients with gliomas. *Journal of neurosurgery* 65:654-658.

Chu, C., C. Abbara, M.S. Noel-Hudson, L. Thomas-Bourgneuf, P. Gonin, R. Farinotti, and L. Bonhomme-Faivre. 2009. Disposition of everolimus in mdr1a-/1b- mice and after a pre-treatment of lapatinib in Swiss mice. *Biochem Pharmacol* 77:1629-1634.

Clark, M.J., N. Homer, B.D. O'Connor, Z. Chen, A. Eskin, H. Lee, B. Merriman, and S.F. Nelson. 2010. U87MG decoded: the genomic sequence of a cytogenetically aberrant human cancer cell line. *PLoS Genet* 6:e1000832.

Fine, R.L., J. Chen, C. Balmaceda, J.N. Bruce, M. Huang, M. Desai, M.B. Sisti, G.M. McKhann, R.R. Goodman, J.S. Bertino, Jr., A.N. Nafziger, and M.R. Fetell. 2006. Randomized study of paclitaxel and tamoxifen deposition into human brain tumors: implications for the treatment of metastatic brain tumors. *Clin Cancer Res* 12:5770-5776.

Galanis, E., J.C. Buckner, M.J. Maurer, J.I. Kreisberg, K. Ballman, J. Boni, J.M. Peralba, R.B. Jenkins, S.R. Dakhil, R.F. Morton, K.A. Jaeckle, B.W. Scheithauer, J. Dancey, M. Hidalgo, and D.J. Walsh. 2005. Phase II trial of temsirolimus (CCI-779) in recurrent glioblastoma multiforme: a North Central Cancer Treatment Group Study. *J Clin Oncol* 23:5294-5304.

Grossman, S.A., X. Ye, S. Piantadosi, S. Desideri, L.B. Nabors, M. Rosenfeld, and J. Fisher. 2010. Survival of patients with newly diagnosed glioblastoma treated with

radiation and temozolomide in research studies in the United States. *Clin Cancer Res* 16:2443-2449.

Guertin, D.A., and D.M. Sabatini. 2007. Defining the role of mTOR in cancer. *Cancer Cell* 12:9-22.

Gulati, N., M. Karsy, L. Albert, R. Murali, and M. Jhanwar-Uniyal. 2009. Involvement of mTORC1 and mTORC2 in regulation of glioblastoma multiforme growth and motility. *Int J Oncol* 35:731-740.

Haar, C.P., P. Hebbar, G.C.t. Wallace, A. Das, W.A. Vandergrift, 3rd, J.A. Smith, P. Giglio, S.J. Patel, S.K. Ray, and N.L. Banik. 2012. Drug resistance in glioblastoma: a mini review. *Neurochem Res* 37:1192-1200.

Hofer, S., and K. Frei. 2007. Gefitinib concentrations in human glioblastoma tissue. *J Neurooncol* 82:175-176.

Huang, T.T., S.M. Sarkaria, T.F. Cloughesy, and P.S. Mischel. 2009. Targeted therapy for malignant glioma patients: lessons learned and the road ahead. *Neurotherapeutics* 6:500-512.

Jiang, B.H., and L.Z. Liu. 2009. PI3K/PTEN signaling in angiogenesis and tumorigenesis. *Adv Cancer Res* 102:19-65.

Karar, J., and A. Maity. 2011. PI3K/AKT/mTOR Pathway in Angiogenesis. *Front Mol Neurosci* 4:51.

Kim, D.H., D.D. Sarbassov, S.M. Ali, J.E. King, R.R. Latek, H. Erdjument-Bromage, P. Tempst, and D.M. Sabatini. 2002. mTOR interacts with raptor to form a nutrient-sensitive complex that signals to the cell growth machinery. *Cell* 110:163-175.

Knobbe, C.B., and G. Reifenberger. 2003. Genetic alterations and aberrant expression of genes related to the phosphatidyl-inositol-3'-kinase/protein kinase B (Akt) signal transduction pathway in glioblastomas. *Brain Pathol* 13:507-518.

Levin, V.A., M. Freeman-Dove, and H.D. Landahl. 1975. Permeability characteristics of brain adjacent to tumors in rats. *Arch Neurol* 32:785-791.

Michaud, K., D.A. Solomon, E. Oermann, J.S. Kim, W.Z. Zhong, M.D. Prados, T. Ozawa, C.D. James, and T. Waldman. 2010. Pharmacologic inhibition of cyclin-

dependent kinases 4 and 6 arrests the growth of glioblastoma multiforme intracranial xenografts. *Cancer Res* 70:3228-3238.

Newcomb, E., and D. Zagzag. 2009. The Murine GL261 Glioma Experimental Model to Assess Novel Brain Tumor Treatments. In CNS Cancer. E.G. Meir, editor Humana Press, 227-241.

Pafundi, D.H., N.N. Laack, R.S. Youland, I.F. Parney, V.J. Lowe, C. Giannini, B.J. Kemp, M.P. Grams, J.M. Morris, J.M. Hoover, L.S. Hu, J.N. Sarkaria, and D.H. Brinkmann. 2013. Biopsy validation of 18F-DOPA PET and biodistribution in gliomas for neurosurgical planning and radiotherapy target delineation: results of a prospective pilot study. *Neuro Oncol* 15:1058-1067.

Pardridge, W.M. 2005. The blood-brain barrier: bottleneck in brain drug development. *NeuroRx* 2:3-14.

Ponten, J., and E.H. Macintyre. 1968. Long term culture of normal and neoplastic human glia. *Acta Pathol Microbiol Scand* 74:465-486.

Rodon, J., R. Dienstmann, V. Serra, and J. Tabernero. 2013. Development of PI3K inhibitors: lessons learned from early clinical trials. *Nat Rev Clin Oncol* 10:143-153.

Rosso, L., C.S. Brock, J.M. Gallo, A. Saleem, P.M. Price, F.E. Turkheimer, and E.O. Aboagye. 2009. A new model for prediction of drug distribution in tumor and normal tissues: pharmacokinetics of temozolomide in glioma patients. *Cancer Res* 69:120-127.

Sabbah, D.A., M.G. Brattain, and H. Zhong. 2011. Dual inhibitors of PI3K/mTOR or mTOR-selective inhibitors: which way shall we go? *Curr Med Chem* 18:5528-5544.

Salphati, L., T.P. Heffron, B. Alicke, M. Nishimura, K. Barck, R.A. Carano, J. Cheong, K.A. Edgar, J. Greve, S. Kharbanda, H. Koeppen, S. Lau, L.B. Lee, J. Pang, E.G. Plise, J.L. Pokorny, H.B. Reslan, J.N. Sarkaria, J.J. Wallin, X. Zhang, S.E. Gould, A.G. Olivero, and H.S. Phillips. 2012a. Targeting the PI3K pathway in the brain--efficacy of a PI3K inhibitor optimized to cross the blood-brain barrier. *Clinical*

cancer research : an official journal of the American Association for Cancer Research 18:6239-6248.

Salphati, L., L.B. Lee, J. Pang, E.G. Plise, and X. Zhang. 2010. Role of P-glycoprotein and breast cancer resistance protein-1 in the brain penetration and brain pharmacodynamic activity of the novel phosphatidylinositol 3-kinase inhibitor GDC-0941. *Drug Metab Dispos* 38:1422-1426.

Salphati, L., J. Pang, E.G. Plise, L.B. Lee, A.G. Olivero, W.W. Prior, D. Sampath, S. Wong, and X. Zhang. 2012b. Preclinical assessment of the absorption and disposition of the phosphatidylinositol 3-kinase/mammalian target of rapamycin inhibitor GDC-0980 and prediction of its pharmacokinetics and efficacy in human. *Drug metabolism and disposition: the biological fate of chemicals* 40:1785-1796.

Sarbassov, D.D., D.A. Guertin, S.M. Ali, and D.M. Sabatini. 2005. Phosphorylation and regulation of Akt/PKB by the rictor-mTOR complex. *Science* 307:1098-1101.

Schinkel, A.H., and J.W. Jonker. 2003. Mammalian drug efflux transporters of the ATP binding cassette (ABC) family: an overview. *Adv Drug Deliv Rev* 55:3-29.

Schmalz, P.G., M.J. Shen, and J.K. Park. 2011. Treatment resistance mechanisms of malignant glioma tumor stem cells. *Cancers (Basel)* 3:621-635.

Stupp, R., W.P. Mason, M.J. van den Bent, M. Weller, B. Fisher, M.J. Taphoorn, K. Belanger, A.A. Brandes, C. Marosi, U. Bogdahn, J. Curschmann, R.C. Janzer, S.K. Ludwin, T. Gorlia, A. Allgeier, D. Lacombe, J.G. Cairncross, E. Eisenhauer, and R.O. Mirimanoff. 2005. Radiotherapy plus concomitant and adjuvant temozolomide for glioblastoma. *N Engl J Med* 352:987-996.

Tamaki, A., C. Ierano, G. Szakacs, R.W. Robey, and S.E. Bates. 2011. The controversial role of ABC transporters in clinical oncology. *Essays Biochem* 50:209-232.

Yang, L., M.J. Clarke, B.L. Carlson, A.C. Mladek, M.A. Schroeder, P. Decker, W. Wu, G.J. Kitange, P.T. Grogan, J.M. Goble, J. Uhm, E. Galanis, C. Giannini, H.A. Lane, C.D. James, and J.N. Sarkaria. 2008. PTEN loss does not predict for response to RAD001 (Everolimus) in a glioblastoma orthotopic xenograft test panel. *Clin Cancer Res* 14:3993-4001.

Zagzag, D., H. Zhong, J.M. Scalzitti, E. Laughner, J.W. Simons, and G.L. Semenza. 2000. Expression of hypoxia-inducible factor 1alpha in brain tumors: association with angiogenesis, invasion, and progression. *Cancer* 88:2606-2618.

APPENDIX

NONMEM CODE for chapter 5

```
;Model Desc: SAME AS 106 BSV 20%
;Project Name: rajneet
;Project ID: NO PROJECT DESCRIPTION



;Project ID: NO PROJECT DESCRIPTION

$PROB RUN# 602
$INPUT C ID TIME DV AMT MDV TYPE CMT RATE EVID POIP
$DATA SUNITINIBPLBRNP_new.CSV IGNORE=C
$SUBROUTINES ADVAN6 TRANS1 TOL=6
$MODEL
  COMP=(PODEPOT)
  COMP=(PLASMA)
  COMP=(BRAIN)
  COMP=(IPDEPOT)
$PK
  KA=THETA(1)
  CL=THETA(2)*EXP(ETA(1))
  V=THETA(3)*EXP(ETA(2))
  CLIN=THETA(4)*EXP(ETA(3))
  S2=V

IF (TYPE.EQ.1) THEN
  KP = THETA(5)
ELSEIF (TYPE.EQ.2) THEN
  KP = THETA(6)
ELSEIF (TYPE.EQ.3) THEN
  KP = THETA(7)
ELSE
  KP = THETA(8)
ENDIF
KP1=KP*EXP(ETA(4))
F1=THETA(9)
CLOUT=CLIN/KP1
HL=0.693*V/CL
SID=TYPE
TAD=TIME
```

```
$DES
CP=A(2)/V
CBR=A(3)
   DADT(1) = -KA*A(1)
   DADT(2) = KA*A(1) + KA*A(4) - CL*CP
   DADT(3) = CLIN*CP-CLOUT*CBR
   DADT(4) = -KA*A(4)

$ERROR
IF(CMT.EQ.2) THEN
   Y = F + F*ERR(1)
ELSE
   Y = F+F*ERR(2)
ENDIF
 IPRE=F

$EST PRINT=5 MAX=9999 SIG=2 SIGL=6 METHOD=1 MSFO=602.msf
$COV
$THETA
  (1.0 FIX) ;[KA]
  (0 .1) ;[CL]
  (0 .5) ;[V]
  (0 2) ;[CLin]
  (0 .5) ;[KP WT]
  (0 2.3) ;[KP PKO]
  (0 .8) ;[KP BKO]
  (0 17) ;[KP TKO]
  (0 .5 1) ;[F4 IP]

$OMEGA
  0.04 FIX ;[P]
  0.04 FIX ;[P]
  0.04 FIX ;[P]
  0.04 FIX ;[P]
$SIGMA
  0.0225 ;[P]
  0.04 ;[P]

$TABLE ID TIME TAD SID CMT POIP TYPE IPRE CWRES HL CL V KP1 CLIN
CLOUT ONEHEADER NOPRINT FILE=602.tab
$TABLE ID CL V CLIN KP1 FIRSTONLY NOAPPEND NOPRINT FILE=602.PAR
$TABLE ID ETA1 ETA2 ETA3 ETA4 FIRSTONLY NOAPPEND NOPRINT
FILE=602.eta
```